NASA Contractor Report 3104

Full-Coverage Film Cooling: 3-Dimensional Measurements of Turbulence Structure and Prediction of Recovery Region Hydrodynamics

S. Yavuzkurt, R. J. Moffat,
and W. M. Kays

CONTRACT NAS3-14336
MARCH 1979

NASA

NASA Contractor Report 3104

Full-Coverage Film Cooling: 3-Dimensional Measurements of Turbulence Structure and Prediction of Recovery Region Hydrodynamics

S. Yavuzkurt, R. J. Moffat,
and W. M. Kays
Stanford University
Stanford, California

Prepared for
Lewis Research Center
under Contract NAS3-14336

National Aeronautics
and Space Administration

Scientific and Technical
Information Office

1979

Table of Contents

		Page
NOMENCLATURE		v
SUMMARY		xi
Chapter		
1	INTRODUCTION	1
	1.1 Background	1
	1.2 Objectives	5
	1.3 Outline of the Work	5
2	APPARATUS AND INSTRUMENTATION	7
	2.1 The Test Surface	7
	2.2 Instrumentation	8
3	REAL-TIME HOT-WIRE MEASUREMENT IN THREE-DIMENSIONAL FLOWS	15
	3.1 Background in Hot-Wire Measurements	15
	3.2 The Present Approach	20
	3.3 The Three-Dimensional Turbulent Flow Analyzer	22
	3.4 Processing of the Data	25
	3.5 Problems Created by the Size of the Triaxial Wire Probe	26
	3.6 Qualification Tests	26
	3.7 Further Work on Triaxial Wire System	31
	3.8 Conclusions and Capabilities	32
4	PREDICTION OF RECOVERY REGION HYDRODYNAMICS WITH A ONE-EQUATION MODEL OF TURBULENCE	45
	4.1 Equations to be Solved	45
	4.2 Mixing-Length Model	48
	4.3 Predictions	58
	4.4 Refining the Model	59
5	MEASUREMENTS AND DISCUSSIONS OF THE DATA	71
	5.1 Experimental Conditions	71
	5.2 Measurement Locations	72
	5.3 Mean Velocity Profiles	73
	5.4 Turbulent Kinetic Energy Profiles	79
	5.5 Streamwise Shear Stress Profiles	86
	5.6 On Spanwise Averaging	88
	5.7 On the Three-Dimensionality of the Flow Field	89
	5.8 Correlation Coefficients	92
	5.9 Mixing Length	93

Table of Contents (cont.)

		Page
Chapter		
6	SUMMARY AND RECOMMENDATIONS	120
	6.1 Summary.	120
	6.2 Recommendations.	122
REFERENCES		123
APPENDIXES		
A	TABULATION OF EXPERIMENTAL DATA	127
	A.1 Individual Profiles.	127
	A.2 Spanwise-Averaged Profiles	159
B	WIRING DIAGRAMS OF THE 3-D TURBULENT FLOW ANALYZER. . .	170

NOMENCLATURE

A_q Production constant for turbulent kinetic energy.

A^+ Effective thickness of laminar sublayer.

B_q Dissipation constant for turbulent kinetic energy.

C Division constant for the total velocity magnitude (R) at the output of 3-D Turbulent Flow Analyzer = 0.576.

D Hole diameter of injection tube.
Van Driest damping function, mixing-length model.

$\mathcal{D}$ Dissipation of turbulent kinetic energy.

E_{eff} Output of linearizers.

F Blowing fraction = $\frac{\rho_{jet} U_{jet}}{\rho_\infty U_\infty} \frac{\pi}{4} \frac{D^2}{P^2}$.

F' Blowing fraction based on momentum = $\frac{\rho_{jet} U_{jet}^2}{\rho_\infty U_\infty^2} \frac{\pi}{4} \frac{D^2}{P^2}$.

g_c Proportionality constant, Newton's Second Law.

H Shape factor = δ_1/δ_2.

J Diffusion of turbulent kinetic energy.

k_1 Pitch sensitivity coefficient for hot wire.

k_2 Yaw sensitivity coefficient for hot-wire.

ℓ Mixing length.

$(\ell/\delta)_a$ Augmentation in mixing-length normalized on outer boundary layer thickness, mixing-length model.

$(\ell/\delta)_{max}$ Maximum value of augmentation in mixing-length normalized on outer boundary layer thickness, mixing-length model.

$(\ell/\delta)_{max,i}$ Initial value of maximum augmentation in mixing-length normalized in outer boundary-layer thickness, mixing-length model.

M	Blowing ratio, $\rho_{jet}U_{jet}/\rho_\infty U_\infty$.
	Inverse Jorgensen matrix, Chapter 3.
N	Coordinate transformation matrix, Chapter 3.
P	Hole spacing, or pitch.
	Pressure.
P	Production of turbulent kinetic energy.
q^2	Turbulent kinetic energy = $\overline{u'^2} + \overline{v'^2} + \overline{w'^2}$.
q_∞^2	Value of the turbulent kinetic energy at free stream.
$\overline{R}$	Magnitude of mean velocity.
Re_x	x-Reynolds number = xU_∞/ν.
Sc_q	Schmidt number of turbulent kinetic energy = $\varepsilon_M/\varepsilon_q$.
T	Temperature.
U	Instantaneous velocity component in x-direction.
U_{jet}	Injectant mean velocity.
U_∞	Freestream velocity.
$\overline{U}$	Mean velocity component in x-direction.
$\overline{U}_{\mathcal{L}}$	Centerline mean velocity in 2-D channel, Chapter 3.
U_{eff}	Instantaneous effective velocity for hot-wire.
$(U_{eff})_{max}$	Maximum value of effective velocity in one calibration.
$\overline{U}_{eff}$	Time-averaged effective velocity.
u_τ	Friction velocity = $g_c\tau_o/\rho_o$.
u'	Fluctuating velocity component in x-direction.
u'_{eff}	Fluctuating effective velocity.
$\overline{u'^2}$	Reynolds normal stress in x-direction.
$\overline{u'v'}$	Longitudinal-normal velocity correlation, Reynolds shear stress.
$\overline{u'w'}$	Longitudinal-tangential velocity correlation, Reynolds shear stress.
$\overline{u'^2_{eff}}$	Mean square of fluctuating effective velocity.

V	Instantaneous velocity component in y-direction.
$\overline{V}$	Mean velocity component in y-direction.
v'	Fluctuating velocity component in y-direction.
$\overline{v'^2}$	Reynolds normal stress in y-direction.
$\overline{v'w'}$	Normal-tangential velocity correlation, Reunolds shear stress.
W	Instantaneous velocity component in z-direction.
$\overline{W}$	Mean velocity component in z-direction.
w'	Fluctuating velocity component in z-direction.
$\overline{w'^2}$	Reynolds normal stress in z-direction.
x	Longitudinal coordinate. Distance along test surface measured from nozzle exit.
x'	Distance along test surface measured from start of recovery region.
x'_o	Distance, start of recovery region to virtual origin of internal two-dimensional layer, Chapter 4.
x''_o	Distance, start of recovery region to virtual origin of effective jet action.
y	Coordinate normal to test surface. Distance normal to test surface.
y^+	Nondimensional distance = yu_τ/ν.
$(y/\delta)_d$	Departure point from κy line in mixing-length model, Chapter 4.
$(y/\delta)_i$	Intersection point of new mixing-length model with $\ell/\delta = \lambda$ line, Chapter 4.
z	Transverse coordinate. Distance in transverse direction on test surface measured from centerline.

Greek Symbols

α	Angle of rotation around probe axis for triaxial hot-wire probe.
α'	Injection angle measured from test surface.
β	Angle between $\overline{U}$ and $\overline{W}$ components of mean velocity.
γ	Angle between $\overline{U}$ and $\overline{V}$ components of mean velocity.
δ	Boundary layer thickness, also $\delta_{.99}$. Thickness of outer boundary layer in mixing-length model, Ch. 4.
δ_1	Displacement thickness.
δ_2	Momentum thickness.
δ'	Thickness of internal two-dimensional layer, also $\delta'_{.99}$, Chapter 4.
ε_M	Eddy diffusivity for momentum.
ε_q	Eddy diffusivity for turbulent kinetic energy.
η	Fmil-cooling effectiveness.
θ	Roll angle for slant hot-wire probe. Non-dimensional temperature = $(T_{jet}-T_\infty)/(T_o-T_\infty)$.
κ	Von Karman constant = 0.41.
λ	Outer region mixing-length proportionality constant = 0.085.
μ	Dynamic viscosity.
ν	Kinematic viscosity.
ρ	Density.
τ	Shear stress = $\sqrt{\overline{u'v'}^2 + \overline{u'w'}^2 + \overline{v'w'}^2}$.
ϕ	Slant angle for slant hot-wire probe.
ω	Pitch angle for triaxial hot-wire probe (angle between probe axis and x-axis when probe body is in x-y plane).

Subscripts

1	Wire number one for triaxial-wire probe, Chapter 3.
2	Wire number two for triaxial-wire probe, Chapter 3.
3	Wire number three for triaxial-wire probe, Chapter 3.
a	Augmented value, mixing length model.
eff	Effective value.
jet	Injectant value.
o	Wall value.
∞	Freestream value

Superscripts

$\overline{\quad}$	Time averaged.

SUMMARY

Hydrodynamic measurements were made with a triaxial hot-wire in the full-coverage region and the recovery region following an array of injection holes inclined downstream, at 30° to the surface. The data were taken under isothermal conditions at ambient temperature and pressure for two blowing ratios: $M = 0.9$ and $M = 0.4$. ($M = \rho_{jet}U_{jet}/\rho_{\infty}U_{\infty}$ where U is the mean velocity and ρ is the density. Subscripts "jet" and "∞" stand for injectant and free stream, respectively.) Profiles of the three mean velocity components and the six Reynolds stresses were obtained at several spanwise positions at each of five locations down the test plate.

High turbulent kinetic energy (TKE) levels were found for low blowing, with low TKE levels for high blowing. This observation is significant when coupled with the fact that the heat transfer coefficient is high for high blowing, and low for low blowing. This apparent paradox can be resolved by the hypothesis that entrainment of the main stream fluid in a 3-D manner along the lanes between wall jets must be more important than the turbulent mixing in heat transfer for the high blowing ratios (close to unity).

The flow in the recovery region can be described approximately in terms of a two-layer model: an outer boundary layer and a two-dimensional (2-D) inner boundary layer.

A one-equation model of turbulence (using TKE with an algebriac mixing length) was used with a 2-D computer program to predict the mean velocity and TKE profiles in the recovery region. Mixing-length values calculated from the data were used in inputs to the program. The mixing-length distribution was assumed to be piecewise continuous, a heuristic fit to the data consistent with the concept of the two quasi-independent layers observed in the recovery region. This mixing length, along with a set of otherwise normal constants (for 2-D boundary layer predictions), successfully predicted the spanwise-averaged features of the flow.

A new hot-wire scheme was developed to make measurements in the three-dimensional (3-D) turbulent boundary layer over the full-coverage surface. The method uses a triaxial hot-wire and an analog device for real-time

data reduction. It does not use the low-fluctuation assumption and can tolerate an unknown flow direction within limits ($\pm 30^{o}$ for the mean velocity). The method is very fast and quite practical for taking large amounts of data in 3D, high-fluctuation turbulent flows.

Chapter 1

INTRODUCTION

1.1 Background

Modern gas turbine technology requires high turbine inlet temperatures to increase thermodynamic efficiency, well above the usable temperature of the materials from which the turbine blades are manufactured. One way to protect the blades is by injecting a coolant through the blade surface, thus forming a cooling film between the hot combustion gases and the metal surface. There are several ways of injecting the coolant onto the blade surface. A comparison of different methods is given by Brunner (1969). Two of the more common are transpiration cooling through a porous plate surface and full-coverage film cooling through an array of closely spaced multiple rows of small holes, as discussed by Esgar (1971). Transpiration cooling achieves lower heat transfer to the surface and has better aerodynamic performance than full-coverage film cooling but has problems with structural strength and is susceptible to plugging (Goldstein, 1971). Full-coverage film cooling seems more practical, but not enough is known about the heat transfer and hydrodynamic mechanisms to allow accurate prediction. Such information is necessary before accurate designs can be developed.

There have been many studies of heat transfer with film cooling. A general review is given by Goldstein (1971). A review of discrete-hole film cooling is given by Choe et al. (1975). Most of the early experimental research on full-coverage film cooling concentrated on measurement of film-cooling effectiveness with the heat transfer coefficients. The hydrodynamics was treated as secondary in importance. A review of the experimental work on this topic is also given by Crawford et al. (1976).

Le Brocq, Launder & Priddin (1971) studied the effects on effectiveness, η, of hole-pattern arrangement, injection angle, ratio of densities of the coolant and mainstream, and blowing ratio. Some profiles of mean velocity were taken near the holes, with a pitot probe. They found that the staggered hole pattern was more effective than the in-line

pattern. A critical blowing ratio was found to exist, which gave maximum effectiveness. Above this blowing ratio effectiveness decreased again. Slant-angle injection was found to be more effective than the normal injection.

Launder & York (1973) studied the effects of mainstream acceleration and turbulence level on film-cooling effectiveness, using a staggered 45° slant-hole test section. Again, only a small number of mean velocity profiles were taken. Acceleration seemed to increase effectiveness, but the free stream turbulence did not have a significant effect.

Metzger, Takeuchi & Kuenstler (1973) studied both effectiveness and heat transfer on a full-coverage surface with normal holes spaced 4.8 diameters apart, arranged in both in-line and staggered patterns. They did not make any measurement of hydrodynamics. Again, it was observed that a staggered pattern was more effective.

Mayle & Camarata (1975) examined the effects of hole spacing and blowing ratio on heat transfer and film effectiveness for a staggered-hole array with compound-angle injection. It was found that for P/D = 10 and 8, higher effectiveness was obtained than with P/D = 14. No measurements were made of the hydrodynamics of the flow field.

Choe et al. (1975) studied the effects on heat transfer of hole spacing, blowing ratio, mainstream velocity and conditions upstream of the discrete-hole array. Normal injection was used with a staggered array of holes spread 5 and 10 diameters apart. Mean velocity profiles were taken with pitot probe to obtain spanwise-averaged values. From the spanwise-averaged profile, mixing length was obtained and used in predictions of heat transfer data with a "zero-equation model" of turbulence. They observed that the P/D = 5 case with a comparable F was more effective than P/D = 10. Furthermore there was no pronounced effect in the initial blowing row.

Crawford et al. (1976) also give a summary of analytical work in the field of full-coverage film cooling. Goldstein et al. (1969) and Ericksen, Eckert & Goldstein (1971) used superposition of film-effectiveness data for individual jets to predict η by modeling injection as a point heat source. Mayle & Camarata (1975) developed an improved superposition method to predict their full-coverage data. Pai & Whitelaw

(1971) and Patankar, Rastogi & Whitelaw (1973) investigated the prediction of wall temperature and effectiveness downstream of 2- and 3-D film-cooling slots. For the 2-D slot injection, the boundary layer equations were used along with an augmented mixing length model to represent the effect of injection. For the 3-D injection, 3-D Navier-Stokes equations were solved numerically by reducing them to elliptic form in the lateral plane and to parabolic form in the streamwise direction.

Herring (1975) used a finite-difference method for predicting the flow over a full-coverage film-cooled surface. Lateral averaging in the full-coverage region was invoked to justify using 2-D boundary layer equations. Terms arising from the spanwise averaging were obtained from consideration of the jet-boundary layer interaction. Predicted velocity profiles were reported but showed some problems in the initial regions of injection near the wall.

Choe et al. (1975) developed a finite-difference method for predicting heat transfer with full-coverage film cooling, solving the two-dimensional boundary layer equations. (These equations have a form similar to those given by Herring, 1975.) Choe et al. (1975) used the concept of local averaging, with a different model for the injection process, the nonlinear terms, and augmented turbulent mixing. By using an augmented mixing length in a zero-equation model for turbulence, he successfully predicted most of their Stanton number data for low and moderate blowing in the full-coverage region. The predictions in the recovery region and for high blowing were less accurate.

Crawford et al. (1976) repeated the conditions covered by Choe et al. (1975); however, they used a different full-coverage surface: 30° slant-hole injection with a staggered array of holes, with two different hole spacings (5 and 10 diameters). For each injection, Stanton number data were taken for two values of injectant temperature, corresponding to θ equal to zero and one. Linear superposition was then used to obtain Stanton numbers as a continuous function of the injectant temperature. Stanton numbers were measured for a range of injection mass flux ratios (M from 0 to 1.3) and Reynolds numbers (Re_x from 1.5×10^5 to 5×10^6).

With the injection temperature equal to the wall temperature, the Stanton number decreased below the normal flat-plate value and reached a minimum at M of 0.4. A higher M caused an increase in the Stanton number. For the recovery region, downstream of the five-diameter hole array, two distinct data trends were observed. For low M the Stanton number began to recover immediately from the effects of blowing, while for high M the Stanton number either remained constant or dropped throughout the recovery region. This latter behavior suggested that interrupted hole patterns may be an effective cooling scheme.

In Crawford's work (Crawford et al., 1976) both integral and differential analyses were carried out on the data sets. A differential prediction method was developed which used a two-dimensional boundary layer program. The injection process was modeled as slot injection, and the turbulence was modeled with a zero-equation model, using an augmented mixing length obtained from the spanwise-averaged mean velocity profiles. Mean velocity profiles were obtained with a pitot probe. Downstream of the jets the profiles may be in error because of the static-pressure islands created around the jets. In Crawford's data, most of the five-hole diameter data were successfully predicted in the full-coverage region. The predictions in the recovery region and for high blowing ratios were not very good, as was also the case with Choe et al. (1975).

Very little of the literature mentioned above gives any information about flow field measurements and, in particular, measurements of turbulence quantities. In the following papers, however, some attempts were made to make measurements of hydrodynamics. Ramsey & Goldstein (1971) measured the mean velocity and turbulence intensity profiles (not the turbulent kinetic energy) for normal injection downstream of a heated jet at blowing ratios of 1.0 and 2.0. Metzger, Carper & Warren (1972) measured the mean velocity profiles both upstream and downstream of a two-dimensional injection slot. Hartnett, Birkebak & Eckert (1961) measured boundary-layer velocity profiles for a number of positions downstream of injection through a single slot. Foster & Haji-Sheikh (1974) measured mean velocities downstream of flush, normal-injection slots.

In these references it was frequently observed that the literature is quite weak from the point of view of hydrodynamic data, especially for full-coverage surfaces.

1.2 Objectives

This research represents an extension of the work by Crawford et al. (1976), whose experiments consisted mainly of heat-transfer coefficient measurements. As explained, the predictions of Crawford were good for low and moderate blowing ratios in the full-coverage region, but problematic in the recovery region and for high blowing ratios. It was felt that the key to understanding these result lay in the structure of the turbulence.

A decision was made to adapt a one-equation model of turbulence for prediction of the hydrodynamics within the recovery region, since the zero-equation model did not give satisfactory results. It was thought that a higher-order model might better represent the real process.

The objectives of this research were twofold:

- to make 3-D measurements of the turbulence structure and mean velocity field in the 3-D turbulent boundary layer over the full-coverage film-cooled surface and in its recovery region,
- to apply a one-equation model of turbulence for predictions of the recovery region hydrodynamics with the empirical input supplied by the experiments.

1.3 Outline of the Work

A new hot-wire anemometer method of measurement was devised to allow measurements of the turbulence structure in the 3-D turbulent boundary layer over the full-coverage surface. Due to the interaction between the mainstream and the jets, a complex flow field is created in the full-coverage region where the local flow is 3-D in the vicinity of the jets, the local flow direction is unknown, and the fluctuations are high.

The new hot-wire method is believed to be an important contribution. The present research could hardly have been done without it. The method is described in Chapter 3 of this thesis.

The physics of the recovery region flow are described in Chapter 4, as well as the predictions of the recovery region hydrodynamics using the one-equation model of turbulence. The physical modeling is accomplished by modeling the length scale of turbulence. The length-scale model introduced in this chapter was successful in predicting the flow with the one-equation model.

Chapter 5 presents the data taken on the full-coverage surface and discussions of the data. The volume of the data taken was so large that only typical results are discussed. As far as the author knows, these data comprise the first detailed study of this process. There will be much to explore in the data beyond the scope of the present report.

Chapter 6 contains the summary and recommendations about the complete research.

The building of the 3-D Turbulent Flow Analyzer was funded by the Thermosciences Affiliates. The Scientific and Technical Research Council of Turkey (Türkiye Bilimsel ve Taknik Arastirma Kurumu) provided all the first author's living expenses and tuition during his four-year stay at Stanford University.

Chapter 2

APPARATUS AND INSTRUMENTATION

The Discrete Hole Rig is the heat transfer apparatus which carries the full-coverage film-cooling test section. It is a closed loop wind tunnel which delivers air at ambient pressure and constant temperature. This system was previously used by Choe et al. (1975) and Crawford et al. (1976). It is described in detail in their work. Only those aspects relevant to the present research will be given here. A flow diagram of the systems which make up the rig is shown in Fig. 2.1; its photograph is given in Fig. 2.2.

2.1 The Test Surface

The test surface of the Discrete Hole Rig is made from copper plates. It has three parts: a preplate, a full-coverage region, and an afterplate.

The preplate is made of 24 individual copper plates, each about 2.6 cm long in the flow direction and 46 cm wide.

The full-coverage section is composed of 12 copper plates, each 0.6 cm thick, 46 cm wide, and 5 cm long in the flow direction. The first plate does not have any holes, but the remaining 11 downstream plates plates have alternately nine and eight holes each. The holes are each 1.03 cm in diameter and are spaced on five-diameter centers to form a staggered hole array. A photograph of the full-coverage section can be seen in Fig. 2.3.

Delivery tubes for secondary air extend beneath the surface at a 30° angle to the plate surface, giving a 30° slant-angle injection in the direction of the main flow. A schematic of the full-coverage surface can be seen in Fig. 2.4.

The afterplate is identical to the preplate. This is the recovery region for the flow after the blown part of the test section. See Crawford et al. (1976) for more detailed information about the test surface. Twenty-four instrumented strips in the afterplate permit measurement of the Stanton number distribution in the recovery region.

2.2 Instrumentation

This section will give information on the instruments used for measurements in the turbulent flow field. The amount of detail given about a certain instrument depends on the importance of its use in the measurements. Detailed information is given about the calibration of the triaxial hot-wire probe.

2.2.1 Temperature

Since the experiments were performed under isothermal conditions and the purpose was to make measurements of hydrodynamics, there was no need for extensive temperature measurements. Only the free-stream temperature was measured. This measurement was made with an iron-constantan thermocouple whose junction was parallel to the flow. The thermocouple probe did not require any special shielding or precautions because the operating temperatures were about ambient and the velocities were low. An integrating digital voltmeter (HP 2401C) was used to read out the thermocouple output.

2.2.2 Pressure

Tunnel static pressure was measured with an inclined Meriam manometer using a 0.824 specific gravity fluid. The manometer had a range of 0.5 in with a smallest division of 0.005 inches of water. Static pressure was measured from the taps located in one of the tunnel sidewalls. Their locations and properties are given by Choe et al. (1976). The mainstream dynamic pressure was measured with a kiel probe corrected to a Combist micromanometer whose smallest division was 0.0005 inches of manometer fluid of specific gravity 0.82. The tunnel geometry was adjusted to achieve a uniform static pressure throughout the test section.

2.2.3 Secondary Air Flow Rate

Flow rates through the secondary air delivery tubes were measured with hot-wire flow meters permanently built into the rig. More information about the flow meters is given by Choe et al. (1975). The digital voltmeter mentioned in section 2.2.1 was used to read out the flow meter outputs. Calibration of the meters was done individually, using reference flow meters.

2.2.4 Turbulent Flow Field

a. Instrumentation

The main instrumentation for the experiments was the hot-wire system used in the measurements of the turbulent flow field. It consists of a DISA claw-type triaxial hot-wire probe, three constant temperature anemometers (TSI 1050), three polynomial linearizers (TSI 1052), and the 3-D Turbulent Flow Analyzer.

An HP-2100 digital computer was used for data acquisition and reduction.

An integrating digital voltmeter (IDVM) (HP-2401C) and an RMS meter (TSI 1076) were used occasionally to reduce and read the outputs of the 3-D Turbulent Flow Analyzer instead of the computer.

More detailed information about the hot-wire instrumentation is given in Chapter 3.

b. Calibration of the triaxial hot-wire probe

The triaxial hot-wire probe was calibrated on the calibrator described by Pimenta et al. (1975). This calibrator produced a uniform flow of air at constant but adjustable temperature, with moderate-to-low turbulence levels (about 0.8%).

The probe was calibrated in the free jet at the exit of the calibrator. After the flow in the calibrator was adjusted to the desired temperature and the anemometers were set, the following procedure was applied for the process of calibration.

The axis of the probe was aligned with the flow direction by trial and error. To check the alignment, the output of each anemometer was recorded at a certain orientation of the probe. Then the probe tip was rotated 180° (the probe holder was designed so that the probe tip could be rotated to 12 positions, each 30° apart) and the anemometer outputs were recorded again. If the probe was aligned properly, the outputs of the same anemometer at 0° and 180° positions of the probe tip should have read the same (for 10 seconds integration of the output signal, the acceptable value is x.xxx $\pm$ 0.002 volts for a velocity about 10 m/sec). If the numbers were not the same, the probe position was readjusted until the alignment criterion was satisfied. It usually took about five trials

to obtain the correct alignment. The final alignment position was within 1-2° of the first visual alignment. During this procedure it was very important to make sure that any change in readings was not caused by a change in either the temperature or the flow rate.

After the probe was aligned with the flow direction the calibration started. First the flow speed was adjusted to the desired value by adjusting the valve of the calibrator. The flow speed was measured through a static pressure tap located on the plenum chamber where the pressure is equal to the total pressure of the jet at the nozzle exit. The pressure was read with the Combist micromanometer mentioned in section 2.2.2. Afterwards, the output of the three anemometers was read with the IDVM, described before. Ten seconds of integration of the output was enough for the calibration.

It was necessary to check the temperature during calibration. This was done by checking the cold resistance of one of the wires from time to time.

Finally, the obtained values of static pressure and anemometer outputs along with the temperature, ambient pressure, and humidity were fed to a computer program prepared by Coleman (Coleman et al., 1975) to obtain the linearized calibration equation.

The typical values used for some of the variables during the calibration were the following:

Cold wire resistances:	$\simeq$ 9.5 Ω
Overheat ratio:	$\simeq$ 1.5
Maximum change in the cold resistance during one calibration:	$\simeq \pm$ .02 Ω
Temperature range (for different calibrations):	18°C-26°C
Velocity range during one calibration:	4-22 m/sec.

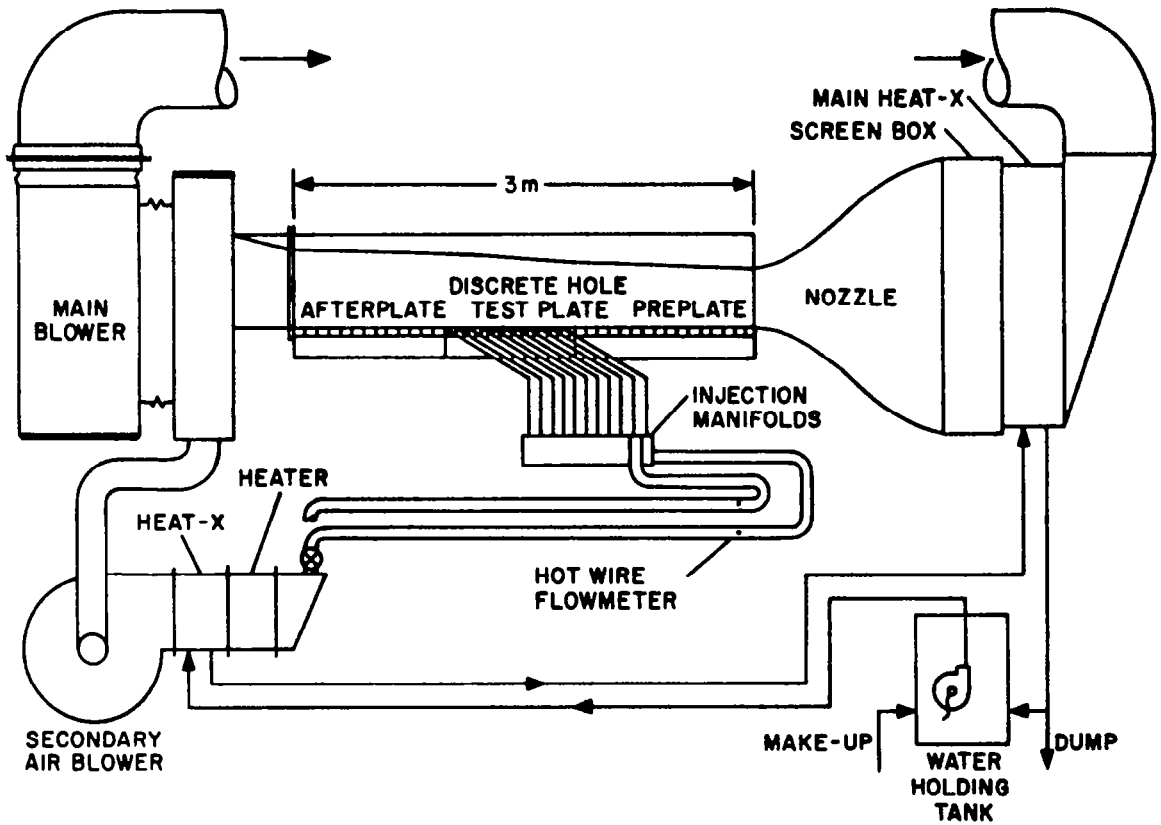

Figure 2.1 Flow schematic of wind tunnel facility, the Discrete Hole Rig

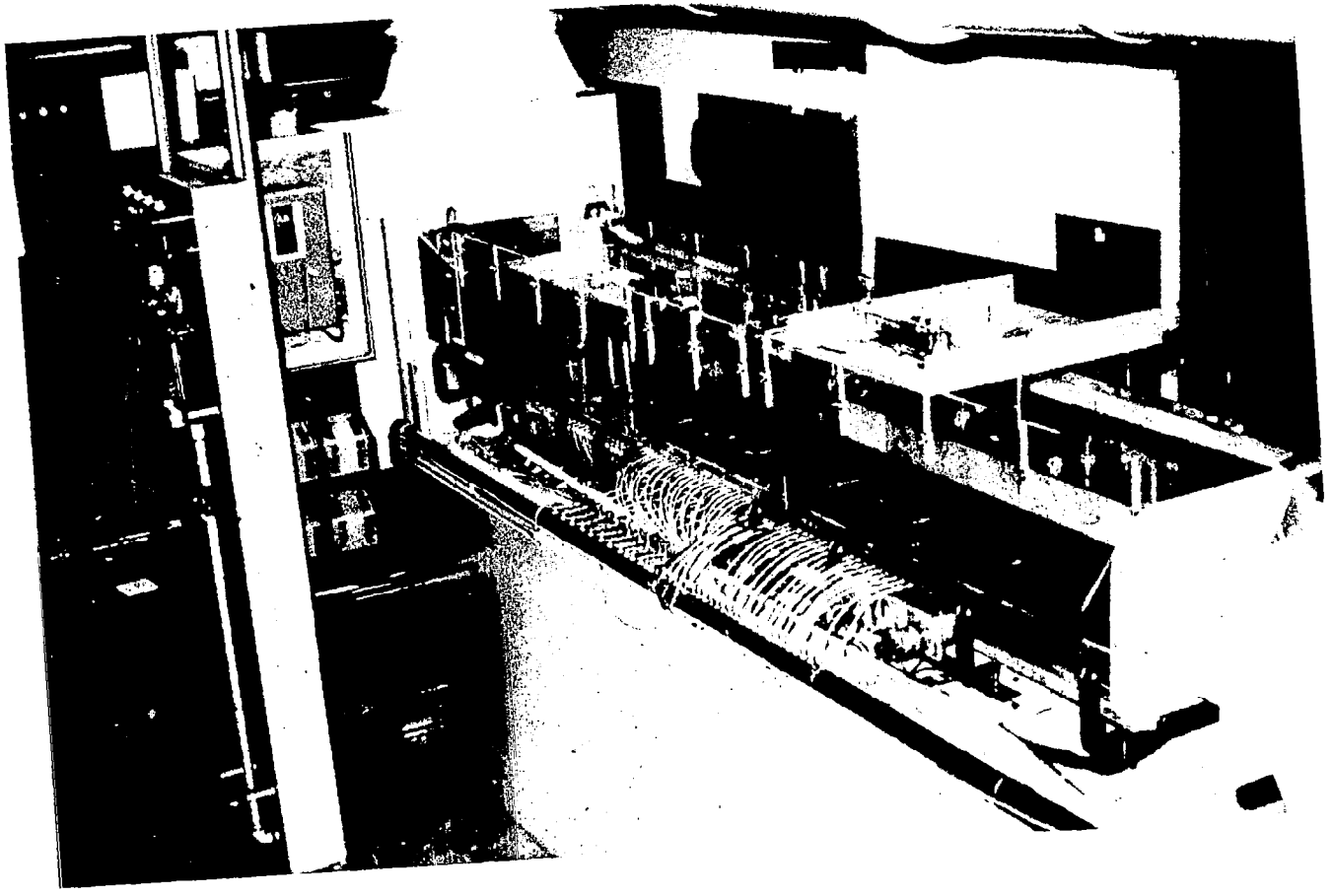

Fig. 2.2. Photograph of Discrete Hole Rig.

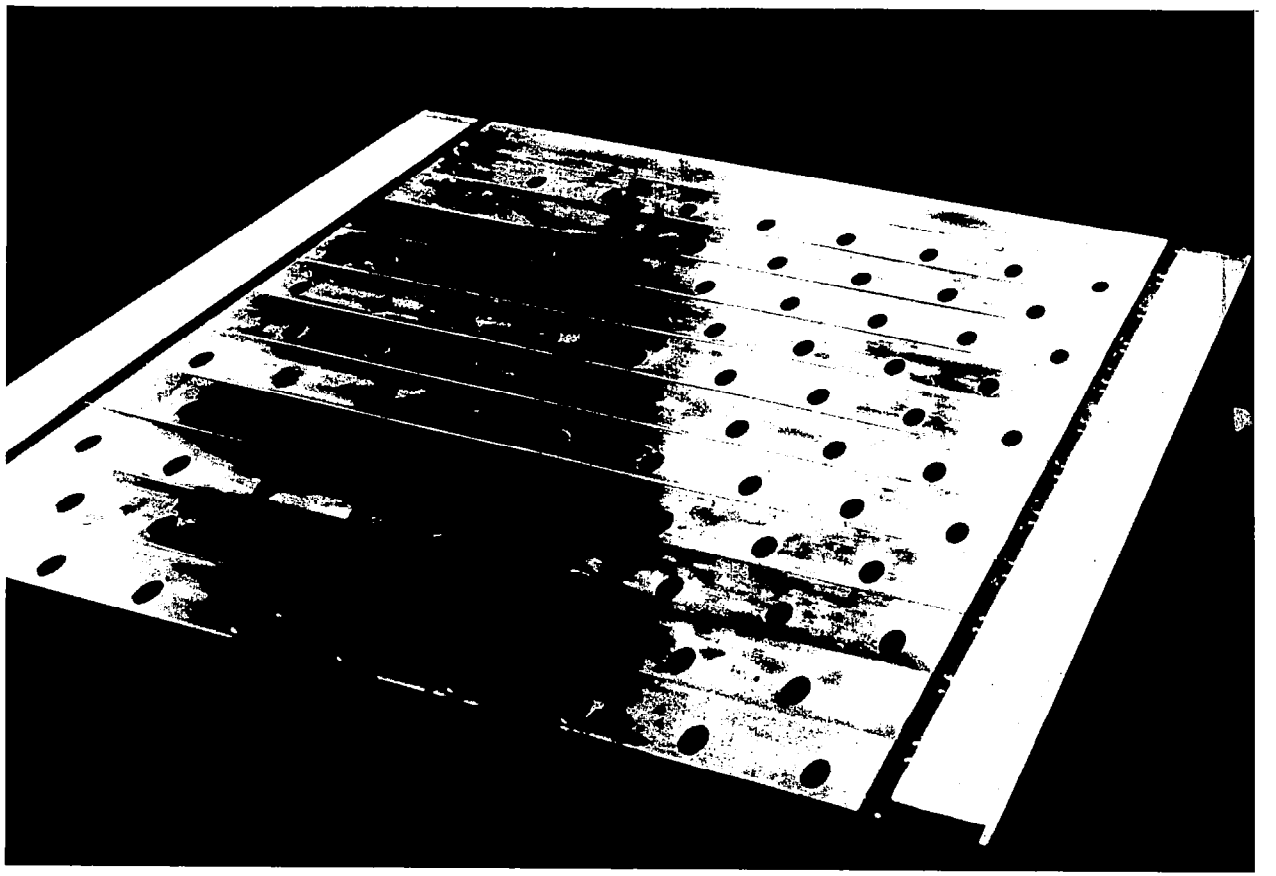

Fig. 2.3. Photograph of full-coverage surface, showing staggered hole array.

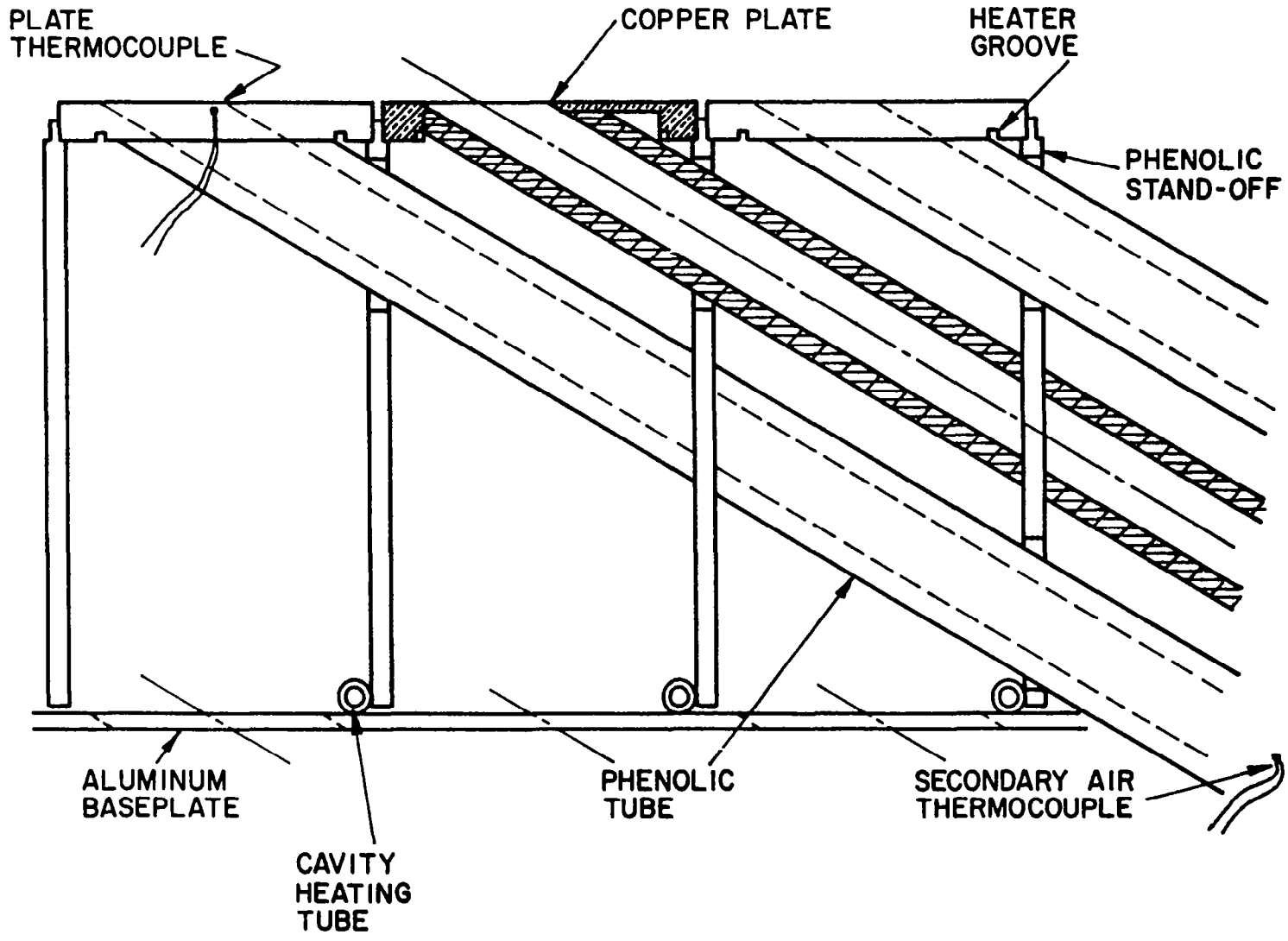

Fig. 2.4. Cross-sectional drawing of the full-coverage section.

Chapter 3

REAL-TIME HOT-WIRE MEASUREMENTS IN THREE-DIMENSIONAL FLOWS

Hot-wire anemometers are the most widely used devices for making measurements in turbulent flow fields. Satisfactory results are obtainable in one- and two-dimensional flows whose directions are known and whose turbulence structures are stationary and of low amplitude (typically on the order of 10% of the mean velocity). Three-dimensional flows of unknown flow direction, with high fluctuations or large intermittent structures, cannot be measured accurately with classical techniques, and even the stationary, low-fluctuation cases are very tedious.

The first step in most classical methods involves finding the time-averaged value of the fluctuating component of the anemometer output. Details of the turbulence structure are deduced by solving sets of simultaneous equations using measurements at different angular positions. These equations are formed by expanding the expression for effective velocity in a Taylor's series around the mean and truncating at second order (usually). When the equations are weakly convergent (as when many angular positions are used), the uncertainty in the calculated values of the turbulence quantities is high, especially for the higher-ordered terms.

The object of this work was to develop a real-time method for hot-wire anemometry which would be applicable to three-dimensional flows of unknown flow direction (within limits) and with high fluctuation levels.

3.1 Background in Hot-Wire Measurements

3.1.1 Classical time-averaged reductions

Most of the existing hot-wire methods are good in 2-D flows with low fluctuations and known flow direction. Almost all use either single horizontal wires, single rotatable slant wires or cross wires. The usual practice in data-taking is to align the probe with the known flow direction, to read the mean output of the anemometer or linearizer with a digital voltmeter, and the average fluctuation value with an RMS meter.

The desired quantities, mean velocities and Reynolds stresses are deduced from the truncated Taylor series expansions of these effective quantities. The truncation and solution process requires some simplifying assumptions, in particular, that the fluctuations are small compared to the mean values.

When the flow direction is unknown, the data-reduction process is quite complicated. To explain this point better, the relation between the effective velocity and the velocity components is given in Eqn. (3.1) taken from Jorgensen (1971), with the nomenclature shown in the following figure.

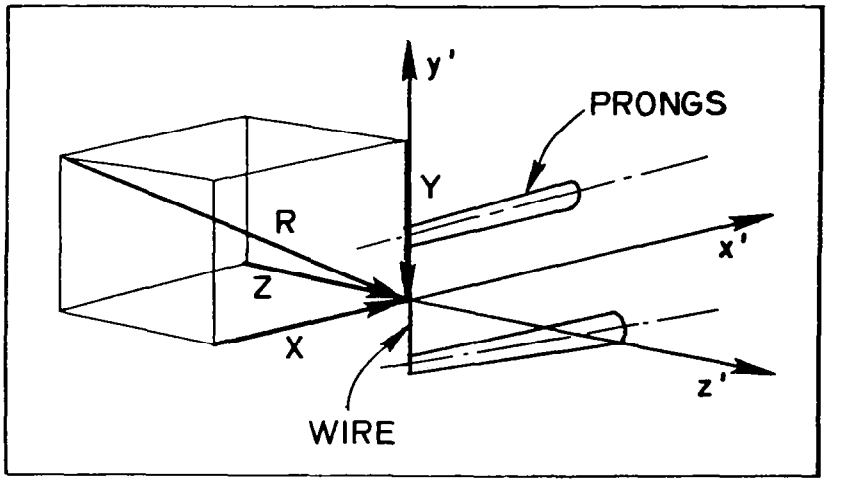

$$U_{eff}^2 = X^2 + k_1^2 Y^2 + k_2^2 Z^2 \qquad (3.1)$$

Here, X, Y, Z are the velocity components in the directions of the wire coordinates x', y', and z', respectively, and k_1 and k_2 are pitch and yaw sensitivities of the wire. The following figure shows a single, rotatable slant wire and the wire orientation with respect to the laboratory coordinates x, y, and z.

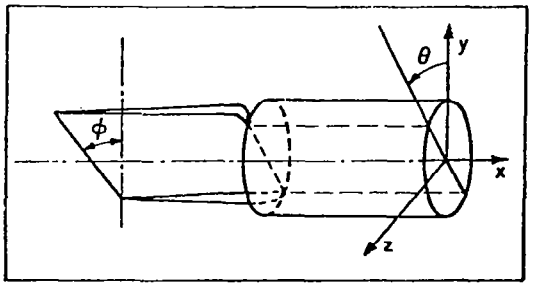

In this figure ϕ is the slant angle, in the plane of prongs, between the wire and the y' direction. The angle ϕ is zero when the wire is perpendicular to the axis of the prongs. The angle θ is the roll angle in the (yz) plane, and is zero when the prongs are in the (xy) plane. Velocity components U, V, and W are in the laboratory coordinates, in the x, y, and z directions, respectively. With this nomenclature, Eqn. (3.1) can be written in terms of velocities in laboratory coordinates, as follows:

$$U_{eff}^2 = A(U^2) + B(V^2) + C(W^2) + D(UV) + E(VW) + F(UW) \qquad (3.2)$$

where

$$\begin{aligned} A &= \cos^2\phi + k_1^2 \sin^2\phi, \\ B &= (\sin^2\phi + k_1^2\cos^2\phi)\cos^2\theta + k_2^2\sin^2\theta, \\ C &= (\sin^2\phi + k_1^2\cos^2\phi)\sin^2\theta + k_2^2\cos^2\theta, \\ D &= (1-k_1^2)\sin 2\phi\cos\theta, \\ E &= (\sin^2\phi + k_1^2\cos^2\phi - k_2^2)\sin 2\theta, \\ F &= (1-k_1^2)\sin 2\phi\sin\theta. \end{aligned} \qquad (3.3)$$

In Eqn. (3.2), each velocity can be written as the sum of the mean and fluctuating parts:

$$\begin{aligned} U &= \overline{U} + u' \\ V &= \overline{V} + v' \\ W &= \overline{W} + w' \end{aligned} \qquad (3.4)$$

and

$$U_{eff} = \overline{U}_{eff} + u'_{eff} \qquad (3.5)$$

In the classical time-averaged method, the quantities recorded are $\overline{U}_{eff}$ and $\overline{u'^2_{eff}}$ for each of several angular positions. If the first-order fluctuation descriptions are substituted into Eqn. (3.2), a very complicated equations results which can be brought to a theoretically solvable form by a Taylor series expansion of both sides. This expansion

is valid only when the flow has a strongly preferred direction and low fluctuations (i.e., $\overline{V}$, $\overline{W}$, and u', v', and w' are each at least one order of magnitude smaller than $\overline{U}$). The resulting equations are given below:

$$\overline{U}_{eff} = \frac{1}{2\sqrt{A}\,\overline{U}}\Big[(2A\overline{U}^2 + B\overline{V}^2 + C\overline{W}^2) + (D\,\overline{U}\,\overline{V} + E\,\overline{V}\,\overline{W} + F\,\overline{U}\,\overline{W}) + (A\overline{u'^2} + B\overline{v'^2} + C\overline{w'^2}) + (D\overline{u'v'} + E\overline{v'w'} + F\overline{u'w'})\Big] + O(3) \tag{3.6}$$

$$\begin{aligned}\overline{u'^2_{eff}} = \frac{1}{4A}\Bigg[&\left(4A^2 + D^2\frac{\overline{V}^2}{\overline{U}^2} + F^2\frac{\overline{W}^2}{\overline{U}^2} + 4AD\frac{\overline{V}}{\overline{U}} + 4AF\frac{\overline{W}}{\overline{U}} + 2DF\frac{\overline{V}\,\overline{W}}{\overline{U}^2}\right)\overline{u'^2} \\ &+ \left(D^2 + 4B^2\frac{\overline{V}^2}{\overline{U}^2} + E^2\frac{\overline{W}^2}{\overline{U}^2} + 4BD\frac{\overline{V}}{\overline{U}} + 2DE\frac{\overline{W}}{\overline{U}} + 4BE\frac{\overline{V}\,\overline{W}}{\overline{U}^2}\right)\overline{v'^2} \\ &+ \left(F^2 + E^2\frac{\overline{V}^2}{\overline{U}^2} + 4C^2\frac{\overline{W}^2}{\overline{U}^2} + 2EF\frac{\overline{V}}{\overline{U}} + 4CF\frac{\overline{W}}{\overline{U}} + 4CE\frac{\overline{V}\,\overline{W}}{\overline{U}^2}\right)\overline{w'^2} \\ &+ \left(4AD + 4BD\frac{\overline{V}^2}{\overline{U}^2} + 2EF\frac{\overline{W}^2}{\overline{U}^2} + (8AB + 2D^2)\frac{\overline{V}}{\overline{U}} + (4AE + 2DF)\frac{\overline{W}}{\overline{U}}\right. \\ &\left. + (2DE + 4BF)\frac{\overline{V}\,\overline{W}}{\overline{U}^2}\right)\overline{u'v'} + \left(4AF + 2DE\frac{\overline{V}^2}{\overline{U}^2} + 4CF\frac{\overline{W}^2}{\overline{U}^2} + (4AE + 2DF)\frac{\overline{V}}{\overline{U}}\right. \\ &\left. + (8AC + 2F^2)\frac{\overline{W}}{\overline{U}} + (2EF + 4CD)\frac{\overline{V}\,\overline{W}}{\overline{U}^2}\right)\overline{u'w'} + \left(2DF + 4BE\frac{\overline{V}^2}{\overline{U}^2} + 4CE\frac{\overline{W}^2}{\overline{U}^2}\right. \\ &\left. + (2DE + 4BF)\frac{\overline{V}}{\overline{U}} + (4CD + 2EF)\frac{\overline{W}}{\overline{U}} + (8BC + 2E^2)\frac{\overline{V}\,\overline{W}}{\overline{U}^2}\right)\overline{v'w'}\Bigg] + O(3)\end{aligned} \tag{3.7}$$

Even with these assumptions the resulting equations are quite complicated. In two-dimensional flows with low fluctuations, where the flow direction is known, aligning the probe with the flow direction sets $\overline{V}$ and $\overline{W}$ to zero, allowing the simplified equation to be used. In cases where there is symmetry ($\overline{u'w'} = 0$ and $\overline{v'w'} = 0$), the equations reduce to the following form, which is generally used for rotatable slant wires:

$$\overline{U}_{eff} = \sqrt{A}\,\overline{U} + O(2) \tag{3.8}$$

$$\overline{u'^2_{eff}} = A\,\overline{u'^2} + \frac{D^2}{4A}\overline{v'^2} + \frac{F}{4A}\overline{w'^2} + D\,\overline{u'v'} + O(3) \tag{3.9}$$

One measures $\overline{U}_{eff}$ and $\overline{u'^2_{eff}}$ in each of four different positions, thus obtaining enough equations to solve for these unknowns.

There are several ways to make measurements in 3-D turbulent flows using the classical time-averaged equations. The most important problem in 3-D flows arises when the mean flow direction is unknown. This direction can be found with one of the following ways. Johnston (1970) measured the local pitch and yaw angles for the mean velocity with a Conrad probe and then measured the Reynolds stresses with a horizontal wire and a rotatable cross wire aligned with the flow. The low-fluctuation assumption was invoked. Moussa & Eskinazi (1975) tried to measure the mean flow direction by using a rotatable slant wire. Making use of the directional properties of hot wires, they calibrated the probe for all possible angles and prepared detailed charts which included the flow angles as functions of four mean voltages obtained at different rotations of the probe. Delleur (1966) used a cross wire to measure the flow direction, arguing that the cross-wire technique was twice as accurate as the single-wire technique. Both methods require the use of a hot-wire calibration curve for flow-direction measurement and consequently require frequent calibration of the hot wire to renew the calibration charts.

Some other 3-D hot-wire methods were developed which do not require the flow direction to be known. Mojola (1974) gives a hot-wire method (rotatable slant wire or cross wire) for measuring the three mean components of the velocity and six Reynolds stresses without knowing the flow direction. His equations are valid when the probe is approximately aligned with the flow (i.e., a strongly preferred mean flow direction) and has only low fluctuations. Hoffmeister (1972) describes a scheme which employs a single rotatable slant wire to obtain three mean velocities and six Reynolds stresses. In this scheme the interpretation of the anemometer voltages is based on calibrations of the probe over the entire range of angles between the wire and the flow which may exist during measurements.

None of the preceding methods is practical for taking large amounts of data. Further, the accuracy with which the higher-ordered terms can be measured is seriously limited. As the number of terms retained in Eqn. (3.7) increases, the number of independent realizations required

increases; thus the number of probe rotational positions increases and the strength with which the equations converge diminishes.

The problem lies, basically, in the time-averaged approach to turbulence measurement. With one or two wires, one does not have enough information to solve for the instantaneous velocities, and, hence, time-averaging is required. With three wires, however, the whole problem is resolved and one can deal directly with the instantaneous velocities.

3.1.2 Real-time reduction

A real-time data-reduction scheme was used by Zimmerman & Abbott (1975). Using a triaxial hot-wire probe and an analog device, they solved for the three unknowns (three instantaneous velocities) in the effective velocity expression, in real time. The outputs of their analog device were the three mean velocities, the three instantaneous fluctuations, and the means of three correlations (off-diagonal components of Reynolds stress tensor). This scheme was used to measure the Reynolds stresses in a 3-D turbulent boundary layer created by a skewed-leading-edged flat plate in zero pressure gradient air flow, which yields high cross-stream gradients of the turbulent quantities.

3.2 The Present Approach

The present approach also uses the real-time data-reduction idea. In fact, this work was finished at the same time as Abbott & Zimmerman's (1975) work, but the publishing of results has been delayed due to unforeseen circumstances.

Equation (3.1) introduced the effective velocity expression. The three unknowns are the three instantaneous velocity components in wire coordinates. To solve for these velocities in real time, one needs three simultaneous and independent values of the U_{eff} at one point in the flow field. Probes are available which have an orthogonal array of wires, such that the x' axis for one is the y' and z' axis for the others. The probe used in the present studies was a DISA triaxial-wire probe.

The DISA triaxial wire probe has three wires each of which has two leads and each of which is driven by a separate anemometer. The wires are mutually orthogonal, forming a right-angled coordinate system. The

sensors provided by DISA are 3.2 mm long, with 5 micron Pt-plated tungsten wires having copper- and gold-plated ends leaving a sensitive length of 1.25 mm. In the present work, bare Pt-plated tungsten wires were used without gold plating, giving 3.2 mm active length. The three wires form a cone of apex angle 70.6° around the axis of the probe stem. The wire coordinate system can be seen in Fig. 3.1. With the special prong structure of the probe, the effective velocity indicated by each wire is related to the velocity components in the wire coordinates in the following manner.

$$\begin{aligned} U^2_{eff_1} &= k^2_{11}X^2 + Y^2 + k^2_{21}Z^2 \\ U^2_{eff_2} &= k^2_{22}X^2 + k^2_{12}Y^2 + Z^2 \\ U^2_{eff_3} &= X^2 + k^2_{23}Y^2 + k^2_{13}Z^2 \end{aligned} \tag{3.10}$$

and the linearized effective voltages (linearizer outputs) are related to the effective velocities as follows:

$$\begin{aligned} U_{eff_1} &= A_1 + B_1 E_{eff_1} \\ U_{eff_2} &= A_2 + B_2 E_{eff_2} \\ U_{eff_3} &= A_3 + B_3 E_{eff_3} \end{aligned} \tag{3.11}$$

In Eqns. (3.11), the A's and B's are constants obtained from calibrations of the wires.

Equations (3.10) have three unknowns -- the instantaneous velocities in the wire coordinates -- which can be obtained from the equations shown below:

$$\begin{bmatrix} X^2 \\ Y^2 \\ Z^2 \end{bmatrix} = \begin{bmatrix} k^2_{11} & 1 & k^2_{21} \\ k^2_{22} & k^2_{12} & 1 \\ 1 & k^2_{23} & k^2_{13} \end{bmatrix}^{-1} \begin{bmatrix} U^2_{eff_1} \\ U^2_{eff_2} \\ U^2_{eff_3} \end{bmatrix} \tag{3.12}$$

or

$$\begin{bmatrix} X^2 \\ Y^2 \\ Z^2 \end{bmatrix} = \underbrace{\begin{bmatrix} k_{11}^2 & 1 & k_{21}^2 \\ k_{22}^2 & k_{12}^2 & 1 \\ 1 & k_{23}^2 & k_{13}^2 \end{bmatrix}}_{M}^{-1} \begin{bmatrix} (A_1 + B_1 E_{eff_1})^2 \\ (A_2 + B_2 E_{eff_2})^2 \\ (A_3 + B_3 E_{eff_3})^2 \end{bmatrix} \tag{3.13}$$

Once the instantaneous velocities in the wire coordinates are obtained, the instantaneous velocities in the laboratory coordinates can be obtained easily with a transformation of coordinates.

$$\begin{bmatrix} U \\ V \\ W \end{bmatrix} = N \begin{bmatrix} X \\ Y \\ Z \end{bmatrix} \tag{3.14}$$

where N is the coordinate transformation matrix from wire coordinates to laboratory coordinates. With the three instantaneous velocity components available in laboratory coordinates, the mean values and the Reynolds stresses can be obtained by using digital voltmeters, RMS meters and turbulence correlators, or with a digital computer having a fast enough A/D (analog-to-digital) converter.

3.3 The Three-Dimensional Turbulent Flow Analyzer

An analog device was built to solve the equations (3.13) and (3.14) using high-speed analog components. All quantities were magnitude-scaled using $(U_{eff})_{max}$, the value which resulted in the maximum output of the linearizer. (For the present case $(U_{eff})_{max}$ can be obtained by substituting 10 volts for E_{eff}, i.e., $(U_{eff})_{max} = A + B \times 10$.) Also, in calibration the problem is scaled such that the output in the real experiment will be between 4 and 8 volts, never reaching the limits of 0 volts and 10 volts. Under these normalization conditions it can be shown that none of the quantities in the equations to be solved goes over 10 volts during an experiment. After normalization, the equations to be solved

by the analog system are (3.13) and (3.14), with all the quantities normalized on $(U_{eff})_{max}$.

A and B values can be set to be the same for all wires during calibration, since they are functions only of the minimum and maximum velocities of the calibration range and the voltages desired. If the stem of the three-wire probe is aligned with the calibration flow, all the wires are exposed to the same minimum and maximum velocities.

The coefficient matrix M can easily be obtained using the known values of k_1 and k_2 for each wire. For example, for $k_1 = 0.15$ and $k_2 = 1.02$, the matrix is:

$$M = \begin{bmatrix} -0.5058 & 0.5155 & 0.4750 \\ 0.4750 & -0.5058 & 0.5155 \\ 0.5155 & 0.4750 & -0.5058 \end{bmatrix} \qquad (3.15)$$

In this matrix the values used for k_1 and k_2 are the same for all three wires. Uniform values of k_1 and k_2 were used in the present study, but the analog system is designed such that it can easily handle different values for k_1 and k_2 for each wire. An uncertainty analysis showed that a 1% change in k_1 causes a change of only 0.02% in the indicated velocity, while a 1% change in k_2 yields a change of 1.04%, regardless of the flow angle. Thus the final results depend only slightly on k_1 but nearly linearly on the value of k_2. As was shown by Jorgensen (1971), the change in k_2 with flow angle is very small.

$$N = \begin{bmatrix} \cos\omega & 0 & -\sin\omega \\ 0 & 1 & 0 \\ \sin\omega & 0 & \cos\omega \end{bmatrix} \begin{bmatrix} 1 & 0 & 0 \\ 0 & \cos\alpha & \sin\alpha \\ 0 & -\sin\alpha & \cos\alpha \end{bmatrix} \begin{bmatrix} \sqrt{3}/3 & \sqrt{3}/3 & \sqrt{3}/3 \\ -\sqrt{6}/6 & -\sqrt{6}/6 & \sqrt{6}/3 \\ -\sqrt{2}/2 & \sqrt{2}/2 & 0 \end{bmatrix} \qquad (3.16)$$

where the angles α and ω are shown in the following figure: α is the angle of rotation around the probe axis and ω is the angle between the probe axis and the x axis when the probe body is in the x-y plane. The angles are measured in the direction indicated by the arrows. Angle α is taken to be zero when the third wire is in the x-y plane and the longer prong is below the shorter one.

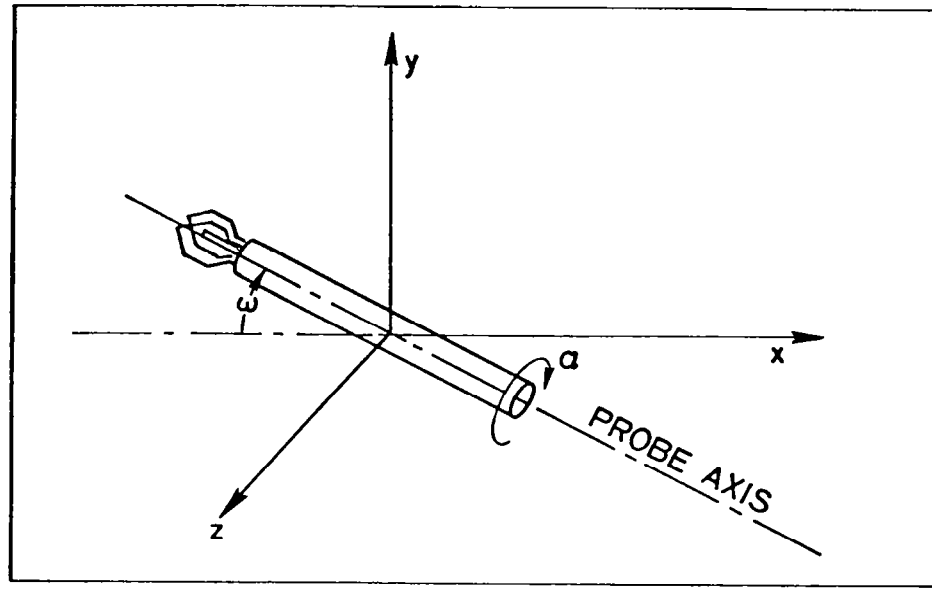

The 3-D Turbulent Flow Analyzer has been designed and built to take the linearizer outputs E_{eff_1}, E_{eff_2}, and E_{eff_3} as inputs and give instantaneous U, V, and W (the normalized velocities in laboratory coordinates) as outputs. Fig. 3.2 shows a photograph of the two control panels of the 3-D Turbulent Flow Analyzer. On the lower panel, there is one potentiometer for setting the A coefficient, and three potentiometers for setting the B coefficients. Three potentiometers are needed for B values because of circuit requirements. The nine coefficient potentiometers for the inverse Jorgensen Matrix (M) are shown, each with its own pair of test points for checking values. The meter provides a continuous display of $\overline{R}/C$, the time-averaged value of the magnitude of the normalized velocity vector. The outputs are the normalized velocity components in wire coordinates X, Y, Z and a value of R/C, the root sum square of the components, divided by three. The upper panel accepts the X, Y, Z as inputs and contains nine potentiometers whose values can be set according to the wire position to calculate the values of U, V, and W, the normalized velocity components in laboratory coordinates. A flow diagram of the complete system is shown in Fig. 3.3.

The electrical performance of the 3-D Turbulent Flow Analyzer was checked up to 20 kHz for phase shift and attenuation of magnitude.

Maximum phase shift was between 1 and 2°, and maximum attenuation of signal magnitude was approximately 0.1%.

3.4 Processing of the Data

There are several options which may be exercised once the instantaneous values of the three components of velocity are available as analog electrical signals. Analog multipliers could be used to form instantaneous products, with integrating voltmeters for time averages and RMS meters for fluctuation measurements. In the work reported here, the three signals were digitized and processed through an HP-2100 system. The A/D converter used had a capability of 45,000 points per second with which to process all three channels. This would have limited the acceptance to about 7500 Hz, using two points per cycle. Peripheral limitations on the current system in fact limited the response to 5882 Hz. Thus the high-frequency events cannot be seen through the present system, but the restriction is in the A/D system, not the analog system. Values of $\overline{u'^2}$ measured by analog and digital methods agreed to within 2-3%; thus the frequency limitation on the digital system seems not to have been important. Data were recorded onto digital tape and processes in computer-idle time, overnight. Twenty-two seconds of data-taking per point required 11 minutes of post-acquisition processing on the HP-2100 to produce the values of the three mean components and the six Reynolds stresses. With all-analog processing, the nine outputs could be generated in whatever time was felt necessary to achieve stationary values, based on the flow.

The functions of the Flow Analyzer could all be performed digitally, by passing the three linearizer outputs through A/D converters by executing the matrix-inversion processes digitally. Using the same HP-2100 system, with the same A/D conversion unit, the total time required for all-digital processing was 75 minutes to process 22.6 seconds of data-taking. The use of analog operations for the two matrix inversions reduced the computing time by a factor of 8.5. Different computer systems, with different A/D conversion and higher speed would surely make the direct digital system look more attractive than these results. Whatever digital system is available, however, the two analog stages presently used will continue to be attractive from a cost-of-running standpoint.

3.5 Problems Created by the Size of the Triaxial Wire Probe

The triaxial wire probe creates some problems in the measurement because of its relatively large size compared to the single- and cross-wire probes. The probe has three wires, with their centers located on a sphere of diameter 3 mm to prevent interference due to the wakes of wires. Measurements made on this sphere must be attributed to the center of the sphere. When making measurements in high shear flows, there may be some uncertainty about where the effective measurement center is, since it will change depending on the orientation of the wires with respect to the gradient. Another problem is the overall size of the probe, about 0.8 cm in diameter. It is not possible to obtain data closer than 0.4 cm to the wall.

3.6 Qualification Tests

The Thermosciences Laboratory in the Mechanical Engineering Department of Stanford University has a two-dimensional channel which gives fully developed mean-velocity and turbulence profiles at least to the second-order turbulence quantities. The performance characteristics of this channel have been fully explored; it has been used by several recent experimenters to calibrate their hot-wire technique, their probes, and their systems. The Flow Analyzer was tested in this channel to qualify its performance and to explore its limitations for turbulence measurements.

For the qualification tests, the probe was mounted in a two-axis probe holder so that it could be rotated around the streamwise axis (roll angle α) and also tilted (pitch angle ω) against the approaching flow, as well as traversed to several different distances from the wall. By measuring at several distances from the wall, the system performance was recorded both for high shear regions (near the wall) and zero shear regions (at the centerline of the channel). The outputs were compared with the outputs of the other acceptable methods of measurement in the channel (single horizontal wire, pitot tube measurements, and linear shear stress distribution calculated from the pressure gradient along the channel).

The two-dimensional channel is 6.35 cm wide and 117 cm high. The experiments were made with air flow at ambient conditions and with a centerline speed of 11.2 m/sec.

In Fig. 3.4 the values of $\overline{U}$ (the streamwise mean velocity) obtained from a pitot probe and from the triaxial probe are compared. The pitot probe was modified to create the same stem blockage effect in the tunnel as did the triaxial probe, as seen in Fig. 3.5. In this test the probe was set to zero roll ($\alpha = 0°$) and the axis was aligned with the flow ($\omega = 0°$). The readings of the pitot probe were corrected for shear displacement effect and for turbulence level. The maximum difference between the pitot probe and the triple wire probe occurs near the wall -- about 2.4%. The difference diminishes rapidly as the distance from the wall increases. The difference near the wall may be due to the finite size of the triaxial probe, as was explained earlier, interacting with the velocity gradient.

The effect of rotation of the probe around its axis was investigated. When the probe axis is aligned with the flow direction ($\omega = 0°$), rotation around its streamwise axis should not affect the result if the velocity is uniform, but may affect the result in a shear flow. To investigate this, the probe was aligned with the flow direction ($\omega = 0°$), and for each transverse position across the tunnel, the probe was rotated around its axis to the values of $\alpha = 0°$, $90°$, $180°$, and $270°$. This angle range covers the extreme positions for the wires and exposes different configurations of wires to the shear at different angles.

Figure 3.6 shows the three mean velocity components ($\overline{U}$, $\overline{V}$, and $\overline{W}$) as a function of the distance from the wall for several values of the roll angle α. Roll around the probe axis does not affect the $\overline{U}$ values. The effect on $\overline{V}$ and $\overline{W}$ is small, but not negligible. In this figure $\overline{V}$ and $\overline{W}$ should be zero, but due to the probe size, some deviation from zero is observed within the shear region. The most meaningful comparison for error in $\overline{V}$ and $\overline{W}$ is to compare them to the $\overline{U}$ at the same location. The largest deviations occur at the point near the wall for $\alpha = 0$, $\overline{V}/\overline{U} = 1\%$, and for $\alpha = 270°$, $\overline{W}/\overline{U} = 4.5\%$. These deviations from zero become smaller as the distance from the wall increases. In the zero gradient region at the centerline there is no deviation.

Figure 3.7 shows the turbulent kinetic energy and shear stress distributions as a function of the distance from the wall for several values of the roll angle. The shear stress ($-\overline{u'v'}$) measurements are compared with the linear shear stress distribution obtained from the pressure gradient along the channel (dP/dx). As is seen, all the experimental data lies inside the ± 10% error band, but at angles $\alpha = 90°$ and $\alpha = 270°$ the deviations are much smaller; therefore, one would like to measure $-\overline{u'v'}$ at these angles. The measured turbulent kinetic energy is not much affected by the roll. The largest difference between results occurs at the high shear region near the wall; it is about 3.5%. In the zero shear region there is no effect of roll.

Figure 3.8 shows the diagonal Reynolds stress components ($\overline{u'^2}$, $\overline{v'^2}$, $\overline{w'^2}$) as a function of the distance from the wall, normalized with centerline velocity. The streamwise normal stress ($\overline{u'^2}$) does not seem to be affected much by roll around the probe axis, even in the high shear regions near the wall. On the same figure the $\overline{u'^2}$ distribution obtained with a conventional single horizontal wire is also given, and its agreement with the triaxial wire data is good. The other normal Reynolds stresses ($\overline{v'^2}$ and $\overline{w'^2}$) are affected by the roll angle, especially in the high shear region, but the data collapse on each other quickly as the shear decreases. In the zero shear region on the centerline there are no deviations. One important point to observe is that, at a certain α value, if $\overline{v'^2}$ reads high compared to the value at $\alpha = 0°$, then $\overline{w'^2}$ reads low, or vice versa, while $\overline{u'^2}$ does not change much with α. This combination leads to q^2 values which are quite insensitive to the changes in α, a fortuitous result for the measurement of q^2 -- the main interest of the general research.

The data discussed above are enough to qualify this system for measurements when the probe axis is aligned with the flow direction. But one of the most important objectives of this research was to find a method which would work in a flow of unknown direction. To investigate this, the probe axis was tilted against the approaching flow direction (ω), again in the 2-D channel. Some rotations around the probe axis (α) were also tested to see the combined effect of both α and ω. The results are discussed in the following paragraphs.

Figure 3.9 shows the three mean velocity components as a function of distance from the wall for several values of the angle between the flow and the probe axis (ω). There the value of α was held constant, because it was seen above that the mean velocities were not much affected by the roll engle. Up to $\omega = 20°$ the data for $\overline{U}$ collapse on top of each other and the deviation for $\omega = 30°$ is not very large. The largest deviation at this angle is about 3.5% in the high shear region near the wall, and about 2% in the zero shear region. Deviation is calculated as the difference between two extremes, not from the pitot probe data. This result means that mean velocity can be measured with good accuracy if the approaching flow direction is within $\pm 30°$ of the probe axis; i.e., one does not have to know the flow direction better than within a cone of half apex angle 30° around the probe axis to measure the mean velocity with acceptable accuracy. (If $\overline{V} = 0.1\ \overline{U}$ this will give an angle of about $\pm 6\%$.) As the angle between the flow direction and the probe axis increases, the errors in $\overline{V}$ and $\overline{W}$ also increase. Some of this may be the effect of the probe size, as was explained earlier, and some may be due to the probe blockage effect in the channel.

In Fig. 3.10 the turbulent kinetic energy (TKE) and shear stress are plotted for several values of roll angle (α) and pitch angle (ω). In the TKE plot the line at the center is faired through the data at $\omega = 0°$, $\alpha = 0°$ (this measurement should be the one closest to reality). The other lines denote the $\pm 10\%$ and $\pm 15\%$ error bands around the reference. Again the data points converge rapidly as the distance from the wall increases. Deviations are much smaller in the zero shear region. In the same figure also, the q^2 distribution for $\alpha = 90°$, $\omega = 20°$ is shown to demonstrate the increase in deviation as ω increases. Another important point to observe from this figure is that for $\alpha = 90°$ and $\omega = 10°$ the data lie very close to the center profile. This shows that, depending on the quantity being measured, there are angle combinations α and ω for which the measurement cone can be enlarged. For example, for $\alpha = 90°$ and $\omega = 10°$ and $20°$, it appears that even in the highest shear region q^2 can be measured within 12% inside a cone of 15° half apex angle around the probe axis. The deviations in q^2 are not like uncertainty scatters, but rather have a preferred direction. It may be

possible to devise a scheme to correct the data based on the first estimate of the flow direction, to improve the accuracy. In the shear stress part of Fig. 3.10, the straight line in the middle of the figure is the shear stress distribution obtained from the pressure gradient in the streamwise direction. The other straight lines are the boundaries for ± 10% and ± 15% error. Most of the data up to the angle $\omega = 10°$ lie within 10% error band, except a few points near the wall for angles $\alpha = 270°$ and $\alpha = 90°$. Almost all the data, including $\omega = 15°$ and $\alpha = 0°$, lie within the ±15% error band. In conclusion, it can be said that the shear stress $-\overline{u'v'}$ can be measured within 10% within a cone of half apex angle 10° and within 15% inside a cone of half apex angle 15°, except very near the wall.

Figure 3.11 shows the normal Reynolds stress $\overline{u'^2}$ as a function of the distance from the wall for several pitch angles. It was shown before that $\overline{u'^2}$ does not change much with roll angle α. For this reason, different α and ω combinations are not included in the figure, and attention is given only to the ω values. Up to $\omega = 15°$ the measurements collapse on top of each other except at the point nearest the wall, where the data for $\omega = 15°$ deviate from others about 5%; but these data converge rapidly to the others with increasing distance from the wall. The data for $\omega = 20°$ deviate about 15% from the data for smaller ω's near the wall, but again converge fast with increasing distance from the wall. The conclusion is that $\overline{u'^2}$ can be measured with good accuracy (maximum error being 5% near the wall) up to the angle $\omega = 15°$, i.e., within a cone of half apex angle 15°. The deviation in the zero shear region is about 1% or 2% up to $\omega = 30°$.

Figure 3.12 shows the normal Reynolds stresses $\overline{v'^2}$ and $\overline{w'^2}$ for different roll and pitch angles. The data for $\overline{v'^2}$ collapse on top of each other for $\omega = 0°$ and $\omega = 5°$. For ($\omega = 10°$, $\alpha = 0°$) and ($\omega = 10°$, $\alpha = 180°$), the data generally lie in the 10% error band, except the next-to-wall point for ($\omega = 10°$, $\alpha = 0°$), for which the deviation is about 15%. Generally, it can be said that within a cone of half apex angle 5°, $\overline{v'^2}$ can be measured with very good accuracy (less than 2% deviation). The measurement cone angle can be enlarged to 15° in a zero

shear region. In the high shear region one can measure $\overline{v'^2}$ within 5% for the case of $\omega = 10°$, $\alpha = 0°$, and within 10-15% for $\omega = 10°$, $\alpha = 180°$.

Considering now the $\overline{w'^2}$ data, in the zero shear region the data converge very well, and good accuracies can be obtained up to $\omega = 15°$. Up to $\omega = 5°$ the data lie within 10% of each other in the high shear region. For the larger values of ω, certain combinations of α and ω are necessary to get the data within 10-15% error bands in a high shear region. For example, all of the $\omega = 10°$ data is out of the 15% error band for all α values, but the data for $\omega = 20°$ and $\alpha = 90°$ fall within the 15% error band.

The qualification data discussed above show that the size of the measurement cone changes, depending on the quantity measured. Some quantities, such as $\overline{v'^2}$ and $\overline{w'^2}$, are affected by rotation around the probe axis, especially in high-velocity gradient regions. The reason for these changes may be the large probe size.

An important point shown by the qualification data is that the major mean velocity component $\overline{U}$ can be measured quite accurately within a cone of 30° half apex angle around the probe axis. In three-dimensional flows where the probe axis makes a large angle with the unknown flow direction, the errors in the measured turbulence quantities may be unacceptable. In critical cases, one might use a two-step process, first finding the flow direction approximately (within 3-4°), and then aligning the probe with this direction. In this position all of the turbulence quantities could be measured quite accurately.

3.7 Further Work on Triaxial Wire System

As has been seen, the size of the probe creates some problems in high shear flows, by causing artificial velocity components to be indicated which depend on the arrangement of the wires in the velocity gradient. Work is in progress currently to predict the magnitude of the artificial velocity components indicated, as a function of the orientation of the probe in flow and the value of the gradient of mean velocity. It is hoped that this work will lead to a method of correcting the turbulence quantities.

Secondly, to eliminate the probe size effects, a new, smaller probe design is being considered for possible future extensions of this work.

3.8 Conclusions and Capabilities

A hot-wire method and system have been developed to make measurements in 3-D turbulent flows with high fluctuations and partially unknown flow direction. The results are summarized below. The error figures are for high-velocity gradient (about 1600 1/sec) regions; for zero or low shear regions the errors are smaller and consequently the measurement cones are larger. With this system:

- The mean velocity can be measured with good accuracy within a cone of 30° half apex angle around the probe axis.
- The turbulence kinetic energy can be measured with 10-15% accuracy within a cone of half apex angle 10-12°.
- The shear stress $(-\overline{u'v'})$ can be measured within ± 10% accuracy in a cone of half apex angle of 10° and ± 15% accuracy within a cone of 15° half apex angle.
- The streamwise normal Reynolds stress component can be measured with a maximum error of 5% within a cone of half apex angle 15°.

The errors in the quantities mentioned above are not random but rather have a preferred direction. Some of these effects can be predicted from the known effects of probe size and position in the velocity field. Work in this area is continuing.

The triple wire method is very fast, with the data-acquisition time being governed by the time required to establish a stationary value of the process being studied. Thus, large amounts of data can be taken.

With the addition of RMS and correlating circuits, quantities such as TKE and mean velocity could be displayed directly with analog instruments. This would eliminate the need for complicated data reduction -- usually the most tedious part of an experiment.

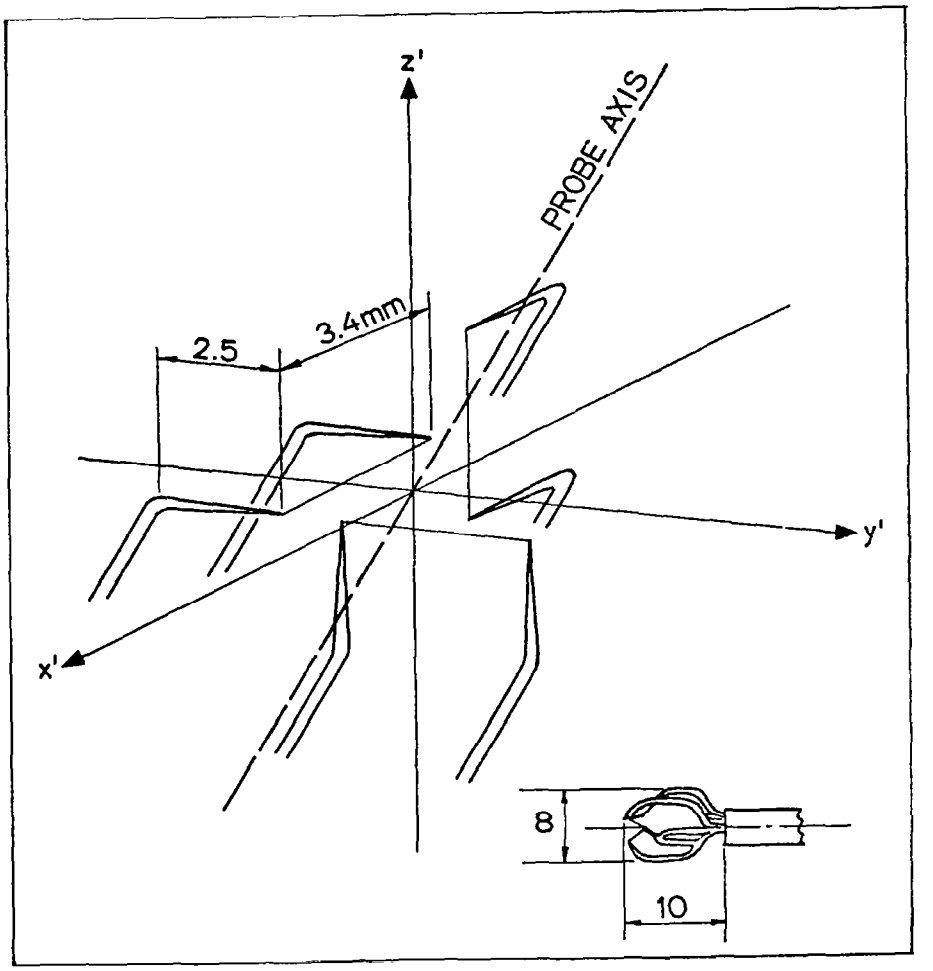

Fig. 3.1. Triaxial wire probe tip and wire coordinate system.

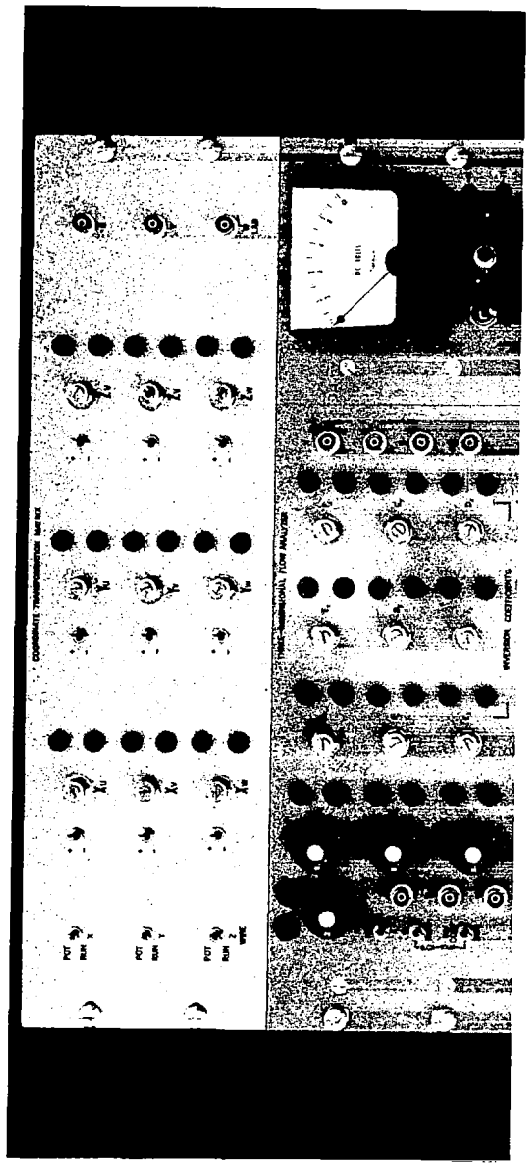

Fig. 3.2. Photograph of the 3-D Turbulent Flow Analyzer.

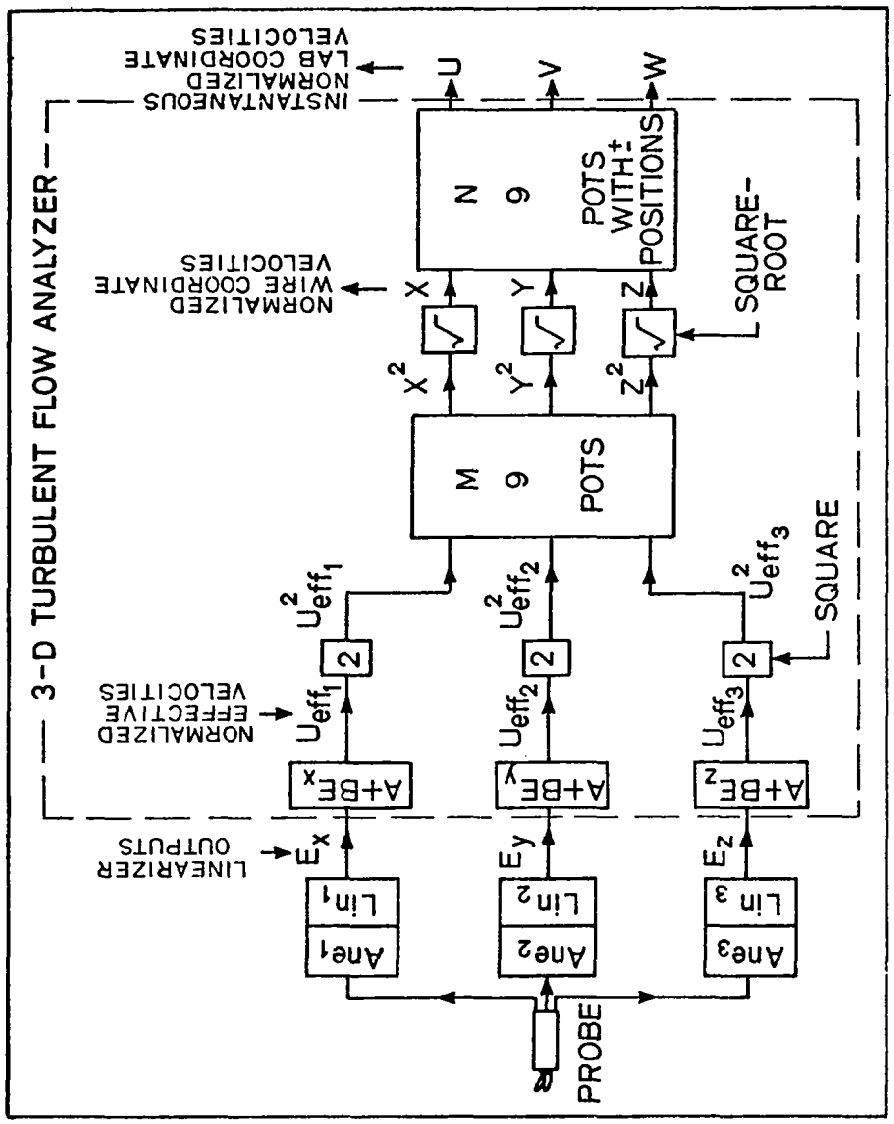

Fig. 3.3. Flow diagram of the complete system.

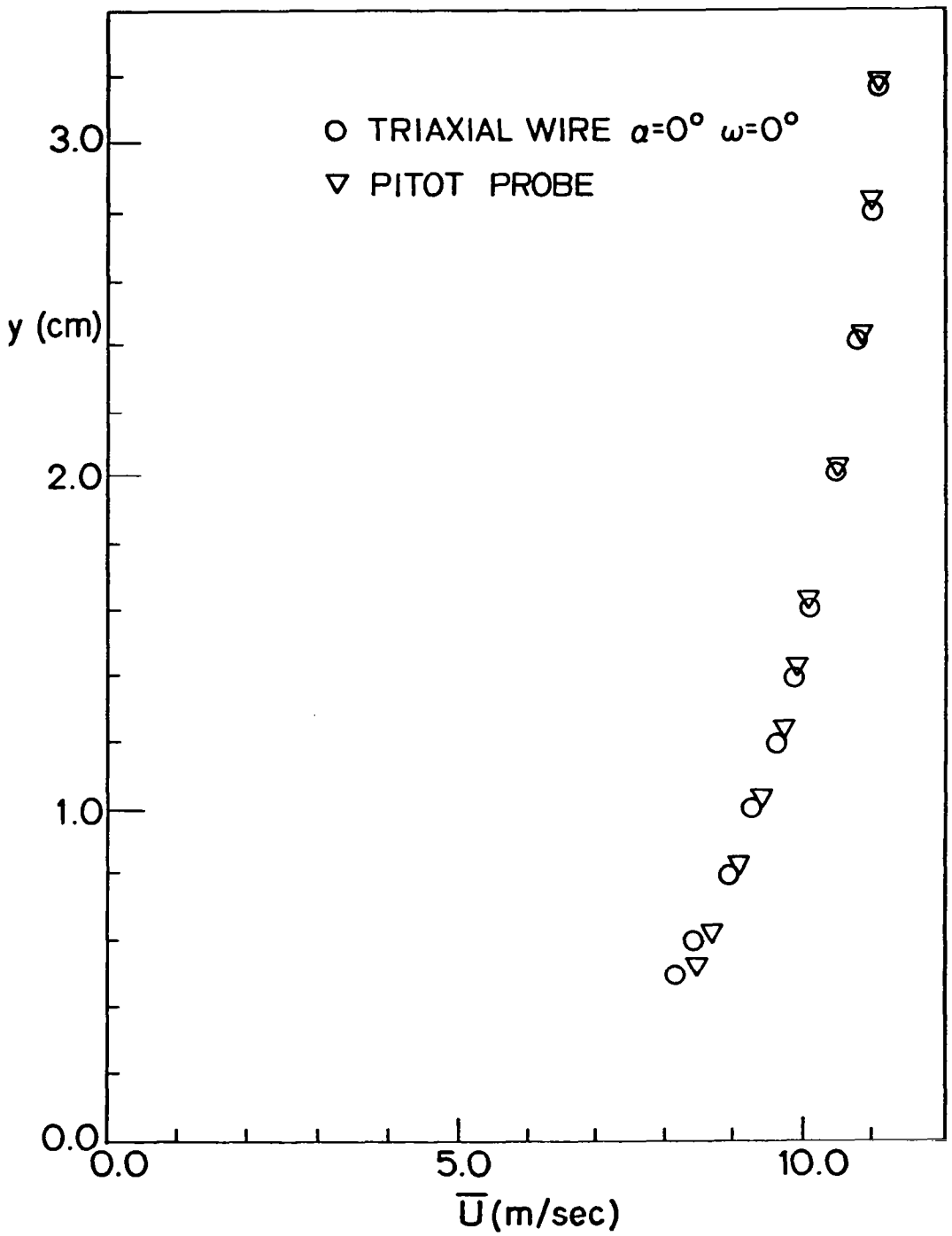

Fig. 3.4. Comparison of triaxial probe and pitot probe measurements of $\overline{U}$ in the 2-D channel.

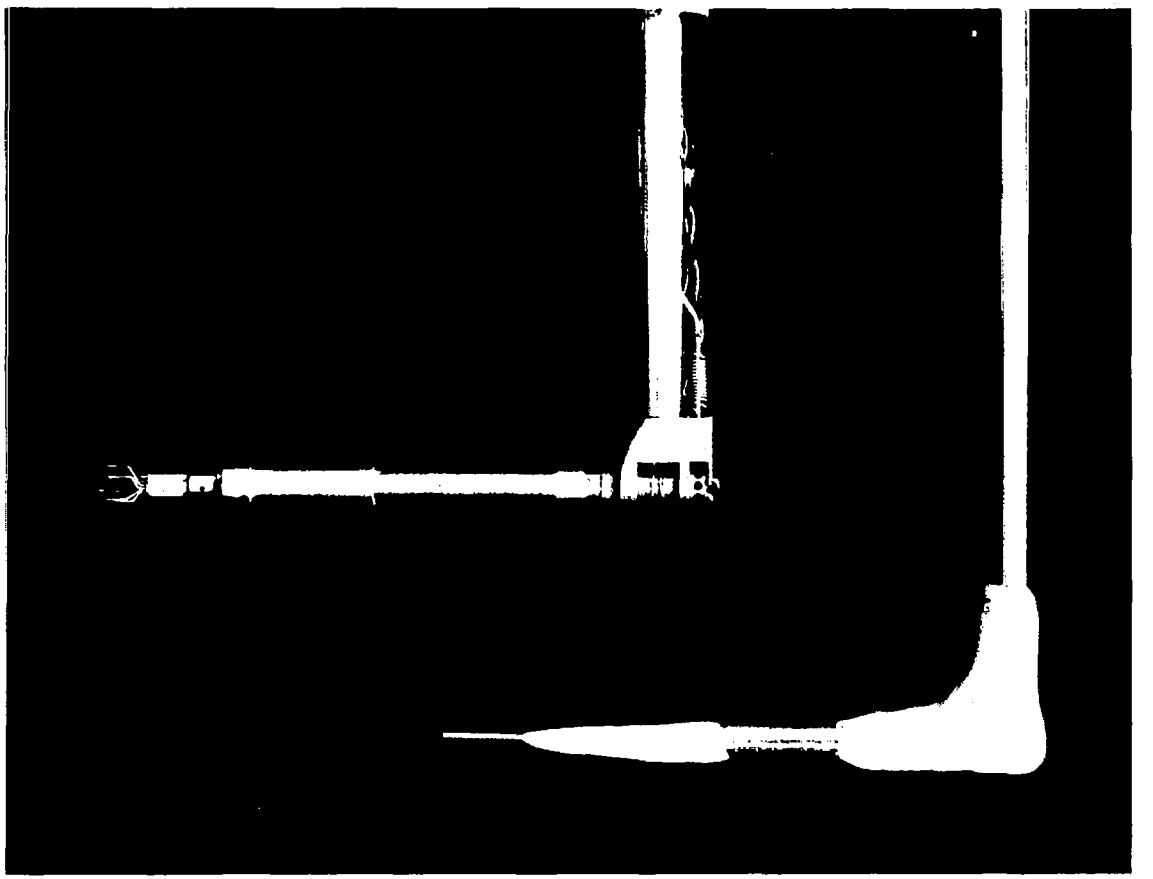

Fig. 3.5. Photograph of the triaxial probe and modified pitot probe.

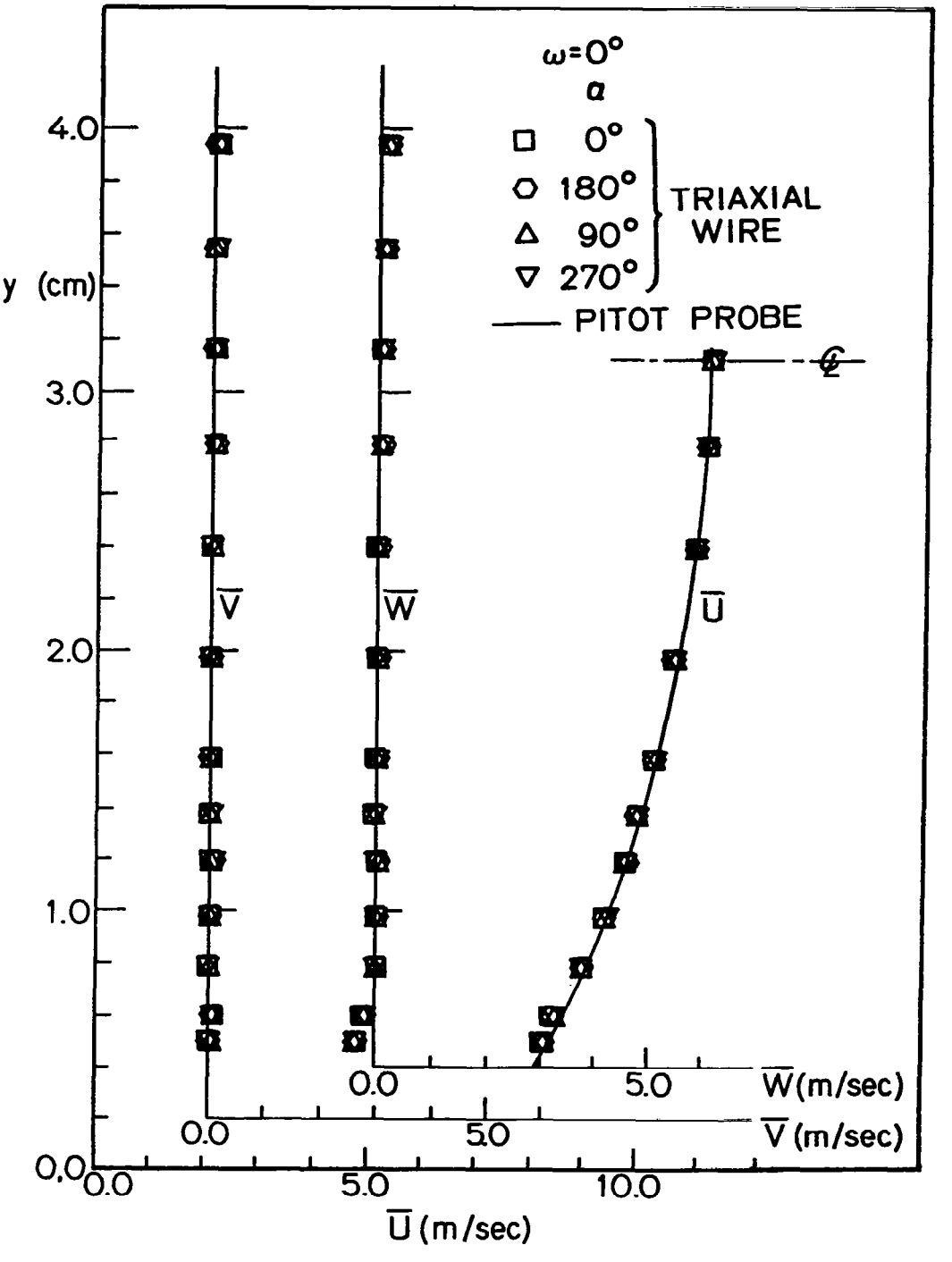

Fig. 3.6. Effect of roll angle about the probe axis on the mean velocity components.

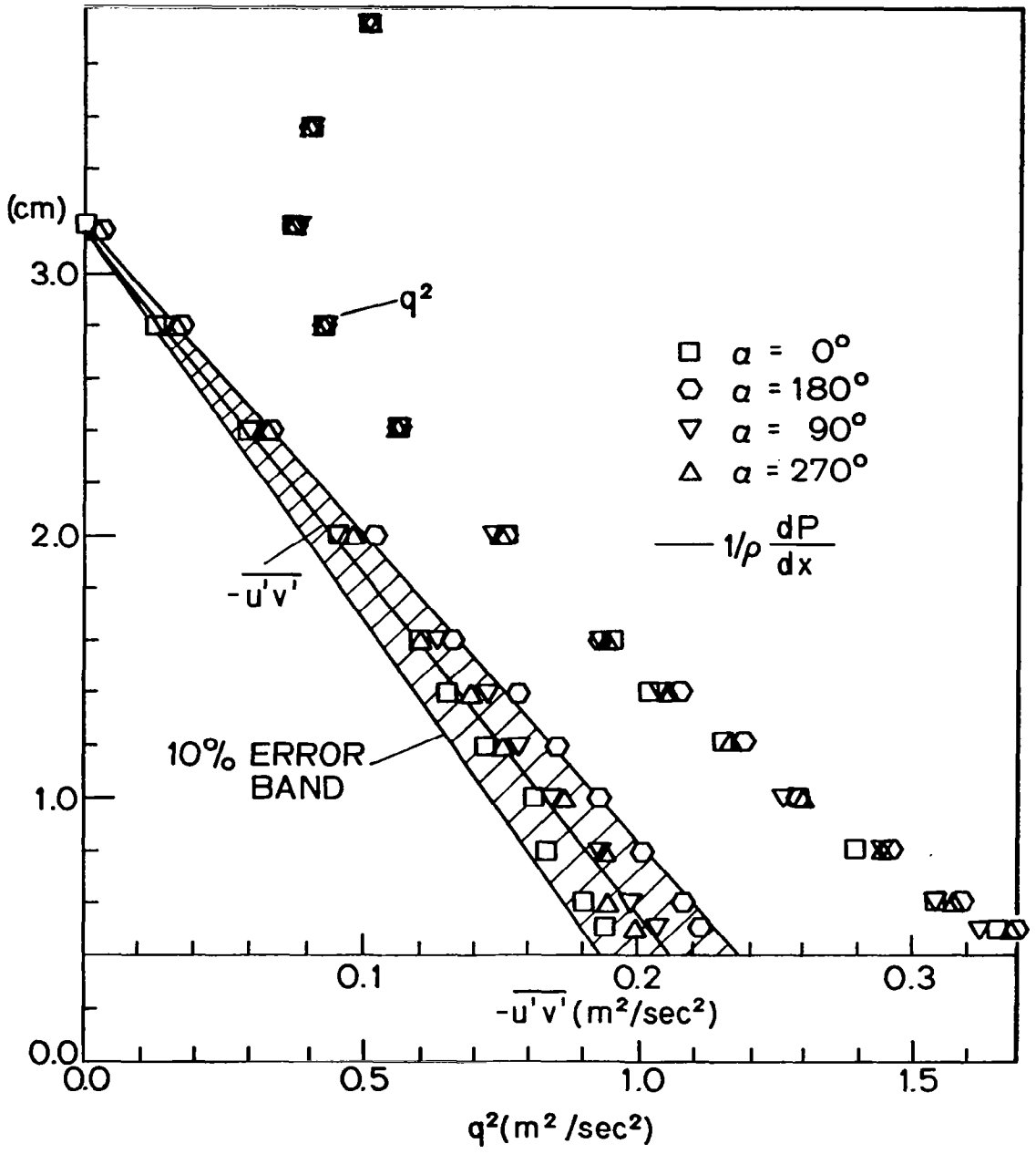

Fig. 3.7. Effect of roll angle about the probe axis on shear stress and turbulent kinetic energy.

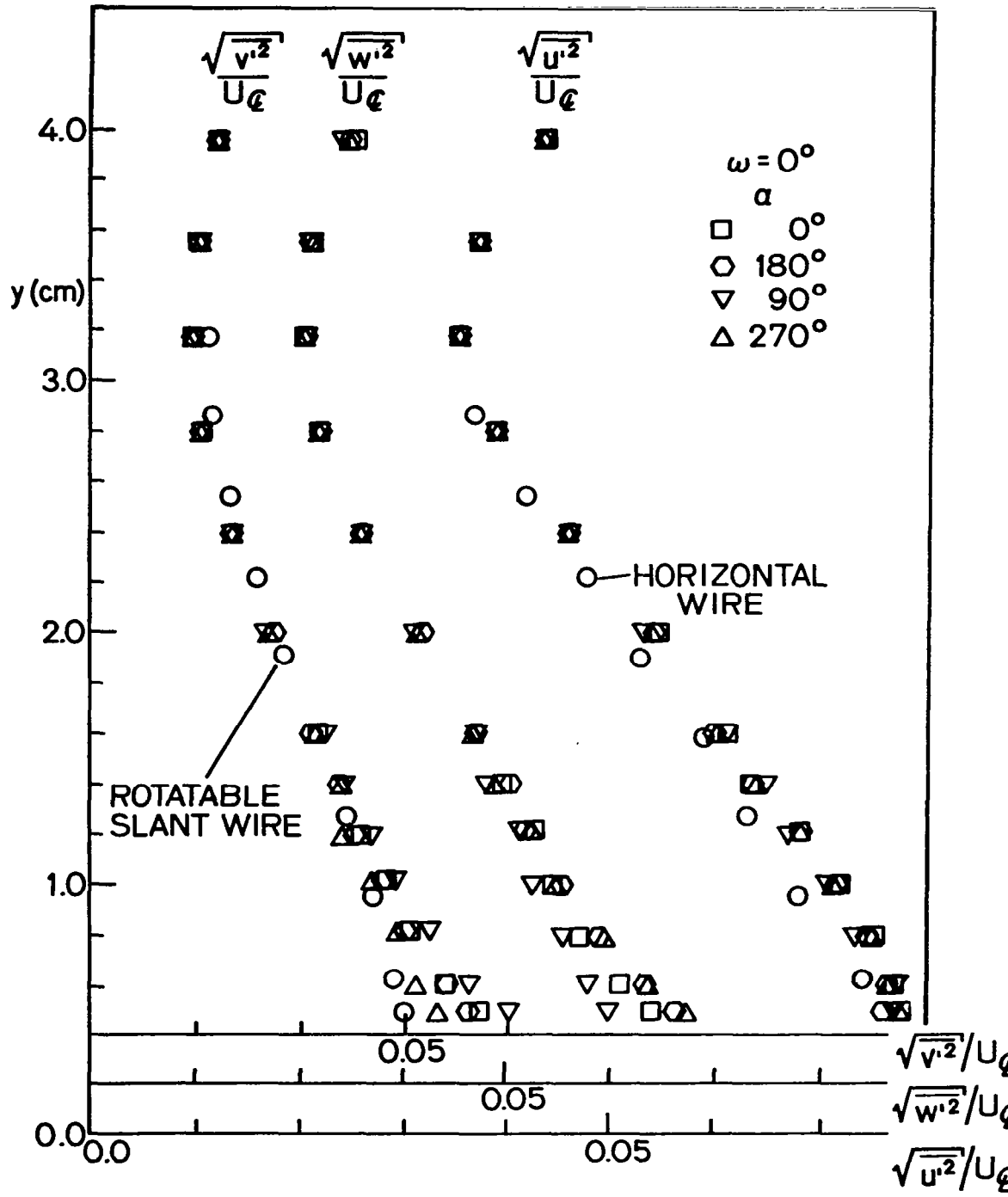

Fig. 3.8. Effect of roll angle about the probe axis on the normal Reynolds stresses.

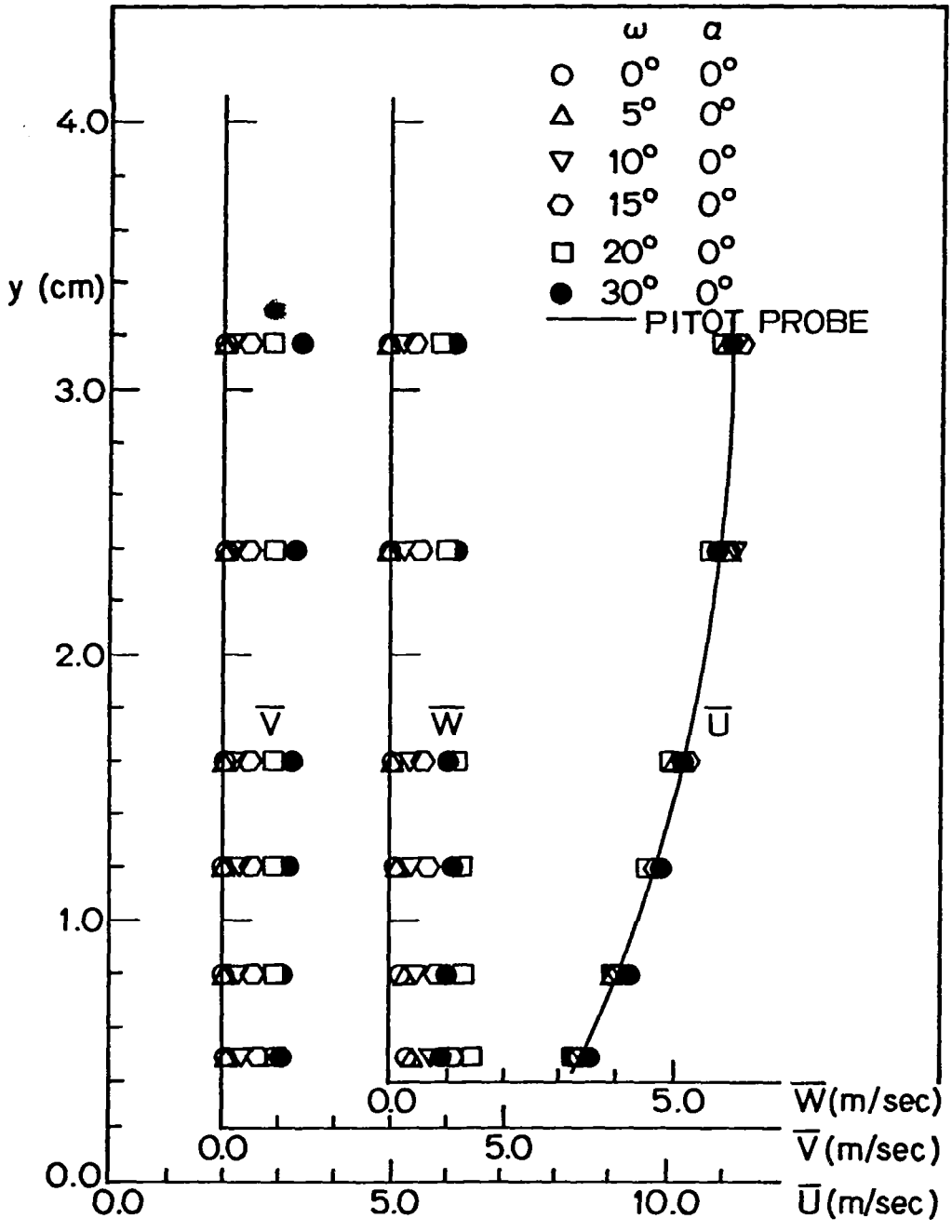

Fig. 3.9. Effect of pitch angle on the mean velocity components.

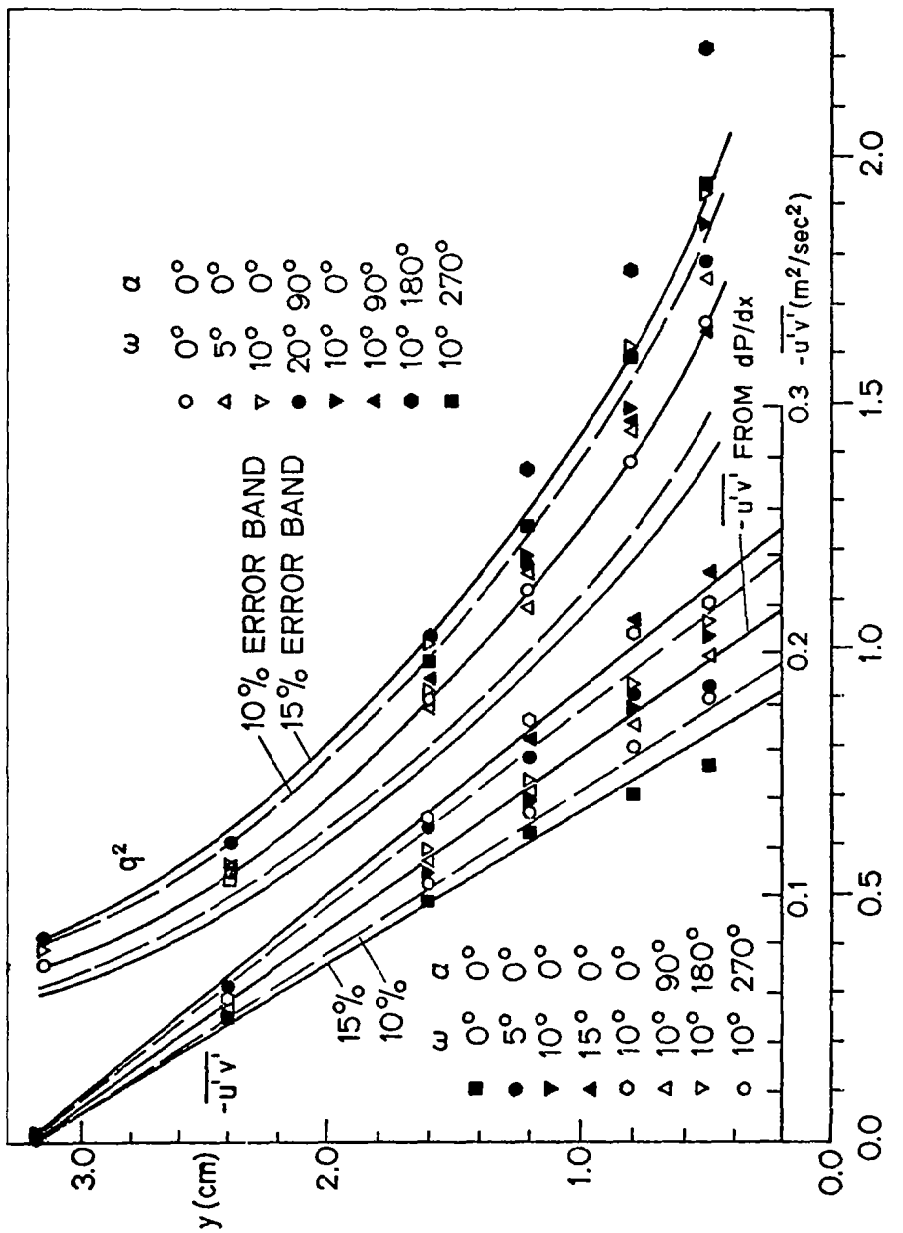

Fig. 3.10. Effect of combined roll and pitch angles on shear stress and turbulent kinetic energy.

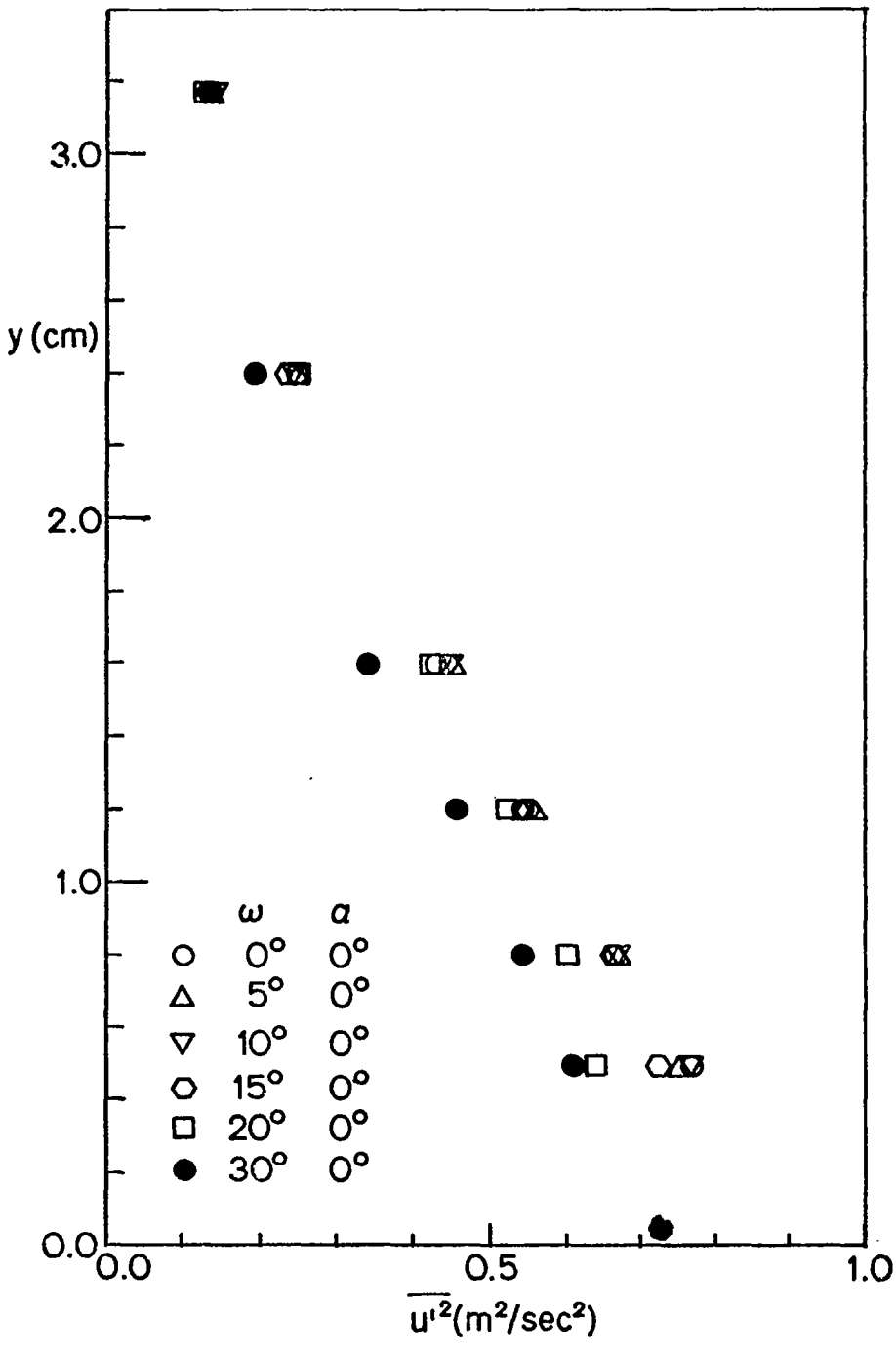

Fig. 3.11. Effect of pitch angle on the $\overline{u'^2}$ Reynolds stress.

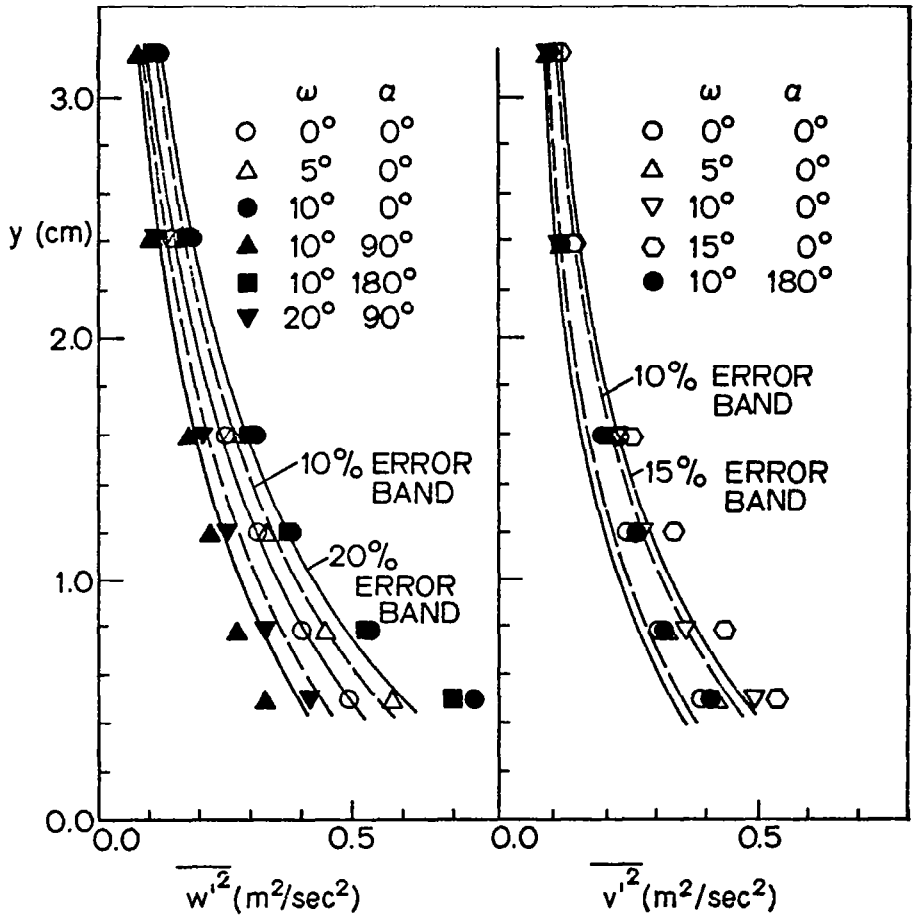

Fig. 3.12. Effect of combined roll and pitch angles on the $\overline{v'^2}$ and $\overline{w'^2}$ Reynolds stresses.

Chapter 4

PREDICTION OF RECOVERY REGION HYDRODYNAMICS WITH A ONE-EQUATION MODEL OF TURBULENCE

One of the main objectives of this research was to see whether or not the recovery region hydrodynamics could be predicted using a one-equation model of turbulence in a two-dimensional boundary layer computation program, STAN5 (Crawford & Kays, 1975).

An algebraic equation for the mixing length was needed for the model. The actual mixing length profiles were first obtained from the experimental profiles ($\overline{u'v'}$ and $\overline{U}$) and purely empirical curve fits were used to model the behavior. The piecewise model was used in STAN5, as a check, and the predictions of the data were very successful. Each region in the mixing-length profile was then interpreted physically and alternative, plausible equations identified. This procedure showed that the recovery region hydrodynamics can be satisfactorily explained by postulating a two-dimensional boundary layer growing inside the thicker initial boundary layer. The following sections present the details of these steps.

4.1 Equations to be Solved

The following equations must be solved to obtain mean velocity and turbulent kinetic energy (TKE) profiles. For a two-dimensional, turbulent boundary layer under isothermal conditions, at ambient temperatures and low speeds, at the constant free stream velocity and without any external body forces:

Continuity:
$$\frac{\partial \overline{U}}{\partial x} + \frac{\partial \overline{V}}{\partial y} = 0 \qquad (4.1)$$

x-Momentum:
$$\rho \overline{U} \frac{\partial \overline{U}}{\partial x} + \rho \overline{V} \frac{\partial \overline{U}}{\partial y} = \frac{\partial}{\partial y} \left(\mu \frac{\partial \overline{U}}{\partial y} - \rho \overline{u'v'} \right) \qquad (4.2)$$

$$\text{TKE:}\quad \rho\bar{U}\frac{\partial q^2}{\partial x} + \rho\bar{V}\frac{\partial q^2}{\partial y} = \underbrace{-\rho\,\overline{u'v'}\frac{\partial \bar{U}}{\partial y}}_{\text{production}} - \underbrace{\mathcal{D}}_{\text{dissipation}} + \underbrace{\frac{\partial}{\partial y}(J)}_{\text{diffusion}} \qquad (4.3)$$

Boundary conditions:

Momentum eqn.

$$y = 0 \begin{cases} \bar{U} = 0 \\ \bar{V} = 0 \end{cases} \qquad (4.4)$$

$$\lim_{y\to\infty} \bar{U} = U_\infty$$

The equation for TKE is not solved all the way to the wall in STAN5, but only to $y^+ = 2A^+$ where A^+ is a measure of sublayer thickness. It is assumed that the flow is in local equilibrium (experiments confirm this assumption) below $y^+ = 2A^+$ and Prandtl's mixing length can be used in this region. The TKE at this point is calculated such that at $y^+ = 2A^+$ the eddy viscosity obtained from the mixing length model is equal to the one obtained from a one-equation model of turbulence. This condition gives the following boundary conditions on TKE:

$$\frac{q^2}{2} = \left(\frac{\kappa}{A_q}\,\ell\,\frac{\partial \bar{U}}{\partial y}\right) \quad \text{at} \quad y^+ = 2A^+ \qquad (4.5)$$

$$\lim_{y\to\infty} \frac{q^2}{2} = \frac{q_\infty^2}{2}$$

The following terms must be modeled in equations (4.2) and (4.3) in order to obtain a soluble set of equations: $\overline{u'v'}$, $\mathcal{D}$, J. The term for $\overline{u'v'}$ will be modeled after Boussinesq (1877) with eddy viscosity model:

$$-\overline{u'v'} = \varepsilon_M \frac{\partial \bar{U}}{\partial y} \qquad (4.6)$$

The term ε_M will be modeled after Prandtl (1945) and Kolmogorov (1942):

$$\varepsilon_M = \frac{Aq}{\kappa}\,\ell\sqrt{\frac{q^2}{2}} \qquad (4.7)$$

The term "$\mathcal{D}$" dissipation of TKE will be modeled as given in Launder & Spalding (1972):

$$\mathcal{D} = B_q \kappa \frac{\left(\sqrt{q^2/2}\right)^3}{\ell} \tag{4.8}$$

and diffusion of TKE "J" is also to be modeled as in Launder & Spalding (1972).

$$J = (\nu + \varepsilon_q) \frac{\partial (q^2/2)}{\partial y} \tag{4.9}$$

where $Sc_q = \varepsilon_M / \varepsilon_q$. The production of TKE, "P", can be expressed as

$$P = -\rho \overline{u'v'} \frac{\partial U}{\partial y} = \rho \left(\frac{A_q}{\kappa}\right) \ell \sqrt{\frac{q^2}{2}} \left(\frac{\partial \bar{U}}{\partial y}\right)^2 \tag{4.10}$$

To complete the model, the following constants or functions need to be specified: ℓ, A_q, B_q, Sc_q. A_q is the production constant and can be obtained from the value of the correlation coefficient $-\overline{u'v'}/q^2$ near the wall. It is generally about 0.22 (Wolfstein, 1969). B_q is called the dissipation constant and can be evaluated under the condition that the production of TKE is equal to its dissipation in the region near the wall. This condition gives the following relation:

$$B_q = \frac{A_q^3}{\kappa^4} \tag{4.11}$$

$$\kappa = 0.41 \tag{4.12}$$

From this equation, $B_q = 0.377$ is obtained.

"Sc_q", the Schmidt number of TKE, is expressed as is shown in the following figure. It has a value of 1.75 near the wall and 0.5 near the

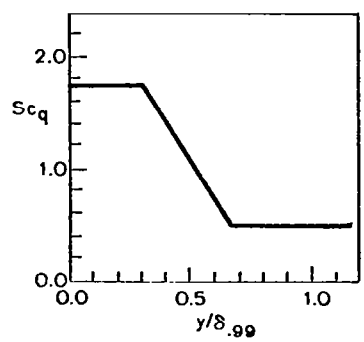

free stream. Launder & Spalding (1972) suggest that for film-cooling applications Sc_q should follow a linear distribution from 1.75 near the wall down to 0.5 near free stream, but during the present predictions, the distribution shown in the preceding figure was found to work better. The extended region of $Sc_q = 0.5$ near free stream played an important role in modeling the correct diffusion of TKE near the edge of the momentum boundary layer. The value near the wall did not seem to be as important because of the dominant role of production and dissipation in this region.

The last quantity to be modeled to complete the set is the mixing length, "ℓ". Predictions and data show that all other constants mentioned above have their usual values (i.e., the values used for 2-D flat-plate boundary predictions). The success of predictions depended very strongly on the correct modeling of "ℓ", as will be shown and discussed in the following sections.

4.2 Mixing-Length Model

A mixing-length model was developed specifically for the recovery region. This same model can later be applied to the full-coverage region, however, because the boundary layer should behave almost like a recovery region between the injection rows.

The following requirements should be met by the mixing-length model for it to have at least some limited universality:

- It should be possible to relate the deviations from the 2-D mixing length to physical events taking place in the flow field.
- The dynamics of the model should allow it to relax back to a 2-D flat-plate mixing length.

The general approach taken in modeling the mixing length was explained at the beginning of this chapter. More specifically, the modeling process will be explained in Sections 4.2.1-4.2.9 in the following order: First the flow structure in the recovery region will be explained briefly (Fig. 4.1). Then each region in the mixing length profiles will be discussed and empirical equations will be given with supporting physical arguments. Figures 5.27, 5.28, 4.1, and 4.2 are used for these discussions, and they will not be mentioned separately in the discussions

of each region. Figures 5.27 and 5.28 show the mixing-length distributions obtained from experiments by

$$\ell = \frac{\sqrt{-\overline{u'v'}}}{\frac{\partial \overline{U}}{\partial y}} \qquad (4.13)$$

Three streamwise positions were used: the start of the recovery region (x = 188 cm) and two downstream recovery region stations (x = 214 cm, 256 cm, or 27 hole diameters and 67 hole diameters downstream of the last row of injection. The mixing length at the start of recovery region was obtained from the spanwise-averaged profiles at this location. Fig. 4.2 shows the modeled mixing length superposed on Fig. 4.1 to show the relation between the regions of mixing length and the flow structure of the recovery region. The new information is on ℓ vs. y coordinates.

4.2.1 Flow structure in the recovery region

Figure 4.1 shows a sketch of the flow structure in the recovery region. The basic structure is an internal two-dimensional (2-D) boundary layer growing inside the thick boundary layer. The thickness of the inner 2-D boundary layer is δ' and the thickness of the overall boundary layer thickened with the injection process in the full-coverage region is δ. In the middle regions the two boundary layers blend (the cross-hatched area) with the help of cumulative jet spread. The region next to the wall is not cross-hatched, however, because the processes in this region are completely controlled by the wall. The 2-D internal boundary layer has an initial thickness at the start of the recovery region which depends on the upstream conditions (e.g., the blowing ratio). This internal boundary layer growth has been observed by several other experimenters whenever there is a sudden change of the surface conditions. For example, Antonia & Luxton (1972) observed such an internal boundary layer in their experiments on the response of a turbulent boundary layer to a step change in surface roughness.

When the mixing-length profiles are examined in Figs. 5.27 and 5.28, five distinguishable mixing length regions can be identified, numbered in Fig. 4.2. In the same figure, three distinguishable flow regions are

shown, numbered I, II, and III. Region I is the near-wall region of the 2-D internal boundary layer, II is the blend region dominated by cumulative jet effects, and region III is the outer region, dominated by the outer region of the thick boundary layer.

4.2.2 Region 1 of the mixing length

A region very close to the wall, where $\ell = \kappa y$, is termed region 1. Experiments show that this region extends up to $y/\delta \simeq 0.14$ for $M = 0.4$, but only up to $y/\delta \simeq 0.055$ for $M = 0.9$.

This is the inner region of the 2-D internal boundary layer where the length scale is based on the distance from the wall "y". For programming convenience, the mixing length and the distance from the wall in all the regions were normalized on the total boundary layer of thickness δ. In this region, however, the wall effects are dominant and determine the heat transfer regardless of the blowing ratio. The effect of blowing is mainly to change the initial thickness of the internal 2-D boundary layer. The proposed model for this region is:

$$\left(\frac{\ell}{\delta}\right) = \kappa \left(\frac{y}{\delta}\right) D \quad \text{for} \quad 0 < \left(\frac{y}{\delta}\right) \leq \left(\frac{y}{\delta}\right)_d \tag{4.14}$$

where D is the damping function (Van Driest) and $(y/\delta)_d$ is the departure point from "κy" line. This point corresponds to $y/\delta' = \lambda/\kappa$ for the inner 2-D boundary layer of thickness δ'.

The following empirical equation is given for $(y/\delta)_d$:

$$\left(\frac{y}{\delta}\right)_d = \frac{\lambda}{\kappa} + C_1 M \left[\left(\frac{x'}{\delta}\right) - C_2\right] \tag{4.15}$$

where $C_1 = 0.0045$ and $C_2 = 37$. It is seen that as M gets large the initial value of $(y/\delta)_d = \lambda/\kappa - C_1 C_2 M$ gets smaller, indicating that a higher blowing ratio destroys the near wall layer, causing a smaller initial thickness for the 2-D internal boundary layer. This fits the physical situation very well. C_2 is the number of boundary layer thicknesses at which $(y/\delta)_d$ reaches the λ/κ point for the outer boundary layer. In fact, then, the recovery is completed. (Antonia* also supports C_2 being 37.) C_1 controls the rate of recovery of $(y/\delta)_d$ point.

* Personal communication.

4.2.3 Region 2 of the mixing length

Experiments show that in this region the mixing length is constant and low, compared to the outer region of a 2-D flat-plate boundary layer of the same thickness. This region is barely visible for $M = 0.4$ but is obvious for $M = 0.9$. It extends up to about $(y/\delta) \simeq 0.2$ for all stations and corresponds to the outer region of the inner 2-D boundary layer, where $\ell = \lambda\delta'$. Here the eddy size does not depend on the distance from the wall, nor does it depend on the total thickness of the outer boundary layer.

The distance of this region from the outer edge means that the outer length scale does not affect it. This region does not extend all the way up to $y = \delta'$ for the reasons stated below.

The following empirical equation is proposed:

$$\ell = \kappa \left(\frac{y}{\delta}\right)_d \quad \text{for} \quad \left(\frac{y}{\delta}\right)_d < \left(\frac{y}{\delta}\right) \leq \frac{\lambda}{\kappa} \tag{4.16}$$

This region does not extend all the way up to δ'. As soon as the edge of the inner layer of the outer boundary layer $(y/\delta = \lambda/\kappa)$ is encountered, the length scale begins to be affected by the outer length scale of the outer boundary layer. The branch point is given as λ/κ.

4.2.4 Region 3 of the mixing length

Experiments show that in this region the mixing length is still below a 2-D flat-plate value. This is barely visible for $M = 0.4$ but is obvious for $M = 0.9$. In this region, the mixing length rises from the value in region 2 to 0.085. The region starts around $y/\delta = \lambda/\kappa \simeq 0.2$ and extends up to $y/\delta \simeq 0.3$ for $M = 0.9$ and $y/\delta \simeq 0.25$ for $M = 0.4$ for the first station. It moves away from the wall in the recovery region.

This is the first section of the blend region of inner and outer boundary layers (region II in Fig. 4.2). Here the length scale changes from the 2-D inner layer value to the value in the outer layer in a medium dominated by the jet flow regime.

The following empirical equation is given for this region:

$$\left(\frac{\ell}{\delta}\right) = a\left(\frac{y}{\delta}\right) + b \quad \text{for} \quad \frac{y}{\kappa} < \left(\frac{y}{\delta}\right) \leq \left(\frac{y}{\delta}\right)_i \tag{4.17}$$

The linear combination is all that is justified and fits the experiments. Here, $(y/\delta)_i$ is the intersection point of the new mixing length line and the $(\ell/\delta) = \lambda$ line. The $(y/\delta)_i$ point is the effective centerline of rising jets and moves out in the recovery region as the jets spread outwards. This will later be shown quantitatively in section 4.4.2. The following empirical equation is given for this point:

$$\left(\frac{y}{\delta}\right)_i = \frac{\lambda}{\kappa} + C_3 M\left[\left(\frac{x'}{\delta}\right) + C_4\right] \tag{4.18}$$

It has an initial value of $\lambda/\kappa + C_3C_4M$ and an advance rate of $C_3M(x'/\delta)$ in the downstream direction. The initial value increases with M, indicating a deeper penetration for high blowing, which fits the physics. The values of the constants are:

$$C_3 = 0.0275 \quad , \quad C_4 = 4.0 \tag{4.19}$$

and the equations for coefficients a and b in equation (4.6) are:

$$a = \frac{\lambda - \kappa(y/\delta)_d}{(y/\delta)_i - \frac{\lambda}{\kappa}} \tag{4.20}$$

$$b = \frac{-\frac{\lambda^2}{\kappa} + \kappa(y/\delta)_d\,(y/\delta)_i}{(y/\delta)_i - \frac{\lambda}{\kappa}} \tag{4.21}$$

4.2.5 Region 4 of the mixing length

Experiments show that a region of augmented mixing length is located between $0.24 \leq (y/\delta) < 0.37$ for $M = 0.4$ and between $0.35 \leq (y/\delta) < 0.55$ for $M = 0.9$ at the start of the recovery region. This region is wider and higher for $M = 0.9$ than for $M = 0.4$. The augmented region vanishes in the recovery regions.

The augmentation in the mixing length occurs due to high shear between the cumulative jet spread and the outer layer fluid. The maximum in the augmentation occurs somewhere between the outer edge of the jet

spread and the effective jet centerline. In the case of higher blowing, this region is moved outwards because of the greater jet penetration. The augmented region also moves outwards in the downstream direction in the recovery region, as jets rise; but at the same time it vanishes, as there is a decrease in shear between the cumulative jet spread and the outer layer. This is discussed further in section 5.9.

This region was modeled as a parabola, the simplest curve which fit the data:

$$\left(\frac{\ell}{\delta}\right)_a = c\left(\frac{y}{\delta}\right)^2 + d\left(\frac{y}{\delta}\right) + e \tag{4.22}$$

and

$$\left(\frac{\ell}{\delta}\right) = \lambda + \left(\frac{\ell}{\delta}\right)_a \quad \text{for} \quad \left(\frac{y}{\delta}\right)_i < \left(\frac{y}{\delta}\right) \leq \left(\frac{y}{\delta}\right) + W \tag{4.23}$$

Here, c, d, and e are constant coefficients. Their values depend on end points and will be given after the discussion of the end points. W is the width of the augmented region at the $(\ell/\delta) = \lambda$ level. Based on the experimental evidence, it was made a function of blowing ratio M. Since no better formulation was possible, it was expressed as a linear function.

$$W = C_7 M \tag{4.24}$$

In Figure 4.2, $(\ell/\delta)_{max}$ is the maximum value of the augmentation. Its decay in the downstream direction was expressed as an exponential function.

$$\left(\frac{\ell}{\delta}\right)_{max} = \left(\frac{\ell}{\delta}\right)_{max,i} \exp\left(-\frac{(x'/\delta)}{C_6}\right) \tag{4.25}$$

$(\ell/\delta)_{max,i}$ is the initial value of augmentation. It is given from the experimental evidence, as follows:

$$\left(\frac{\ell}{\delta}\right)_{max,i} = C_5 M \tag{4.26}$$

The coefficients for the parabola are given as:

$$c = \frac{4(\ell/\delta)_{max}}{W^2} \tag{4.27}$$

$$d = \frac{8(\ell/\delta)_{max}}{W^2}\left[\left(\frac{y}{\delta}\right)_i + \frac{W}{2}\right] \tag{4.28}$$

$$e = -\frac{4(\ell/\delta)_{max}}{W^2}\left(\frac{y}{\delta}\right)_i\left[\left(\frac{y}{\delta}\right)_i + W\right] \tag{4.29}$$

The values of the constants are:

$$C_5 = 0.496 \quad , \quad C_6 = 0.435 \quad , \quad C_7 = 0.333 \tag{4.30}$$

4.2.6 Region 5 of the mixing length

Experiments show that in this region the length scale is constant and it is $(\ell/\delta) = \lambda \cong 0.085$. The region begins after the augmented region and continues up to the free stream for both blowing ratios.

This region is the outer layer of the outer boundary layer, where the mixing length scales on the total thickness δ. In this region, the following empirical equation is given:

$$\left(\frac{\ell}{\delta}\right) = \lambda \quad \text{for} \quad \left(\frac{y}{\delta}\right)_i + W < \left(\frac{y}{\delta}\right) \tag{4.31}$$

4.2.7 Summary of the model equations

Region 1 (4.14): $\left(\frac{\ell}{\delta}\right) = \kappa\left(\frac{y}{\delta}\right)D \quad , \quad 0 < \left(\frac{y}{\delta}\right) \leq \left(\frac{y}{\delta}\right)_d$

Region 2 (4.16): $\left(\frac{\ell}{\delta}\right) = \kappa\left(\frac{y}{\delta}\right)_d \quad , \quad \left(\frac{y}{\delta}\right)_d < \left(\frac{y}{\delta}\right) \leq \frac{\lambda}{\kappa}$

Region 3 (4.17) $\left(\frac{\ell}{\delta}\right) = a\left(\frac{y}{\delta}\right) + b \quad , \quad \frac{\lambda}{\kappa} < \left(\frac{y}{\delta}\right) \leq \left(\frac{y}{\delta}\right)_i$

Region 4 (4.23) $\left(\frac{\ell}{\delta}\right) = \lambda + \left(\frac{\ell}{\delta}\right)_a \quad , \quad \left(\frac{y}{\delta}\right)_i < \left(\frac{y}{\delta}\right) \leq \left(\frac{y}{\delta}\right)_i + W$

Region 5 (4.31): $\left(\frac{\ell}{\delta}\right) = \lambda \quad , \quad \left(\frac{y}{\delta}\right)_i + W < \left(\frac{y}{\delta}\right)$

Unknowns in the above equations are:

Region 1 (4.15): $\left(\frac{y}{\delta}\right)_d = \frac{\lambda}{\kappa} + C_1 M \left[(x'/\delta) - C_2\right]$

$$D = 1.0 - \exp(-y^+/A^+) \qquad (4.32)$$

Region 3 (4.20): $$a = \frac{\lambda - \kappa(y/\delta)_d}{(y/\delta)_i - \lambda/\kappa}$$

(4.21): $$b = \frac{-\frac{\lambda^2}{\kappa} + \kappa(y/\delta)_d (y/\delta)_i}{(y/\delta)_i - \frac{\lambda}{\kappa}}$$

(4.18): $\left(\frac{y}{\delta}\right)_i = \frac{\lambda}{\kappa} + C_3 M \left[\left(\frac{x'}{\delta}\right) + C_4\right]$

Region 4 (4.22) $\left(\frac{\ell}{\delta}\right)_a = c\left(\frac{y}{\delta}\right)^2 + d\left(\frac{y}{\delta}\right) + e$

(4.27) $$c = -\frac{4(\ell/\delta)_{max}}{W^2}$$

(4.28) $$d = \frac{8(\ell/\delta)_{max}}{W^2}\left[\left(\frac{y}{\delta}\right)_i + \frac{W}{2}\right]$$

(4.29) $$d = -\frac{4(\ell/\delta)_{max}}{W^2}\left(\frac{y}{\delta}\right)_i\left[\left(\frac{y}{\delta}\right)_i + \frac{W}{2}\right]$$

(4.25) $\left(\frac{\ell}{\delta}\right)_{max} = \left(\frac{\ell}{\delta}\right)_{max,i} \exp\left(-\frac{(x'/\delta)}{C_6}\right)$

(4.26) $$\left(\frac{\ell}{\delta}\right)_{max,i} = C_5 M$$

(4.24): $W = C_7 M$

Constants:

C_1 = 0.0045 (controls the rate of recovery of $(y/\delta)_d$).

C_2 = 37.0 (number of boundary layer thicknesses at which $(y/\delta)_d$ approaches (λ/κ) or the 2-D internal layer coalesces with outer layer).

C_3 = 0.0275 (controls the rate at which the $(y/\delta)_i$ point advances, i.e., the rising of the effective jet centerline).

C_4 = 4.0 (controls the initial value of the $(y/\delta)_i$ point at the start of the recovery region).

C_5 = 0.496 (controls the magnitude of the initial augmentation).

C_6 = 0.435 (decay rate of augmentation).

C_7 = 0.333 (controls the width of the augmented region).

Figure 4.3 shows the experimental and modeled mixing lengths for $M = 0.4$ and $M = 0.9$ at the three different stations in the recovery region.

4.2.8 Comments on the number of constants

Except for the usual universal values of $\kappa = 0.41$ and $\lambda = 0.085$, seven constants were used to model the mixing length. The number of constants looks very large at first glance, but when examined more closely one can see that this number is reasonable. Three different flow structures are being modeled: inner and outer boundary layers and blend region in between, as well as their dynamics in the streamwise direction.

During the prediction process it was observed that the most important constants in the mixing length model were C_1, C_2, C_3, and C_4. The constants used to specify the augmented region (C_5, C_6, and C_7) did not prove significant. The augmented region did not have much effect on the predictions because it lies in the outer region of the boundary layer. It also decays rapidly. During computer experiments with W and

$(\ell/\delta)_{max}$, changing the values of C_5 and C_7 did not affect the results at all. It is possible that the augmented region can be completely eliminated for the recovery region predictions, thus reducing the number of constants to four. The constants were obtained from the empirical data rather than from computer experiments. Kacker & Whitelaw (1970) used five constants to model the mixing length for prediction of wall jet and wall-wake flows, which is similar to, but not more complicated than, the recovery region of the present full-coverage film-cooled surface. In the present model the augmented region is kept for convenience and for easy adaptation of this mixing length model to the full-coverage region where the peak of augmentation moves closer to the wall and is important for the prediction of heat transfer.

In the recovery region predictions, especially for $M = 0.9$, the most important region of the mixing length turned out to be the reduced mixing length region near the wall. Without correct modeling of this region predictions always failed. The first four constants are the important ones in the recovery region predictions.

4.2.9 General remarks about the mixing length

It was observed that only regions 2, 3, and 4 show deviations from a usual 2-D mixing length model. Region 2 proved especially interesting, because it had been thought that the jet mainstream interaction would increase the mixing length above the 2-D value (Choe et al., 1975; Crawford et al., 1976). Choe et al. (1975) and Crawford et al. (1976) calculated the mixing length for low blowing and in the full-coverage region. They observed that the augmented region (Region 4) moved closer to the wall and did not observe Regions 2 and 3, which are more easily observable for high blowing. In reality, Regions 2 and 3 are very important in predictions, as is explained in Section 4.3.1.

4.2.10 Physical explanation of recovery to 2-D state in the mixing-length model

The relaxation to the 2-D state takes place in the following manner. As the cumulative effects of jets move downstream and diffuse out, they lose their strength and the augmentation dies out (~ 3 or 4δ), but the

effective centerline of the jets (the $(y/\delta)_i$ point) continues to rise. At the same time the inner 2-D boundary layer thickness δ' grows faster than δ (δ almost stops growing after the injection stops), and finally, when they merge (in approximately 40δ), the recovery process is complete.

4.3 Predictions

The mixing length model, along with the TKE equation, was used as a one-equation model of turbulence in the 2-D boundary layer program STAN5 (Crawford & Kays, 1975). Starting with the spanwise-averaged mean velocity and TKE profiles at the beginning of the recovery region ($x = 188$ cm), very successful predictions of TKE and the mean velocity profiles for $M = 0.4$ and $M = 0.9$ were obtained at two downstream stations in the recovery region ($x = 214$ cm, 256 cm).

Figure 4.4 shows a comparison of the predicted mean velocity and TKE profiles with the experimental data for $M = 0.4$ on the two stations in the recovery region, starting with the spanwise-averaged initial profiles. The prediction of mean velocity on plate 11 ($x = 214$ cm) is somewhat high in the middle region of the boundary layer, but the difference lessens by the 27th plate ($x = 256$ cm). For TKE profiles the predictions are somewhat low. These figures show that the model predicts a slightly faster recovery to the 2-D state than the physical process, but the difference is not that great. The reason for lower TKE predictions might be the mixing length. In Fig. 4.3 the mixing-length model for $M = 0.4$ is slightly lower compared to measurements in the region $0.15 < (y/\delta) < 0.3$. This means that the model results in a smaller production and a higher dissipation than the reality, yielding lower TKE values compared to the experiment.

Figure 4.5 shows a comparison of the mean velocity and TKE profiles with the experimental data for $M = 0.9$ on the two stations in the recovery region, starting with the spanwise-averaged initial profiles. The suggested model predicts the $M = 0.4$ case well. The predictions for the $M = 0.9$ case are excellent. It is important to remember that the constants do not change with the blowing ratio. Both cases were predicted with the same set of constants for the mixing length and the other

constants in the one-equation model are the usual ones employed for 2-D boundary layer predictions. The author believes that the model will successfully predict blowing ratios up to M = 1.0. Further extrapolation of the model might be dangerous due to the changing hydrodynamic character of the flows.

4.3.1 The effect of reduced mixing on predictions

As previously mentioned, it is important to consider the effect of the reduced mixing near the wall in making predictions. This is demonstrated by Fig. 4.6. This figure shows the comparisons of the experimental data with the predictions of TKE (in the recovery region on the 27th plate for M = 0.9). The predictions were made with two different mixing length models. One of them is the normal 2-D flat-plate mixing length, and the other is the model developed in this study, which has a smaller value near the wall relative to the former. The new model predicts perfectly, whereas the usual 2-D mixing length predicts much higher TKEs almost up to the first half of the boundary layer. The reason lies in the relationship between the mixing length and the production and dissipation of TKE. Higher mixing lengths increase the production and reduce the dissipation, giving rise to higher TKEs.

The reduced mixing region did not have a significant effect on near-velocity profiles; however, it is important in heat transfer behavior because of its influence on the turbulence level.

4.4 Refining the Model

The empirical curve fits described in section 4.2.7 do in fact match the boundary layer behavior. The physical arguments are plausible and suggest that the empirical relations could be replaced (if desired) by more conventional forms. In this section some possible alternative equations are examined -- without changing the physical arguments -- both for the purpose of testing the physical argument for reasonableness of the magnitudes and to take advantage of established forms where possible.

4.4.1 The outer edge of the inner boundary layer

$$\left(\frac{y}{\delta}\right)_d = \frac{\lambda}{\kappa} + 0.0045\ M\left[\left(\frac{x'}{\delta}\right) - 37\right] \tag{4.15}$$

Using a conventional equation to describe the growth of the internal boundary layer growth (Schlichting, 1968) yields:

$$\frac{\delta'}{(x+x_o')} = 0.37\left(\frac{\rho\overline{U}(x+x_o')}{\mu}\right)^{-1/5} \tag{4.33}$$

δ' and $(y/\delta)_d$ are related as follows:

$$\text{At } \left(\frac{y}{\delta}\right)_d, \quad \left(\frac{y}{\delta'}\right) = \frac{\lambda}{\kappa} \tag{4.34}$$

Therefore,

$$\frac{(y/\delta)_d}{(y/\delta')} = \frac{(y/\delta)_d}{(\lambda/\kappa)} \tag{4.35}$$

or

$$\frac{\delta'}{\delta} = \frac{(y/\delta)_d}{(\lambda/\kappa)} \tag{4.36}$$

Consequently, if one knows the initial value of δ and $(y/\delta)_d$ at $x' = 0$, then the initial δ' can be calculated and x_o' determined from the formula. After x_o' is found, the rest of δ' and $(y/\delta)_d$ can be obtained from the boundary layer growth formula.

In Eqn. (4.33) the value of U_∞ can be used for the value of $\overline{U}$ since $\overline{U}$ at $\delta'_{.99}$ is never far from U_∞. For example, for $M = 0.9$ the velocity profile is so flat that near $\delta'_{.99}$

$$\overline{U} \sim U_\infty$$

For $M = 0.4$ the initial thickness of this boundary layer is large (because there is less disturbance), and again around $y \sim \delta'$, $\overline{U} \sim U_\infty$. One might question the use of Eqn. (4.33) to predict the growth of the inner layer, since it neglects the effect of the turbulence of the outer regions. It seems justified, however, because around δ' the turbulence levels are quite small for both cases studied here (3%-5%).

By using $\overline{U} \simeq U_\infty = 16.7$ m/sec, $\rho = 1.2$ kg/m^3, $\mu = 0.9 \times 10^{-5}$ kg/msec, the virtual origin of the internal 2-D boundary layer can be calculated for both cases from the initial value of $(y/\delta)_d$. The following values were obtained:

$$\text{For } M = 0.4 \quad , \quad x'_o = 1.29 \text{ m}$$

$$\text{For } M = 0.9 \quad , \quad x'_o = 0.41 \text{ m}$$

$(x'_o)_{M=0.4}$ is greater than $(x'_o)_{M=0.9}$, which is normal because for low blowing, the undisturbed region near the wall is larger. After calculation of virtual origins, the following comparisons were obtained between the piecewise model and the internal boundary layer growth formula.

M = 0.4

δ'(m) \ (x'/δ)	0	~ 5	~ 12
Piecewise Model	0.028	0.036	0.045
Boundary Layer Formula	0.028	0.033	0.040

M = 0.9

δ'(m) \ (x'/δ)	0	~ 5	~ 12
Piecewise Model	0.011	0.018	0.028
Boundary Layer Formula	0.011	0.017	0.025

As is seen from the comparison, the present linear model and the boundary layer growth results compare quite well. In fact, when one looks at the data, the boundary layer formula seems to be closer.

The following changes can be suggested in the present model. Instead of calculating $(y/\delta)_d$ from the piecewise linear formula (Eqn. (4.15)), $(y/\delta)_{d,\text{initial}}$ can be calculated, which involves only one empirical constant. Then, using

$$\frac{\delta'_{initial}}{\delta} = \frac{(y/\delta)_{d,initial}}{(\lambda/\kappa)} \tag{4.37}$$

$\delta'_{initial}$ can be found, and

$$x'_o = \left[\frac{\delta'_{initial}}{0.37\left(\frac{\rho U_\infty}{\mu}\right)^{-1/5}}\right]^{5/4} \tag{4.38}$$

Other δ' can be calculated as follows:

$$\delta' = (x' + x'_o)\ 0.37\left(\frac{\rho\bar{U}\ (x' + x'_o)}{\mu}\right)^{-1/5} \tag{4.39}$$

and

$$\left(\frac{y}{\delta}\right)_d = \left(\frac{\lambda}{\kappa}\right)\left(\frac{\delta'}{\delta}\right) \tag{4.40}$$

Here, even though the equation for boundary layer growth is still empirical, it is more universal than the constant supplied in the formula for $(y/\delta)_d$. So the $(y/\delta)_d$ formula can be reduced to one empirical constant supplied by the present experiments and a more universally accepted empirical equation.

4.4.2 Comparison of the development of the $(y/\delta)_i$ point with jet spreading theory

It is argued that the dynamics of the $(y/\delta)_i$ point corresponds to the rising of the effective jet centerline. In this section, the output of the empirical equation for $(y/\delta)_i$ (Eqn. (4.18)) is compared with the results of an equation describing the rising of the centerline of a jet in crossflow (Abramovich, 1960):

$$\left(\frac{x' + x''_o}{D}\right) = \left(\frac{1}{M^2}\right)^{1/3}\left(\frac{y}{D}\right)^3 + \left(\frac{y}{D}\right)\cot\alpha' \tag{4.41}$$

Here x''_o is the virtual origin for the effective jet action, D is the diameter of a single jet, and α' is the injection angle. The solution of this equation depends on four parameters: x''_o, D, M and α'. The last three are supplied by the problem physics, and the only unknown is the virtual origin, which can be calculated from the empirical input, i.e.,

from the initial value of $(y/\delta)_i$, assuming that effective jet spread occurs according to the equation (4.41).

The results of the virtual origin calculation are:

$$\text{For } M = 0.4 \quad , \quad x_o'' = 0.13 \text{ m}$$

$$\text{For } M = 0.9 \quad , \quad x_o'' = 0.055 \text{ m}$$

Then, with these results and from Eqn. (4.41), the spreading of the jets can be calculated and compared with the present model values of $(y/\delta)_i$. The results:

M = 0.4

$(y/\delta)_i$ \ (x'/δ)	0	∿5	∿12
Piecewise Model	0.244	0.3	0.37
Jet Spread Formula	0.244	0.3	0.333

M = 0.9

$(y/\delta)_i$ \ (x'/δ)	0	∿5	∿12
Piecewise Model	0.3	0.424	0.59
Jet Spread Formula	0.3	0.55	0.67

As is seen again, the comparison is not bad. This supports the argument that $(y/\delta)_i$ point moves out with distance similar to the jet centerline.

The following changes can be made in the model to replace the constant C_3 with the more accepted empirical equation; or with this physically supporting agreement, the old model for $(y/\delta)_i$ can be left as it is. The change is as follows. Calculate

$$\left(\frac{y}{\delta}\right)_{i,\text{initial}} = \frac{\lambda}{\kappa} + C_3 C_4 M \qquad (4.42)$$

Then

$$y_{initial} = \delta\left(\frac{y}{\delta}\right)_{i,initial} \tag{4.43}$$

Calculate x''_o from

$$\frac{x''_o}{D} = \left(\frac{1}{M^2}\right)^{1.3} \left(\frac{y_{initial}}{D}\right)^3 + \frac{y_{initial}}{D} \cot \alpha' \tag{4.44}$$

Then calculate new y_i's from

$$\frac{x' + x''_o}{D} = \left(\frac{1}{M^2}\right)^{1/3} \left(\frac{y}{D}\right)^3 + \frac{y}{D} \cot \alpha' \tag{4.41}$$

4.4.3 Other changes suggested

To include the effect of P/D (pitch-to-diameter ratio, the blowing ratio M in the formulas can be replaced by

$$F = M\left(\frac{D^2}{4P^2}\right)$$

or by

$$F' = M^2\left(\frac{D^2}{4P^2}\right)$$

which reflects the relative effects of the jet and free stream momentum. It is thought that it will be better to replace them by F'; by inclusion of an empirical jet spread equation (4.10), the variation in the injection angle (α') can be represented in the model.

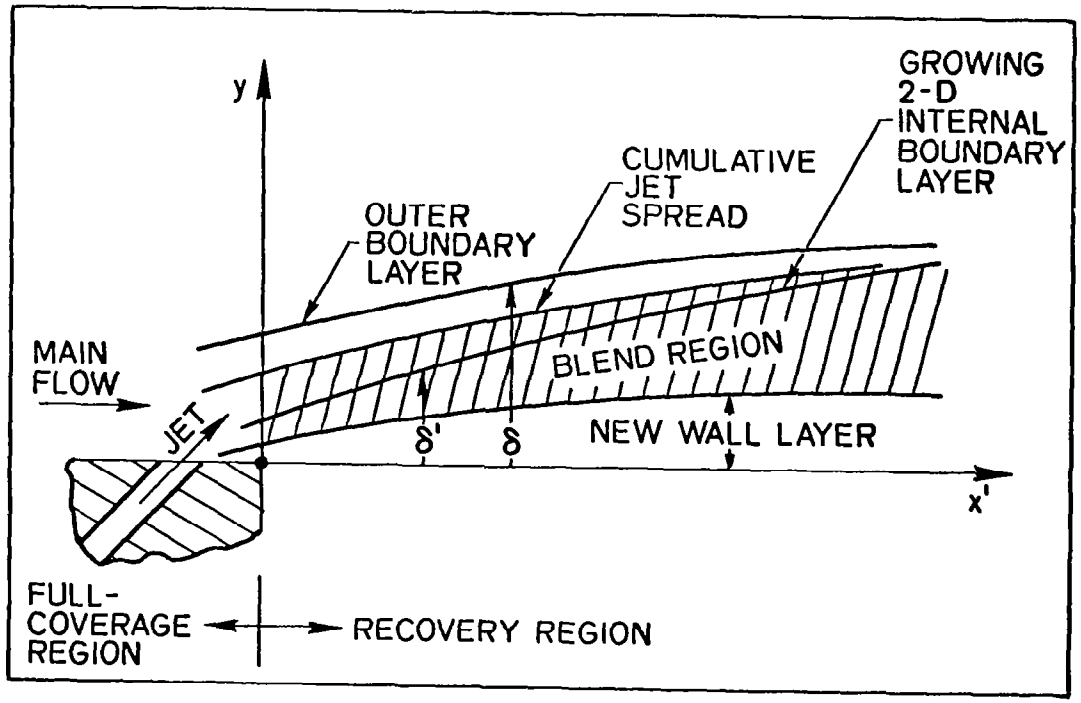

Fig. 4.1. Flow structure in the recovery region.

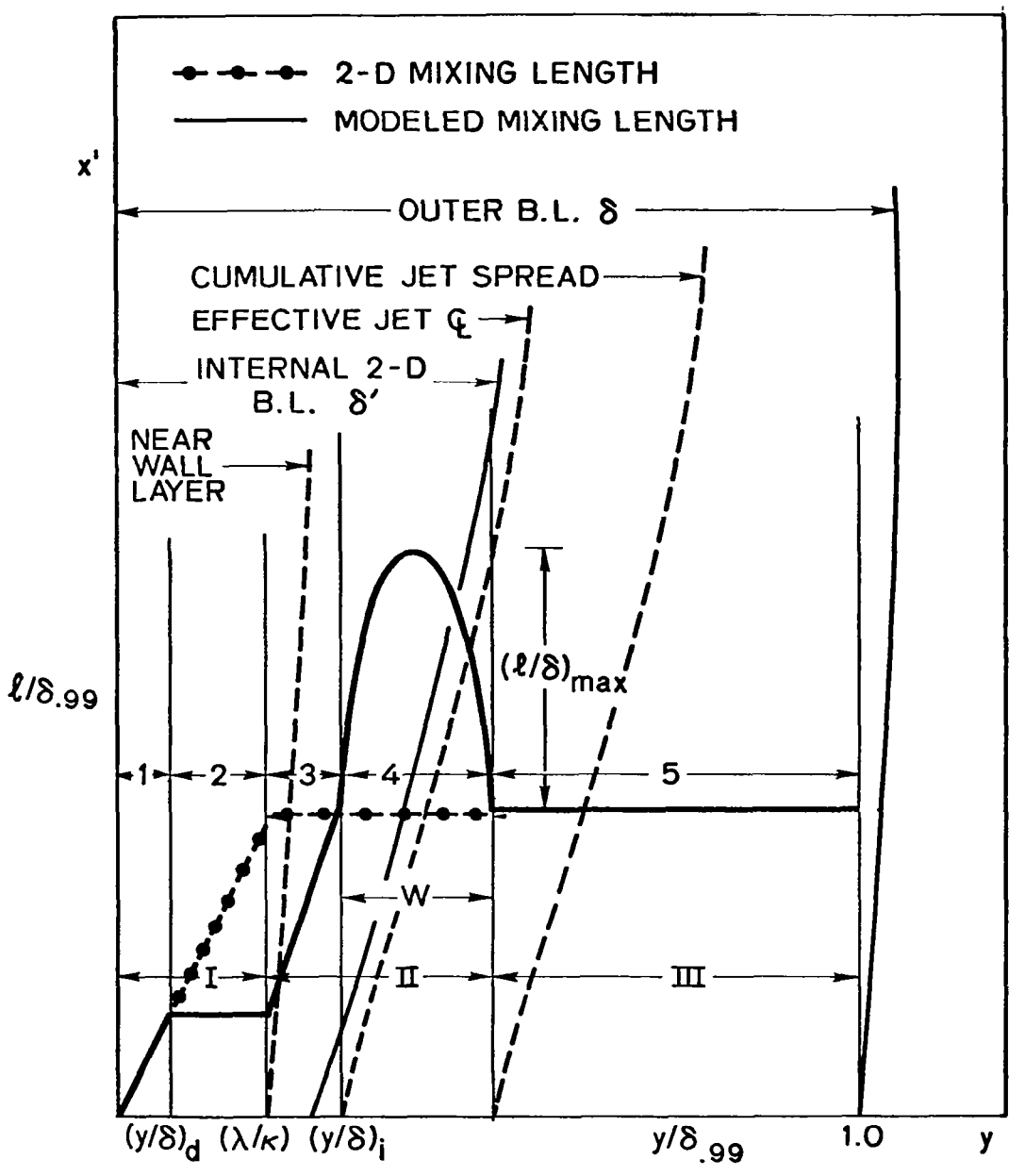

Fig. 4.2. Mixing-length model and flow structure in the recovery region.

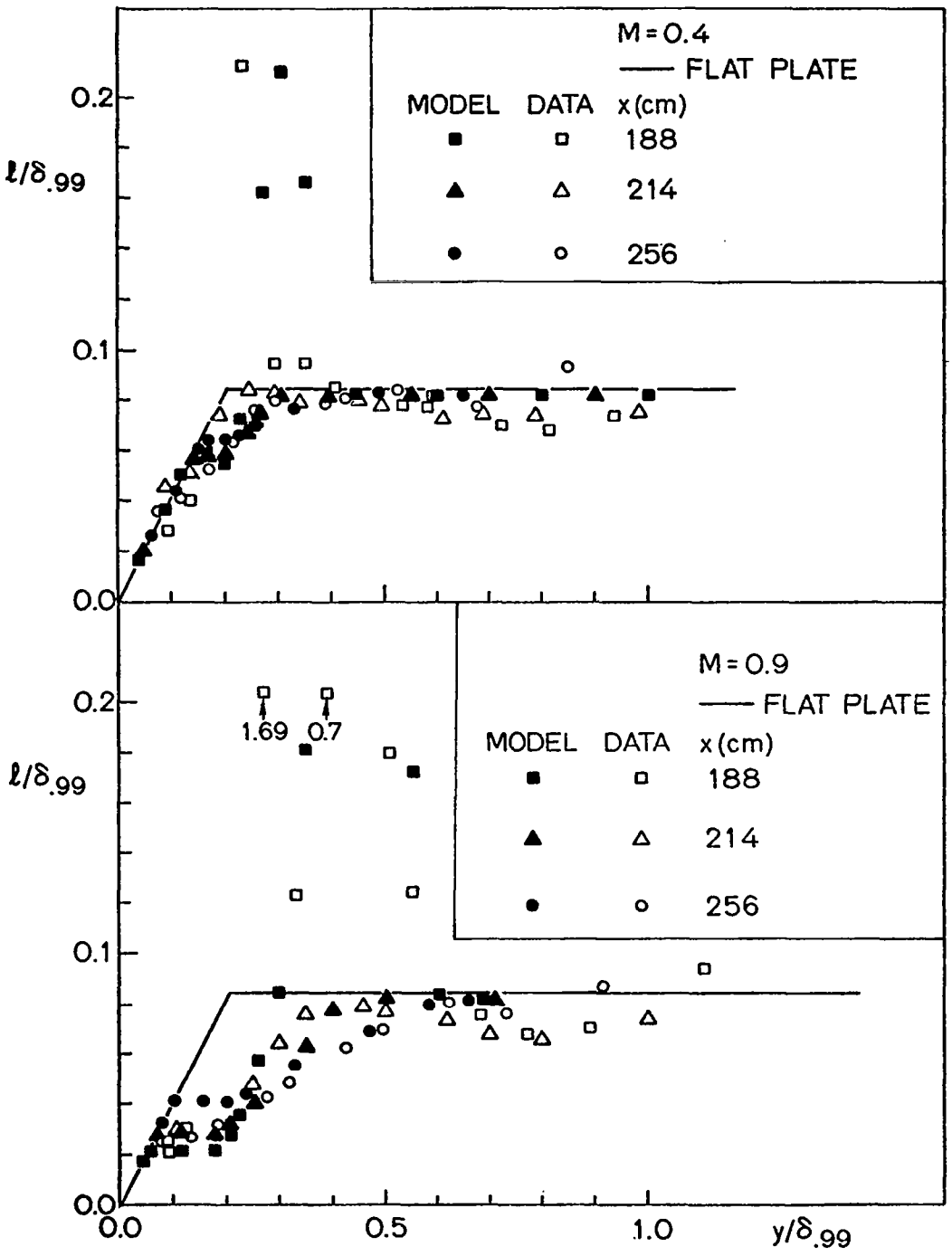

Fig. 4.3. Comparisons of the piecewise mixing-length model and the data in the recovery region.

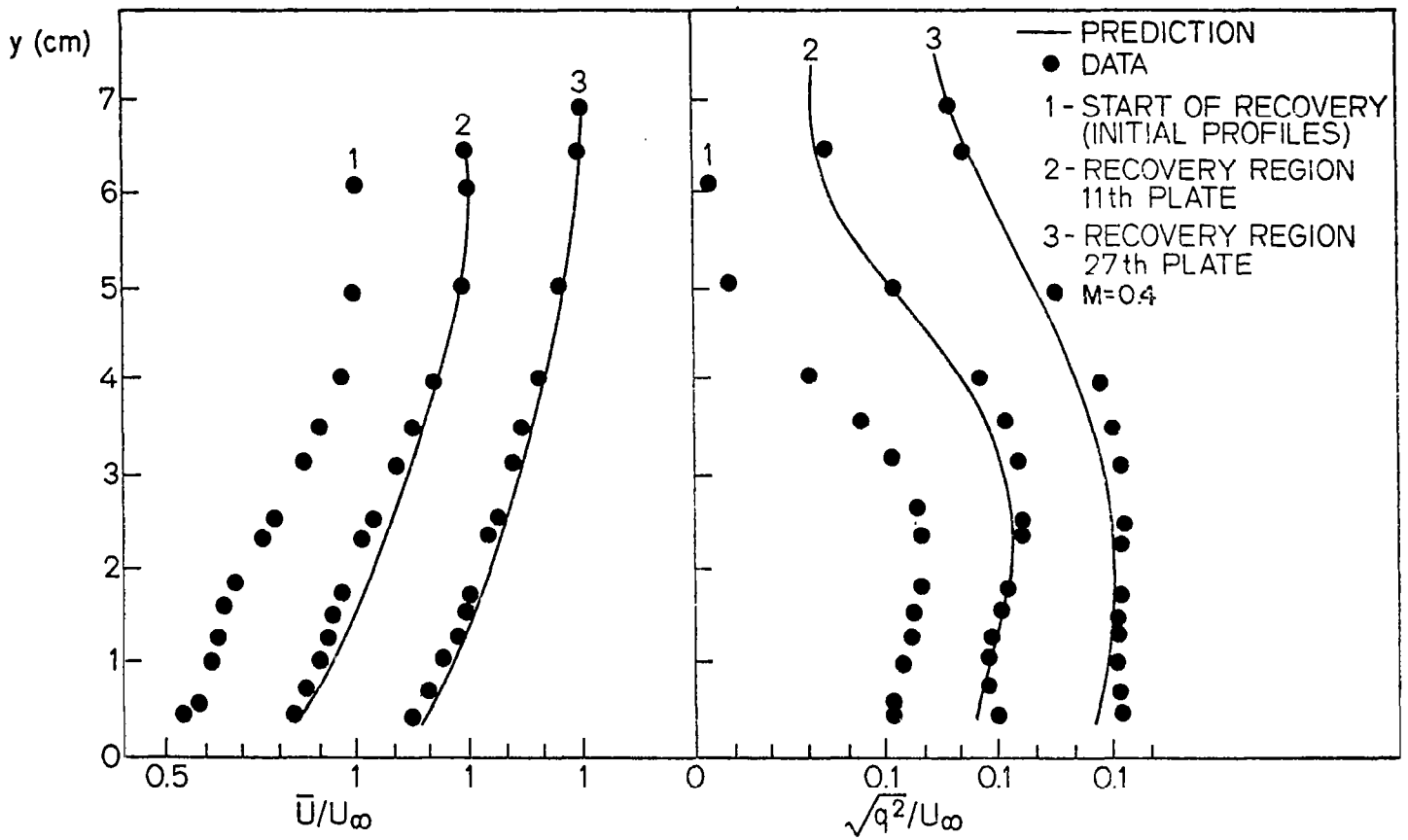

Fig. 4.4. Predictions of streamwise mean velocity component $(\bar{U})$ and turbulent kinetic energy (q^2) for M = 0.4.

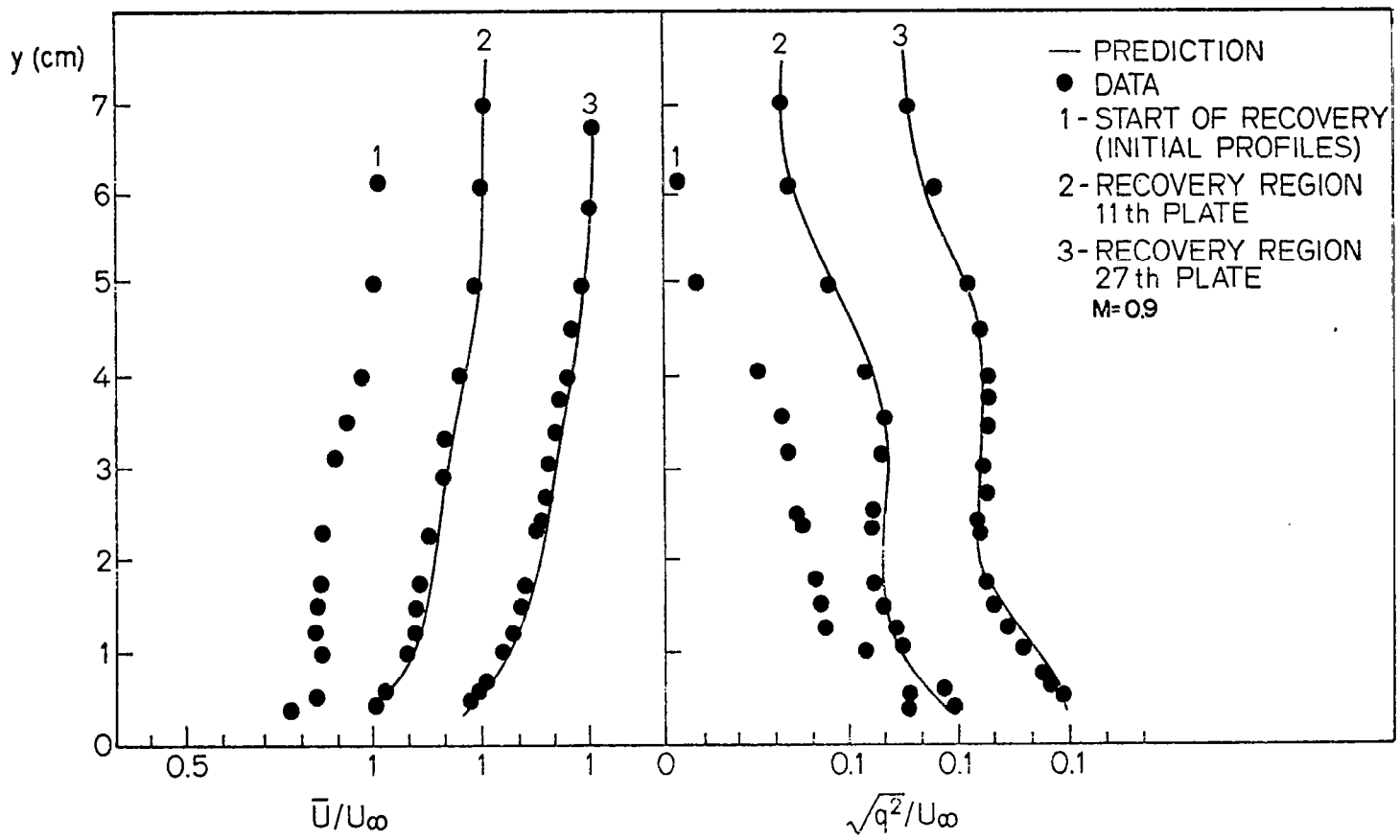

Fig. 4.5. Predictions of streamwise mean velocity component ($\bar{U}$) and turbulent kinetic energy (q^2) for M = 0.9.

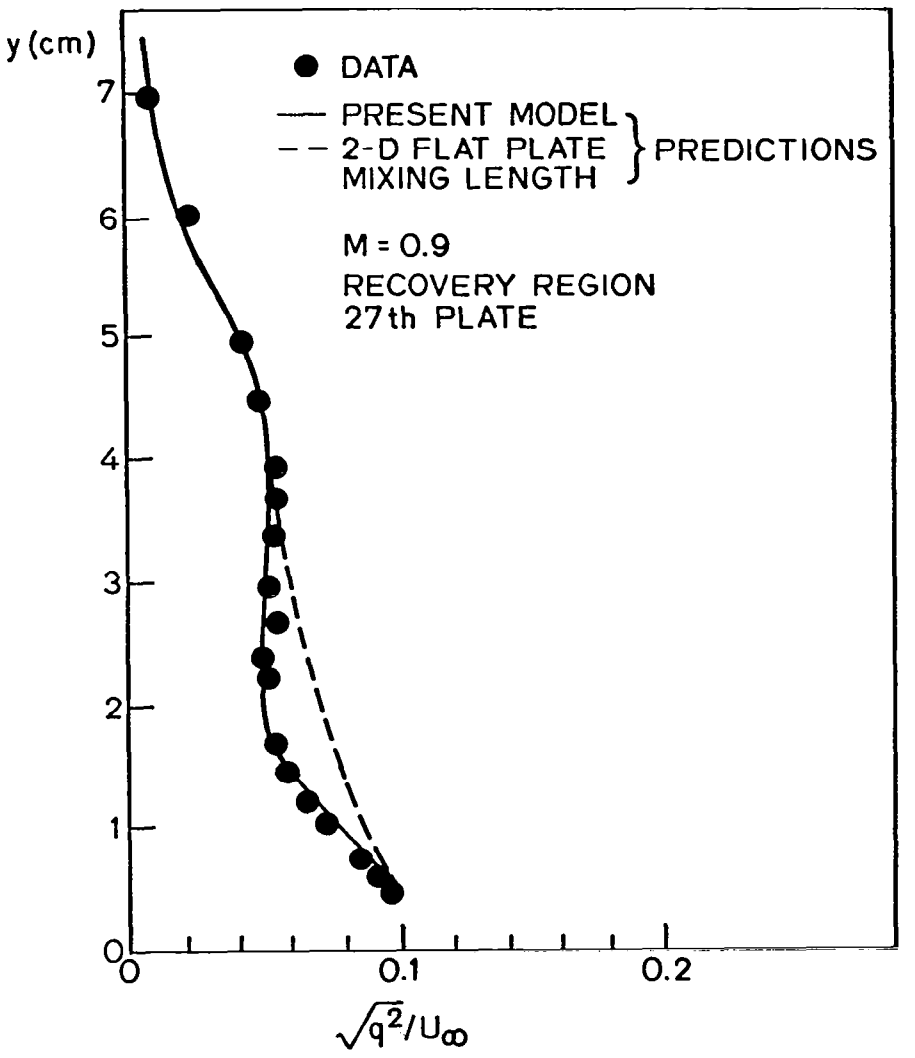

Fig. 4.6. Effect of mixing-length on predictions of turbulent kinetic energy.

Chapter 5

MEASUREMENTS AND DISCUSSIONS OF THE DATA

Measurements were made to supply the necessary empirical input for development of turbulence models for the recovery region following a full-coverage, film-cooled region. The final objective of the turbulence modeling was to obtain correct predictions of the heat transfer coefficient. This chapter will discuss the experimental conditions, measurement locations, and the data. Due to the large volume of the data, only the parts which directly concern the prediction process will be discussed in detail.

5.1 Experimental Conditions

The experiments were made under isothermal conditions, with air temperatures around 22-25°C. Since the heat transfer experiments were made with small temperature differences (16°), it was believed that the hydrodynamics of the isothermal flow field would be the same as that of non-isothermal heat transfer experiments. This question was investigated by Harnett, Birkebak & Eckert (1961). The pressure levels were about atmospheric ($\sim$ 760 mm of mercury), and the experiments were made at a uniform free stream velocity of approximately 16 m/sec. The velocity of the free stream was kept uniform along the test section by adjusting the top wall (as explained in Crawford et al., 1976), so that the static pressure change along the tunnel was less than $\pm 0.8\%$ of freestream dynamic head ($\pm$ 0.005 inches of water).

Experiments were made at two different blowing ratios: $M = 0.4$ and $M = 0.9$ ($M = U_{jet}/U_{\infty}$). The $M = 0.4$ blowing ratio was chosen because, during heat transfer experiments, minimum Stanton numbers on the test section were obtained here, as demonstrated by Crawford et al. (1976). The second blowing ratio, $M = 0.9$, was chosen because a definite change in the heat transfer behavior was seen at this high blowing ratio.

5.2 Measurement Locations

The schematic of the test section is given in Fig. 2.4. The jets are injected into the main stream at a 30° angle with the horizontal plane, and the injection is in line with the main flow direction. Due to the interaction of the jets and the main flow, a 3-D high-fluctuation flow field is created, at least locally, around the secondary air jets. All the measurements of the velocity field were made with the 3-D Turbulent Flow Analyzer system introduced in Chapter 3.

The measurement locations can be seen in Fig. 5.1. Five streamwise positions were selected for measurements to observe the development of the flow field on the full-coverage surface and its relaxation in the recovery region. The first is located at the center of the 5th plate (x = 148 cm) after three rows of blowing, and the second is at the center of the 9th plate (x = 168 cm) after seven rows of blowing in the full-coverage region. The third one is at the center of the first plate (x = 188 cm) in the recovery region after 11 rows of blowing. The last two are at the centers of the 11th (x = 214 cm) and 27th plates (x = 256 cm) and are, respectively, 27 and 67 hole diameters downstream from the last row of injection holes. In order to see spanwise variations in the flow, several measurements were made at each streamwise position. At the first and third stations, five spanwise locations were used, situated at z/P = + 05, + 0.3, 0.0, -0.3, and -0.5. Since the flow field is periodic, it repeats itself after $z/P = + 0.5$ and $- 0.5$. At the second streamwise location three spanwise locations were selected at $z/P = + 0.5$, 0.0, and $- 0.5$. In the recovery region for $M = 0.9$, at each streamwise location three spanwise locations were used. After the experiments it was seen that the profiles in the recovery region station were the same in all three spanwise locations, as illustrated by Figures 5.4 and 5.9. So for $M = 0.4$ these spanwise locations were eliminated in the recovery region. The profiles were used to obtain the necessary spanwise-averaged input to the 2-D boundary layer program STAN5. Measurements were made at each location of the three mean velocities and the six Reynolds stresses. Each quantity was averaged over 22 seconds to include the effects of low-frequency fluctuations.

5.3 Mean Velocity Profiles

In this section attention will be given to the streamwise component of the mean velocity $\overline{U}$, rather than discussing the three-dimensionality of the flow around the holes. Two sets of profiles for different blowing ratios will be discussed and compared with each other.

5.3.1 Mean velocity profiles for M = 0.4

Figure 5.2 shows the mean velocity profiles at each spanwise location, at each of the five streamwise stations, for the blowing ratio M = 0.4. The location of each of the traversing stations is marked on each figure with respect to the injection locations.

The first observation on this figure is the remarkable symmetry of the profiles from positions which are symmetric with respect to the centerline. This proves that there is periodicity in the spanwise direction and that the coalescing of the upstream jets is regular. Periodicity is very helpful in spanwise averaging.

In the full-coverage section, two distinct regions appear in each of the profiles. In the outer region all spanwise profiles are the same; however, in the near-wall region, differences are observed in the spanwise profiles because of injection. The same observation was made by LeBrocq, Launder & Priddin (1971) for a 45° injection. The spanwise profiles also show some common behavior. The central profiles just downstream of a jet show the greatest velocity defect, because they are affected directly by injection. The profiles at the outer edges show less defect than the central profiles but more defect than the intermediate positions (between two holes). This is expected, because the outer profiles are affected by the injection one row upstream and are still recovering from the effect of that injection, while the profiles between two holes have no injection in line with them and are affected only by the lateral spreading of jets. This is clearly seen in Fig. 5.2, where, after three rows of blowing, the intermediate profiles show almost no defect, thus indicating that the effect of lateral spreading has not reached them with its full force yet. After 11 rows of blowing, however, the momentum defect in the intermediate profiles can easily be observed.

The size of the near-wall momentum defect region increases downstream. The velocity defect region after 11 rows of blowing is almost twice as large as after three rows of blowing. This indicates the cumulative effect of upstream jets which keep rising as they spread downstream. The jets penetrate only about 2 cm, immediately after injection, as can be seen from the figure, the point where there is an abrupt change in the slope of the profiles. The immediate penetration distance is about two jet diameters for this blowing ratio. This means that the mass shed into the boundary layer by each injection row penetrates to an almost constant distance for a certain blowing ratio at the injection location before jets are knocked down by the main stream. The immediate penetration distance increases slightly in a downstream direction as the boundary layer loses momentum due to the effect of previous injections. This constant penetration distance was also observed by Le Brocq, Launder & Priddin (1971), Crawford et al. (1976), Colladay & Russel (1975), and Ramsey & Goldstein (1971).

There is no indication of a reverse flow and separation of the jet from the surface in any of the full-coverage region profiles. This might be due to the fact that the profiles were measured at locations where jets have already reattached themselves to the surface. The measurement locations were 2.5 hole diameters downstream from the edge of the closest hole. The separation of jet from the surface was observed by Bergeles, Gosman & Launder (1975) for normal blowing at a blowing ratio of $M = 0.24$, and extended only to 1.5 diameters downstream of the hole. It is generally agreed in the literature (Le Brocq, Launder & Priddin, 1971; Colladay & Russell, 1972) that slant-injection jets stay attached to the surface at much higher blowing ratios compared to a normal injection. Launder & York (1973) state that for a 45° in-line injection with $P/D = 8$, jets attach to the surface at 3-4 hole diameters downstream of the last injection for $M \approx 0.6$. These observations help one arrive at the conclusion that the jets for the 30° slant injection for $M = 0.4$ reattach to the surface in a very short distance downstream or perhaps don't separate at all.

The points which are closest to the wall in all the mean velocity profiles have almost the same value of $\bar{U}/U_\infty$ for the same spanwise

locations at all streamwise stations. For the central profiles the value is $\overline{U}/U_\infty = 0.35\text{-}0.4$. This number can be obtained by multiplying the value of the blowing ratio ($\overline{U}_{jet}/U_\infty = 0.4$) with the cosine of the injection angle (30°). This is a definite indication of the average jet velocity in the near-wall region. It was observed by Bergeles, Gosman & Launder (1975) that the velocity in the exit plane of jets is not uniform at all; however, the present work shows that even though the velocity is not uniform, the effect is governed by the average jet velocity given by $M \times U_\infty$.

In Fig. 5.2, curves representing $(1/7)^{th}$ power profiles are shown at the start of the recovery region (after the last row of injection) and at the two measurement stations in the recovery region as reference lines to make the cross-comparisons easier. It was expected that, finally, in the recovery region, the boundary layer would return to a normal 2-D flat-plate boundary layer. A $(1/7)^{th}$ power profile was chosen to represent the flat-plate mean velocity profile, although any curve which is close to a 2-D turbulent boundary layer profile could have been chosen as a reference line. A spanwise-averaged profile is also shown (for the profiles at the start of the recovery region only). When compared to the $(1/7)^{th}$ power profiles, it can be seen that the momentum defect decreases as the boundary layer recovers from the blowing. However, there is a considerable momentum deficit even at the last recovery region station due to the large initial deficit. The reason for the long recovery distance is the "momentum-sink" action of the wall. The diffusion of momentum from the free stream is the only way for these profiles to recover to 2-D flat-plate profiles, and diffusion is a slow process. The long recovery distance indicates that the effects of jets near the wall prevail over long distances for low blowing.

Velocity gradients at the wall are smaller than for a 2-D flat-plate profile; this will give lower friction factors. There is also no indication of boundary layer separation except locally at the injection points. Thus, the aerodynamic behavior of the 30° slant-hole in-line injection with $M = 0.4$ is quite good. Since this blowing also gives the lowest heat transfer coefficients (Crawford et al., 1976), it is a very important

blowing ratio in full-coverage film-cooling applications. Le. Brocq, Launder & Priddin (1971) agree with this conclusion.

Even though the jets initially penetrate to a constant distance (two hole diameters), comparisons with the $(1/7)^{th}$ power profiles show that their cumulative effect on the momentum deficit can be observed at much larger distances from the surface due to the rising of the effective jet centerlines in the downstream direction. The jets continue to rise even at large distances from the last row of holes. This observation was also made by Keffer and Baines (1963).

Figure 5.3 shows the spanwise-averaged mean velocity for $M = 0.4$ in (y/δ) and $\overline{U}/U_\infty$ coordinates. The profile at $x = 168$ cm is not to be trusted quantitatively near the wall. Only three spanwise profiles were taken at this location, and the spanwise averaging of three profiles does not represent a physically correct average. This point is further explained in section 5.6. It is plotted here, however, for comparisons in the outer layers where the spanwise profiles are not very different from each other, and the resulting average is correct. The profile after three rows of blowing ($x = 148$ cm) has the largest momentum defect, but the difference from the others is not great. This means that the region near the wall is governed by the latest injection and stays almost at the same level of $\overline{U}/U_\infty$. The effects of previous rows can be seen in the outer layers. For example, in the outer regions, the profile at $x = 148$ cm is very close to the profile at the last recovery station ($x = 256$ cm). This means that the jets cannot strongly affect the outer layers at this distance. The outer region profiles are very similar after 7 and 11 rows of blowing ($x = 168$, 188 cm, respectively) and in the recovery region profile at 27 hole diameters downstream of the last row of injection ($x = 214$ cm). The result of these observations can be summarized as follows: after four or five rows of blowing it appears that the boundary layer reaches a state of equilibrium in a large part of the boundary layer (almost above $y/\delta \geq 0.1$) for low blowing. This may be very helpful in the modeling of the injection process in the full-coverage region.

5.3.2 Mean velocity profiles for M = 0.9

Figure 5.4 shows the spanwise mean velocity profiles at five streamwise stations for the blowing ratio of M = 0.9. Spanwise symmetry can be observed, as in M = 0.4. This indicates uniform lateral jet spread. Nina & Whitelaw (1971) cautioned against non-uniform coalescing of jets in full-coverage film-cooling applications; such a phenomenon is not observed here.

Again, two distinct regions can be observed in the profiles, an outer and an inner one. In the outer region all the spanwise profiles are the same at a certain streamwise station. In the inner region, however, there are differences in the profiles, depending on the spanwise location. The size of the inner region is very large compared to the M = 0.4 case because of the higher rate of blowing and deeper penetration of the jets. The jets penetrate up to three hole diameters at M = 0.9, and this distance is almost the same for all the stations.

Another difference between the cases is the excess momentum near the wall in M = 0.9 because of the high blowing ratio. This can be observed by comparing the spanwise-averaged profile to the $(1/7)^{th}$ power reference curve at the third streamwise location.

In the central profiles just downstream of a jet, a local maximum in velocity occurs around y = 1 cm with $\overline{U}/U_\infty$ = 0.85-0.9 (this was not observed for M = 0.4). This point is the centerline of the new injected jet, about one hole diameter above the surface. This can be observed at the same location in every station of the full-coverage region. This maximum in the streamwise mean velocity was also observed by Le Brocq, Launder & Priddin (1971) for M = 0.5 and P/D = 8 for 45° injection. This is another indication of the fact that the depth of immediate penetration is constant.

It is important to observe that at the point closest to the wall in the central profiles, there is a sharp decrease in the velocity. This indicates that the jet has separated from the surface and has not reattached yet at the measurement location (about 2.5 diameters downstream of the hole). However, the same phenomenon is not observed in the side profiles, which are 7.5 hole diameters away from the last injection location. Therefore, it can be concluded that, for the case of M = 0.9,

jets reattach to the surface somewhere between 2.5 and 7.5 hole diameters downstream of their injection location. This was also observed by Colladay & Russell (1975) and by Launder & York (1973). The separation of the protective jet from the surface explains the poor heat transfer behavior (high heat transfer coefficients) of the $M = 0.9$ case observed by Crawford et al. (1976).

In Fig. 5.4, $(1/7)^{th}$ power profiles are shown at the start of the recovery region and at the two recovery region stations as reference lines for comparison. A spanwise average is also shown for the profiles at the beginning of the recovery region.

The spanwise-averaged mean velocity profile has a region of negative slope (as can be seen in section 5) which gives rise to a locally negative shear stress.

There is a rapid relaxation back to the 2-D state in the recovery region, as can be seen from the comparison of the profiles in this region with $(1/7)^{th}$ power profiles. In fact, the profile at the last recovery region station is almost the same as the $(1/7)^{th}$ profiles, except for a small momentum deficit in the outer layer. Relaxation back to the 2-D state is much faster for $M = 0.9$ than for $M = 0.4$ because of the excess momentum near the wall. The wall acts as a momentum sink and facilitates the relaxation process. In the outer layer, where there is some momentum deficit, the relaxation process is very slow. The momentum supplied by the free stream entrainment and by the transport is not large enough for rapid relaxation.

Higher velocity gradients near the wall (when compared with the $(1/7)^{th}$ profile and the $M = 0.4$ profiles) lead to larger skin friction coefficients, thus increasing the aerodynamic drag. Increase in the skin friction coefficitn with blowing was observed by Kacker & Whitelaw (1970) for a 2-D wall jet.

One observes generally the lack of velocity gradient all over the $M = 0.9$ mean profiles except at the wall. This yields low shear stresses and low TKEs (low turbulent mixing) in a large part of the boundary layer. Samuel & Joubert (1965) also observed that the closer the M is to unity, the lower the turbulent mixing is for a 2-D

injection. Seban & Back (1962) made the same observation in the case of a 2-D tangential injection.

In Fig. 5.5, spanwise-averaged profiles for five streamwise locations are plotted on (y/δ) and $\overline{U}/U_\infty$ coordinates for $M = 0.9$. A very clear outer layer similarity is observed in these coordinates; the profiles lie much closer to each other than in the same case for $M = 0.4$. The similarity is not observable below $(y/\delta) = 0.25$. The high rate of blowing causes non-equilibrium in the region near the wall. Another indication of this non-equilibrium can be seen in Fig. 5.4. The intermediate profiles in each streamwise location get fuller downstream as the preceding jets expand laterally; they do not reach an equilibrium even after 11 rows of blowing.

Figure 5.6 shows the spanwise-averaged mean velocity components in semi-logarithmic coordinates $(\overline{U}/U_\infty$ vs. $\ell n\ y)$ for $M = 0.4$ and $M = 0.9$. No logarithmic region can be seen in the profiles for either case, in the full-coverage region. The signs of the curvatures of the profiles in the full-coverage region are opposite for different blowing ratios; this is an indication of the momentum deficit in one case and of the momentum excess in the other. In the recovery region, however, there is a definite indication of a logarithmic region near the wall. The two profiles at $x = 214$ cm and $x = 256$ cm exhibit linear regions for both blowing ratios; this proves that as soon as the blowing stops, wall effects are dominant and the "law of the wall" seems to apply.

5.4 Turbulent Kinetic Energy Profiles

Turbulent kinetic energy will be discussed, like the mean velocity profiles, in the form of two sets -- first for $M = 0.4$, second for $M = 0.9$. Comparisons between the two cases will be deferred until the section discussing the $M = 0.9$ data.

5.4.1 Turbulent kinetic energy profiles for $M = 0.4$

Figure 5.7 shows the TKE profiles at several spanwise locations at each of five streamwise stations for $M = 0.4$. Spanwise symmetry can be observed in these profiles, indicating an orderly behavior of the turbulent flow field.

The position of the $\delta_{.99}$ thickness is marked on the profiles in the full-coverage region. As seen, the TKE boundary layer extends up to $y \approx 1.3\ \delta_{.99}$. This was also observed by several other workers -- for example, Klebanoff (1955).

In the full-coverage region, there is a strong convergence above $y = 2$ cm in the TKE profiles at all spanwise locations, but large differences exist between the profiles below $y = 2$ cm. This relates to the 2 cm penetration distance and indicates that the region near the wall is locally affected by the jets.

Near the wall, the highest TKE is observed in the central profiles; the second-highest one is observed in the side profiles. The intermediate profiles have the lowest TKE, as expected (no jets are in line with them). There is a dip in the center profiles around $y = 1$ cm. This can be explained as follows. There is a high velocity gradient near the wall which causes high shear, resulting in higher TKEs. However, there exists a very low velocity gradient region (see Fig. 5.2) just above it, because of injection. In this region the local TKE production is decreased but local dissipation is high, leading to low TKE values. The low velocity gradient region ends at about $y = 2$ cm (penetration distance). Above this level, higher velocity gradients lead to higher TKE. As a result, a double maximum is observed in the central TKE profiles. The side TKE profiles have only one maximum. At some distance from the injection location, the TKE near the wall dissipates and the maximum near the wall vanishes. TKE diffuses from the second maximum towards the wall. The result is a smooth profile with one maximum.

In Fig. 5.7, 2-D flat-plate TKEs are also shown both at the start of the recovery region and at the two recovery region stations as references for comparisons. The 2-D flat-plate TKE profiles were obtained with the STAN5 computer program (Crawford & Kays, 1975) for the same free stream turbulence level as the experimental profiles. A spanwise-averaged TKE profile is shown for the start of the recovery region. Comparisons with the 2-D profile show that there is excess TKE throughout the region, but most of the excess energy lies in the middle section of the boundary layer. There is more violent turbulent mixing in the outer layers relative to layers next to the wall. Even though the jets do not penetrate

very far into the boundary layer, the TKE diffuses towards the free stream, causing large TKE values far from the wall.

In the recovery region, there is still high TKE compared to the 2-D value. The reversion of the turbulence quantities to the 2-D state is very slow. This interesting process is shown in the following sketch.

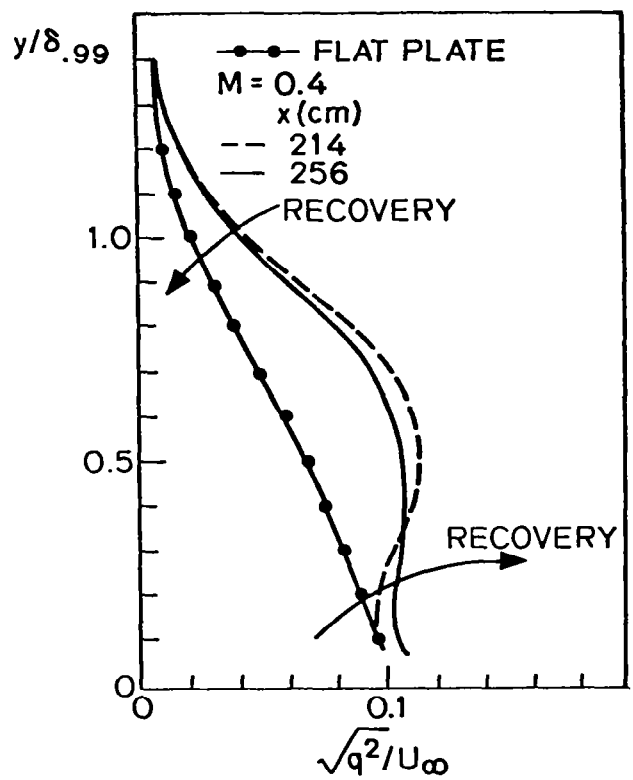

Again, there are two distinct regions in the relaxation process, an outer region and an inner region. The relaxation to the 2-D state is in the expected direction in the outer region and is caused by the diffusion of TKE. However, an opposite "relaxation" is seen in the inner layer. This means that the rate of diffusion of the TKE toward the wall exceeds the rate of dissipation near the wall. After the profile

becomes flat in the last recovery region station (67 diameters downstream), the diffusion will stop and the dissipation will dominate, causing the reversion of the profile to the 2-D state.

The high TKE (turbulent mixing) levels in the recovery region must be the reason for the slowly rising Stanton numbers here for $M = 0.4$. Crawford et al. (1976) observed that Stanton numbers for $M = 0.4$ decrease in the full-coverage region and rise slowly in the recovery region. This process can be explained by the TKE levels, as follows. The TKE levels are higher than the 2-D boundary layer values. This higher turbulence level should cause high Stanton numbers; however, at the same time, an energy sink is created in the full-coverage region by the cold injection. The combination of these two opposing phenomena results in the low and decreasing Stanton numbers in this region. There is no injection in the recovery region (i.e., the energy sink is lost), but the turbulence level (turbulent mixing) is still high. The mixing process, unopposed, increases the Stanton numbers and they rise gradually in the recovery region.

In Fig. 5.8, spanwise-averaged TKE profiles are plotted in (y/δ) and $\sqrt{q^2}/U_\infty$ coordinates for each streamwise station. There is no definite similarity in any region, even though all the profiles seem very similar (again, for the $x = 168$ cm profile, the points near the wall are to be neglected, as discussed in Sec. 5.6). There is an indication of invariance in the TKE profiles in the full-coverage region after four or five rows of blowing (over $(y/\delta) = 0.3$). This was also the case with the streamwise mean velocity profiles.

5.4.2 Turbulent kinetic energy profiles for $M = 0.9$

Figure 5.9 shows the TKE profiles for several spanwise locations at each of five streamwise stations for $M = 0.9$.

Spanwise symmetry can be observed in the profiles within the experimental uncertainty limits.

The behavior of the TKE is qualitatively similar to the $M = 0.4$ case -- contrary to the mean velocity profiles which exhibit different behavior. Once more, the highest TKE is seen in the central profiles, the next highest in the side profiles, and the lowest in the intermediate

profiles. However, quantitatively, there are big differences between the TKE profiles for the $M = 0.4$ case and the $M = 0.9$ case.

The double maximum observed in the $M = 0.4$ TKE profiles is not found here. The highest TKE occurs next to the wall rather than in the outer region, owing to the high velocity gradient there. Above $y = 2.0$ cm there is a sharp drop in TKE. Also, the TKE levels for $M = 0.9$ are much lower than in the case of $M = 0.4$ within a large region of the boundary layer outboard of $y/\delta \cong 0.15$ (compare the spanwise-averaged profile at the start of the recovery region with the 2-D TKE profile). This is clear evidence of a decrease in turbulence level as the blowing ratio approaches 1. The TKE levels are lower because of the lack of velocity gradients for the $M = 0.9$ case, as shown in Fig. 5.11. This figure shows the central profiles of mean velocity and TKE at the start of the recovery region for $M = 0.4$ and $M = 0.9$. The mean velocity gradient is smaller and the TKE is lower for the $M = 0.9$ case than for the $M = 0.4$ case everywhere above $(y/\delta) \simeq 0.2$. This behavior may be due primarily to the dependence of the TKE production on the mean velocity gradient -- the larger the mean velocity gradient, the larger the TKE production and the TKE itself.

The lower TKE levels for the higher blowing case seem, at first glance, to be inconsistent with the heat transfer data obtained by Crawford et al. (1976), but when examined closely it can be seen that there may be an explanation: the governing process for the heat transfer may be different. Crawford et al. (1976) observed that the Stanton number for the $M = 0.9$ case is below the 2-D flat-plate value and above the value for the $M = 0.4$ case. The Stanton number values decreased in the downstream direction in the full-coverage region and also in the recovery region. If turbulent mixing were the governing process in the heat transfer, one would expect the Stanton numbers for the $M = 0.9$ case to be lower than for the $M = 0.4$ case, for two reasons: first, more cold fluid is injected into the boundary layer for high blowing and, second, there is less turbulent mixing. Instead, higher Stanton numbers were observed. The reason could be that, for high blowing, the jets separate from the wall and penetrate deeply into the boundary layer, entraining the

hot free stream fluid towards the wall in the middle lanes. This process is schematically explained in the following figure.

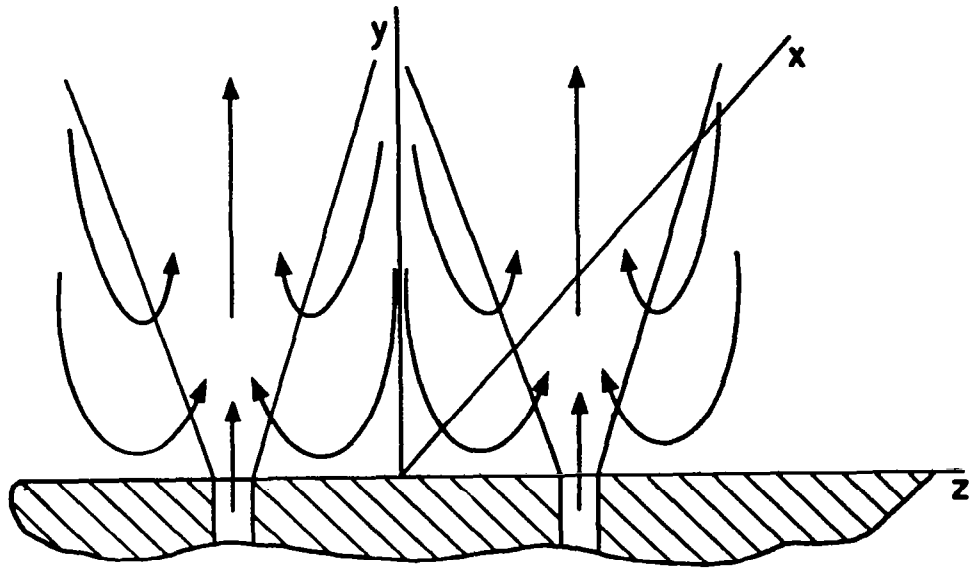

This figure was also used by Le Brocq, Launder & Priddin (1971) to describe the in-line blowing process. This same process seems to occur in a staggered array, at high blowing. Thie hypothesis is also supported by the $\overline{V}$ component of the mean velocity, as can be seen in Figs. 5.16 and 5.17.

In addition to the entrainment process, the cold fluid (energy sink) is also deposited in the outer layer due to the separation of the jets from the surface. Thus, two opposing mechanisms result in the decreasing Stanton numbers in the full-coverage region. (They are, nevertheless, higher than the low-blowing values.)

In summary, the two pairs of opposing processes which control the heat transfer are: (i) turbulent mixing versus energy sink near the wall for low blowing, and (ii) outer-layer fluid entrainment versus energy sink in the outer layer for high blowing.

In the recovery region, the Stanton numbers continue to decrease because there is rapid decay of entrainment of the outer-layer fluid by the jets and the energy sink is no longer being injected at the wall. In the absence of these mechanisms, the process continues

in its natural direction until the turbulent mixing is strong enough to reverse the trend. Since the three-dimensionality is important in heat transfer for high blowing, any 2-D computer program will have difficulty in predicting the heat transfer in the full-coverage region for these cases.

In Fig. 5.9, the recovery region TKE profiles are compared with 2-D flat-plate TKE profiles. The behavior of the TKE is very interesting. At the start of the recovery region, the spanwise-averaged TKE is higher than the 2-D value; however, by 27 hole diameters into the recovery region, TKE values are lower than the 2-D value below $y \simeq 3$ cm. In fact, the deviation from the 2-D value increases in the downstream direction. Normally one would expect the difference to decrease. This can be explained as follows. In Fig. 5.4, the spanwise-averaged mean velocity profile at the start of the recovery region has negative velocity gradients close to the wall. There are also negative shear stresses in the same area as seen in Fig. 5.13. In fact, since the flow is three-dimensional, there are y locations where the mean velocity gradient is positive and the shear stress negative, and vice versa. This results in the apparent negative production of TKE. The high TKE near the wall is dissipated rapidly as soon as the injection stops and thus cannot feed the low TKE regions by diffusion. As a result of the "negative production", the dissipation, and the decreased diffusion, the TKE falls below the 2-D flat-plate value. Even though the negative velocity gradient region diminishes rapidly after the last row of injection, its effect on TKE continues because the turbulence profiles respond slowly to changes. The production first becomes zero and then positive. A considerable distance is required before the production can adjust itself to increase the TKE level.

The relaxation of TKE in the recovery region occurs in the expected direction in the outer layer. This rate is again slow, as was observed in the $M = 0.4$ case. In the near-wall region, TKE responds rapidly. At the point nearest the wall, TKE drops from $\sqrt{q^2}/U_\infty = 0.134$ to 0.1 quickly, after the last row of injection, and remains at that level throughout the recovery region. This is also true for $M = 0.4$, in the

recovery region (see Fig. 5.7) and for a 2-D flat-plate boundary layer. These observations illustrate the rapid recovery to the 2-D state in the near-wall layer ($y/\delta \leq 0.1$), which occurs as soon as the injection stops.

Figure 5.10 shows the spanwise-averaged TKE profiles for $M = 0.9$ at the five streamwise stations (discard the $x = 168$ cm, as discussed in Section 5.6). There is a fair similarity above $(y/\delta) = 0.8$. This is due to the undisturbed TKE region here. Below $(y/\delta) = 0.8$, there is similarity between the full-coverage region profiles and the recovery region profiles. This may mean that a state of invariance for TKE is reached in the full-coverage region. This phenomenon may simplify predictions of the full-coverage region and might lead to better insight into the injection process. The similarity observed in the recovery region may be due to the slow rate of relaxation to the 2-D state.

5.5 Streamwise Shear Stress Profiles

Figures 5.12 and 5.13 show the streamwise shear stress profiles at the start of the recovery region (just after the last row of injections) for $M = 0.4$ and $M = 0.9$, respectively. The 2-D flat-plate shear stress profiles (Klebanoff, 1955) are also shown in these figures as reference lines for comparison. In both cases there is some symmetry observed for the profiles which are in symmetrical positions with respect to the centerline. Compared to the 2-D shear stress, excesses are observed for the $M = 0.4$ case, above $y/\delta \simeq 0.2$, for all of the spanwise profiles. In general, for the $M = 0.9$ case, however, defects can be seen when compared to the reference profiles below $y/\delta \simeq 0.6$. Above $y/\delta \simeq 0.6$, there are some excesses, but the magnitudes of these are less than for the $M = 0.4$ case owing to the higher shear action of the effective jet spread for the low blowing. Thus, the shear stress levels are much higher for $M = 0.4$ than for $M = 0.9$, as was expected from the mean velocity gradients. This is another indication of high turbulence mixing for the low blowing. The extremely high shear stress next to the wall in the central profile for the $M = 0.9$ case must be due to the separated jet, which creates a high-shear and vortex region there.

Some negative shear stresses can be seen for $M = 0.9$ in the central (No. 3) and side profiles (Nos. 1 and 5) due to the separation of jets. These negative shear stress regions occur close to and at the points of negative streamwise mean velocity gradients. It appears that $-\overline{u'v'}$ is more or less following the direction of $\partial\overline{U}/\partial y$. Shear stress regions close to zero can be seen in the intermediate profiles (Nos. 2 and 4) next to the wall. These regions correspond to the $\partial\overline{U}/\partial y = 0$ region of the mean velocity profiles.

Another indication of the jet separation from the surface for $M = 0.9$ is the highly disturbed region of shear stress in the central profile extending up to $(y/\delta) \simeq 0.5$ (about $y \simeq 3$ cm or three hole diameters). This is the penetration distance for the last row of injections. In fact, the same disturbed region can also be observed in the side profiles because of the jets injected one row before. However, the profiles in the middle lanes are very smooth and do not show any sign of disturbance. They also indicate the low level of turbulence for the $M = 0.9$ case.

Figure 5.14 shows spanwise-averaged streamwise shear stress profiles at five streamwise positions for $M = 0.4$. The 2-D flat-plate shear stress profiles are also shown for comparison. The development of the shear stress in the full-coverage region and its relaxation in the recovery region can easily be observed. In the full-coverage region the profiles grow fuller in the downstream direction as the injection effects diffuse outwards. In the recovery region the relaxation process is quite slow. The shear stress levels are much higher in comparison to the 2-D values at each station, indicating high turbulent mixing.

Figure 5.15 shows spanwise-averaged streamwise shear stress profiles at the start of the recovery region, as well as at the two recovery region stations for $M = 0.9$. As can be seen, the relaxation process in the recovery region is also slow for this case. When compared to the 2-D values, the shear stresses are quite small, indicating low turbulent mixing below $(y/\delta) \simeq 0.65$. In the outer layers (above $(y/\delta) \simeq 0.65$), there is some excess shear, but it is not significant. The low shear level is consistent with the mean velocity gradients at the start of the

recovery region. The spanwise-averaged mean velocity profile is quite flat, resulting in small gradients and small shear (see Fig. 5.4). The mean velocity reverts back to the 2-D flat-plate value rapidly in the recovery region. However, because of the slow relaxation speed of the turbulence field, the shear stress remains low for long distances.

5.6 On Spanwise Averaging

Most of the data above was discussed on spanwise-averaged bases. This section will explain the hows and whys of spanwise averaging.

In section 5.7 it is shown that the three dimensionality of the flow field was local and restricted to the vicinity of the jets. The flow field was expected to be periodic due to the fact that the jets are in a regular array. The spanwise uniformity and the symmetry of the flow field were shown in the discussions of the mean velocity, TKE, and the shear stress profiles.

The values of the heat transfer coefficients sought here are not the local values, but rather the average behavior of the Stanton numbers in the streamwise direction. This requirement plus the properties from the preceding paragraph allow for a simpler two-dimensional analysis instead of a 3-D one.

The following method was used to spanwise average the flow properties. A spline fit in the lateral (z) direction was made to the profiles at each y level within a pitch. Each point of the spanwise averaged profiles was obtained from the following formulas. To be consistent with the physics, mean velocities and TKEs were mass averaged.

$$G_{average} = \frac{\int_{-P/2}^{+P/2} \bar{U}\, G\, dz}{\int_{-P/2}^{+P/2} \bar{U}\, dz} \tag{5.1}$$

where G stands for $\bar{U}$ or q^2, as the case may be. Shear stresses were area averaged.

$$(\overline{-u'v'})_{average} = \frac{\int_{-P/2}^{+P/2} (\overline{-u'v'})\, dz}{P} \tag{5.2}$$

As was seen in section 5.2, five profiles were taken at the first and last full-coverage stations and three profiles at the second station. Results of spanwise averaging showed that three profiles were not enough to obtain a good spanwise average, since this process gave more weight than was proper to the central profile. Therefore, for the profiles at $x = 168$ cm (second full-coverage region station), little importance is attached to the results of spanwise averaging near the wall, when the spanwise profiles differ significantly from each other due to the injection. However, spanwise averages obtained from five profiles appear to represent the physics adequately. The spanwise-averaged profiles of mean velocity and TKE at the start of the recovery region bears a strong resemblance (at least from the standpoint of qualitative tendencies) to the profiles in the recovery region, where no spanwise averaging was done because all the spanwise profiles are the same. From this it can be concluded that the physical averaging process taking place in the flow must coincide with the spanwise averaging of five profiles here.

5.7 On the Three-Dimensionality of the Flow Field

As noted, the three-dimensionality of the flow field was limited to the close vicinity of jets; the flow had a strongly preferred direction. Elaboration follows in sections 5.7.1 and 5.7.2. Space and time did not permit plotting all the data (such as the components of the mean velocity and Reynolds stress tensor) at every measurement location. Some interesting representative data of this nature are given, however, as an aid to understanding the three-dimensionality and its implications for heat transfer.

5.7.1 $\overline{V}$ and $\overline{W}$ components of the mean velocity

Figure 5.16 shows the $\overline{V}$ component of the mean velocity after the last row of injection for several spanwise locations for the case of $M = 0.4$. Together with the $\overline{V}$, the flow angle γ is also shown. Only the profiles on one side of the centerline are plotted because of symmetry. As expected, because of the inline jet, the highest $\overline{V}$ occurs in the centerline profile at the point next to the wall. The smallest $\overline{V}$ values occur in the intermediate profile, which has no jet in line

with it. It is significant that the direction of $\overline{V}$ depends on the profile position. At the central and side positions, V is in the positive direction (towards the free stream), whereas for the intermediate profile it is in the negative direction. The fluid is pushed upwards by jets at the position in line with them and is entrained towards the wall in between. Maximum values of $\overline{V}$ occur near the wall, reaching approximately 8% of the free stream velocity; whereas in most of the boundary layer they are only from 0-4% of the free stream velocity. The largest flow angle is about 10° and occurs next to the wall. The flow angles get smaller rapidly as the distance from the wall increases.

Figure 5.17 shows the $\overline{V}$ component of mean velocity after the last row of injection at several spanwise locations, for $M = 0.9$. The observations for $M = 0.4$ also apply here qualitatively. Quantitatively, the values of $\overline{V}$ are higher because of the higher rate of blowing -- there is a larger drift towards the wall in the middle lanes. This is evidence of the strong role which entrainment must play in the heat transfer for high blowing ratios.

The largest value of $\overline{V}$ is around 16% of the free stream. The largest flow angle is about 12°.

Figure 5.18 shows the $\overline{W}$ component for $M = 0.4$ at the same streamwise location as the $\overline{V}$ components. An additional spanwise profile on the other side of the centerline is also shown. $\overline{W}$ is biased, not symmetric. Except for a few points near the wall, the $\overline{W}$ values are insignificantly small (1-3% of the U_∞). The flow angles β are also plotted on the same figure. Generally, $\overline{V}$ and $\overline{W}$ values for the $M = 0.4$ case are small enough so that locating the spanwise-averaged flow as a 2-D boundary layer is a valid approximation.

Figure 5.19 shows the $\overline{W}$ component for $M = 0.9$. The profile locations are the same as on Figure 5.18. There is no preferred direction of the $\overline{W}$, as seen in the case of $M = 0.4$; indeed, the $\overline{W}$ values are smaller than the values for $M = 0.4$. This is because of the low spanwise gradients in the streamwise mean velocity as compared to the low blowing case. The lower $\overline{W}$ values support both the spanwise averaging and the weak three-dimensionality argument, except perhaps very close to the wall, where $\overline{W}$ values are about $\pm$ 2% of the U_∞.

The large and highly disturbed values of $\overline{V}$ and $\overline{W}$ near the wall for $M = 0.9$ in the central profile are indications of vortices created by the separated jet.

In both cases of blowing, the angle range of the flow field is entirely suitable for measurements, within a good accuracy, of most of the turbulence quantities with the triaxial wire system, except perhaps at the point next to the wall just downstream of a jet for the $M = 0.9$ case.

5.7.2 Reynolds stresses

Figure 5.20 shows the Reynolds shear stresses for the first station in the recovery region (27 hole diameters downstream of the last row of injection) for $M = 0.4$ and 0.9. These profiles are given to show a sample of the data; the rest are found in Appendix A. These profiles are not discussed in detail because of their secondary importance in the present work.

The $(\overline{u'v'})$ component of shear stress for $M = 0.4$ is significantly higher than for the others. The $(\overline{u'w'})$ and $(\overline{v'w'})$ components are almost one order of magnitude smaller than $(\overline{u'v'})$, except for a few points near the wall. This indicates a return to two-dimensionality for the stress field.

All of the shear stress values for $M = 0.9$ are low in comparison to $M = 0.4$ as expected, with the exception of $(\overline{u'v'})$ near the wall, which is high (still remembering its upstream history).

Figure 5.21 shows the normal Reynolds stresses at the same station as in Fig. 5.19 for $M = 0.4$ and $M = 0.9$. Again, the general observation is of the expected low turbulence level of $M = 0.9$ in the outer region. The two cases also differ in the near isotropy of the $M = 0.9$ case. All the normal stress components are very close in magnitude, which is not the case for $M = 0.4$. This distribution of the normal stress may be attributed to the flat mean velocity profiles and the small spanwise gradients in the $M = 0.9$ case.

For $M = 0.4$ the u'^2 profile looks very much like the $\overline{u'^2}$ profile obtained by Wilson & Goldstein (1976) in a turbulent plane wall jet,

except that here the levels are lower. The reason is that the plane wall jet was injected to a still environment, thus causing higher shear rate.

5.8 Correlation Coefficients

Figure 5.22 shows the spanwise-averaged stress-energy ratio $(-\overline{u'v'}/q^2)$ for $M = 0.4$ at five streamwise stations. The 2-D flat-plate value (0.15) is also given in the same figure for comparison (taken from Hinze, 1975). The values near the wall are smaller than the 2-D values because of the disturbance caused by the injection there. The values reach the 2-D level above $(y/\delta) \simeq 0.5$, where the jet effects are weak. Recovery to the 2-D values near the wall can be observed in the recovery region stations.

The first profile after three rows of blowing does not show the large area of low stress-energy ratio shown in the other full-coverage region profiles. This must be because the effects of injection have not yet penetrated that far.

Figure 5.23 shows the same profiles for $M = 0.9$. A much larger area of reduced and disturbed stress-energy ratio is observed, attributed to the deeper jet penetration; otherwise the same observations can be made for this case as in $M = 0.4$.

Figures 5.24 and 5.25 show the spanwise-averaged 3-D stress-energy ratio, $(|\tau|/\rho)/q^2$, for $M = 0.4$ and $M = 0.9$, respectively. Since there is some three-dimensionality in the flow field, it was thought that it would be interesting to see the effect of three-dimensionality. Fig. 5.24 shows that the total stress-energy ratio lies closer to the 2-D value than $-\overline{u'v'}/q^2$, except for a few points near the wall. This suggests that the value of 0.15 may not be restricted to 2-D boundary layers, but may be useful in weakly 3-D flow such as this one. The same observations can be made for $M = 0.9$, also, except that the effect of high blowing still shows itself in large disturbances.

Figure 5.26 shows the correlation coefficient, $-\overline{u'v'}/\sqrt{\overline{u'^2}}\sqrt{\overline{v'^2}}$, for both blowing ratios at the two recovery region stations. The flat plate value (0.45) of the correlation coefficient is also shown for

comparison (Schlichting, 1968). Again, for low blowing, the values are much closer to the flat-plate value than for high blowing. The effect of the injection can be observed near the wall in the form of decreased correlation coefficients for both cases. Reversion to the 2-D flat-plate state can be seen in the downstream direction for both blowing ratios.

5.9 Mixing Length

The mixing length can be obtained using Prandtl's (1925) definition

$$\ell = \frac{\sqrt{-\overline{u'v'}}}{\left(\frac{\partial \overline{U}}{\partial y}\right)} \qquad (4.13)$$

Figures 5.27 and 5.28 show the mixing length obtained from the shear stress and the mean velocity data using the above formula in the recovery region for $M = 0.4$ and 0.9. The same figures also show the mixing-length profile for a 2-D flat plate boundary layer (from Escudier, 1966). An augmented mixing-length region is observed at the station just after the last row of blowing ($x = 188$ cm) for both cases. This augmentation is a result of the injection process, which creates shear stresses as well as regions of low $\partial\overline{U}/\partial y$. Evidence in support of this hypothesis is found in the large region of augmentation for the $M = 0.9$ case, where the velocity profiles are quite flat. Having a high mixing length does not always imply a high rate of mixing; it may just be a result of definition. For example, even though low shear stress and TKE levels are observed for $M = 0.9$ (Figs. 5.9 and 5.13), the height and width of the augmented region are much larger than for $M = 0.4$. This is an indication of the inadequacy of the mixing-length models in regions with a zero mean velocity gradient. Fortunately, the augmented region moved out at the start of recovery region so that its effect on the near wall behavior is negligible. Furthermore, the peak in the mixing length dies out quite fast, and is not observable in the recovery region stations.

Another interesting point is the existence of regions of low mixing length near the wall, as compared to the 2-D flat-plate case. This region cannot be seen clearly for $M = 0.4$, but is quite clear for $M = 0.9$. The details of this region were discussed in Chapter 4, along with the

predictions. Except for these two regions, the mixing length behaves like a 2-D mixing length.

Figure 5.29 shows the mixing-length distributions obtained from the spanwise-averaged profiles in the full-coverage region for both blowing ratios, as compared to a 2-D flat-plate boundary layer. Some very general remarks can be made on these trends, even though the whole picture is quite complex. In the outer layers, the mixing length is similar to that for a 2-D layer. In the inner layer, the profile for $M = 0.9$ is reduced below the reference. However, a different behavior can be observed for $M = 0.4$. It appears that the profiles at the first and second recovery region stations have higher values than the 2-D below $(y/\delta) \simeq 0.15$, at which point their values drop below the reference between $(y/\delta) \simeq 0.15 - 0.4$. This leads one to the conclusion that for low blowing ratios, the peak in the mixing length occurs near the wall and moves outwards in the downstream direction in the full-coverage region, whereas for high blowing, it occurs in the outer layers to start with, due to deeper jet penetration. The points which are outside the figure limits are shown on top of the figure, with arrows indicating their magnitude.

Figure 5.30 shows the mixing length obtained from the TKE using the following definitions:

$$- \overline{u'v'} = \varepsilon_M \frac{\partial \overline{U}}{\partial y} , \qquad \varepsilon_M = \ell \sqrt{q^2/2} \tag{5-3}$$

It was interesting to observe its behavior, since a one-equation model of turbulence was used in predictions. Again, there is some scatter in the data; the same trends discussed before apply here. Therefore it was decided to use the mixing length obtained from Eqn. (4.13) -- since it was already programmed in the computer program by Crawford & Kays (1975).

Finally, as a point of interest, the shape factor H is shown in Fig. 5.31 for both blowing ratios. It was obtained from the spanwise-averaged profiles. A representative value of H for a 2-D boundary layer (by Hinze, 1975) is also shown for comparison. The shape factor lies very close to the 2-D value for both blowing ratios. This is an indication of spanwise-averaged aerodynamic behavior which is not violently damaged.

It is over the 2-D value for $M = 0.4$ and below it for $M = 0.9$. The shape factor converges towards the 2-D value downstream in the recovery region for both blowing ratios.

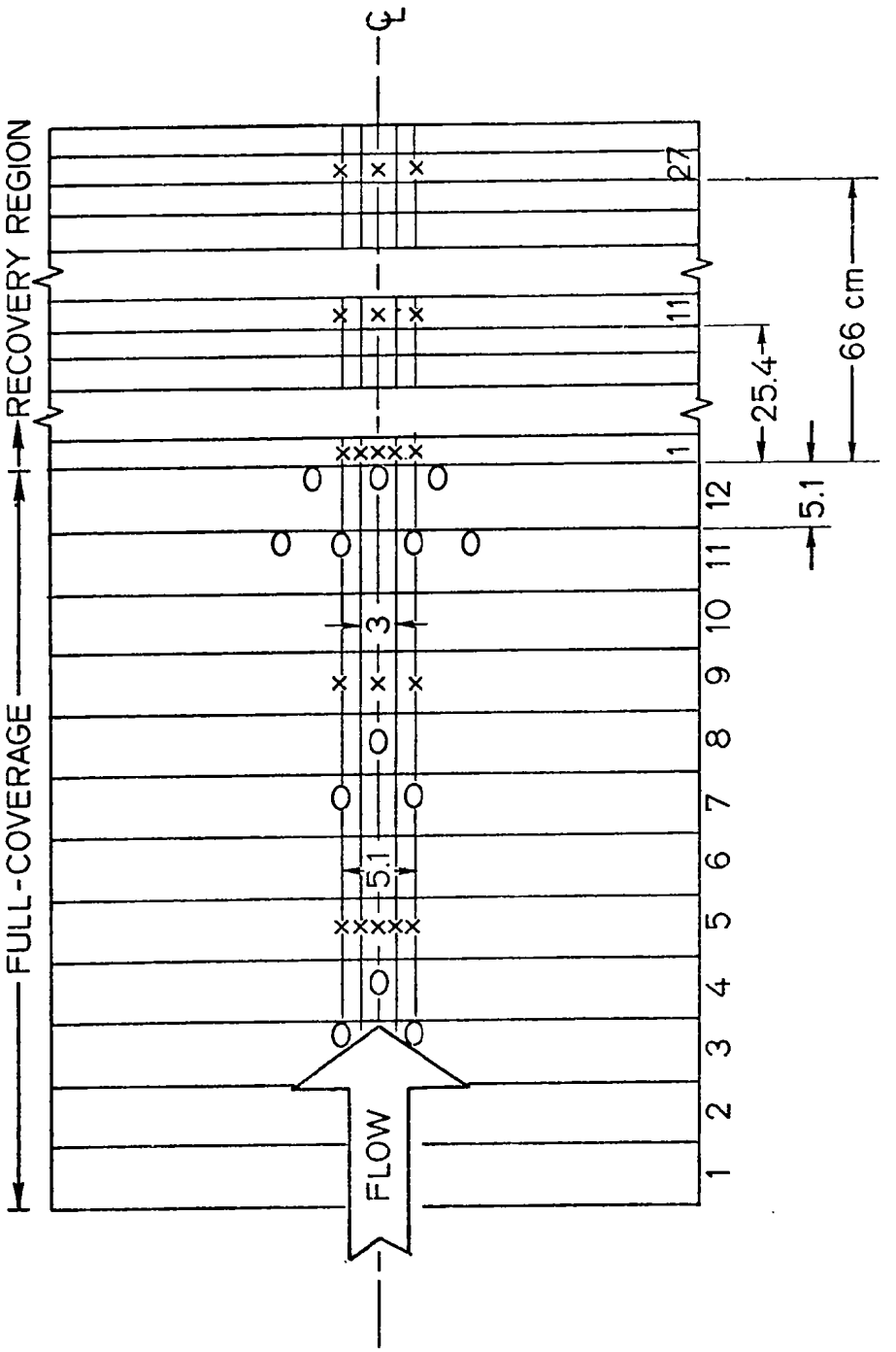

Fig. 5.1. Measurement positions.

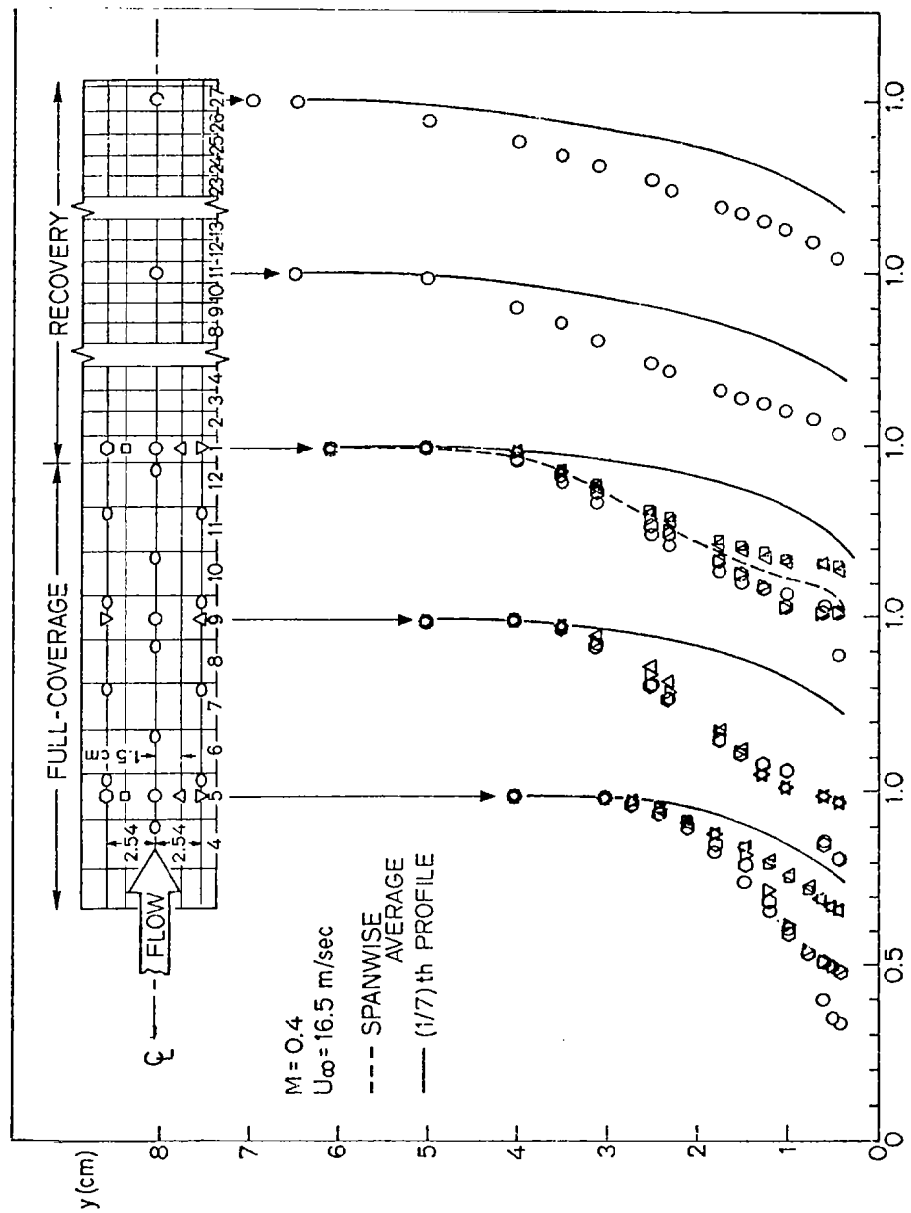

Fig. 5.2. Profiles of the streamwise mean velocity component ($\bar{U}$) for M = 0.4.

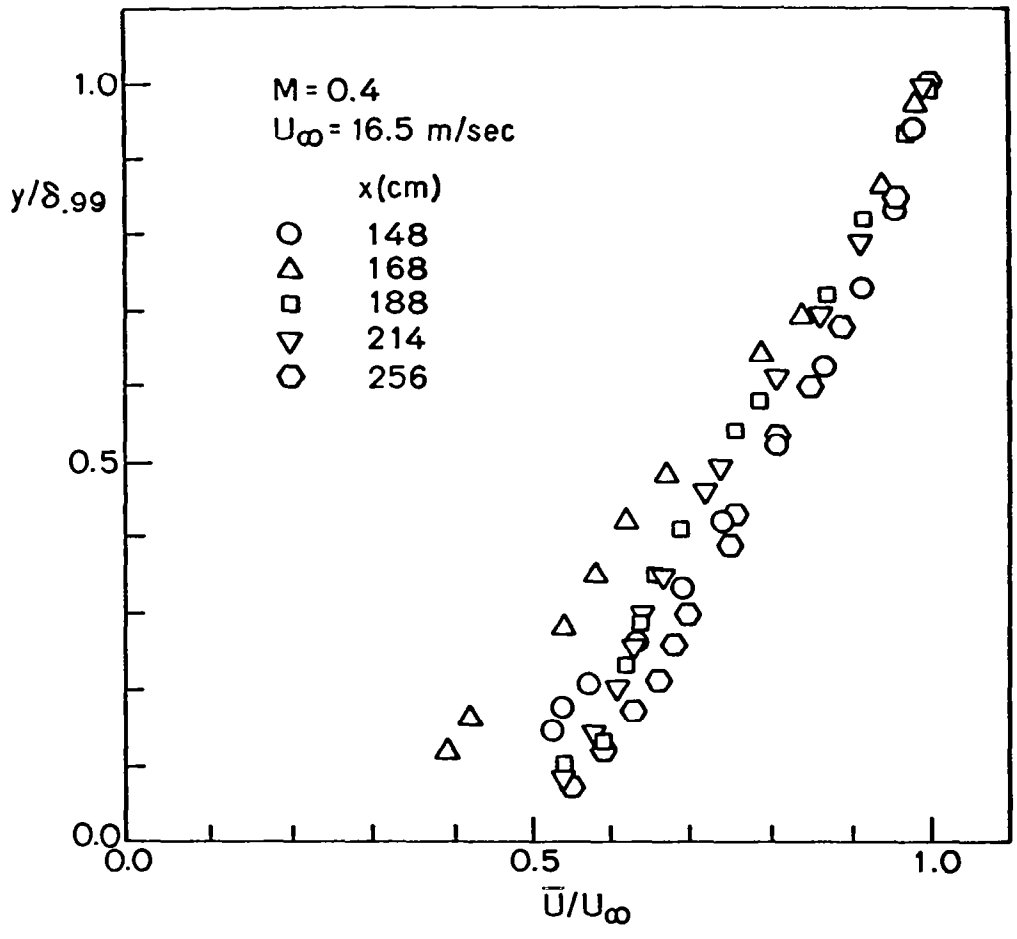

Fig. 5.3. Spanwise-averaged profiles of the streamwise mean velocity component ($\bar{U}$) for M = 0.4.

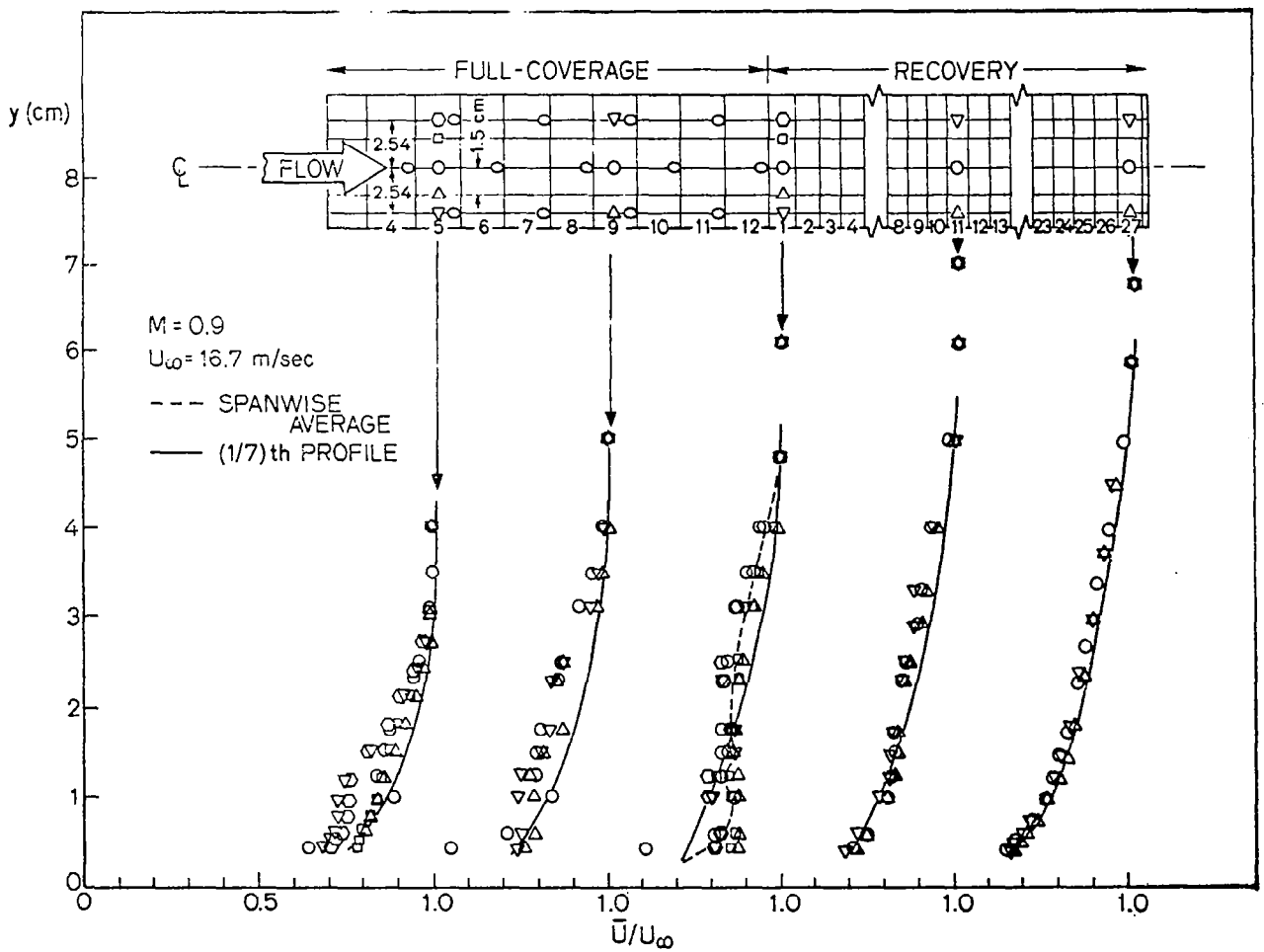

Fig. 5.4. Profiles of the streamwise mean velocity component ($\bar{U}$) for M = 0.9.

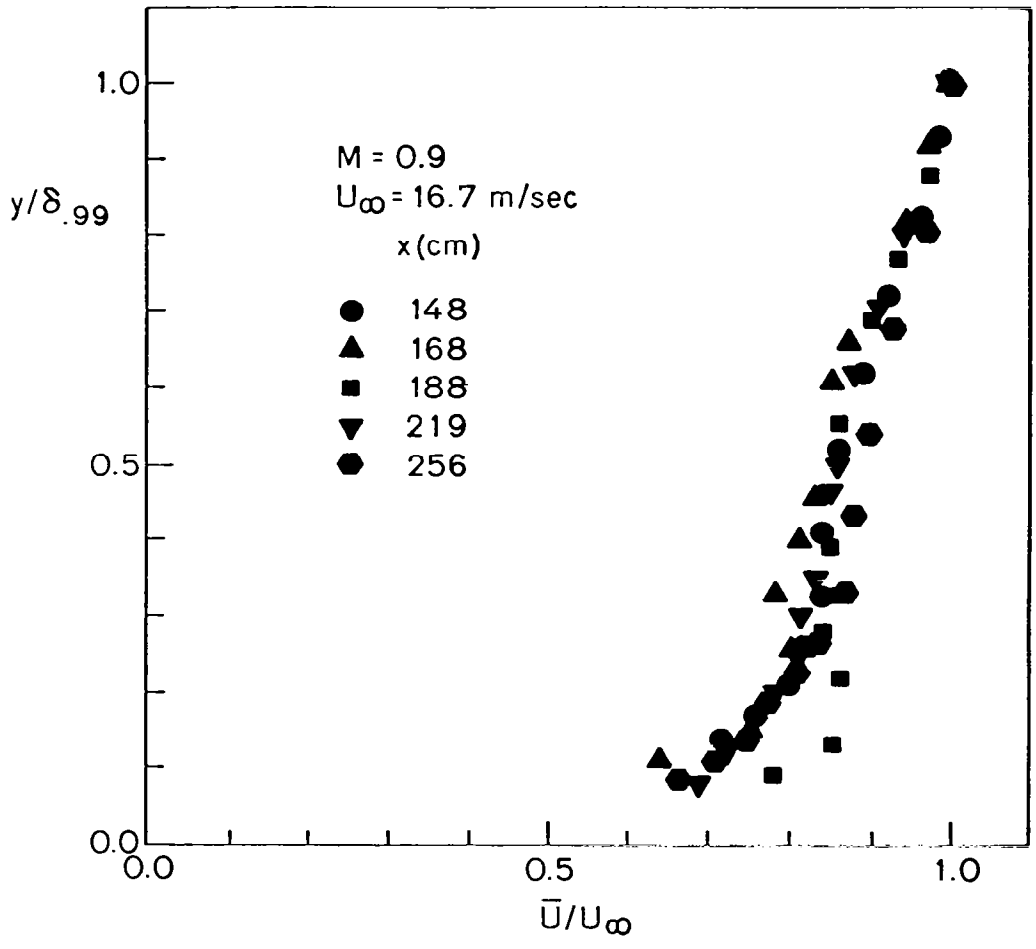

Fig. 5.5. Spanwise-averaged profiles of the streamwise mean velocity component ($\bar{U}$) for M = 0.9.

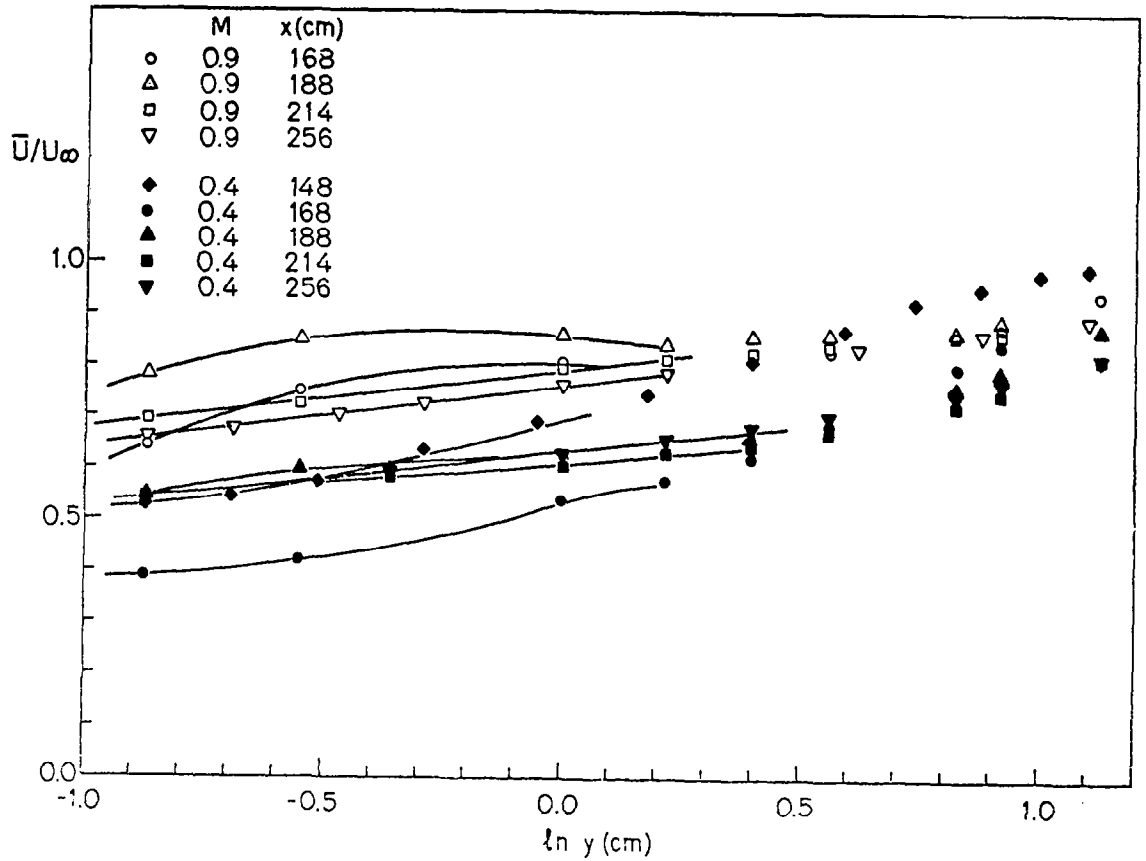

Fig. 5.6. Spanwise-averaged profiles of the streamwise mean velocity component ($\bar{U}$) plotted in semi-log coordinates.

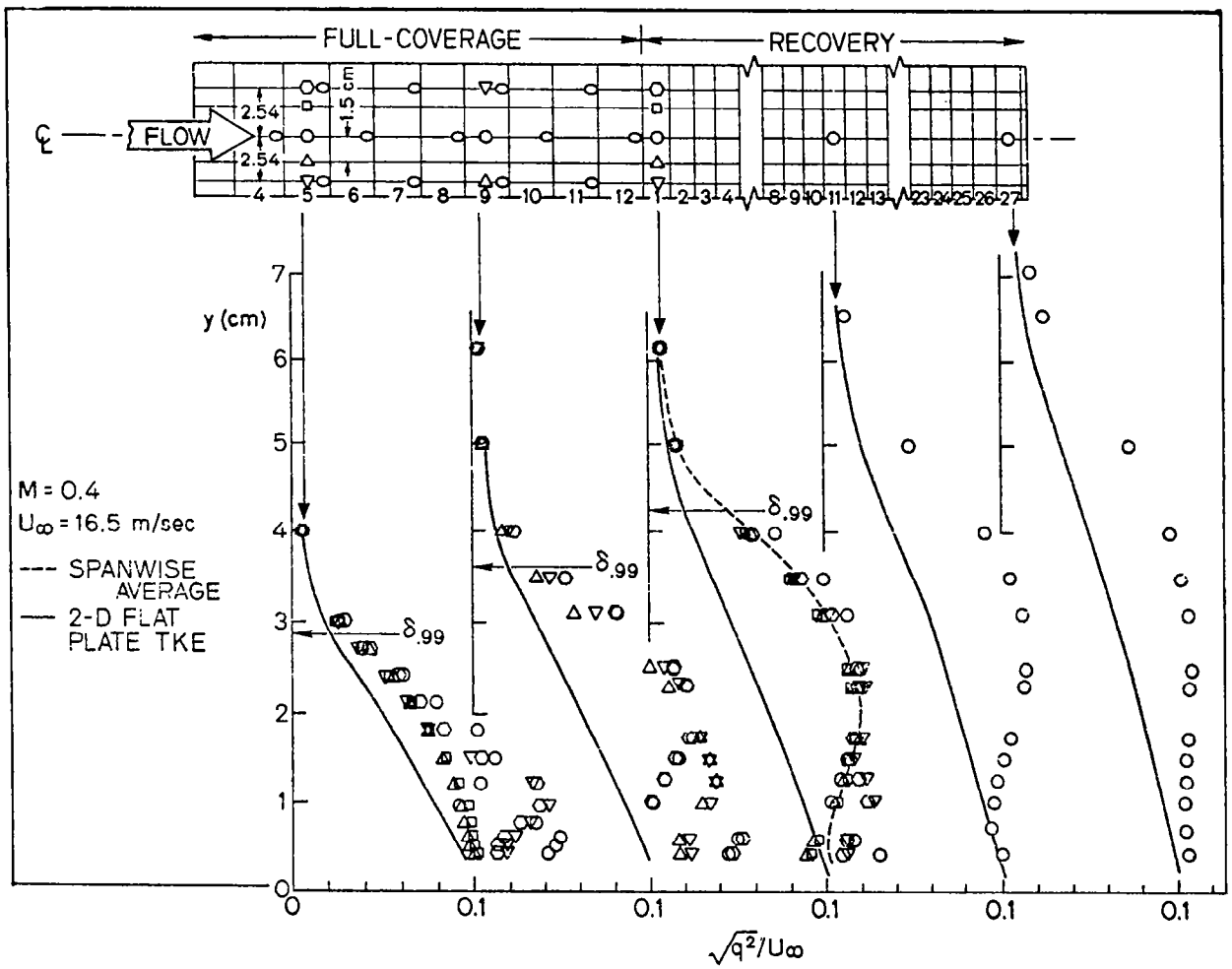

Fig. 5.7. Turbulent kinetic energy profiles for M = 0.4.

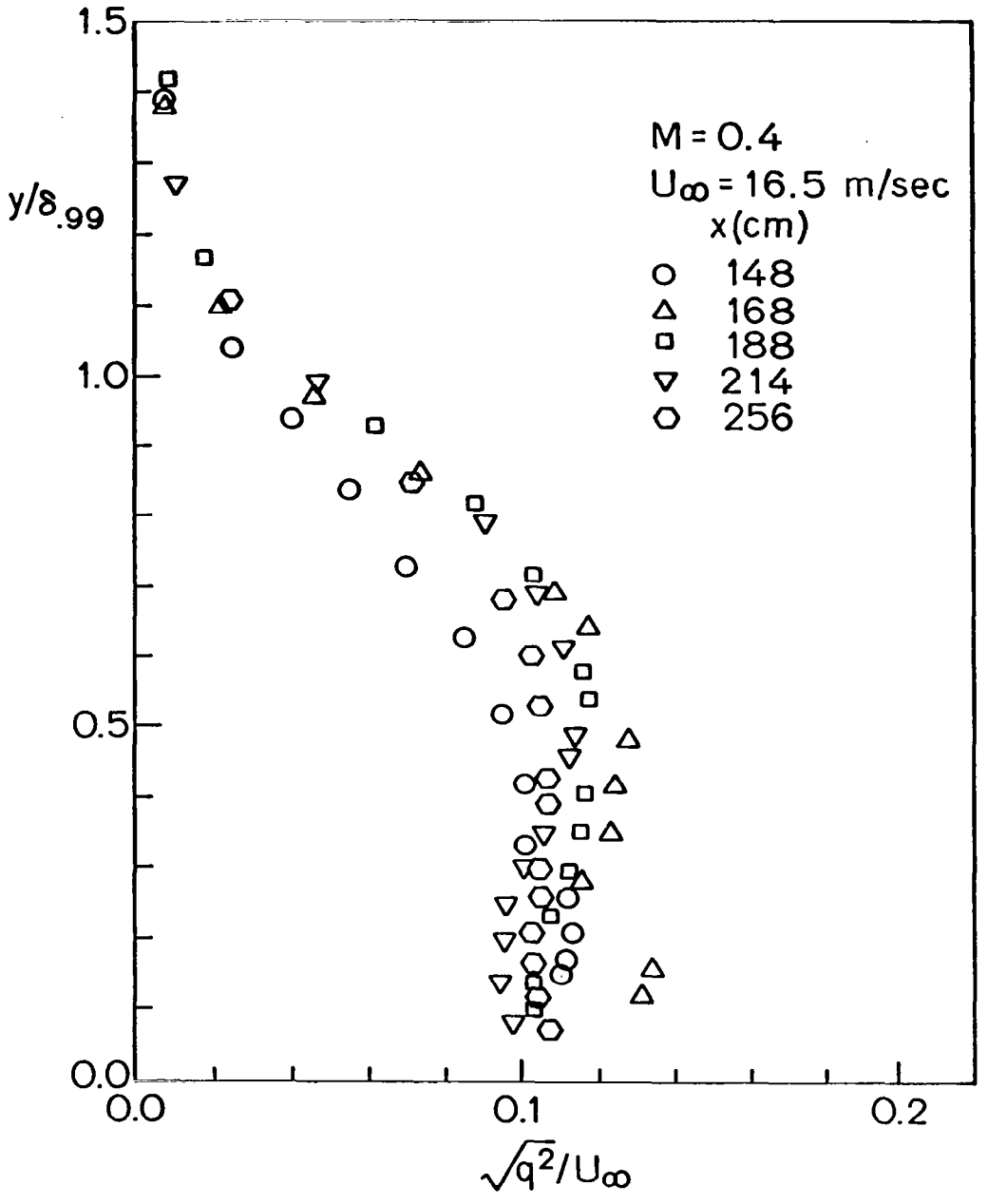

Fig. 5.8. Spanwise-averaged turbulent kinetic energy profiles for M = 0.4.

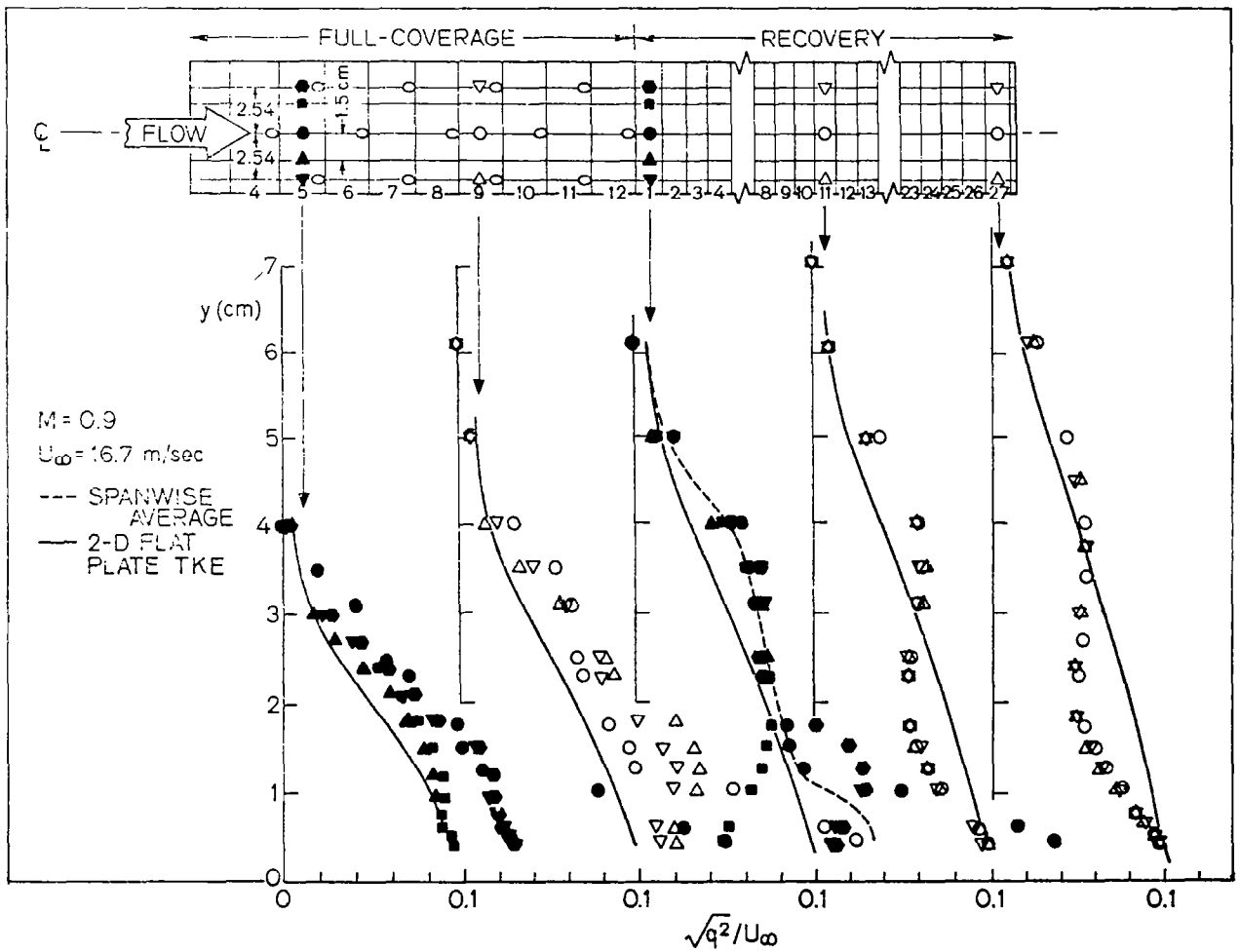

Fig. 5.9. Turbulent kinetic energy profiles for M = 0.9.

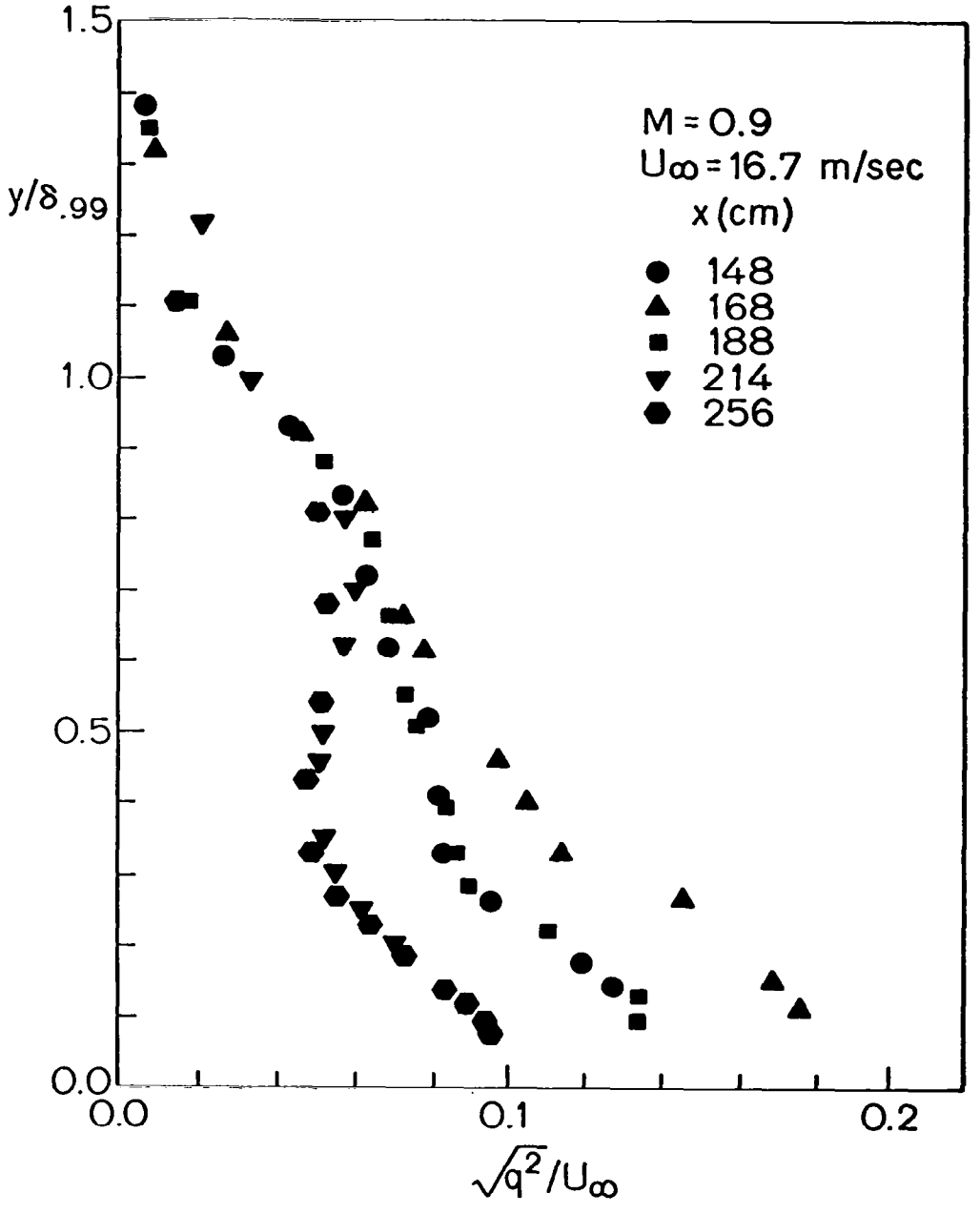

Fig. 5.10. Spanwise-averaged turbulent kinetic energy profiles for M = 0.9.

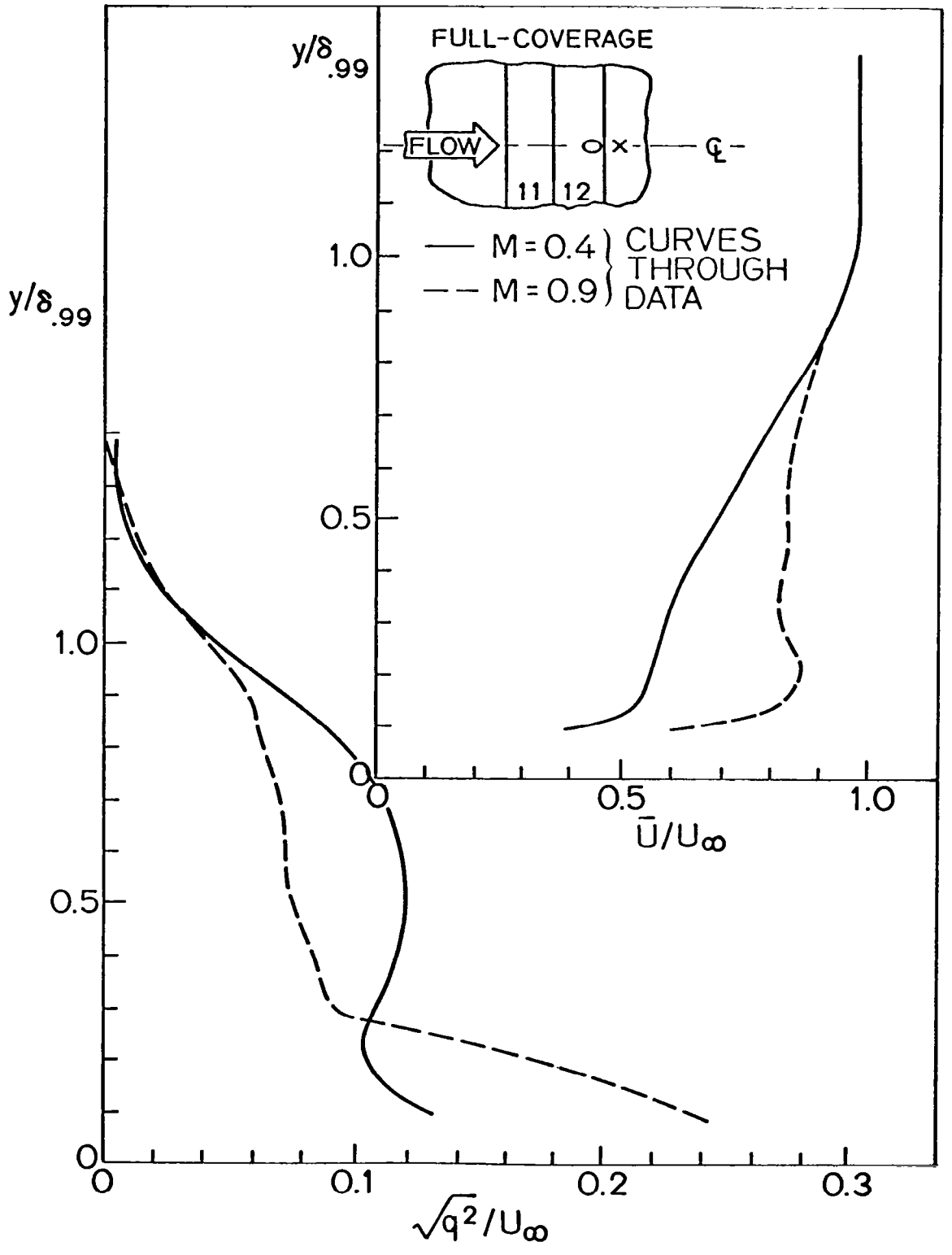

Fig. 5.11. Relation between mean velocity gradient and turbulent kinetic energy level.

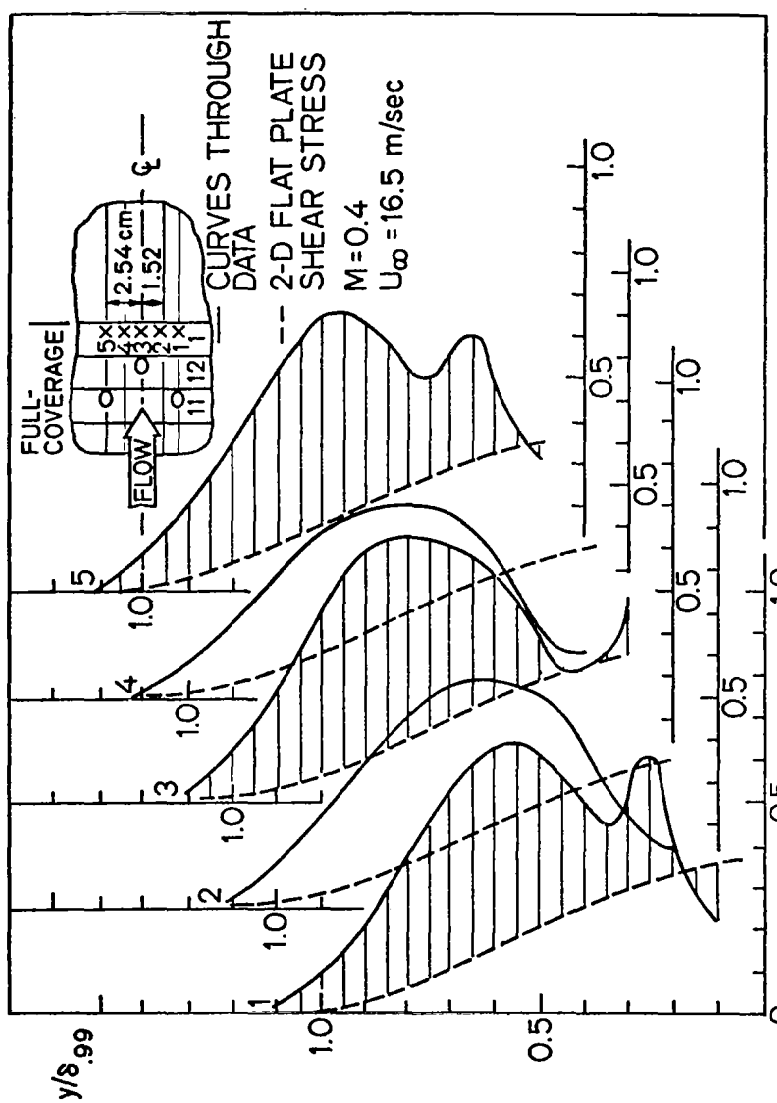

Fig. 5.12. Streamwise turbulent shear stress component $(-\overline{u'v'})$ at the start of the recovery region for M = 0.4.

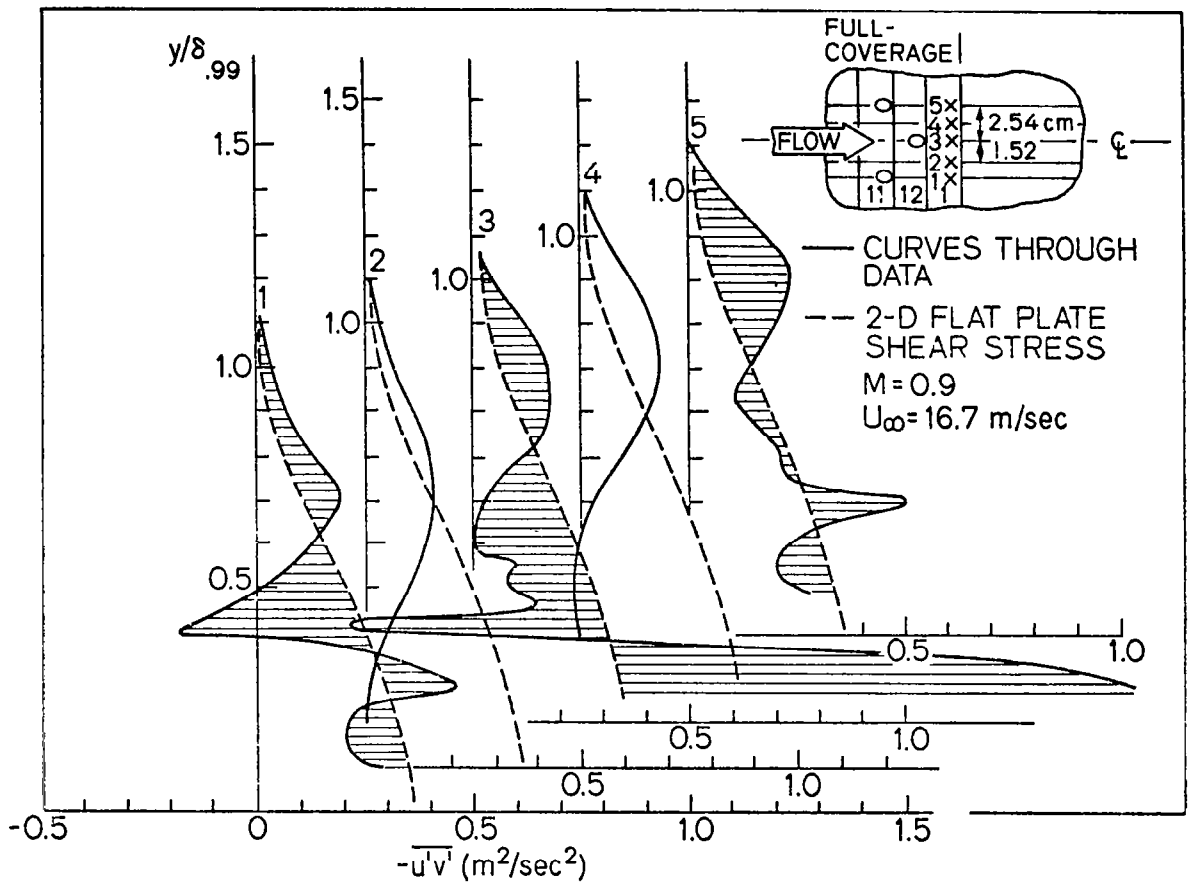

Fig. 5.13. Streamwise turbulent shear stress component ($-\overline{u'v'}$) at the start of the recovery region for M = 0.9.

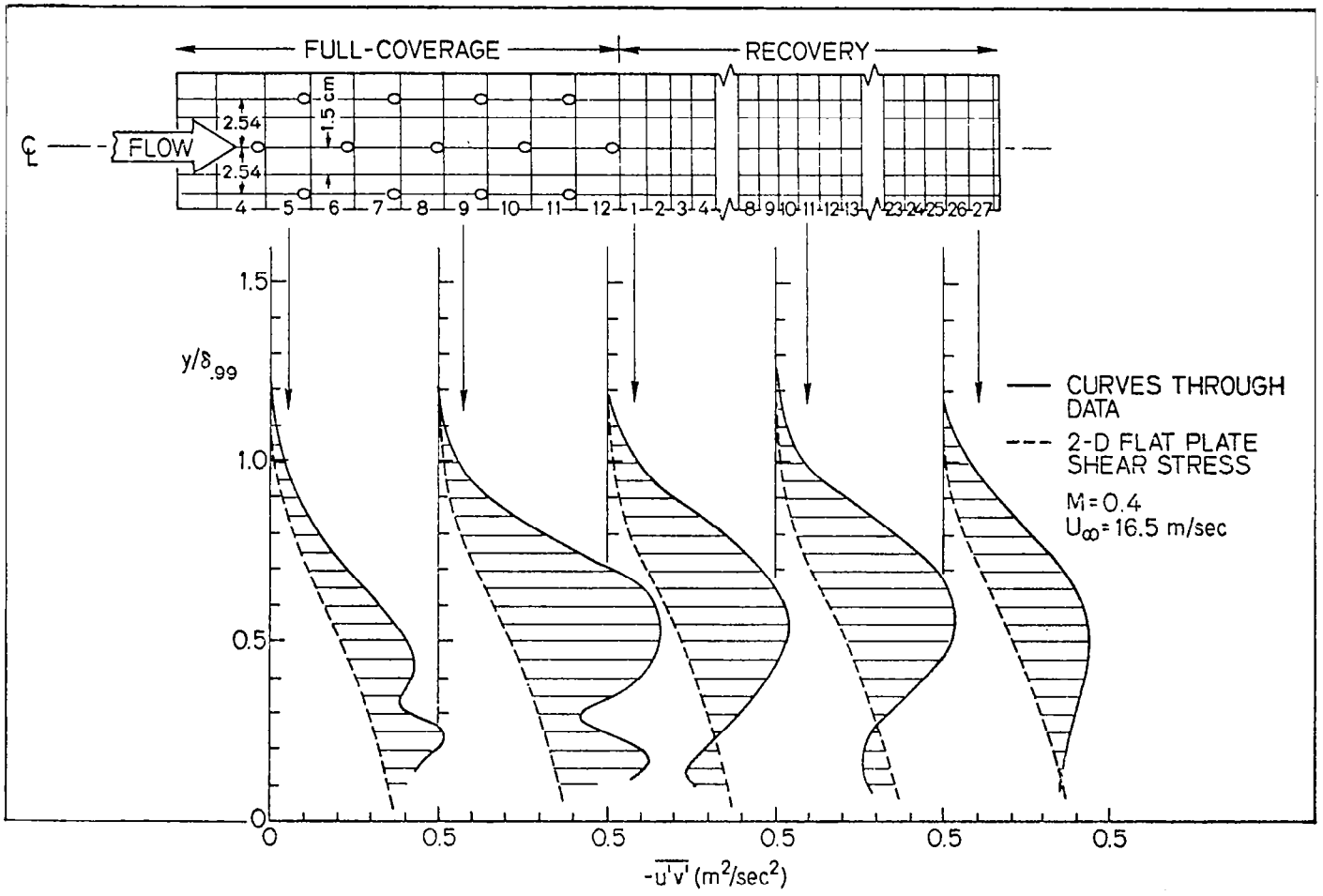

Fig. 5.14. Spanwise-averaged profiles of the streamwise turbulent shear stress component for M = 0.4.

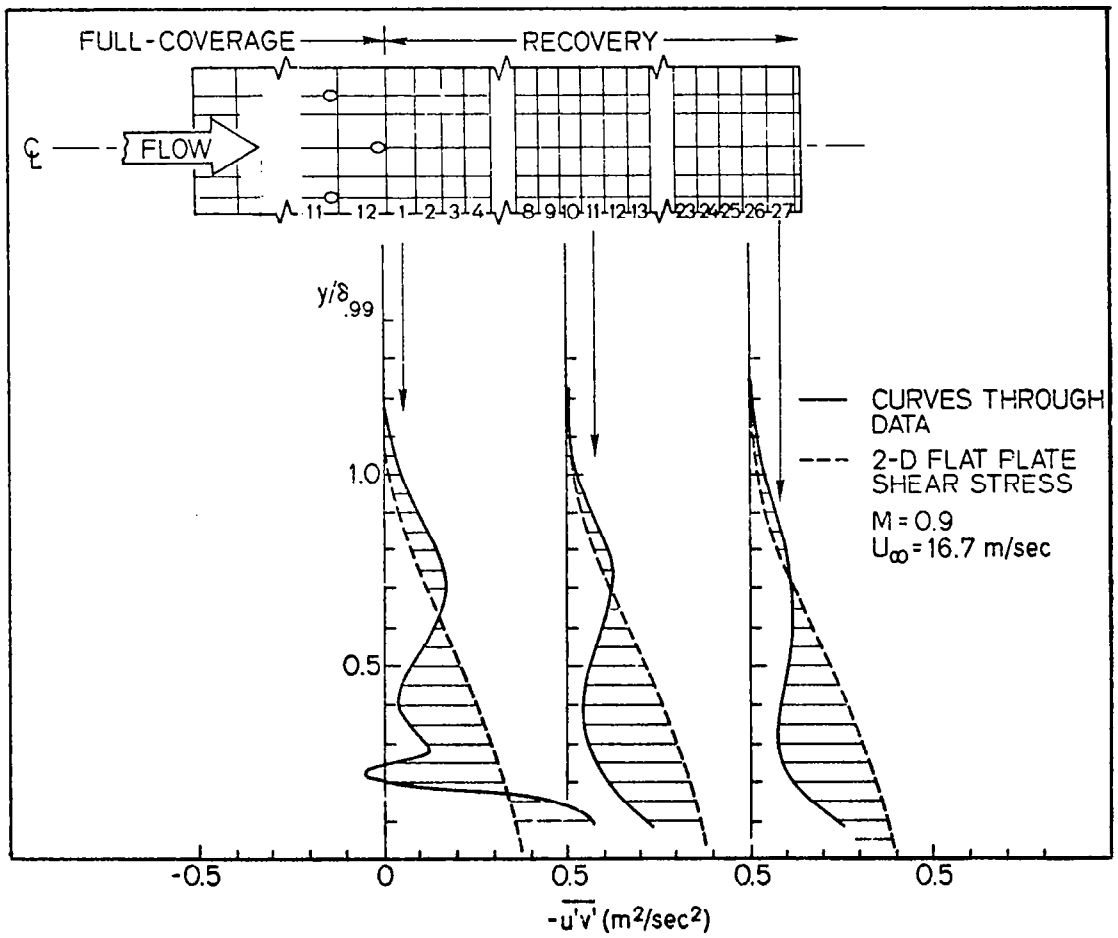

Fig. 5.15. Spanwise-averaged profiles of the streamwise turbulent shear stress component for M = 0.9.

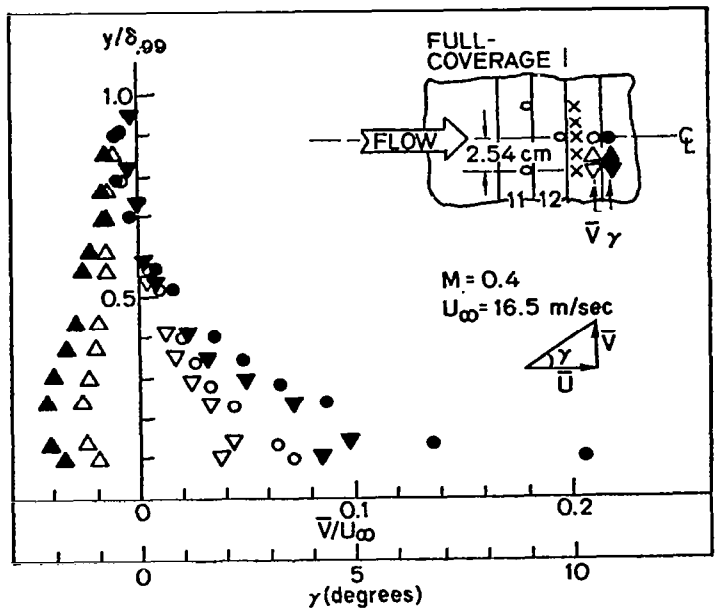

Fig. 5.16. $\bar{V}$ component of the mean velocity at the start of the recovery region for M = 0.4.

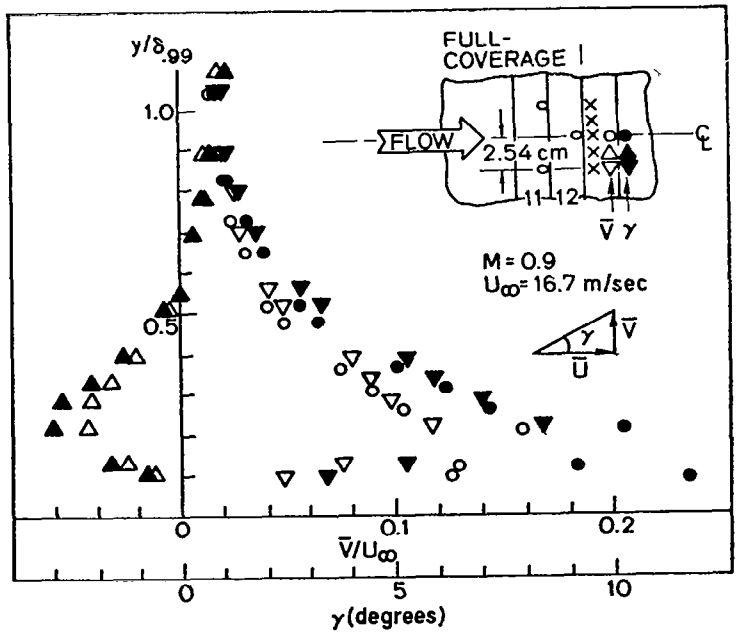

Fig. 5.17. $\bar{V}$ component of the mean velocity at the start of the recovery region for M = 0.9.

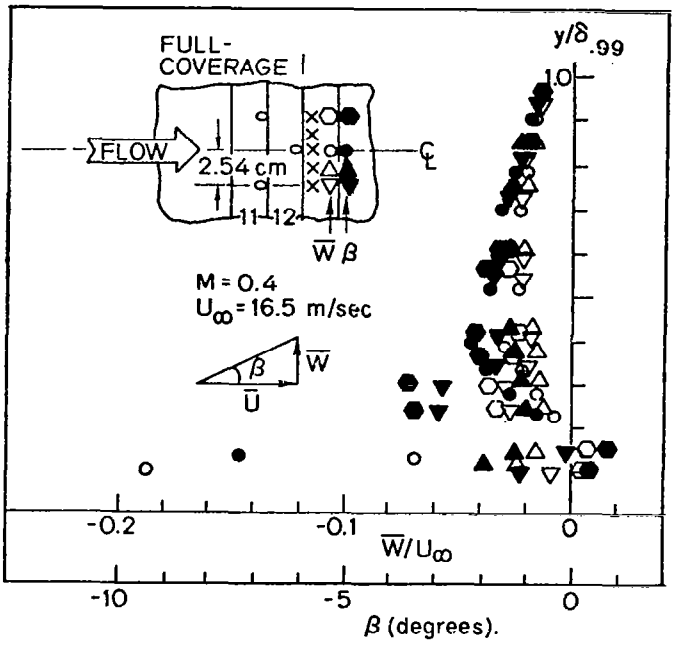

Fig. 5.18. $\overline{W}$ component of the mean velocity at the start of the recovery region for M = 0.4.

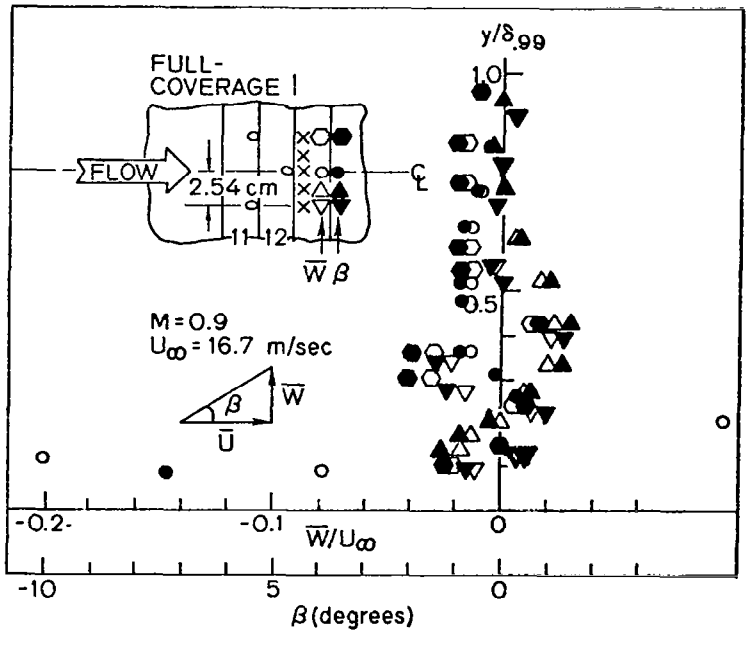

Fig. 5.19. $\overline{W}$ component of the mean velocity at the start of the recovery region for M = 0.9.

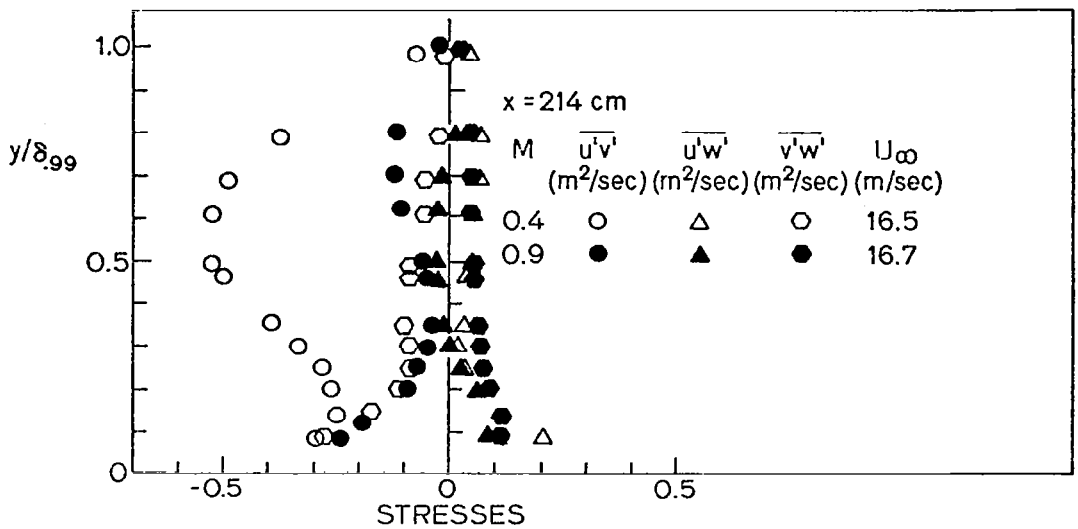

Fig. 5.20. Reynolds shear stresses at the first recovery region station.

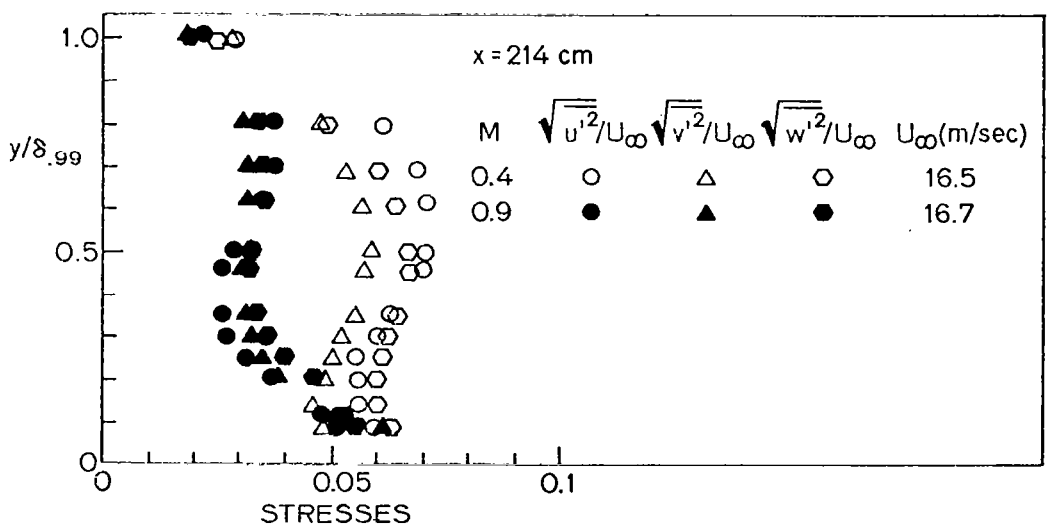

Fig. 5.21. Reynolds normal stresses at the first recovery region station.

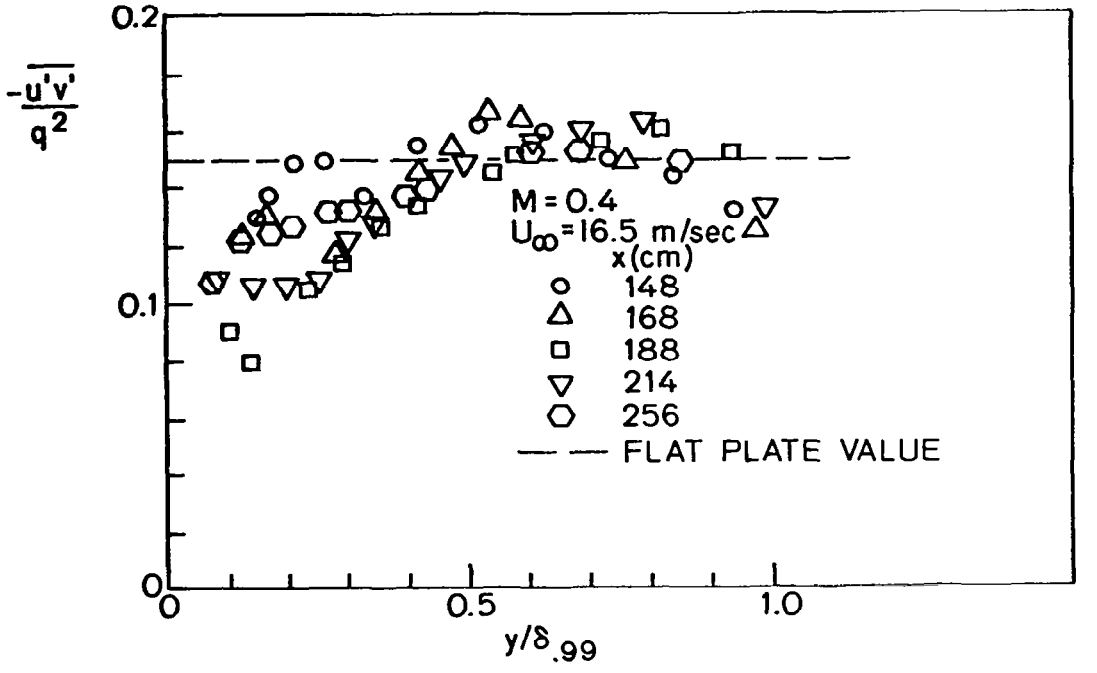

Fig. 5.22. Spanwise-averaged stress-energy ratio for M = 0.4.

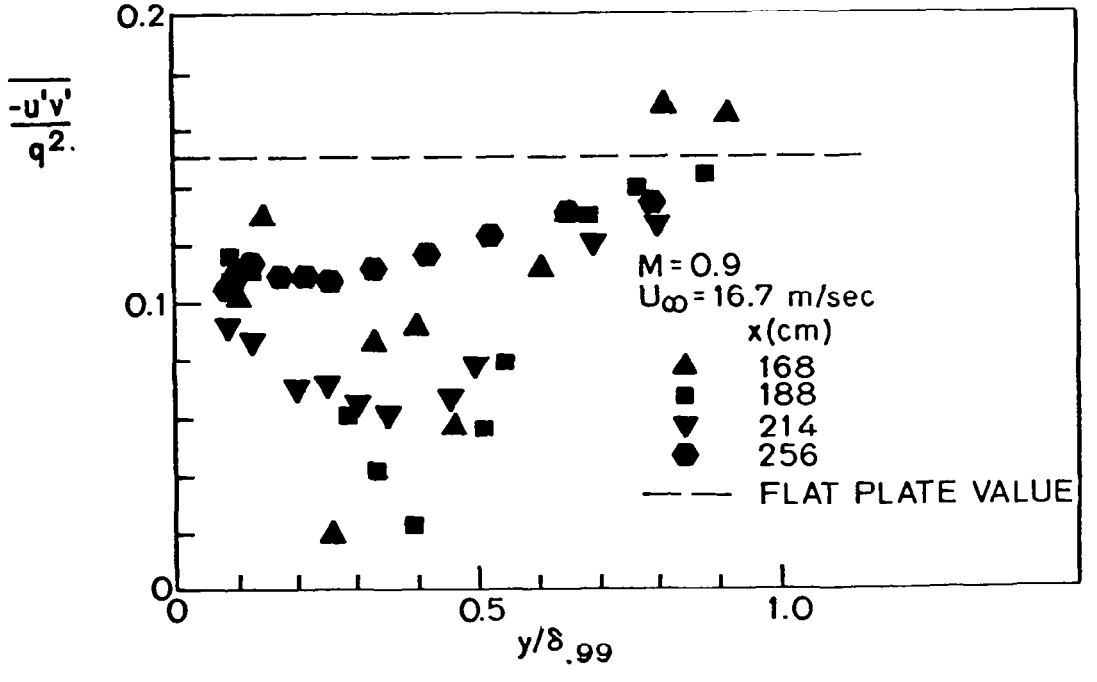

Fig. 5.23. Spanwise-averaged stress-energy ratio for M = 0.9.

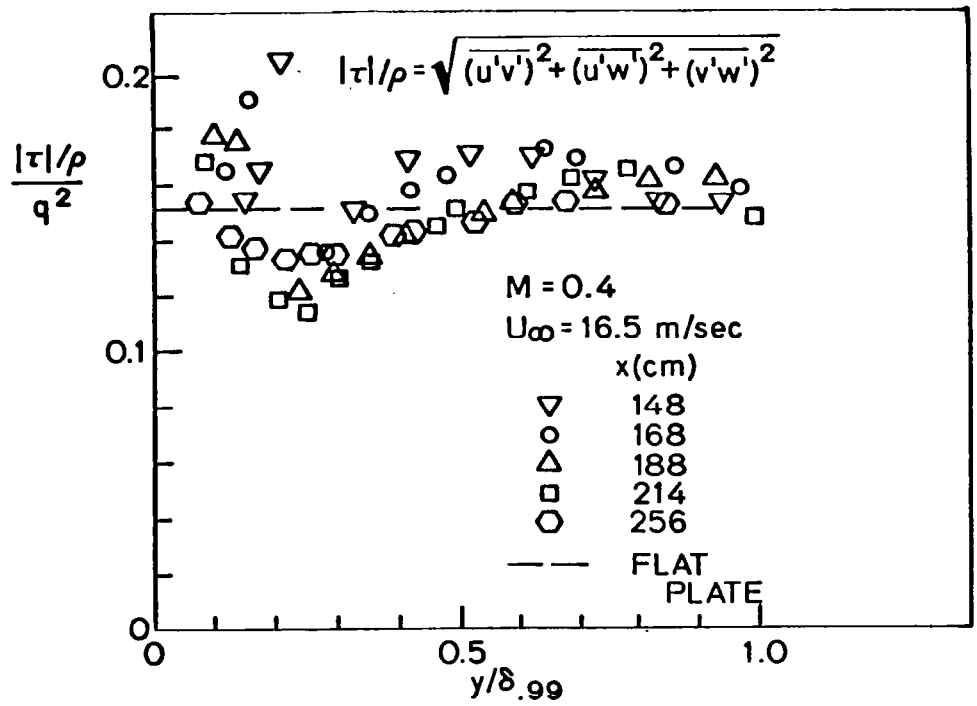

Fig. 5.24. Spanwise-averaged 3-D stress-energy ratio for M = 0.4.

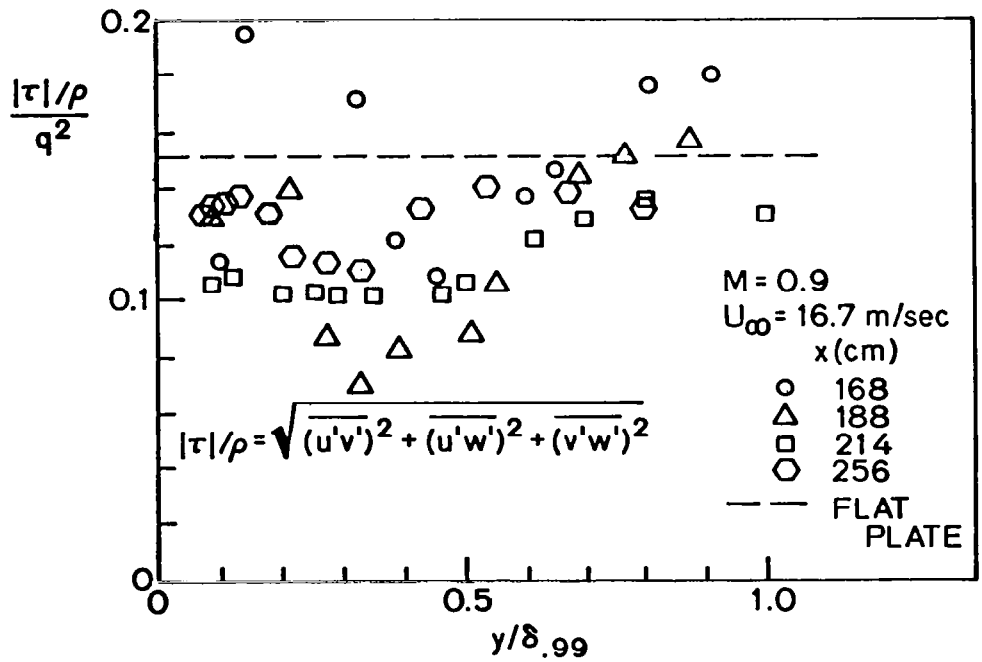

Fig. 5.25. Spanwise-averaged 3-D stress-energy ratio for M = 0.9.

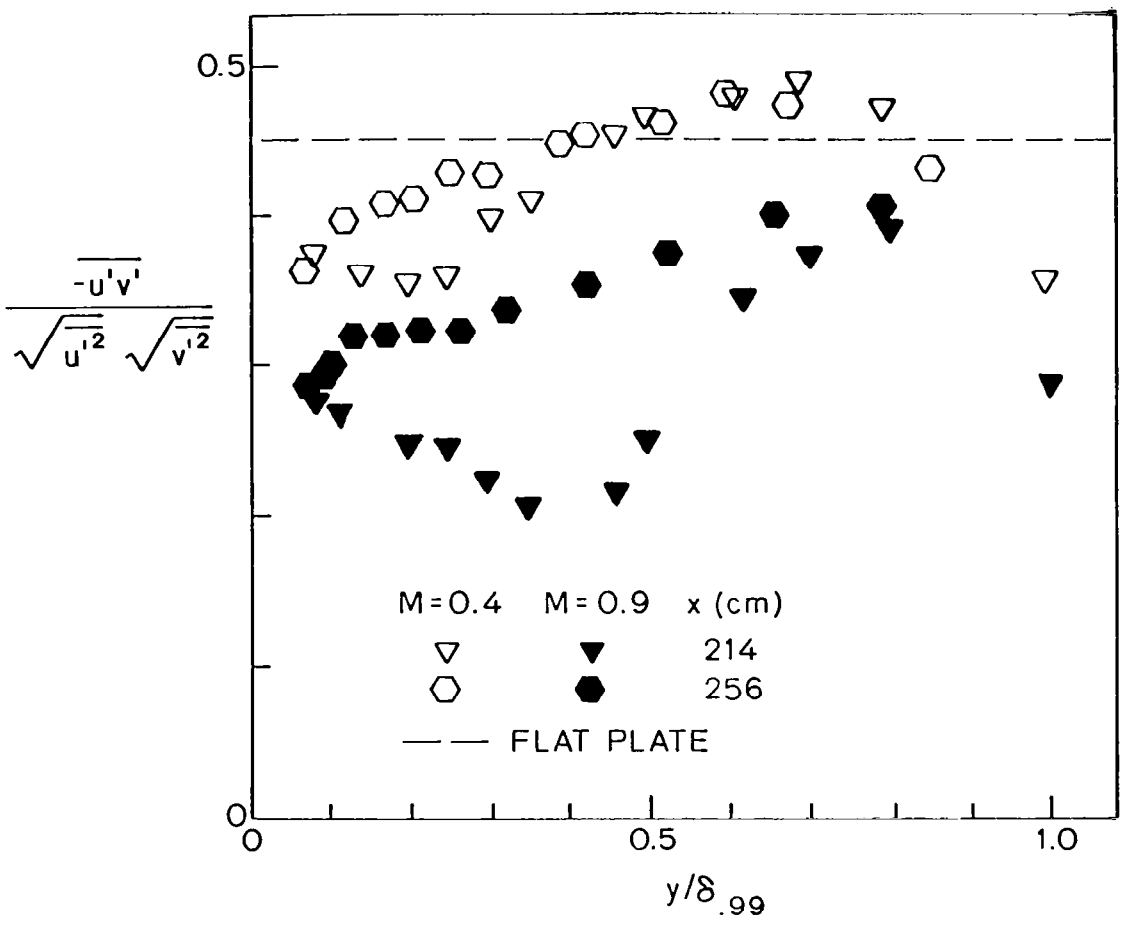

Fig. 5.26. Correlation coefficient for M = 0.4, 0.9 at the two recovery region stations.

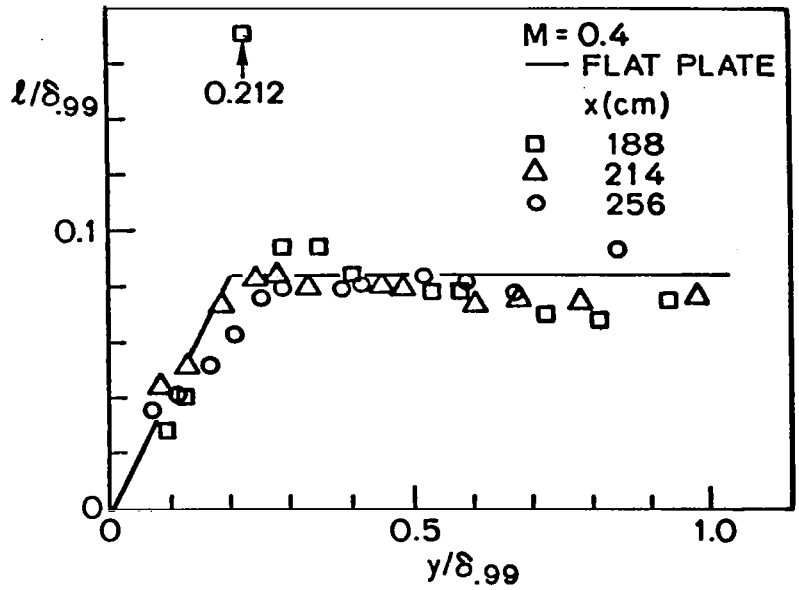

Fig. 5.27. Mixing-length distribution in the recovery region for M = 0.4.

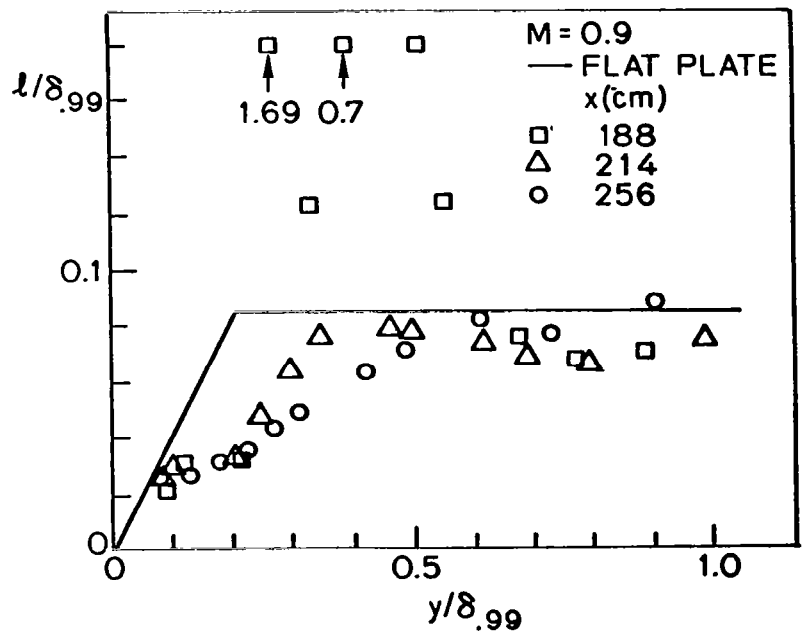

Fig. 5.28. Mixing-length distribution in the recovery region for M = 0.9.

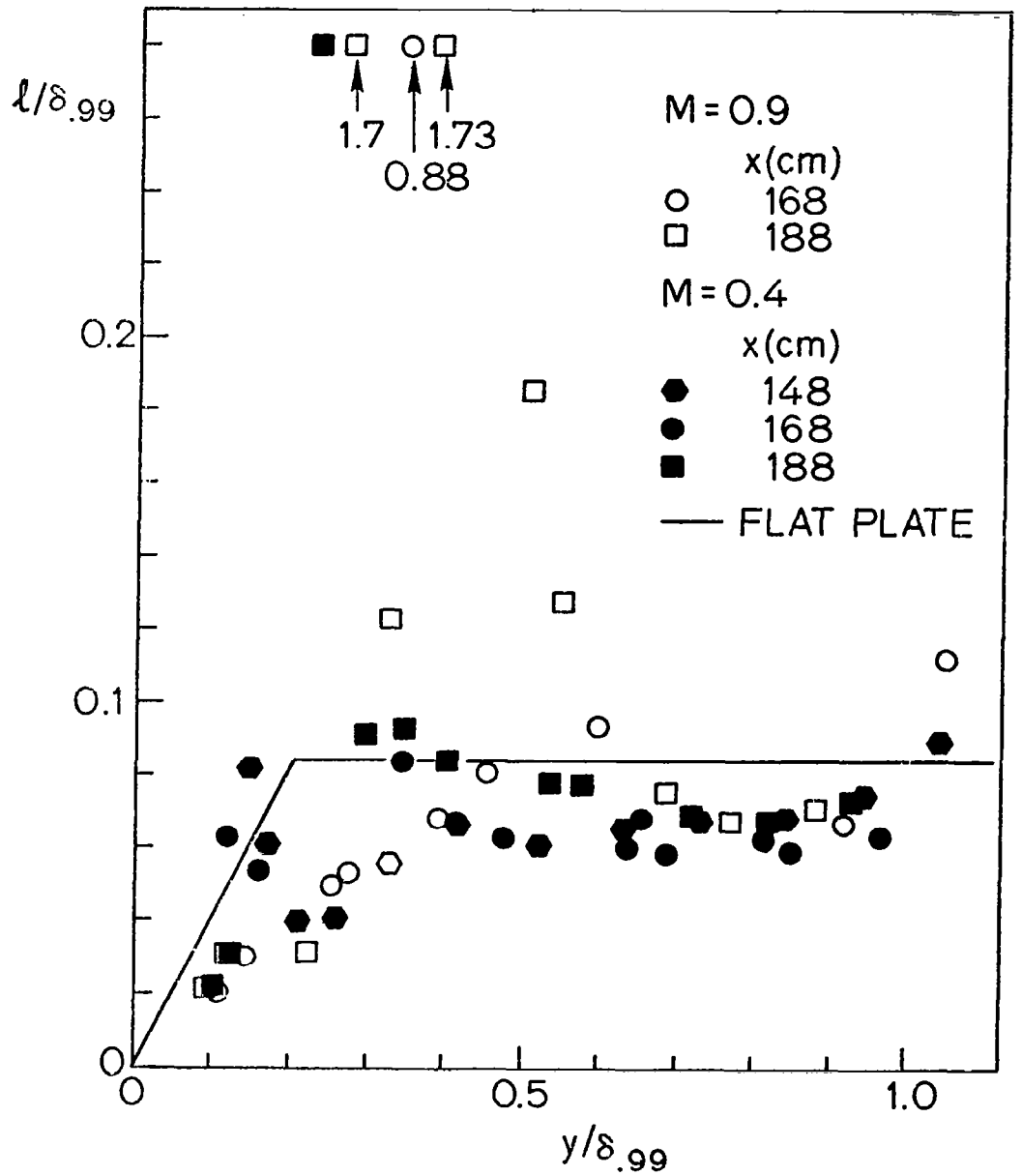

Fig. 5.29. Spanwise-averaged mixing-length distribution in the full-coverage region for M = 0.4 and M = 0.9.

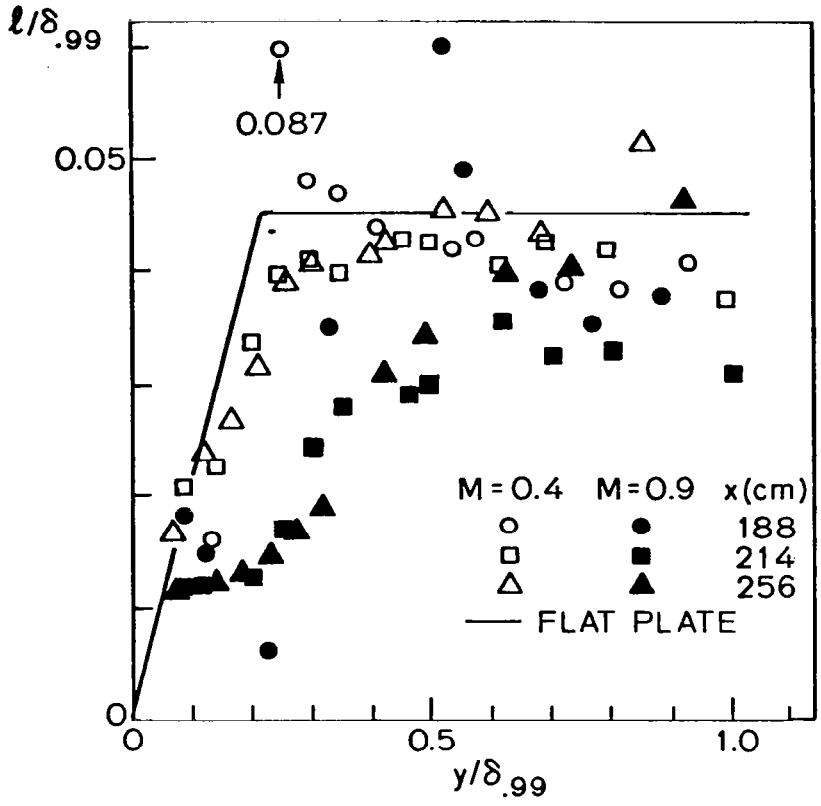

Fig. 5.30. Mixing-length obtained from the turbulent kinetic energy in the recovery region.

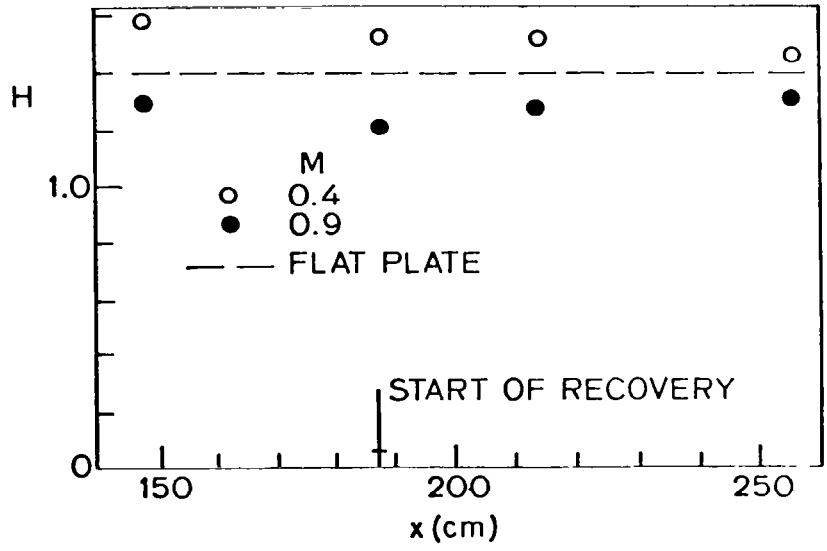

Fig. 5.31. Shape factor.

Chapter 6

SUMMARY AND RECOMMENDATIONS

6.1 Summary

The work reported here is a part of continuing study of the heat transfer and hydrodynamics associated with full-coverage film cooling. In the present work, hydrodynamic measurements were made with a triaxial hot-wire in the full-coverage region and the recovery region of a 30° slant-angle injection pattern. These measurements were made in isothermal flows at ambient temperature and pressure (about 20°C and 760 mm Hg) for two blowing ratios: $M = 0.9$ and $M = 0.4$. Profiles of the three mean velocity components and the six Reynolds stresses were obtained at several spanwise positions at each of five locations down the test plate: two within the full-coverage region, two within the recovery region, and one at the dividing line between the two regions.

One of the most important observations from these experiments is the peculiar dependence of TKE on the blowing ratio: high TKEs were observed for low blowing ($M = 0.4$), low TKEs for high blowing ($M = 0.9$). This phenomenon results from the low mean velocity gradients for high blowing (close to unity). The difference in the TKE levels has a significant effect on heat transfer behavior.

As a result, it was concluded that two different pairs of processes compete to govern the heat transfer, depending on the level of blowing: for low blowing, the energy sink near the wall competes with high turbulent mixing; for high blowing, the energy sink in the outer layer competes with the entrainment and convection of mainstream fluid toward the wall in the lanes between the jets. The present 2-D spanwise-averaged solution methods are not expected to predict the heat transfer well for high blowing ratios -- except in a purely formal way -- because they cannot handle the entrainment process and by definition neglect the spanwise 3-D flows.

The flow in the recovery region can be described in terms of a two-layer model: an outer boundary layer where the length scale scales on the total thickness of the layer, and an inner layer where the mixing

length is the usual κy and $\lambda\delta$. The two layers blend into each other with the spreading of jets. Recovery to a 2-D boundary layer is completed when the inner and outer layers finally merge.

A one-equation model of turbulence was used in the 2-D finite-difference boundary layer computer program (STAN5) to predict the mean velocity and TKE profiles in the recovery region. The one-equation model employs the TKE conservation equation with an algebraic relationship for the mixing length. Mixing-length values calculated from the data were input to the program using a piecewise continuous, heuristic fit consistent with the concept of the two quasi-independent layers observed in the recovery region. This mixing length pattern, used with a set of otherwise normal constants (for 2-D boundary layer predictions), successfully predicted all the spanwise-averaged features of the flow. This strongly suggests that the principal mechanisms were modeled adequately by the mixing-length formulation. It was also shown that the piecewise continuous heuristic model can be replaced by a set of relations taken from the literature describing the spreading of jets and the growth of boundary layers, thus supporting the physical arguments behind the mixing-length model.

Large amounts of data were required by the present program, and a new hot-wire scheme was developed for this work: a triaxial hot-wire with an analog device for real-time data reduction. The method is basically simple; i.e., with three orthogonal wires, the components of the instantaneous velocity vector can be deduced without recourse to any time averaging and without invoking the low-fluctuation assumption. The present method can tolerate an unknown flow direction within the following limits. The mean velocity was measured within a cone of $\pm$ 30° half apex angle around the probe axis with a maximum error of 4%, even in a high-velocity gradient (about 1600 1/sec). The turbulent kinetic energy was measured within a cone of 12° half apex angle with a maximum error of 12% up to the same velocity gradient point and within 5.5% in a region of zero velocity gradient. The method is very fast and practical for taking large amounts of data in three-dimensional, high-fluctuation turbulent flows.

6.2 Recommendations

- The present model for the length scale, developed for the recovery region, can probably be used also for the full-coverage region provided that the injection process is modeled correctly.
- Either 3-D solution methods should be used or new 2-D solution procedures should be devised to simulate the entrainment process for high blowing ratios, in order to better predict the heat transfer.
- For the 3-D turbulent flow measurement scheme, a smaller probe should be manufactured to decrease the errors arising from the probe size and to permit a closer approach to the wall.

RMS and correlator circuits can be added to the 3-D Turbulent Flow Analyzer which will increase the speed of data-taking, as well as allowing for reading important quantities such as mean velocity and TKE directly from the dials. This will greatly increase the range of applicability.

REFERENCES

Abramovich, G. N., 1960, The Theory of Turbulent Jets, MIT Press, p. 544.

Antonia, R. A., & Luxton, R. E., 1972, "The Response of a Turbulent Boundary Layer to a Step Change in Surface Roughness. Part 2. Rough to Smooth," J. Fluid Mechanics, 53, Part 4, 737-757.

Bergeles, G., Gosman, A. D., & Launder, B. E., 1975, "The Prediction of Three-Dimensional Discrete-Hole Cooling Processes: I - Laminar Flow," ASME Paper 75-WA/HT-109.

Boussinesq, J., 1877, "Theorie de l'ecoulement Tourbillant," Mem. Pre. Par. Div. Sav. 23, Paris.

Brunner, M. S., 1969, "Active Cooling Heat Protection," J. Space Craft, June 1969, Vol. 6, No. 6.

Choe, H., et al., 1975, "Turbulent Boundary Layer on a Full-Coverage Film-Cooled Surface -- An Experimental Heat Transfer Study with Normal Injection," NASA Rep. CR-2642 (also Stanford Univ., Mech. Engrg. Dept. Rep. HMT-22).

Colladay, R. S., & Russell, L. M., 1975, "Flow Visualization of Discrete-Hole Film Cooling for Gas Turbine Applications," NASA Rep. TM X-71766.

Crawford, M. E., & Kays, W. M., 1975, "STAN5 -- A Program for Numerical Computation of Two-Dimensional Internal/External Boundary Layer Flows," Stanford Univ., Mech. Engrg. Dept. Rep. HMT-23.

Crawford, M. E., et al., 1976, "Heat Transfer to a Full-Coverage Film-Cooled Surface with 30-Deg. Slant-Hole Injection," Stanford Univ., Mech. Engrg. Dept. Rep. HMT-25.

Delleur, J. W., 1966, "Flow Direction Measurement by Hot-Wire Anemometry," Journal A.S.C.E., Engineering Mechanics Division, Aug. 1966, Vol. 92, p. 45.

Eriksen, V. L., Eckert, E. R. G., & Goldstein, R. J., 1971, "A Model for Analysis of the Temperature Field Downstream of a Heated Jet Injected into an Isothermal Crossflow at an Angle of 90°," NASA Rep. CR-72990.

Escudier, M. P., 1966, "The Distribution of Mixing-Length in Turbulent Flows Near Walls," Imperial College, Heat Transfer Section, Rep. TWF/TN/1.

Esgar, J. B., 1971, "Turbine Cooling -- Its Limitations and Its Future," High Temperature Turbines, AGARD Conf. Proc. No. 73: 14.1-14.24.

Foster, R. C., Haji-Sheikh, A., 1974, "An Experimental Investigation of Boundary Layer Heat Transfer in the Region of Separated Flow Downstream of Normal Injection Slots," ASME Paper No. 74-HT-12.

Goldstein, R. J., 1971, "Film Cooling," Advances in Heat Transfer 7, 321-279.

Goldstein, R. J., et al., 1969, "Film Cooling Following Injection through Inclined Circular Tubes," NASA Rep. CR-73612.

Hartnett, J. P., Birkebak, R. C., & Eckert, E. R. G., 1961, "Velocity Distributions, Temperature Distributions, Effectiveness and Heat Transfer for Air Injected through a Tangential Slot into a Turbulent Boundary Layer," J. Heat Transfer, Aug. 1961, 293-306.

Herring, H. J., 1975, "A Method of Predicting the Behavior of a Turbulent Boundary Layer with Discrete Transpiration Jets," J. Eng. Power, 97, 214-224.

Hinze, J. O., 1975, Turbulence, McGraw-Hill Book Co., Second Edition, p. 643.

Hoffmeister, M., 1972, "Using a Single Hot-Wire Probe in Three-Dimensional Turbulent Flow Fields," DISA Information, May 1972, No. 13, 26-28.

Johnston, J. P., 1970, "Measurements in a Three-Dimensional Turbulent Boundary Layer Induced by a Swept Forward-Facing Step," J. Fluid Mechanics, 42, Part 4, 823-844.

Jorgensen, F. E., 1971, "Directional Sensitivity of Wire and Fiber Film Probes, An Experiemntal Study," DISA Information, May 1971, No. 11, 31-37.

Kacker, S. C., & Whitelaw, J. H., 1970, "Prediction of Wall-Jet and Wall-Wake Flows," J. Mech. Engrg. Science, 12, No. 6.

Keffer, J. F., & Bains, W. D., 1963, "The Round Turbulent Jet in a Cross-wind," J. Fluid Mechanics, 15, 481-496.

Klebanoff, P. S., 1955, "Characteristics of Turbulence in a Boundary Layer with Zero Pressure Gradient," NACA TN 1247.

Kolmogorov, A. N., 1942, "Equations of Turbulent Motion of an Incompressible Turbulent Fluid," Izv. Akad. Nauk SSSR, ser Phys. VI, No. 1-2, p. 56.

Launder, B. E., & Spalding, D. B., 1972, Lectures in Mathematical Models of Turbulence, Academic Press, London and New York.

LeBrocq, P. V., Launder, B. E., & Priddin, C. H., 1971, "Discrete Hole Injection as a Means of Transpiration Cooling -- An Experimental Study," Imp. Coll. Rep. HTS/71/37.

Mayle, R. E., & Camarata, F. J., 1975, "Multihole Cooling Film Effectiveness and Heat Transfer," J. Heat Transfer, 97, 534-538.

Metzger, D. E., Carper, H. J., & Warren, J. M., 1972, "Predicted Film Cooling near Flush Slots -- Comparison with Experiment," J. Aircraft, Dec. 1972, 9, No. 12, 857-863.

Metzger, D. E., Takeuchi, D. I., & Kuenstler, P. A., 1973, "Effectiveness and Heat Transfer with Full-Coverage Film-Cooling," J. Eng. Power, 95, 180-184.

Mojola, O. O., 1974, "A Hot-Wire Method for Three-Dimensional Shear Flows," DISA Information, July 1974, 16, 11-14.

Moussa, Z. M., & Eskinazi, S., 1975, "Directional Mean Flow Measurements Using a Single Inclined Hot-Wire," Physics of Fluids, March 1975, 18, No. 3, 298-305.

Nina, M. N. R., & Whitelaw, J. H., 1971, "The Effectiveness of Film Cooling with Three-Dimensional Slot Geometry," Gas Turbine Conference and Products Show, Houston, Texas, March 1971, ASME Paper No. 71-GT-11.

Pai, B. R., & Whitelaw, J. H., 1971, "The Prediction of Wall Temperature in the Presence of Film-Cooling," Int. J. Heat Mass Transfer 14, 409-426.

Patankar, S. V., Rastogi, A. K., & Whitelaw, J. H., 1973, "The Effectiveness of Three-Dimensional Film-Cooling Slots -- II. Predictions," Int. J. Heat Mass Transfer, 16, 1673-1681.

Pimenta, M. M., 1975, "The Turbulent Boundary Layer: An Experimental Study of the Transport of Momentum and Heat with the Effect of Roughness," Stanford Univ. Mech. Engrg. Dept. Rep. HMT-21.

Prandtl, L., 1925, "Über die Ausgebildete Turbulenz," ZAMM5, 136-139; and Proc. 2nd Intern. Congr. Applied Mech., Zurich, 1926, 62-75; also Coll. Works II, 736-751.

Prandtl, L., 1945, "Über ein Neues Formelsystem fur die Ausgebildete Turbulenz," Nachrichten von der Akad. de Wissenschaft in Gottingen.

Ramsey, J. W., & Goldstein, R. J., 1971, "Interaction of a Heated Jet with a Deflecting Stream," J. Heat Transfer, Nov. 1971, 365-372.

Samuel, A. E., & Joubert, P. N., 1965, "Film Cooling of an Adiabatic Flat Plate in Zero Pressure Gradient in the Presence of a Hot Mainstream and Cold Tangential Secondary Injection," J. Heat Transfer, 87, 409-419.

Schlichting, H., 1968, Boundary-Layer Theory, Sixth Edition, McGraw-Hill Book Company, p. 533.

Seban, R. A., & Back, L. H., 1962, "Velocity and Temperature Profiles in Turbulent Boundary Layers with Tangential Injection," J. Heat Transfer, 84, 45-54.

Wilson, D. J., & Goldstein, R. J., 1976, "Turbulent Wall Jets with Cylindrical Streamwise Surface Curvature," J. Fluids Engineering, Sept. 1976, 550-556.

Wolfshtein, M., 1969, "The Velocity and Temperature Distribution in One-Dimensional Flow with Turbulence Augmentation and Pressure Gradient," J. Heat Mass Transfer, 12, 301-318.

Zimmerman, D. R., & Abbott, D. E., 1975, "An Experimental Investigation of a Three-Dimensional Turbulent Boundary Layer," Tech. Rep. CFMTR-75-1, May 1975.

APPENDIX A

TABULATION OF EXPERIMENTAL DATA

A.1. Individual Profiles

This section contains the dimensional and non-dimensional profiles of three mean velocity components and six Reynolds stresses at each measurement location for blowing ratios M = 0.4 and 0.9. Profiles of turbulent kinetic energy, flow angles, mixing-length, and correlation coefficients are also given. The number of diameters downstream at the top of appropriate pages represents the distance of the measurement location from the last row of injection in terms of jet diameter D. The nomenclature given in this section also applies in Section A.2.

Nomenclature

BETA	β, angle between $\overline{U}$ and $\overline{W}$ components of mean velocity in degrees.
CM	cm.
DELM	δ, boundary layer thickness.
DELM1	δ_1, displacement thickness.
DELM2	δ_2, momentum thickness.
GAMA	γ, angle between $\overline{U}$ and $\overline{V}$ components of mean velocity in degrees.
L	ℓ, mixing-length.
M	$\rho_{jet}U_{jet}/\rho_\infty U_\infty$, blowing ratio.
M/S	m/sec.
M2/S2	m^2/sec^2.
P	P, hole spacing or pitch.
PR	P, pressure
Q	$\sqrt{q^2} = \sqrt{\overline{u'^2} + \overline{v'^2} + \overline{w'^2}}$
Q2	$q^2 = \overline{u'^2} + \overline{v'^2} + \overline{w'^2}$, turbulent kinetic energy.
R	$\overline{R} = \sqrt{\overline{U}^2 + \overline{V}^2 + \overline{W}^2}$, magnitude of mean velocity.

RF	U_∞, value of $\overline{R}$ at freestream.
RF2	$\overline{R}^2$ at freestream.
TF	T_∞, freestream temperature (°C).
U	$\overline{U}$, component of mean velocity in x-direction.
UDERV	$\partial\overline{U}/\partial y$, gradient of $\overline{U}$ component of mean velocity.
UF	U_∞, freestream velocity.
UF2	U_∞^2, freestream velocity squared.
UINF	U_∞, freestream velocity.
UP	u', component of fluctuating velocity in x-direction.
UP2	$\overline{u'^2}$, Reynolds normal stress in x-direction.
UV	$\overline{u'v'}$, longitudinal-normal velocity correlation, Reynolds shear stress.
UW	$\overline{u'w'}$, longitudinal-tangential velocity correlation, Reynolds shear stress.
V	$\overline{V}$, component of mean velocity in y-direction.
VP	v', component of fluctuating velocity in y-direction.
VP2	$\overline{v'^2}$, Reynolds normal stress in y-direction.
VW	$\overline{v'w'}$, normal-tangential velocity correlation, Reynolds shear stress.
W	$\overline{W}$, component of mean velocity in z-direction.
WP	w', component of fluctuating velocity in z-direction.
WP2	$\overline{w'^2}$, Reynolds normal stress in z-direction.
X	x, distance along test surface measured from nozzle exit.
Y	y, distance normal to test surface.
Z	z, distance in transverse direction on test surface measured from centerline.

M=0.4 BLOWING REGION AFTER 3 ROWS OF HOLES, X=148 CM AND Z/P=+0.5

RUN 12157602 TF= 20.00 C PR= 760.00 MM-HG DELM= 2.952 CM DELM1= 0.782 CM DELM2= 0.455 CM

DIMENSIONAL PROFILES

Y (CM)	U (M/S)	V (M/S)	W (M/S)	R (M/S)	UP2 (M2/S2)	VP2 (M2/S2)	WP2 (M2/S2)	Q2 (M2/S2)	UV (M2/S2)	UW (M2/S2)	VW (M2/S2)
0.419	8.00	0.29	-0.28	8.01	0.793	1.207	1.362	3.363	-0.354	0.260	-0.401
0.500	8.17	0.27	-0.22	8.18	0.795	1.225	1.380	3.400	-0.341	0.213	-0.344
0.600	8.38	0.30	-0.21	8.39	0.856	1.310	1.458	3.624	-0.397	0.141	-0.275
0.750	8.78	0.29	-0.37	8.79	1.169	1.456	1.560	4.186	-0.589	0.079	-0.253
0.950	9.68	0.18	-0.69	9.71	1.853	1.605	1.575	5.034	-0.824	0.085	-0.317
1.200	11.30	0.07	-0.79	11.33	2.236	1.350	1.357	4.943	-0.824	0.350	-0.338
1.500	13.06	-0.04	-0.47	13.07	1.356	0.790	0.869	3.015	-0.458	0.267	-0.159
1.800	14.12	-0.09	-0.28	14.13	0.833	0.515	0.548	1.896	-0.283	0.091	-0.048
2.100	14.91	-0.12	-0.21	14.91	0.587	0.378	0.379	1.345	-0.202	0.047	-0.019
2.400	15.52	-0.14	-0.16	15.53	0.404	0.263	0.246	0.913	-0.130	0.037	-0.005
2.700	16.02	-0.13	-0.08	16.02	0.224	0.155	0.137	0.517	-0.068	0.031	0.000
3.000	16.32	-0.11	-0.01	16.32	0.088	0.077	0.062	0.227	-0.025	0.021	0.002
4.000	16.45	-0.09	0.12	16.46	0.010	0.006	0.003	0.019	0.000	0.001	0.000

NON-DIMENSIONAL PROFILES

Y/DELM	U/RF	V/RF	W/RF	GAMA	BETA	UP/RF	VP/RF	WP/RF	Q/RF	UV/RF2	UW/RF2	VW/RF2
0.142	0.486	0.018	-0.017	2.1	-2.0	0.054	0.067	0.071	0.111	-0.13D-02	0.96D-03	-0.15D-02
0.169	0.496	0.016	-0.013	1.9	-1.5	0.054	0.067	0.071	0.112	-0.13D-02	0.79D-03	-0.13D-02
0.203	0.509	0.018	-0.013	2.1	-1.4	0.056	0.070	0.073	0.116	-0.15D-02	0.52D-03	-0.10D-02
0.254	0.533	0.018	-0.022	1.9	-2.4	0.066	0.073	0.076	0.124	-0.22D-02	0.29D-03	-0.93D-03
0.322	0.588	0.011	-0.042	1.1	-4.1	0.083	0.077	0.076	0.136	-0.30D-02	0.31D-03	-0.12D-02
0.406	0.687	0.004	-0.048	0.4	-4.0	0.091	0.071	0.071	0.135	-0.30D-02	0.13D-02	-0.12D-02
0.508	0.793	-0.002	-0.029	-0.2	-2.1	0.071	0.054	0.057	0.105	-0.17D-02	0.99D-03	-0.59D-03
0.610	0.858	-0.005	-0.017	-0.4	-1.1	0.055	0.044	0.045	0.084	-0.10D-02	0.34D-03	-0.18D-03
0.711	0.906	-0.007	-0.013	-0.5	-0.8	0.047	0.037	0.037	0.070	-0.75D-03	0.17D-03	-0.70D-04
0.813	0.943	-0.009	-0.010	-0.5	-0.6	0.039	0.031	0.030	0.058	-0.48D-03	0.14D-03	-0.16D-04
0.915	0.973	-0.008	-0.005	-0.5	-0.3	0.029	0.024	0.022	0.044	-0.25D-03	0.11D-03	0.00D 00
1.016	0.991	-0.007	-0.001	-0.4	-0.0	0.018	0.017	0.015	0.029	-0.92D-04	0.78D-04	0.74D-05
1.355	0.999	-0.005	0.007	-0.3	0.4	0.006	0.005	0.003	0.008	0.00D 00	0.37D-05	0.00D 00

Y/DELM	L/DELM	UV/Q2	UV/(UP*VP)
0.142	0.099	-0.105	-0.362
0.169	0.096	-0.100	-0.346
0.203	0.093	-0.110	-0.375
0.254	0.076	-0.141	-0.451
0.322	0.055	-0.164	-0.478
0.406	0.047	-0.167	-0.474
0.508	0.048	-0.152	-0.443
0.610	0.061	-0.149	-0.432
0.711	0.067	-0.150	-0.429
0.813	0.066	-0.142	-0.399
0.915	0.066	-0.132	-0.365
1.016	0.074	-0.110	-0.304
1.355	0.000	0.000	0.000

M=0.4 BLOWING REGION AFTER 3 ROWS OF HOLES, X=148 CM AND Z/P=+0.3

RUN 12157601 TF= 20.00 C PR= 760.00 MM-HG DELM= 2.783 CM DELM1= 0.523 CM DELM2= 0.374 CM

DIMENSIONAL PROFILES

Y (CM)	U (M/S)	V (M/S)	W (M/S)	R (M/S)	UP2 (M2/S2)	VP2 (M2/S2)	WP2 (M2/S2)	Q2 (M2/S2)	UV (M2/S2)	UW (M2/S2)	VW (M2/S2)
0.419	10.96	-0.21	-0.35	10.97	1.036	0.820	0.901	2.757	-0.295	-0.053	-0.190
0.500	11.14	-0.26	-0.28	11.15	1.008	0.820	0.866	2.694	-0.298	-0.093	-0.191
0.600	11.54	-0.28	-0.22	11.54	0.993	0.809	0.824	2.626	-0.306	-0.142	-0.115
0.750	11.99	-0.27	-0.16	12.00	1.001	0.820	0.774	2.596	-0.324	-0.175	-0.077
0.950	12.57	-0.24	-0.14	12.58	1.027	0.800	0.711	2.538	-0.356	-0.175	-0.055
1.200	13.20	-0.21	-0.14	13.21	0.923	0.710	0.633	2.266	-0.332	-0.113	-0.052
1.500	13.96	-0.18	-0.15	13.96	0.796	0.588	0.535	1.920	-0.293	-0.058	-0.037
1.800	14.66	-0.17	-0.13	14.67	0.643	0.464	0.426	1.534	-0.239	-0.033	-0.025
2.100	15.28	-0.16	-0.12	15.28	0.494	0.344	0.309	1.147	-0.179	-0.011	-0.015
2.400	15.83	-0.16	-0.09	15.83	0.320	0.230	0.193	0.743	-0.116	0.007	-0.004
2.700	16.23	-0.16	-0.04	16.23	0.163	0.135	0.100	0.398	-0.061	0.018	0.000
3.000	16.43	-0.16	0.04	16.43	0.058	0.065	0.040	0.164	-0.021	0.011	0.002
4.000	16.47	-0.17	0.13	16.47	0.011	0.005	0.003	0.020	0.000	0.001	0.001

NON-DIMENSIONAL PROFILES

Y/DELM	U/RF	V/RF	W/RF	GAMA	BETA	UP/RF	VP/RF	WP/RF	Q/RF	UV/RF2	UW/RF2	VW/RF2
0.151	0.665	-0.013	-0.021	-1.1	-1.8	0.062	0.055	0.058	0.101	-0.11D-02	-0.20D-03	-0.70D-03
0.180	0.676	-0.016	-0.017	-1.3	-1.4	0.061	0.055	0.057	0.100	-0.11D-02	-0.34D-03	-0.56D-03
0.216	0.701	-0.017	-0.013	-1.4	-1.1	0.061	0.055	0.055	0.098	-0.11D-02	-0.52D-03	-0.42D-03
0.270	0.728	-0.016	-0.010	-1.3	-0.8	0.061	0.055	0.053	0.098	-0.12D-02	-0.65D-03	-0.28D-03
0.341	0.763	-0.015	-0.009	-1.1	-0.6	0.062	0.054	0.051	0.097	-0.13D-02	-0.65D-03	-0.20D-03
0.431	0.801	-0.013	-0.009	-0.9	-0.6	0.058	0.051	0.048	0.091	-0.12D-02	-0.42D-03	-0.19D-03
0.539	0.848	-0.011	-0.009	-0.7	-0.6	0.054	0.047	0.044	0.084	-0.11D-02	-0.21D-03	-0.14D-03
0.647	0.890	-0.010	-0.008	-0.7	-0.5	0.049	0.041	0.040	0.075	-0.88D-03	-0.12D-03	-0.92D-04
0.755	0.928	-0.010	-0.007	-0.6	-0.4	0.043	0.036	0.034	0.065	-0.66D-03	-0.41D-04	-0.55D-04
0.862	0.961	-0.010	-0.005	-0.6	-0.3	0.034	0.029	0.027	0.052	-0.43D-03	0.26D-04	-0.15D-04
0.970	0.985	-0.010	-0.002	-0.6	-0.1	0.025	0.022	0.019	0.038	-0.22D-03	0.66D-04	0.00D 00
1.078	0.998	-0.010	0.002	-0.6	0.1	0.015	0.015	0.012	0.025	-0.77D-04	0.41D-04	0.74D-05
1.437	1.000	-0.010	0.008	-0.6	0.5	0.006	0.004	0.003	0.009	0.00D 00	0.37D-05	0.37D-05

Y/DELM	L/DELM	UV/Q2	UV/(UP*VP)
0.151	0.075	-0.107	-0.320
0.180	0.063	-0.111	-0.328
0.216	0.057	-0.117	-0.341
0.270	0.068	-0.125	-0.358
0.341	0.080	-0.140	-0.393
0.431	0.083	-0.147	-0.410
0.539	0.079	-0.153	-0.428
0.647	0.080	-0.156	-0.438
0.755	0.077	-0.156	-0.434
0.862	0.075	-0.156	-0.428
0.970	0.090	-0.153	-0.411
1.078	0.121	-0.128	-0.342
1.437	0.000	0.000	0.000

M=0.4 BLOWING REGION AFTER 3 ROWS OF HOLES, X=148 CM AND Z/P= 0.0

RUN 12147604 TF= 21.00 C PR= 760.00 MM-HG DELM= 2.934 CM DELM1= 0.898 CM DELM2= 0.449 CM

DIMENSIONAL PROFILES

Y (CM)	U (M/S)	V (M/S)	W (M/S)	R (M/S)	UP2 (M2/S2)	VP2 (M2/S2)	WP2 (M2/S2)	Q2 (M2/S2)	UV (M2/S2)	UW (M2/S2)	VW (M2/S2)
0.419	5.40	0.59	-0.35	5.45	0.754	2.346	2.195	5.295	-0.655	-0.024	-0.056
0.500	5.65	0.49	-0.93	5.75	0.906	2.566	2.195	5.667	-0.772	0.034	-0.383
0.600	6.54	0.61	-1.96	6.85	1.333	2.510	1.981	5.825	-0.916	0.357	-0.965
0.750	8.60	0.60	-1.61	8.77	1.255	1.537	2.012	4.804	-0.780	0.970	-0.906
0.950	10.06	0.56	-0.27	10.08	0.548	0.780	0.894	2.223	-0.258	0.031	-0.093
1.200	10.84	0.40	-0.45	10.85	0.964	0.910	0.939	2.813	-0.462	-0.019	-0.122
1.500	12.23	0.23	-0.54	12.24	1.480	0.956	0.947	3.383	-0.591	0.049	-0.122
1.800	13.64	0.11	-0.45	13.64	1.323	0.741	0.742	2.806	-0.474	0.190	-0.100
2.100	14.77	0.04	-0.28	14.78	0.757	0.447	0.464	1.668	-0.242	0.145	-0.038
2.400	15.49	0.01	-0.17	15.49	0.425	0.266	0.269	0.961	-0.127	0.081	-0.005
2.700	15.97	0.02	-0.07	15.97	0.221	0.146	0.145	0.512	-0.055	0.053	0.004
3.000	16.28	0.05	0.01	16.28	0.081	0.067	0.062	0.210	-0.017	0.025	0.004
4.000	16.39	0.07	0.13	16.39	0.010	0.006	0.003	0.019	0.000	0.001	0.000

NON-DIMENSIONAL PROFILES

Y/DELM	U/RF	V/RF	W/RF	GAMA	BETA	UP/RF	VP/RF	WP/RF	Q/RF	UV/RF2	UW/RF2	VW/RF2
0.143	0.329	0.036	-0.021	6.2	-3.7	0.053	0.093	0.090	0.140	-0.24D-02	-0.89D-04	-0.21D-03
0.170	0.345	0.030	-0.057	5.0	-9.3	0.058	0.098	0.090	0.145	-0.29D-02	0.13D-03	-0.14D-02
0.205	0.399	0.037	-0.120	5.3	-16.7	0.070	0.097	0.086	0.147	-0.34D-02	0.13D-02	-0.36D-02
0.256	0.525	0.037	-0.098	4.0	-10.6	0.068	0.076	0.087	0.134	-0.29D-02	0.36D-02	-0.34D-02
0.324	0.614	0.034	-0.016	3.2	-1.5	0.045	0.054	0.058	0.091	-0.96D-03	0.12D-03	-0.35D-03
0.409	0.661	0.024	-0.027	2.1	-2.4	0.060	0.058	0.059	0.102	-0.17D-02	-0.71D-04	-0.45D-03
0.511	0.746	0.014	-0.033	1.1	-2.5	0.074	0.060	0.059	0.112	-0.22D-02	0.18D-03	-0.45D-03
0.614	0.832	0.007	-0.027	0.5	-1.9	0.070	0.053	0.053	0.102	-0.18D-02	0.71D-03	-0.37D-03
0.716	0.901	0.002	-0.017	0.2	-1.1	0.053	0.041	0.042	0.079	-0.90D-03	0.54D-03	-0.14D-03
0.818	0.945	0.001	-0.010	0.0	-0.6	0.040	0.031	0.032	0.060	-0.47D-03	0.30D-03	-0.19D-04
0.920	0.974	0.001	-0.004	0.1	-0.3	0.029	0.023	0.023	0.044	-0.20D-03	0.20D-03	0.15D-04
1.023	0.993	0.003	0.001	0.2	0.0	0.017	0.016	0.015	0.028	-0.63D-04	0.93D-04	0.15D-04
1.363	1.000	0.004	0.008	0.2	0.5	0.006	0.005	0.003	0.008	0.00D 00	0.37D-05	0.00D 00

Y/DELM	L/DELM	UV/Q2	UV/(UP*VP)
0.143	0.121	-0.124	-0.492
0.170	0.056	-0.136	-0.506
0.205	0.027	-0.157	-0.501
0.256	0.025	-0.162	-0.562
0.324	0.042	-0.116	-0.395
0.409	0.068	-0.164	-0.493
0.511	0.052	-0.175	-0.497
0.614	0.054	-0.169	-0.479
0.716	0.055	-0.145	-0.416
0.818	0.064	-0.132	-0.378
0.920	0.061	-0.107	-0.306
1.023	0.059	-0.081	-0.231
1.363	0.000	0.000	0.000

M=0.4 BLOWING REGION AFTER 3 ROWS OF HOLES, X=148 CM AND Z/P=-0.3

RUN 12157603 TF= 20.00 C PR= 760.00 MM-HG DELM= 2.852 CM DELM1= 0.530 CM DELM2= 0.379 CM

DIMENSIONAL PROFILES

Y (CM)	U (M/S)	V (M/S)	W (M/S)	R (M/S)	UP2 (M2/S2)	VP2 (M2/S2)	WP2 (M2/S2)	Q2 (M2/S2)	UV (M2/S2)	UW (M2/S2)	VW (M2/S2)
0.419	10.68	-0.25	-0.72	10.71	0.989	0.799	0.743	2.532	-0.335	0.129	-0.213
0.500	10.92	-0.32	-0.66	10.94	0.956	0.783	0.706	2.445	-0.306	0.109	-0.184
0.600	11.34	-0.42	-0.57	11.37	0.914	0.761	0.669	2.344	-0.261	0.093	-0.140
0.750	11.85	-0.45	-0.52	11.87	0.865	0.761	0.674	2.300	-0.248	0.076	-0.101
0.950	12.44	-0.45	-0.46	12.45	0.847	0.714	0.657	2.218	-0.240	0.056	-0.069
1.200	13.07	-0.36	-0.39	13.08	0.789	0.631	0.627	2.047	-0.243	0.010	-0.048
1.500	13.78	-0.27	-0.30	13.79	0.709	0.527	0.539	1.775	-0.245	-0.015	-0.035
1.800	14.43	-0.19	-0.25	14.44	0.611	0.442	0.431	1.484	-0.217	-0.018	-0.020
2.100	15.02	-0.15	-0.20	15.02	0.484	0.337	0.322	1.143	-0.174	-0.013	-0.010
2.400	15.54	-0.11	-0.16	15.54	0.336	0.236	0.206	0.778	-0.118	0.006	-0.002
2.700	15.95	-0.09	-0.11	15.95	0.183	0.143	0.110	0.436	-0.065	0.018	0.001
3.000	16.15	-0.09	-0.04	16.15	0.071	0.070	0.049	0.190	-0.025	0.013	0.002
4.000	16.24	-0.08	0.05	16.24	0.010	0.005	0.002	0.018	0.000	0.001	0.000

NON-DIMENSIONAL PROFILES

Y/DELM	U/RF	V/RF	W/RF	GAMA	BETA	UP/RF	VP/RF	WP/RF	Q/RF	UV/RF2	UW/RF2	VW/RF2
0.147	0.658	-0.015	-0.044	-1.3	-3.9	0.061	0.055	0.053	0.098	-0.13D-02	0.49D-03	-0.81D-03
0.175	0.672	-0.020	-0.041	-1.7	-3.5	0.060	0.054	0.052	0.096	-0.12D-02	0.41D-03	-0.70D-03
0.210	0.698	-0.026	-0.035	-2.1	-2.9	0.059	0.054	0.050	0.094	-0.99D-03	0.35D-03	-0.53D-03
0.263	0.730	-0.028	-0.032	-2.2	-2.5	0.057	0.054	0.051	0.093	-0.94D-03	0.29D-03	-0.38D-03
0.333	0.766	-0.028	-0.028	-2.1	-2.1	0.057	0.052	0.050	0.092	-0.91D-03	0.21D-03	-0.26D-03
0.421	0.805	-0.022	-0.024	-1.6	-1.7	0.055	0.049	0.049	0.088	-0.92D-03	0.38D-04	-0.18D-03
0.526	0.849	-0.017	-0.018	-1.1	-1.2	0.052	0.045	0.045	0.082	-0.93D-03	-0.57D-04	-0.13D-03
0.631	0.889	-0.012	-0.015	-0.8	-1.0	0.048	0.041	0.040	0.075	-0.82D-03	-0.68D-04	-0.76D-04
0.736	0.925	-0.009	-0.012	-0.6	-0.8	0.043	0.036	0.035	0.066	-0.66D-03	-0.49D-04	-0.38D-04
0.842	0.957	-0.007	-0.010	-0.4	-0.6	0.036	0.030	0.028	0.054	-0.45D-03	0.23D-04	-0.76D-05
0.947	0.982	-0.006	-0.007	-0.3	-0.4	0.026	0.023	0.020	0.041	-0.25D-03	0.68D-04	0.38D-05
1.052	0.994	-0.006	-0.002	-0.3	-0.1	0.016	0.016	0.014	0.027	-0.95D-04	0.49D-04	0.76D-05
1.403	1.000	-0.005	0.003	-0.3	0.2	0.006	0.004	0.003	0.008	0.00D 00	0.38D-05	0.00D 00

Y/DELM	L/DELM	UV/Q2	UV/(UP*VP)
0.147	0.058	-0.132	-0.377
0.175	0.054	-0.125	-0.354
0.210	0.049	-0.111	-0.313
0.263	0.054	-0.108	-0.306
0.333	0.063	-0.108	-0.309
0.421	0.071	-0.119	-0.344
0.526	0.076	-0.138	-0.401
0.631	0.079	-0.146	-0.418
0.736	0.078	-0.152	-0.431
0.842	0.076	-0.152	-0.419
0.947	0.088	-0.149	-0.402
1.052	0.122	-0.132	-0.355
1.403	0.000	0.000	0.000

M=0.4 BLOWING REGION AFTER 3 ROWS OF HOLES, X=148 CM AND Z/P=-0.5

RUN 12157604 TF= 20.00 C PR= 760.00 MM-HG DELM= 2.803 CM DELM1= 0.735 CM DELM2= 0.425 CM

DIMENSIONAL PROFILES

Y (CM)	U (M/S)	V (M/S)	W (M/S)	R (M/S)	UP2 (M2/S2)	VP2 (M2/S2)	WP2 (M2/S2)	Q2 (M2/S2)	UV (M2/S2)	UW (M2/S2)	VW (M2/S2)
0.419	7.96	0.41	-0.42	7.98	0.825	1.330	1.621	3.777	-0.371	0.165	-0.408
0.500	8.16	0.36	-0.39	8.18	0.835	1.352	1.600	3.788	-0.381	0.138	-0.414
0.600	8.45	0.38	-0.38	8.46	0.958	1.418	1.665	4.041	-0.477	0.052	-0.315
0.750	9.01	0.33	-0.56	9.03	1.387	1.574	1.737	4.698	-0.690	-0.011	-0.307
0.950	10.12	0.22	-0.83	10.15	2.120	1.664	1.636	5.421	-0.923	0.063	-0.376
1.200	11.90	0.05	-0.85	11.93	2.191	1.293	1.277	4.761	-0.818	0.373	-0.349
1.500	13.61	-0.11	-0.47	13.62	1.138	0.688	0.729	2.556	-0.387	0.203	-0.124
1.800	14.60	-0.17	-0.30	14.60	0.708	0.453	0.449	1.610	-0.233	0.066	-0.035
2.100	15.28	-0.17	-0.24	15.28	0.490	0.323	0.304	1.117	-0.163	0.044	-0.014
2.400	15.84	-0.18	-0.18	15.84	0.317	0.210	0.194	0.721	-0.098	0.037	-0.001
2.700	16.25	-0.17	-0.10	16.25	0.154	0.118	0.100	0.372	-0.047	0.032	0.000
3.000	16.46	-0.16	-0.01	16.46	0.051	0.055	0.040	0.146	-0.015	0.013	0.001
4.000	16.51	-0.13	0.06	16.51	0.009	0.004	0.003	0.017	0.000	0.001	0.000

NON-DIMENSIONAL PROFILES

Y/DELM	U/RF	V/RF	W/RF	GAMA	BETA	UP/RF	VP/RF	WP/RF	Q/RF	UV/RF2	UW/RF2	VW/RF2
0.149	0.482	0.025	-0.025	2.9	-3.0	0.055	0.070	0.077	0.118	-0.14D-02	0.61D-03	-0.17D-02
0.178	0.494	0.022	-0.024	2.5	-2.7	0.055	0.070	0.077	0.118	-0.14D-02	0.51D-03	-0.15D-02
0.214	0.512	0.023	-0.023	2.6	-2.6	0.059	0.072	0.078	0.122	-0.17D-02	0.19D-03	-0.12D-02
0.268	0.546	0.020	-0.034	2.1	-3.6	0.071	0.076	0.080	0.131	-0.25D-02	-0.40D-04	-0.11D-02
0.339	0.613	0.013	-0.050	1.2	-4.7	0.088	0.078	0.077	0.141	-0.34D-02	0.23D-03	-0.14D-02
0.428	0.721	0.003	-0.051	0.2	-4.1	0.090	0.069	0.068	0.132	-0.30D-02	0.14D-02	-0.13D-02
0.535	0.824	-0.007	-0.028	-0.5	-2.0	0.065	0.050	0.052	0.097	-0.14D-02	0.74D-03	-0.45D-03
0.642	0.884	-0.010	-0.018	-0.7	-1.2	0.051	0.041	0.041	0.077	-0.85D-03	0.24D-03	-0.13D-03
0.749	0.925	-0.010	-0.015	-0.6	-0.9	0.042	0.034	0.033	0.064	-0.60D-03	0.16D-03	-0.51D-04
0.856	0.959	-0.011	-0.011	-0.7	-0.7	0.034	0.028	0.027	0.051	-0.36D-03	0.14D-03	-0.37D-05
0.963	0.984	-0.010	-0.006	-0.6	-0.4	0.024	0.021	0.019	0.037	-0.17D-03	0.12D-03	0.00D 00
1.070	0.997	-0.010	-0.001	-0.6	-0.0	0.014	0.014	0.012	0.023	-0.55D-04	0.48D-04	0.37D-05
1.427	1.000	-0.008	0.004	-0.5	0.2	0.006	0.004	0.003	0.008	0.00D 00	0.37D-05	0.00D 00

Y/DELM	L/DELM	UV/Q2	UV/(UP*VP)
0.149	0.085	-0.098	-0.354
0.178	0.082	-0.101	-0.359
0.214	0.077	-0.118	-0.409
0.268	0.065	-0.147	-0.467
0.339	0.053	-0.170	-0.491
0.428	0.047	-0.172	-0.486
0.535	0.050	-0.151	-0.437
0.642	0.066	-0.145	-0.411
0.749	0.072	-0.146	-0.410
0.856	0.069	-0.136	-0.380
0.963	0.075	-0.126	-0.349
1.070	0.091	-0.103	-0.283
1.427	0.000	0.000	0.000

M=0.4 BLOWING REGION AFTER 7 ROWS OF HOLES, X=168 CM AND Z/P=+0.5

RUN 12147601 TF= 21.00 C PR= 760.00 MM-HG DELM= 3.629 CM DELM1= 1.105 CM DELM2= 0.629 CM

DIMENSIONAL PROFILES

Y (CM)	U (M/S)	V (M/S)	W (M/S)	R (M/S)	UP2 (M2/S2)	VP2 (M2/S2)	WP2 (M2/S2)	Q2 (M2/S2)	UV (M2/S2)	UW (M2/S2)	VW (M2/S2)
0.419	7.82	0.48	-0.21	7.84	1.100	1.215	1.798	4.113	-0.400	0.396	-0.572
0.575	8.07	0.55	0.01	8.09	1.071	1.233	1.768	4.073	-0.366	0.265	-0.379
1.000	8.43	0.52	-0.21	8.45	1.425	1.462	1.914	4.802	-0.603	0.127	-0.242
1.250	9.23	0.40	-0.42	9.24	1.781	1.472	1.891	5.144	-0.722	0.220	-0.315
1.500	10.26	0.30	-0.40	10.27	1.867	1.337	1.736	4.940	-0.734	0.245	-0.260
1.750	11.19	0.21	-0.35	11.20	1.747	1.230	1.495	4.472	-0.692	0.159	-0.179
2.300	13.19	0.07	-0.30	13.20	1.688	0.994	1.080	3.762	-0.619	0.120	-0.091
2.500	13.94	0.00	-0.26	13.94	1.450	0.827	0.886	3.164	-0.505	0.141	-0.061
3.100	15.56	-0.04	-0.08	15.56	0.592	0.363	0.360	1.316	-0.183	0.088	-0.006
3.500	16.21	-0.02	0.04	16.21	0.217	0.164	0.143	0.524	-0.063	0.042	0.004
4.000	16.53	0.02	0.16	16.53	0.043	0.049	0.033	0.125	-0.011	0.011	0.003
5.000	16.54	0.02	0.21	16.54	0.010	0.007	0.003	0.021	0.000	0.001	0.001
6.100	16.51	0.01	0.19	16.51	0.008	0.003	0.002	0.014	0.000	0.001	0.000

NON-DIMENSIONAL PROFILES

Y/DELM	U/RF	V/RF	W/RF	GAMA	BETA	UP/RF	VP/RF	WP/RF	Q/RF	UV/RF2	UW/RF2	VW/RF2
0.115	0.474	0.029	-0.013	3.5	-1.5	0.064	0.067	0.081	0.123	-0.15D-02	0.15D-02	-0.21D-02
0.158	0.489	0.033	0.001	3.9	0.1	0.063	0.067	0.081	0.122	-0.13D-02	0.97D-03	-0.14D-02
0.276	0.511	0.031	-0.013	3.5	-1.4	0.072	0.073	0.084	0.133	-0.22D-02	0.47D-03	-0.89D-03
0.344	0.559	0.024	-0.025	2.5	-2.6	0.081	0.073	0.083	0.137	-0.26D-02	0.81D-03	-0.12D-02
0.413	0.621	0.018	-0.024	1.7	-2.2	0.083	0.070	0.080	0.135	-0.27D-02	0.90D-03	-0.95D-03
0.482	0.678	0.013	-0.021	1.1	-1.8	0.080	0.067	0.074	0.128	-0.25D-02	0.58D-03	-0.66D-03
0.634	0.799	0.004	-0.018	0.3	-1.3	0.079	0.060	0.063	0.117	-0.23D-02	0.44D-03	-0.33D-03
0.689	0.844	0.000	-0.016	0.0	-1.1	0.073	0.055	0.057	0.108	-0.19D-02	0.52D-03	-0.22D-03
0.854	0.942	-0.002	-0.005	-0.1	-0.3	0.047	0.036	0.036	0.069	-0.67D-03	0.32D-03	-0.29D-04
0.965	0.982	-0.001	0.002	-0.1	0.1	0.028	0.025	0.023	0.044	-0.23D-03	0.15D-03	0.15D-04
1.102	1.001	0.001	0.010	0.1	0.6	0.013	0.013	0.011	0.021	-0.40D-04	0.40D-04	0.11D-04
1.378	1.002	0.001	0.013	0.1	0.7	0.006	0.005	0.003	0.009	0.00D 00	0.37D-05	0.37D-05
1.681	1.000	0.001	0.012	0.0	0.7	0.005	0.003	0.003	0.007	0.00D 00	0.37D-05	0.00D 00

Y/DELM	L/DELM	UV/Q2	UV/(UP*VP)
0.115	0.109	-0.097	-0.346
0.158	0.154	-0.090	-0.318
0.276	0.105	-0.126	-0.418
0.344	0.060	-0.140	-0.446
0.413	0.059	-0.149	-0.465
0.482	0.063	-0.155	-0.472
0.634	0.058	-0.165	-0.478
0.689	0.056	-0.160	-0.461
0.854	0.058	-0.139	-0.395
0.965	0.060	-0.120	-0.334
1.102	0.100	-0.088	-0.240
1.378	0.000	0.000	0.000
1.681	0.000	0.000	0.000

M=0.4 BLOWING REGION AFTER 7 ROWS OF HOLES, X=168 CM AND Z/P= 0.0

RUN 12137606 TF= 20.50 C PR= 760.50 MM-HG DELM= 3.628 CM DELM1= 1.204 CM DELM2= 0.614 CM

DIMENSIONAL PROFILES

Y (CM)	U (M/S)	V (M/S)	W (M/S)	R (M/S)	UP2 (M2/S2)	VP2 (M2/S2)	WP2 (M2/S2)	Q2 (M2/S2)	UV (M2/S2)	UW (M2/S2)	VW (M2/S2)
0.419	5.06	0.56	-0.33	5.10	0.909	2.450	2.125	5.485	-0.747	0.000	-0.203
0.575	5.85	0.55	-1.55	6.08	1.377	2.475	2.034	5.886	-0.881	0.240	-0.891
1.000	9.12	0.75	-0.28	9.16	0.710	0.847	1.190	2.747	-0.280	0.111	-0.214
1.250	9.48	0.65	-0.33	9.51	0.886	0.974	1.288	3.149	-0.357	0.076	-0.198
1.500	9.94	0.56	-0.40	9.96	1.124	1.080	1.383	3.587	-0.473	0.056	-0.177
1.750	10.63	0.43	-0.49	10.65	1.469	1.156	1.427	4.052	-0.609	0.083	-0.184
2.300	12.59	0.25	-0.53	12.60	1.697	1.010	1.190	3.897	-0.641	0.149	-0.132
2.500	13.26	0.22	-0.50	13.27	1.560	0.887	1.023	3.470	-0.570	0.132	-0.099
3.100	15.10	0.13	-0.36	15.11	0.831	0.456	0.473	1.760	-0.268	0.140	-0.031
3.500	15.85	0.13	-0.22	15.85	0.316	0.210	0.198	0.725	-0.093	0.077	-0.005
4.000	16.24	0.17	-0.06	16.24	0.050	0.055	0.040	0.145	-0.011	0.014	0.002
5.000	16.24	0.16	-0.01	16.24	0.010	0.008	0.003	0.021	0.000	0.001	0.000
6.100	16.17	0.13	-0.03	16.17	0.007	0.003	0.002	0.012	0.000	0.001	0.000

NON-DIMENSIONAL PROFILES

Y/DELM	U/RF	V/RF	W/RF	GAMA	BETA	UP/RF	VP/RF	WP/RF	Q/RF	UV/RF2	UW/RF2	VW/RF2
0.115	0.313	0.035	-0.020	6.3	-3.7	0.059	0.097	0.090	0.145	-0.29D-02	0.00D 00	-0.78D-03
0.158	0.362	0.034	-0.096	5.4	-14.8	0.073	0.097	0.088	0.150	-0.34D-02	0.92D-03	-0.33D-02
0.276	0.564	0.046	-0.017	4.7	-1.8	0.052	0.057	0.067	0.102	-0.11D-02	0.42D-03	-0.82D-03
0.345	0.586	0.040	-0.020	3.9	-2.0	0.058	0.061	0.070	0.110	-0.14D-02	0.29D-03	-0.76D-03
0.413	0.615	0.035	-0.025	3.2	-2.3	0.066	0.064	0.073	0.117	-0.18D-02	0.21D-03	-0.68D-03
0.482	0.657	0.027	-0.030	2.3	-2.6	0.075	0.066	0.074	0.124	-0.23D-02	0.32D-03	-0.70D-03
0.634	0.779	0.015	-0.033	1.1	-2.4	0.081	0.062	0.067	0.122	-0.25D-02	0.57D-03	-0.50D-03
0.689	0.820	0.014	-0.031	1.0	-2.2	0.077	0.058	0.063	0.115	-0.22D-02	0.50D-03	-0.38D-03
0.854	0.934	0.008	-0.022	0.5	-1.4	0.056	0.042	0.043	0.082	-0.10D-02	0.54D-03	-0.12D-03
0.965	0.980	0.008	-0.014	0.5	-0.8	0.035	0.028	0.028	0.053	-0.36D-03	0.29D-03	-0.19D-04
1.102	1.004	0.011	-0.004	0.6	-0.2	0.014	0.015	0.012	0.024	-0.42D-04	0.54D-04	0.76D-05
1.378	1.004	0.010	-0.001	0.6	-0.0	0.006	0.006	0.003	0.009	0.00D 00	0.38D-05	0.00D 00
1.681	1.000	0.008	-0.002	0.5	-0.1	0.005	0.003	0.003	0.007	0.00D 00	0.38D-05	0.00D 00

Y/DELM	L/DELM	UV/Q2.	UV/(UP*VP)
0.115	0.053	-0.136	-0.501
0.158	0.040	-0.150	-0.477
0.276	0.034	-0.102	-0.361
0.345	0.192	-0.113	-0.384
0.413	0.079	-0.132	-0.429
0.482	0.068	-0.150	-0.467
0.634	0.063	-0.164	-0.490
0.689	0.063	-0.164	-0.485
0.854	0.058	-0.152	-0.435
0.965	0.064	-0.128	-0.361
1.102	0.079	-0.076	-0.210
1.378	0.000	0.000	0.000
1.681	0.000	0.000	0.000

M=0.4 BLOWING REGION AFTER 7 ROWS OF HOLES, X=168 CM AND Z/P=-0.5

RUN 12147602 TF= 21.00 C PR= 760.00 MM-HG DELM= 3.543 CM DELM1= 1.065 CM DELM2= 0.604 CM

DIMENSIONAL PROFILES

Y (CM)	U (M/S)	V (M/S)	W (M/S)	R (M/S)	UP2 (M2/S2)	VP2 (M2/S2)	WP2 (M2/S2)	Q2 (M2/S2)	UV (M2/S2)	UW (M2/S2)	VW (M2/S2)
0.419	7.75	0.60	-0.30	7.78	0.873	1.042	1.711	3.626	-0.314	0.260	-0.533
0.575	7.98	0.67	-0.08	8.01	0.843	1.066	1.694	3.603	-0.274	0.138	-0.354
1.000	8.38	0.59	-0.30	8.40	1.305	1.341	1.852	4.499	-0.555	-0.010	-0.221
1.250	9.25	0.46	-0.52	9.28	1.806	1.377	1.810	4.993	-0.739	0.128	-0.330
1.500	10.33	0.33	-0.49	10.35	1.902	1.298	1.609	4.809	-0.787	0.198	-0.309
1.750	11.39	0.24	-0.42	11.40	1.815	1.172	1.401	4.389	-0.716	0.113	-0.204
2.300	13.49	0.05	-0.35	13.50	1.552	0.864	0.933	3.349	-0.554	0.121	-0.094
2.500	14.18	0.00	-0.30	14.18	1.242	0.699	0.719	2.660	-0.433	0.118	-0.058
3.100	15.66	-0.02	-0.10	15.66	0.397	0.265	0.250	0.912	-0.131	0.060	-0.005
3.500	16.16	-0.01	0.02	16.16	0.134	0.117	0.094	0.345	-0.040	0.026	0.004
4.000	16.37	0.01	0.12	16.37	0.026	0.035	0.020	0.081	-0.005	0.006	0.003
5.000	16.38	0.03	0.19	16.38	0.010	0.006	0.003	0.019	0.000	0.001	0.000
6.100	16.36	0.02	0.18	16.36	0.007	0.003	0.002	0.012	0.000	0.001	0.000

NON-DIMENSIONAL PROFILES

Y/DELM	U/RF	V/RF	W/RF	GAMA	BETA	UP/RF	VP/RF	WP/RF	Q/RF	UV/RF2	UW/RF2	VW/RF2
0.118	0.474	0.037	-0.018	4.4	-2.2	0.057	0.062	0.080	0.116	-0.12D-02	0.97D-03	-0.20D-02
0.162	0.488	0.041	-0.005	4.8	-0.6	0.056	0.063	0.080	0.116	-0.10D-02	0.52D-03	-0.13D-02
0.282	0.512	0.036	-0.018	4.0	-2.1	0.070	0.071	0.083	0.130	-0.21D-02	-0.37D-04	-0.83D-03
0.353	0.565	0.028	-0.032	2.8	-3.2	0.082	0.072	0.082	0.137	-0.28D-02	0.48D-03	-0.12D-02
0.423	0.631	0.020	-0.030	1.8	-2.7	0.084	0.070	0.078	0.134	-0.29D-02	0.74D-03	-0.12D-02
0.494	0.696	0.015	-0.026	1.2	-2.1	0.082	0.066	0.072	0.128	-0.27D-02	0.42D-03	-0.76D-03
0.649	0.825	0.003	-0.021	0.2	-1.5	0.076	0.057	0.059	0.112	-0.21D-02	0.45D-03	-0.35D-03
0.706	0.867	0.000	-0.018	0.0	-1.2	0.068	0.051	0.052	0.100	-0.16D-02	0.44D-03	-0.22D-03
0.875	0.957	-0.001	-0.006	-0.1	-0.4	0.039	0.031	0.031	0.058	-0.49D-03	0.22D-03	-0.19D-04
0.988	0.988	-0.001	0.001	-0.0	0.1	0.022	0.021	0.019	0.036	-0.15D-03	0.97D-04	0.15D-04
1.129	1.001	0.001	0.007	0.0	0.4	0.010	0.011	0.009	0.017	-0.19D-04	0.22D-04	0.11D-04
1.411	1.001	0.002	0.012	0.1	0.7	0.006	0.005	0.003	0.008	0.00D 00	0.37D-05	0.00D 00
1.722	1.000	0.001	0.011	0.1	0.6	0.005	0.003	0.003	0.007	0.00D 00	0.37D-05	0.00D 00

Y/DELM	L/DELM	UV/Q2	UV/(UP*VP)
0.118	0.109	-0.087	-0.329
0.162	0.146	-0.076	-0.289
0.282	0.092	-0.123	-0.420
0.353	0.059	-0.148	-0.469
0.423	0.057	-0.164	-0.501
0.494	0.058	-0.163	-0.491
0.649	0.059	-0.165	-0.478
0.706	0.058	-0.163	-0.465
0.875	0.059	-0.144	-0.404
0.988	0.070	-0.116	-0.319
1.129	0.117	-0.062	-0.166
1.411	0.000	0.000	0.000
1.722	0.000	0.000	0.000

M=0.4 START OF RECOVERY AFTER 11 ROWS OF HOLES, X=188 CM AND Z/P=+0.5

RUN 12137605 TF= 20.50 C PR= 760.50 MM-HG DELM= 4.264 CM DELM1= 1.181 CM DELM2= 0.725 CM

DIMENSIONAL PROFILES

Y (CM)	U (M/S)	V (M/S)	W (M/S)	R (M/S)	UP2 (M2/S2)	VP2 (M2/S2)	WP2 (M2/S2)	Q2 (M2/S2)	UV (M2/S2)	UW (M2/S2)	VW (M2/S2)
0.419	8.59	0.64	-0.16	8.61	0.672	0.941	1.622	3.235	-0.223	0.107	-0.468
0.575	8.55	0.73	-0.01	8.58	0.710	1.046	1.628	3.384	-0.238	0.018	-0.318
1.000	8.97	0.56	-0.45	8.99	1.300	1.259	1.612	4.172	-0.588	0.055	-0.335
1.250	9.76	0.42	-0.47	9.78	1.310	1.119	1.480	3.909	-0.564	0.197	-0.341
1.500	10.48	0.29	-0.31	10.49	1.125	1.015	1.327	3.468	-0.444	0.066	-0.202
1.750	11.00	0.22	-0.30	11.00	1.260	1.065	1.302	3.627	-0.513	-0.028	-0.129
2.300	12.30	0.08	-0.37	12.31	1.590	1.086	1.277	3.953	-0.627	0.031	-0.148
2.500	12.81	0.05	-0.37	12.82	1.591	1.054	1.234	3.879	-0.624	0.044	-0.139
3.100	14.33	-0.03	-0.36	14.33	1.259	0.780	0.857	2.896	-0.469	0.062	-0.075
3.500	15.21	-0.05	-0.31	15.21	0.943	0.558	0.557	2.058	-0.335	0.062	-0.035
4.000	16.04	-0.05	-0.21	16.05	0.422	0.284	0.249	0.955	-0.143	0.052	-0.006
5.000	16.56	-0.02	-0.03	16.56	0.027	0.036	0.015	0.079	-0.004	0.004	0.003
6.100	16.49	-0.02	-0.04	16.49	0.012	0.008	0.003	0.023	0.000	0.002	0.001

NON-DIMENSIONAL PROFILES

Y/DELM	U/RF	V/RF	W/RF	GAMA	BETA	UP/RF	VP/RF	WP/RF	Q/RF	UV/RF2	UW/RF2	VW/RF2
0.098	0.521	0.039	-0.010	4.3	-1.1	0.050	0.059	0.077	0.109	-0.82D-03	0.39D-03	-0.17D-02
0.135	0.518	0.044	-0.001	4.9	-0.1	0.051	0.062	0.077	0.112	-0.88D-03	0.66D-04	-0.12D-02
0.235	0.544	0.034	-0.027	3.6	-2.9	0.069	0.068	0.077	0.124	-0.22D-02	0.20D-03	-0.12D-02
0.293	0.592	0.025	-0.029	2.5	-2.8	0.069	0.064	0.074	0.120	-0.21D-02	0.72D-03	-0.13D-02
0.352	0.636	0.018	-0.019	1.6	-1.7	0.064	0.061	0.070	0.113	-0.16D-02	0.24D-03	-0.74D-03
0.410	0.667	0.013	-0.018	1.1	-1.6	0.068	0.063	0.069	0.115	-0.19D-02	-0.10D-03	-0.47D-03
0.539	0.746	0.005	-0.022	0.4	-1.7	0.076	0.063	0.069	0.121	-0.23D-02	0.11D-03	-0.54D-03
0.586	0.777	0.003	-0.022	0.2	-1.7	0.076	0.062	0.067	0.119	-0.23D-02	0.16D-03	-0.51D-03
0.727	0.869	-0.002	-0.022	-0.1	-1.4	0.068	0.054	0.056	0.103	-0.17D-02	0.23D-03	-0.28D-03
0.821	0.922	-0.003	-0.019	-0.2	-1.2	0.059	0.045	0.045	0.087	-0.12D-02	0.23D-03	-0.13D-03
0.938	0.973	-0.003	-0.013	-0.2	-0.8	0.039	0.032	0.030	0.059	-0.53D-03	0.19D-03	-0.22D-04
1.173	1.004	-0.001	-0.002	-0.1	-0.1	0.010	0.012	0.007	0.017	-0.15D-04	0.15D-04	0.11D-04
1.431	1.000	-0.001	-0.002	-0.1	-0.1	0.007	0.005	0.003	0.009	0.00D 00	0.74D-05	0.37D-05

Y/DELM	L/DELM	UV/Q2	UV/(UP*VP)
0.098	0.415	-0.069	-0.280
0.135	10.737	-0.070	-0.276
0.235	0.075	-0.141	-0.460
0.293	0.055	-0.144	-0.466
0.352	0.063	-0.128	-0.416
0.410	0.079	-0.141	-0.443
0.539	0.074	-0.159	-0.477
0.586	0.072	-0.161	-0.482
0.727	0.067	-0.162	-0.473
0.821	0.068	-0.163	-0.462
0.938	0.072	-0.150	-0.413
1.173	0.195	-0.051	-0.128
1.431	0.000	0.000	0.000

M=0.4 START OF RECOVERY AFTER 11 ROWS OF HOLES, X=188 CM AND Z/P=+0.3

RUN 12137604 TF= 20.50 C PR= 760.50 MM-HG DELM= 4.103 CM DELM1= 0.912 CM DELM2= 0.640 CM

DIMENSIONAL PROFILES

Y (CM)	U (M/S)	V (M/S)	W (M/S)	R (M/S)	UP2 (M2/S2)	VP2 (M2/S2)	WP2 (M2/S2)	Q2 (M2/S2)	UV (M2/S2)	UW (M2/S2)	VW (M2/S2)
0.419	10.69	-0.34	-0.37	10.70	0.831	0.593	0.788	2.212	-0.138	-0.084	-0.144
0.575	10.80	-0.42	-0.24	10.81	0.942	0.672	0.773	2.387	-0.150	-0.178	-0.055
1.000	10.99	-0.44	-0.19	11.00	1.121	0.935	0.957	3.013	-0.295	-0.207	0.038
1.250	11.25	-0.40	-0.23	11.26	1.223	1.020	1.056	3.300	-0.383	-0.225	0.053
1.500	11.58	-0.35	-0.27	11.59	1.310	1.093	1.116	3.520	-0.467	-0.178	0.019
1.750	11.97	-0.31	-0.30	11.98	1.374	1.115	1.130	3.620	-0.501	-0.172	0.009
2.300	13.01	-0.28	-0.35	13.02	1.419	1.033	1.089	3.541	-0.516	-0.069	-0.013
2.500	13.40	-0.27	-0.35	13.41	1.374	0.977	1.031	3.382	-0.511	-0.046	-0.021
3.100	14.64	-0.21	-0.34	14.65	1.081	0.713	0.747	2.541	-0.378	0.010	-0.005
3.500	15.39	-0.18	-0.30	15.39	0.770	0.503	0.496	1.770	-0.264	0.032	-0.001
4.000	16.13	-0.16	-0.22	16.13	0.314	0.258	0.217	0.789	-0.115	0.038	0.000
5.000	16.48	-0.15	-0.05	16.48	0.027	0.038	0.017	0.083	-0.003	0.003	0.002
6.100	16.40	-0.12	-0.06	16.40	0.012	0.007	0.002	0.021	0.000	0.001	0.000

NON-DIMENSIONAL PROFILES

Y/DELM	U/RF	V/RF	W/RF	GAMA	BETA	UP/RF	VP/RF	WP/RF	Q/RF	UV/RF2	UW/RF2	VW/RF2
0.102	0.652	-0.021	-0.023	-1.8	-2.0	0.056	0.047	0.054	0.091	-0.51D-03	-0.31D-03	-0.54D-03
0.140	0.659	-0.026	-0.015	-2.2	-1.3	0.059	0.050	0.054	0.094	-0.56D-03	-0.66D-03	-0.20D-03
0.244	0.670	-0.027	-0.012	-2.3	-1.0	0.065	0.059	0.060	0.106	-0.11D-02	-0.77D-03	0.14D-03
0.305	0.686	-0.024	-0.014	-2.0	-1.2	0.067	0.062	0.063	0.111	-0.14D-02	-0.84D-03	0.20D-03
0.366	0.706	-0.021	-0.016	-1.7	-1.3	0.070	0.064	0.064	0.114	-0.17D-02	-0.66D-03	0.71D-04
0.426	0.730	-0.019	-0.018	-1.5	-1.4	0.071	0.064	0.065	0.116	-0.19D-02	-0.64D-03	0.33D-04
0.561	0.793	-0.017	-0.021	-1.2	-1.5	0.073	0.062	0.064	0.115	-0.19D-02	-0.26D-03	-0.48D-04
0.609	0.817	-0.016	-0.021	-1.2	-1.5	0.071	0.060	0.062	0.112	-0.19D-02	-0.17D-03	-0.78D-04
0.755	0.893	-0.013	-0.021	-0.8	-1.3	0.063	0.051	0.053	0.097	-0.14D-02	0.37D-04	-0.19D-04
0.853	0.938	-0.011	-0.018	-0.7	-1.1	0.054	0.043	0.043	0.081	-0.98D-03	0.12D-03	-0.37D-05
0.975	0.984	-0.010	-0.013	-0.6	-0.8	0.034	0.031	0.028	0.054	-0.43D-03	0.14D-03	0.00D 00
1.219	1.005	-0.009	-0.003	-0.5	-0.2	0.010	0.012	0.008	0.018	-0.11D-04	0.11D-04	0.74D-05
1.487	1.000	-0.007	-0.004	-0.4	-0.2	0.007	0.005	0.003	0.009	0.00D 00	0.37D-05	0.00D 00

Y/DELM	L/DELM	UV/Q2	UV/(UP*VP)
0.102	0.177	-0.062	-0.197
0.140	0.195	-0.063	-0.189
0.244	0.173	-0.098	-0.288
0.305	0.132	-0.116	-0.343
0.366	0.115	-0.133	-0.390
0.426	0.102	-0.138	-0.405
0.561	0.088	-0.146	-0.426
0.609	0.085	-0.151	-0.441
0.755	0.075	-0.149	-0.431
0.853	0.072	-0.149	-0.424
0.975	0.080	-0.146	-0.404
1.219	2.967	-0.036	-0.094
1.487	0.000	0.000	0.000

M=0.4 START OF RECOVERY AFTER 11 ROWS OF HOLES, X=188 CM AND Z/P= 0.0

RUN 12137603 TF= 20.50 C PR= 760.50 MM-HG DELM= 4.419 CM DELM1= 1.301 CM DELM2= 0.760 CM

DIMENSIONAL PROFILES

Y (CM)	U (M/S)	V (M/S)	W (M/S)	R (M/S)	UP2 (M2/S2)	VP2 (M2/S2)	WP2 (M2/S2)	Q2 (M2/S2)	UV (M2/S2)	UW (M2/S2)	VW (M2/S2)
0.419	6.51	1.18	-3.10	7.31	0.898	2.180	1.494	4.573	-0.474	0.278	-0.850
0.575	8.85	1.07	-1.14	8.99	0.665	0.833	2.154	3.652	-0.364	0.726	-0.664
1.000	9.44	0.73	-0.14	9.47	0.784	0.861	1.247	2.893	-0.303	0.027	-0.161
1.250	9.66	0.56	-0.23	9.68	0.907	0.979	1.356	3.243	-0.351	0.023	-0.148
1.500	10.02	0.44	-0.33	10.04	1.123	1.050	1.417	3.590	-0.461	0.012	-0.160
1.750	10.53	0.33	-0.40	10.54	1.314	1.112	1.449	3.876	-0.531	0.053	-0.204
2.300	11.85	0.16	-0.38	11.86	1.441	1.120	1.372	3.933	-0.590	0.064	-0.168
2.500	12.34	0.09	-0.37	12.34	1.487	1.105	1.313	3.906	-0.621	0.057	-0.137
3.100	13.84	-0.07	-0.38	13.85	1.465	0.944	1.017	3.426	-0.577	0.073	-0.075
3.500	14.86	-0.13	-0.35	14.86	1.191	0.725	0.710	2.627	-0.450	0.083	-0.040
4.000	15.86	-0.17	-0.26	15.86	0.640	0.417	0.354	1.411	-0.222	0.094	-0.018
5.000	16.60	-0.15	-0.02	16.60	0.031	0.050	0.022	0.104	-0.005	0.006	0.002
6.100	16.54	-0.18	-0.06	16.54	0.010	0.008	0.003	0.022	0.000	0.001	0.000

NON-DIMENSIONAL PROFILES

Y/DELM	U/RF	V/RF	W/RF	GAMA	BETA	UP/RF	VP/RF	WP/RF	Q/RF	UV/RF2	UW/RF2	VW/RF2
0.095	0.394	0.071	-0.187	10.3	-25.5	0.057	0.089	0.074	0.129	-0.17D-02	0.10D-02	-0.31D-02
0.130	0.535	0.065	-0.069	6.9	-7.3	0.049	0.055	0.089	0.116	-0.13D-02	0.27D-02	-0.24D-02
0.226	0.571	0.044	-0.008	4.4	-0.8	0.054	0.056	0.068	0.103	-0.11D-02	0.99D-04	-0.59D-03
0.283	0.584	0.034	-0.014	3.3	-1.4	0.058	0.060	0.070	0.109	-0.13D-02	0.84D-04	-0.54D-03
0.339	0.606	0.027	-0.020	2.5	-1.9	0.064	0.062	0.072	0.115	-0.17D-02	0.44D-04	-0.58D-03
0.396	0.637	0.020	-0.024	1.8	-2.2	0.069	0.064	0.073	0.119	-0.19D-02	0.19D-03	-0.75D-03
0.520	0.716	0.010	-0.023	0.8	-1.8	0.073	0.064	0.071	0.120	-0.22D-02	0.23D-03	-0.61D-03
0.566	0.746	0.005	-0.022	0.4	-1.7	0.074	0.064	0.069	0.119	-0.23D-02	0.21D-03	-0.50D-03
0.702	0.837	-0.004	-0.023	-0.3	-1.6	0.073	0.059	0.061	0.112	-0.21D-02	0.27D-03	-0.27D-03
0.792	0.898	-0.008	-0.021	-0.5	-1.3	0.066	0.051	0.051	0.098	-0.16D-02	0.30D-03	-0.15D-03
0.905	0.959	-0.010	-0.016	-0.6	-0.9	0.048	0.039	0.036	0.072	-0.81D-03	0.34D-03	-0.66D-04
1.131	1.004	-0.009	-0.001	-0.5	-0.1	0.011	0.014	0.009	0.019	-0.18D-04	0.22D-04	0.73D-05
1.380	1.000	-0.011	-0.004	-0.6	-0.2	0.006	0.005	0.003	0.009	0.00D 00	0.37D-05	0.00D 00

Y/DELM	L/DELM	UV/Q2	UV/(UP*VP)
0.095	0.009	-0.104	-0.339
0.130	0.013	-0.100	-0.489
0.226	0.140	-0.105	-0.369
0.283	0.089	-0.108	-0.372
0.339	0.091	-0.128	-0.425
0.396	0.073	-0.137	-0.439
0.520	0.071	-0.150	-0.464
0.566	0.073	-0.159	-0.484
0.702	0.067	-0.168	-0.491
0.792	0.063	-0.171	-0.484
0.905	0.069	-0.157	-0.430
1.131	0.089	-0.048	-0.127
1.380	0.000	0.000	0.000

M=0.4 START OF RECOVERY AFTER 11 ROWS OF HOLES, X=188 CM AND Z/P=-0.3

RUN 12177601 TF= 21.50 C PR= 761.00 MM-HG DELM= 4.317 CM DELM1= 0.958 CM DELM2= 0.669 CM

DIMENSIONAL PROFILES

Y (CM)	U (M/S)	V (M/S)	W (M/S)	R (M/S)	UP2 (M2/S2)	VP2 (M2/S2)	WP2 (M2/S2)	Q2 (M2/S2)	UV (M2/S2)	UW (M2/S2)	VW (M2/S2)
0.419	10.40	-0.52	-0.08	10.41	0.769	0.573	0.689	2.031	-0.112	0.057	-0.066
0.575	10.59	-0.65	-0.01	10.61	0.855	0.660	0.701	2.216	-0.097	0.053	0.000
1.000	10.80	-0.71	-0.13	10.83	1.091	0.930	0.908	2.930	-0.224	0.093	0.035
1.250	11.03	-0.60	-0.21	11.05	1.213	1.026	1.029	3.269	-0.317	0.101	0.011
1.500	11.34	-0.51	-0.27	11.36	1.301	1.056	1.071	3.428	-0.389	0.120	-0.011
1.750	11.71	-0.44	-0.30	11.73	1.361	1.071	1.131	3.564	-0.436	0.076	-0.008
2.300	12.75	-0.30	-0.35	12.76	1.359	0.987	1.114	3.461	-0.451	0.021	-0.038
2.500	13.13	-0.24	-0.34	13.14	1.318	0.922	1.056	3.297	-0.439	-0.003	-0.023
3.100	14.32	-0.13	-0.31	14.32	1.029	0.688	0.765	2.483	-0.350	-0.027	-0.014
3.500	15.07	-0.08	-0.29	15.08	0.745	0.514	0.512	1.771	-0.263	-0.012	-0.005
4.000	15.80	-0.06	-0.22	15.80	0.355	0.278	0.233	0.866	-0.130	0.011	0.010
5.000	16.30	-0.04	-0.08	16.30	0.026	0.040	0.018	0.085	-0.004	0.002	0.004
6.100	16.26	-0.01	-0.04	16.26	0.010	0.008	0.003	0.021	0.000	0.001	0.000

NON-DIMENSIONAL PROFILES

Y/DELM	U/RF	V/RF	W/RF	GAMA	BETA	UP/RF	VP/RF	WP/RF	Q/RF	UV/RF2	UW/RF2	VW/RF2
0.097	0.640	-0.032	-0.005	-2.9	-0.4	0.054	0.047	0.051	0.088	-0.42D-03	0.22D-03	-0.25D-03
0.133	0.651	-0.040	-0.001	-3.5	-0.1	0.057	0.050	0.051	0.092	-0.37D-03	0.20D-03	0.00D 00
0.232	0.664	-0.044	-0.008	-3.8	-0.7	0.064	0.059	0.059	0.105	-0.85D-03	0.35D-03	0.13D-03
0.290	0.678	-0.037	-0.013	-3.1	-1.1	0.068	0.062	0.062	0.111	-0.12D-02	0.38D-03	0.42D-04
0.347	0.697	-0.031	-0.017	-2.6	-1.4	0.070	0.063	0.064	0.114	-0.15D-02	0.45D-03	-0.42D-04
0.405	0.720	-0.027	-0.018	-2.2	-1.5	0.072	0.064	0.065	0.116	-0.16D-02	0.29D-03	-0.30D-04
0.533	0.784	-0.018	-0.022	-1.3	-1.6	0.072	0.061	0.065	0.114	-0.17D-02	0.79D-04	-0.14D-03
0.579	0.808	-0.015	-0.021	-1.0	-1.5	0.071	0.059	0.063	0.112	-0.17D-02	-0.11D-04	-0.87D-04
0.718	0.881	-0.008	-0.019	-0.5	-1.2	0.062	0.051	0.054	0.097	-0.13D-02	-0.10D-03	-0.53D-04
0.811	0.927	-0.005	-0.018	-0.3	-1.1	0.053	0.044	0.044	0.082	-0.99D-03	-0.45D-04	-0.19D-04
0.926	0.972	-0.004	-0.014	-0.2	-0.8	0.037	0.032	0.030	0.057	-0.49D-03	0.42D-04	0.38D-04
1.158	1.002	-0.002	-0.005	-0.1	-0.3	0.010	0.012	0.008	0.018	-0.15D-04	0.76D-05	0.15D-04
1.413	1.000	-0.001	-0.002	-0.0	-0.1	0.006	0.006	0.003	0.009	0.00D 00	0.38D-05	0.00D 00

Y/DELM	L/DELM	UV/Q2	UV/(UP*VP)
0.097	0.079	-0.055	-0.169
0.133	0.090	-0.044	-0.129
0.232	0.163	-0.076	-0.222
0.290	0.123	-0.097	-0.284
0.347	0.105	-0.113	-0.332
0.405	0.092	-0.122	-0.361
0.533	0.079	-0.130	-0.389
0.579	0.078	-0.133	-0.398
0.718	0.070	-0.141	-0.416
0.811	0.069	-0.149	-0.425
0.926	0.075	-0.150	-0.414
1.158	0.133	-0.047	-0.124
1.413	0.000	0.000	0.000

M=0.4 START OF RECOVERY AFTER 11 ROWS OF HOLES, X=188 CM AND Z/P=-0.5

RUN 12177602 TF= 21.50 C PR= 761.00 MM-HG DELM= 4.135 CM DELM1= 1.171 CM DELM2= 0.710 CM

DIMENSIONAL PROFILES

Y (CM)	U (M/S)	V (M/S)	W (M/S)	R (M/S)	UP2 (M2/S2)	VP2 (M2/S2)	WP2 (M2/S2)	Q2 (M2/S2)	UV (M2/S2)	UW (M2/S2)	VW (M2/S2)
0.419	8.35	0.35	0.06	8.36	0.786	0.942	1.463	3.191	-0.307	0.345	-0.392
0.575	8.33	0.43	0.11	8.34	0.837	1.089	1.480	3.407	-0.337	0.279	-0.276
1.000	8.64	0.36	-0.51	8.66	1.310	1.286	1.584	4.180	-0.590	0.218	-0.362
1.250	9.44	0.29	-0.58	9.46	1.306	1.154	1.465	3.925	-0.545	0.248	-0.345
1.500	10.14	0.22	-0.40	10.15	1.180	1.077	1.319	3.577	-0.483	0.124	-0.206
1.750	10.70	0.16	-0.38	10.71	1.341	1.104	1.317	3.762	-0.538	0.016	-0.147
2.300	12.18	0.04	-0.45	12.19	1.674	1.107	1.300	4.081	-0.659	0.091	-0.150
2.500	12.71	0.03	-0.43	12.71	1.609	1.010	1.195	3.814	-0.607	0.092	-0.120
3.100	14.25	-0.01	-0.39	14.26	1.168	0.699	0.792	2.659	-0.405	0.079	-0.046
3.500	15.11	0.00	-0.35	15.11	0.770	0.477	0.488	1.735	-0.267	0.069	-0.020
4.000	15.87	0.01	-0.23	15.87	0.290	0.230	0.199	0.719	-0.099	0.047	-0.001
5.000	16.22	0.04	-0.06	16.22	0.021	0.029	0.013	0.064	-0.002	0.002	0.002
6.100	16.17	0.02	-0.05	16.17	0.011	0.006	0.003	0.021	0.000	0.001	0.000

NON-DIMENSIONAL PROFILES

Y/DELM	U/RF	V/RF	W/RF	GAMA	BETA	UP/RF	VP/RF	WP/RF	Q/RF	UV/RF2	UW/RF2	VW/RF2
0.101	0.516	0.022	0.004	2.4	0.4	0.055	0.060	0.075	0.110	-0.12D-02	0.13D-02	-0.15D-02
0.139	0.515	0.027	0.007	3.0	0.8	0.057	0.065	0.075	0.114	-0.13D-02	0.11D-02	-0.11D-02
0.242	0.534	0.022	-0.032	2.4	-3.4	0.071	0.070	0.078	0.126	-0.23D-02	0.83D-03	-0.14D-02
0.302	0.584	0.018	-0.036	1.8	-3.5	0.071	0.066	0.075	0.123	-0.21D-02	0.95D-03	-0.13D-02
0.363	0.627	0.014	-0.025	1.2	-2.3	0.067	0.064	0.071	0.117	-0.18D-02	0.47D-03	-0.79D-03
0.423	0.662	0.010	-0.024	0.9	-2.0	0.072	0.065	0.071	0.120	-0.21D-02	0.61D-04	-0.56D-03
0.556	0.753	0.002	-0.028	0.2	-2.1	0.080	0.065	0.071	0.125	-0.25D-02	0.35D-03	-0.57D-03
0.605	0.786	0.002	-0.027	0.1	-1.9	0.078	0.062	0.068	0.121	-0.23D-02	0.35D-03	-0.46D-03
0.750	0.881	-0.001	-0.024	-0.0	-1.6	0.067	0.052	0.055	0.101	-0.15D-02	0.30D-03	-0.18D-03
0.846	0.934	0.000	-0.022	0.0	-1.3	0.054	0.043	0.043	0.081	-0.10D-02	0.26D-03	-0.76D-04
0.967	0.981	0.001	-0.014	0.0	-0.8	0.033	0.030	0.028	0.052	-0.38D-03	0.18D-03	-0.38D-05
1.209	1.003	0.002	-0.004	0.1	-0.2	0.009	0.011	0.007	0.016	-0.76D-05	0.76D-05	0.76D-05
1.475	1.000	0.001	-0.003	0.1	-0.2	0.006	0.005	0.003	0.009	0.00D 00	0.38D-05	0.00D 00

Y/DELM	L/DELM	UV/Q2	UV/(UP*VP)
0.101	0.789	-0.096	-0.357
0.139	1.664	-0.099	-0.353
0.242	0.080	-0.141	-0.455
0.302	0.056	-0.139	-0.444
0.363	0.068	-0.135	-0.428
0.423	0.075	-0.143	-0.442
0.556	0.072	-0.161	-0.484
0.605	0.071	-0.159	-0.476
0.750	0.065	-0.152	-0.448
0.846	0.065	-0.154	-0.441
0.967	0.072	-0.138	-0.383
1.209	0.669	-0.031	-0.081
1.475	0.000	0.000	0.000

M=0.4 RECOVERY REGION, 27 DIAM DOWNSTREAM, X=214 CM AND Z/P= 0.0

RUN 12137601 TF= 20.50 C PR= 760.50 MM-HG DELM= 5.056 CM DELM1= 1.258 CM DELM2= 0.820 CM

DIMENSIONAL PROFILES

Y (CM)	U (M/S)	V (M/S)	W (M/S)	R (M/S)	UP2 (M2/S2)	VP2 (M2/S2)	WP2 (M2/S2)	Q2 (M2/S2)	UV (M2/S2)	UW (M2/S2)	VW (M2/S2)
0.419	8.94	0.28	-0.52	8.96	0.959	0.633	1.081	2.673	-0.291	0.204	-0.278
0.700	9.61	0.24	-0.33	9.62	0.874	0.574	0.977	2.425	-0.256	0.108	-0.155
1.000	10.06	0.22	-0.28	10.07	0.861	0.630	0.982	2.474	-0.263	0.074	-0.109
1.250	10.40	0.20	-0.28	10.40	0.873	0.678	1.016	2.567	-0.276	0.036	-0.088
1.500	10.70	0.18	-0.29	10.71	0.978	0.756	1.073	2.808	-0.341	0.017	-0.093
1.750	11.10	0.15	-0.32	11.10	1.111	0.821	1.142	3.074	-0.392	0.032	-0.102
2.300	12.00	0.11	-0.35	12.01	1.335	0.907	1.250	3.492	-0.498	0.029	-0.095
2.500	12.34	0.11	-0.34	12.34	1.385	0.917	1.253	3.556	-0.526	0.046	-0.090
3.100	13.52	0.04	-0.35	13.53	1.374	0.866	1.131	3.371	-0.524	0.048	-0.060
3.500	14.27	0.03	-0.35	14.27	1.261	0.787	0.982	3.030	-0.485	0.059	-0.054
4.000	15.14	0.00	-0.31	15.14	1.017	0.617	0.662	2.297	-0.372	0.065	-0.020
5.000	16.40	-0.01	-0.16	16.40	0.240	0.220	0.163	0.623	-0.082	0.042	-0.003
6.500	16.61	-0.01	-0.09	16.61	0.017	0.020	0.006	0.043	0.000	0.002	0.001

NON-DIMENSIONAL PROFILES

Y/DELM	U/RF	V/RF	W/RF	GAMA	BETA	UP/RF	VP/RF	WP/RF	Q/RF	UV/RF2	UW/RF2	VW/RF2
0.083	0.538	0.017	-0.031	1.8	-3.3	0.059	0.048	0.063	0.098	-0.11D-02	0.74D-03	-0.10D-02
0.138	0.579	0.014	-0.020	1.4	-2.0	0.056	0.046	0.060	0.094	-0.93D-03	0.39D-03	-0.56D-03
0.198	0.606	0.013	-0.017	1.3	-1.6	0.056	0.048	0.060	0.095	-0.95D-03	0.27D-03	-0.40D-03
0.247	0.626	0.012	-0.017	1.1	-1.5	0.056	0.050	0.061	0.096	-0.10D-02	0.13D-03	-0.32D-03
0.297	0.644	0.011	-0.017	1.0	-1.6	0.060	0.052	0.062	0.101	-0.12D-02	0.62D-04	-0.34D-03
0.346	0.668	0.009	-0.019	0.8	-1.7	0.063	0.055	0.064	0.106	-0.14D-02	0.12D-03	-0.37D-03
0.455	0.722	0.007	-0.021	0.5	-1.7	0.070	0.057	0.067	0.113	-0.18D-02	0.11D-03	-0.34D-03
0.494	0.743	0.007	-0.020	0.5	-1.6	0.071	0.058	0.067	0.114	-0.19D-02	0.17D-03	-0.33D-03
0.613	0.814	0.002	-0.021	0.2	-1.5	0.071	0.056	0.064	0.111	-0.19D-02	0.17D-03	-0.22D-03
0.692	0.859	0.002	-0.021	0.1	-1.4	0.068	0.053	0.060	0.105	-0.18D-02	0.21D-03	-0.20D-03
0.791	0.911	0.000	-0.019	0.0	-1.2	0.061	0.047	0.049	0.091	-0.13D-02	0.24D-03	-0.72D-04
0.989	0.987	-0.001	-0.010	-0.0	-0.6	0.029	0.028	0.024	0.048	-0.30D-03	0.15D-03	-0.11D-04
1.286	1.000	-0.001	-0.005	-0.0	-0.3	0.008	0.009	0.005	0.012	0.00D 00	0.72D-05	0.36D-05

Y/DELM	L/DELM	UV/Q2	UV/(UP*VP)
0.083	0.044	-0.109	-0.373
0.138	0.051	-0.106	-0.361
0.198	0.074	-0.106	-0.357
0.247	0.083	-0.108	-0.359
0.297	0.083	-0.121	-0.397
0.346	0.079	-0.128	-0.410
0.455	0.081	-0.143	-0.453
0.494	0.079	-0.148	-0.467
0.613	0.073	-0.155	-0.480
0.692	0.075	-0.160	-0.487
0.791	0.074	-0.162	-0.470
0.989	0.075	-0.132	-0.357
1.286	0.000	0.000	0.000

M=0.4 RECOVERY REGION, 67 DIAM DOWNSTREAM, X=256 CM AND Z/P= 0.0

RUN 12137602 TF= 20.50 C PR= 760.50 MM-HG DELM= 5.879 CM DELM1= 1.269 CM DELM2= 0.865 CM

DIMENSIONAL PROFILES

Y (CM)	U (M/S)	V (M/S)	W (M/S)	R (M/S)	UP2 (M2/S2)	VP2 (M2/S2)	WP2 (M2/S2)	Q2 (M2/S2)	UV (M2/S2)	UW (M2/S2)	VW (M2/S2)
0.419	8.93	0.28	-0.68	8.96	1.291	0.650	1.131	3.073	-0.333	0.163	-0.292
0.700	9.71	0.21	-0.51	9.73	1.264	0.619	1.017	2.901	-0.350	0.116	-0.183
1.000	10.33	0.19	-0.43	10.34	1.224	0.630	0.992	2.847	-0.357	0.070	-0.138
1.250	10.77	0.17	-0.42	10.78	1.211	0.648	1.017	2.876	-0.364	0.050	-0.105
1.500	11.16	0.17	-0.40	11.17	1.257	0.675	1.038	2.971	-0.394	0.012	-0.088
1.750	11.47	0.18	-0.40	11.48	1.244	0.687	1.058	2.989	-0.394	0.020	-0.082
2.300	12.24	0.15	-0.40	12.25	1.268	0.719	1.082	3.069	-0.425	0.028	-0.080
2.500	12.52	0.15	-0.38	12.53	1.264	0.722	1.096	3.082	-0.433	0.009	-0.064
3.100	13.34	0.12	-0.38	13.34	1.219	0.709	1.044	2.972	-0.428	0.036	-0.065
3.500	13.85	0.13	-0.40	13.86	1.174	0.684	0.979	2.838	-0.431	0.014	-0.045
4.000	14.54	0.10	-0.39	14.55	1.038	0.608	0.813	2.459	-0.377	0.031	-0.031
5.000	15.66	0.09	-0.35	15.67	0.618	0.378	0.400	1.397	-0.208	0.041	-0.036
6.500	16.39	0.09	-0.23	16.39	0.055	0.075	0.041	0.172	-0.012	0.008	0.000

NON-DIMENSIONAL PROFILES

Y/DELM	U/RF	V/RF	W/RF	GAMA	BETA	UP/RF	VP/RF	WP/RF	Q/RF	UV/RF2	UW/RF2	VW/RF2
0.071	0.545	0.017	-0.041	1.8	-4.4	0.069	0.049	0.065	0.107	-0.12D-02	0.61D-03	-0.11D-02
0.119	0.592	0.013	-0.031	1.2	-3.0	0.069	0.048	0.062	0.104	-0.13D-02	0.43D-03	-0.68D-03
0.170	0.630	0.012	-0.026	1.1	-2.4	0.068	0.048	0.061	0.103	-0.13D-02	0.26D-03	-0.51D-03
0.213	0.657	0.010	-0.026	0.9	-2.2	0.067	0.049	0.062	0.103	-0.14D-02	0.19D-03	-0.39D-03
0.255	0.681	0.010	-0.024	0.9	-2.1	0.068	0.050	0.062	0.105	-0.15D-02	0.45D-04	-0.33D-03
0.298	0.700	0.011	-0.024	0.9	-2.0	0.068	0.051	0.063	0.105	-0.15D-02	0.74D-04	-0.31D-03
0.391	0.747	0.009	-0.024	0.7	-1.9	0.069	0.052	0.063	0.107	-0.16D-02	0.10D-03	-0.30D-03
0.425	0.764	0.009	-0.023	0.7	-1.7	0.069	0.052	0.064	0.107	-0.16D-02	0.34D-04	-0.24D-03
0.527	0.814	0.007	-0.023	0.5	-1.6	0.067	0.051	0.062	0.105	-0.16D-02	0.13D-03	-0.24D-03
0.595	0.845	0.008	-0.024	0.5	-1.7	0.066	0.050	0.060	0.103	-0.16D-02	0.52D-04	-0.17D-03
0.680	0.887	0.006	-0.024	0.4	-1.5	0.062	0.048	0.055	0.096	-0.14D-02	0.12D-03	-0.12D-03
0.851	0.955	0.005	-0.021	0.3	-1.3	0.048	0.038	0.039	0.072	-0.77D-03	0.15D-03	-0.30D-04
1.106	1.000	0.005	-0.014	0.3	-0.8	0.014	0.017	0.012	0.025	-0.45D-04	0.30D-04	0.00D 00

Y/DELM	L/DELM	UV/Q2	UV/(UP*VP)
0.071	0.036	-0.108	-0.364
0.119	0.041	-0.121	-0.396
0.170	0.053	-0.125	-0.407
0.213	0.063	-0.127	-0.411
0.255	0.076	-0.133	-0.428
0.298	0.080	-0.132	-0.426
0.391	0.079	-0.138	-0.445
0.425	0.081	-0.140	-0.453
0.527	0.084	-0.144	-0.460
0.595	0.084	-0.152	-0.481
0.680	0.079	-0.153	-0.475
0.851	0.092	-0.149	-0.430
1.106	******	-0.070	-0.187

M=0.9 BLOWING REGION AFTER 3 ROWS OF HOLES, X=148 CM AND Z/P=+0.5

RUN 12177604 TF= 21.00 C PR= 761.00 MM-HG DELM= 2.995 CM DELM1= 0.548 CM DELM2= 0.404 CM

DIMENSIONAL PROFILES

Y (CM)	U (M/S)	V (M/S)	W (M/S)	R (M/S)	UP2 (M2/S2)	VP2 (M2/S2)	WP2 (M2/S2)	Q2 (M2/S2)	UV (M2/S2)	UW (M2/S2)	VW (M2/S2)
0.419	11.52	0.74	-0.59	11.56	1.044	1.408	1.896	4.349	-0.493	0.525	-0.637
0.500	11.78	0.79	-0.44	11.82	0.948	1.294	1.865	4.108	-0.431	0.473	-0.539
0.600	12.07	1.00	-0.24	12.11	0.832	1.190	1.857	3.879	-0.353	0.368	-0.443
0.750	12.29	1.23	-0.04	12.35	0.734	1.172	1.806	3.713	-0.270	0.247	-0.324
0.950	12.32	1.29	0.11	12.39	0.702	1.337	1.560	3.599	-0.219	0.121	-0.101
1.200	12.44	0.98	-0.14	12.48	0.735	1.537	1.378	3.650	-0.356	0.033	0.135
1.500	13.33	0.52	-0.49	13.35	0.837	1.253	1.059	3.149	-0.432	0.113	-0.100
1.800	14.21	0.24	-0.28	14.22	0.603	0.761	0.642	2.006	-0.207	0.072	-0.031
2.100	14.80	0.07	-0.28	14.80	0.552	0.452	0.395	1.399	-0.189	0.037	0.016
2.400	15.42	0.00	-0.25	15.42	0.409	0.269	0.255	0.934	-0.135	0.053	-0.005
2.700	15.91	0.02	-0.17	15.91	0.228	0.155	0.142	0.525	-0.068	0.042	-0.001
3.000	16.23	0.04	-0.08	16.23	0.088	0.074	0.065	0.228	-0.023	0.023	0.003
4.000	16.39	0.08	0.04	16.39	0.010	0.005	0.004	0.019	0.000	0.001	0.000

NON-DIMENSIONAL PROFILES

Y/DELM	U/RF	V/RF	W/RF	GAMA	BETA	UP/RF	VP/RF	WP/RF	Q/RF	UV/RF2	UW/RF2	VW/RF2
0.140	0.703	0.045	-0.036	3.7	-2.9	0.062	0.072	0.084	0.127	-0.18D-02	0.20D-02	-0.24D-02
0.167	0.719	0.048	-0.027	3.8	-2.1	0.059	0.069	0.083	0.124	-0.16D-02	0.18D-02	-0.20D-02
0.200	0.736	0.061	-0.015	4.7	-1.1	0.056	0.067	0.083	0.120	-0.13D-02	0.14D-02	-0.16D-02
0.250	0.750	0.075	-0.002	5.7	-0.2	0.052	0.066	0.082	0.118	-0.10D-02	0.92D-03	-0.12D-02
0.317	0.752	0.079	0.007	6.0	0.5	0.051	0.071	0.076	0.116	-0.82D-03	0.45D-03	-0.38D-03
0.401	0.759	0.060	-0.009	4.5	-0.6	0.052	0.076	0.072	0.117	-0.13D-02	0.12D-03	0.50D-03
0.501	0.813	0.032	-0.030	2.2	-2.1	0.056	0.068	0.063	0.108	-0.16D-02	0.42D-03	-0.37D-03
0.601	0.867	0.015	-0.017	1.0	-1.1	0.047	0.053	0.049	0.086	-0.77D-03	0.27D-03	-0.12D-03
0.701	0.903	0.004	-0.017	0.3	-1.1	0.045	0.041	0.038	0.072	-0.70D-03	0.14D-03	0.60D-04
0.801	0.941	0.000	-0.015	0.0	-0.9	0.039	0.032	0.031	0.059	-0.50D-03	0.20D-03	-0.19D-04
0.901	0.971	0.001	-0.010	0.1	-0.6	0.029	0.024	0.023	0.044	-0.25D-03	0.16D-03	-0.37D-05
1.002	0.990	0.002	-0.005	0.1	-0.3	0.018	0.017	0.016	0.029	-0.86D-04	0.86D-04	0.11D-04
1.336	1.000	0.005	0.002	0.3	0.1	0.006	0.004	0.004	0.008	0.00D 00	0.37D-05	0.00D 00

Y/DELM	L/DELM	UV/Q2	UV/(UP*VP)
0.140	0.075	-0.113	-0.407
0.167	0.074	-0.105	-0.389
0.200	0.088	-0.091	-0.355
0.250	0.217	-0.073	-0.291
0.317	11.191	-0.061	-0.226
0.401	0.120	-0.098	-0.335
0.501	0.066	-0.137	-0.422
0.601	0.063	-0.103	-0.306
0.701	0.074	-0.135	-0.378
0.801	0.064	-0.145	-0.407
0.901	0.064	-0.130	-0.362
1.002	0.065	-0.101	-0.285
1.336	0.000	0.000	0.000

M=0.9 BLOWING REGION AFTER 3 ROWS OF HOLES, X=148 CM AND Z/P=+0.3

RUN 12177603 TF= 21.00 C PR= 761.00 MM-HG DELM= 2.887 CM DELM1= 0.408 CM DELM2= 0.322 CM

DIMENSIONAL PROFILES

Y (CM)	U (M/S)	V (M/S)	W (M/S)	R (M/S)	UP2 (M2/S2)	VP2 (M2/S2)	WP2 (M2/S2)	Q2 (M2/S2)	UV (M2/S2)	UW (M2/S2)	VW (M2/S2)
0.419	12.66	-0.65	-0.30	12.68	0.701	0.896	0.730	2.328	-0.204	0.116	-0.170
0.500	12.85	-0.76	-0.21	12.88	0.643	0.872	0.705	2.221	-0.165	0.089	-0.147
0.600	13.14	-0.89	-0.04	13.17	0.555	0.836	0.677	2.068	-0.097	0.048	-0.096
0.750	13.40	-1.00	0.15	13.44	0.517	0.811	0.689	2.017	-0.049	-0.006	-0.021
0.950	13.62	-0.97	0.31	13.66	0.514	0.851	0.725	2.090	-0.047	-0.053	0.059
1.200	13.86	-0.75	0.37	13.89	0.524	0.803	0.714	2.042	-0.074	-0.081	0.089
1.500	14.17	-0.43	0.27	14.18	0.542	0.623	0.620	1.786	-0.110	-0.088	0.057
1.800	14.60	-0.20	0.08	14.60	0.556	0.484	0.461	1.501	-0.171	-0.077	0.033
2.100	15.13	-0.09	-0.02	15.13	0.470	0.367	0.314	1.151	-0.170	-0.024	0.009
2.400	15.62	-0.04	-0.06	15.62	0.334	0.249	0.202	0.785	-0.121	0.011	0.005
2.700	16.00	-0.01	-0.02	16.00	0.175	0.143	0.112	0.430	-0.064	0.023	0.002
3.000	16.24	0.00	0.06	16.24	0.064	0.067	0.050	0.181	-0.025	0.014	0.002
4.000	16.33	0.02	0.20	16.33	0.009	0.005	0.003	0.018	0.000	0.001	0.000

NON-DIMENSIONAL PROFILES

Y/DELM	U/RF	V/RF	W/RF	GAMA	BETA	UP/RF	VP/RF	WP/RF	Q/RF	UV/RF2	UW/RF2	VW/RF2
0.145	0.775	-0.040	-0.018	-2.9	-1.4	0.051	0.058	0.052	0.093	-0.76D-03	0.43D-03	-0.64D-03
0.173	0.787	-0.047	-0.013	-3.4	-0.9	0.049	0.057	0.051	0.091	-0.62D-03	0.33D-03	-0.55D-03
0.208	0.805	-0.055	-0.002	-3.9	-0.2	0.046	0.056	0.050	0.088	-0.36D-03	0.18D-03	-0.36D-03
0.260	0.821	-0.061	0.009	-4.3	0.6	0.044	0.055	0.051	0.087	-0.18D-03	-0.22D-04	-0.79D-04
0.329	0.834	-0.059	0.019	-4.1	1.3	0.044	0.056	0.052	0.089	-0.18D-03	-0.20D-03	0.22D-03
0.416	0.849	-0.046	0.023	-3.1	1.5	0.044	0.055	0.052	0.088	-0.28D-03	-0.30D-03	0.33D-03
0.520	0.868	-0.026	0.017	-1.7	1.1	0.045	0.048	0.048	0.082	-0.41D-03	-0.33D-03	0.21D-03
0.623	0.894	-0.012	0.005	-0.8	0.3	0.046	0.043	0.042	0.075	-0.64D-03	-0.29D-03	0.12D-03
0.727	0.927	-0.006	-0.001	-0.3	-0.1	0.042	0.037	0.034	0.066	-0.64D-03	-0.90D-04	0.34D-04
0.831	0.957	-0.002	-0.004	-0.1	-0.2	0.035	0.031	0.028	0.054	-0.45D-03	0.41D-04	0.19D-04
0.935	0.980	-0.001	-0.001	-0.0	-0.1	0.026	0.023	0.020	0.040	-0.24D-03	0.86D-04	0.75D-05
1.039	0.994	0.000	0.004	0.0	0.2	0.015	0.016	0.014	0.026	-0.94D-04	0.52D-04	0.75D-05
1.385	1.000	0.001	0.012	0.1	0.7	0.006	0.004	0.003	0.008	0.00D 00	0.37D-05	0.00D 00

Y/DELM	L/DELM	UV/Q2	UV/(UP*VP)
0.145	0.063	-0.088	-0.257
0.173	0.058	-0.074	-0.220
0.208	0.049	-0.047	-0.142
0.260	0.050	-0.024	-0.076
0.329	0.074	-0.022	-0.071
0.416	0.102	-0.036	-0.114
0.520	0.094	-0.062	-0.189
0.623	0.088	-0.114	-0.330
0.727	0.082	-0.148	-0.409
0.831	0.081	-0.154	-0.420
0.935	0.084	-0.149	-0.405
1.039	0.095	-0.138	-0.382
1.385	0.000	0.000	0.000

M=0.9 BLOWING REGION AFTER 3 ROWS OF HOLES, X=148 CM AND Z/P=-0.5

RUN 12177605 TF= 21.00 C PR= 761.00 MM-HG DELM= 2.824 CM DELM1= 0.551 CM DELM2= 0.394 CM

DIMENSIONAL PROFILES

Y (CM)	U (M/S)	V (M/S)	W (M/S)	R (M/S)	UP2 (M2/S2)	VP2 (M2/S2)	WP2 (M2/S2)	Q2 (M2/S2)	UV (M2/S2)	UW (M2/S2)	VW (M2/S2)
0.419	11.07	0.76	-0.54	11.11	1.074	1.397	1.916	4.387	-0.488	0.632	-0.614
0.500	11.35	0.84	-0.38	11.39	0.970	1.298	1.913	4.181	-0.431	0.563	-0.523
0.600	11.64	1.08	-0.21	11.69	0.842	1.159	1.938	3.939	-0.341	0.420	-0.389
0.750	11.80	1.33	-0.05	11.87	0.712	1.088	1.808	3.608	-0.247	0.242	-0.240
0.950	11.80	1.37	0.01	11.88	0.651	1.234	1.523	3.408	-0.205	0.089	-0.031
1.200	12.11	0.98	-0.29	12.16	0.752	1.393	1.332	3.477	-0.418	-0.009	0.091
1.500	13.32	0.50	-0.50	13.34	0.877	1.137	0.974	2.989	-0.476	0.147	-0.141
1.800	14.33	0.22	-0.23	14.33	0.588	0.629	0.542	1.759	-0.219	0.051	-0.015
2.100	14.96	0.07	-0.21	14.97	0.491	0.369	0.333	1.194	-0.171	0.033	0.007
2.400	15.56	0.02	-0.19	15.56	0.328	0.227	0.201	0.756	-0.113	0.040	-0.002
2.700	15.97	0.02	-0.10	15.97	0.159	0.125	0.108	0.392	-0.054	0.032	0.001
3.000	16.20	0.03	-0.01	16.20	0.054	0.058	0.045	0.158	-0.017	0.016	0.002
4.000	16.25	0.09	0.08	16.25	0.010	0.005	0.004	0.019	0.000	0.001	0.000

NON-DIMENSIONAL PROFILES

Y/DELM	U/RF	V/RF	W/RF	GAMA	BETA	UP/RF	VP/RF	WP/RF	Q/RF	UV/RF2	UW/RF2	VW/RF2
0.148	0.681	0.047	-0.033	3.9	-2.8	0.064	0.073	0.085	0.129	-0.18D-02	0.24D-02	-0.23D-02
0.177	0.698	0.052	-0.023	4.2	-1.9	0.061	0.070	0.085	0.126	-0.16D-02	0.21D-02	-0.20D-02
0.212	0.716	0.066	-0.013	5.3	-1.0	0.056	0.066	0.086	0.122	-0.13D-02	0.16D-02	-0.15D-02
0.266	0.726	0.082	-0.003	6.4	-0.2	0.052	0.064	0.083	0.117	-0.94D-03	0.92D-03	-0.91D-03
0.336	0.726	0.084	0.001	6.6	0.0	0.050	0.068	0.076	0.114	-0.78D-03	0.34D-03	-0.12D-03
0.425	0.745	0.060	-0.018	4.6	-1.4	0.053	0.073	0.071	0.115	-0.16D-02	-0.34D-04	0.34D-03
0.531	0.820	0.031	-0.031	2.1	-2.1	0.058	0.066	0.061	0.106	-0.18D-02	0.56D-03	-0.53D-03
0.637	0.882	0.014	-0.014	0.9	-0.9	0.047	0.049	0.045	0.082	-0.83D-03	0.19D-03	-0.57D-04
0.743	0.921	0.004	-0.013	0.3	-0.8	0.043	0.037	0.036	0.067	-0.65D-03	0.12D-03	0.27D-04
0.850	0.958	0.001	-0.012	0.1	-0.7	0.035	0.029	0.028	0.054	-0.43D-03	0.15D-03	-0.76D-05
0.956	0.983	0.001	-0.006	0.1	-0.4	0.025	0.022	0.020	0.039	-0.20D-03	0.12D-03	0.38D-05
1.062	0.997	0.002	-0.001	0.1	-0.0	0.014	0.015	0.013	0.024	-0.64D-04	0.61D-04	0.76D-05
1.416	1.000	0.006	0.005	0.3	0.3	0.006	0.004	0.004	0.008	0.00D 00	0.38D-05	0.00D 00

Y/DELM	L/DELM	UV/Q2	UV/(UP*VP)
0.148	0.074	-0.111	-0.398
0.177	0.075	-0.103	-0.384
0.212	0.099	-0.087	-0.345
0.266	0.415	-0.068	-0.281
0.336	0.784	-0.060	-0.229
0.425	0.084	-0.120	-0.408
0.531	0.059	-0.159	-0.477
0.637	0.063	-0.125	-0.360
0.743	0.074	-0.143	-0.402
0.850	0.068	-0.149	-0.414
0.956	0.079	-0.138	-0.383
1.062	0.088	-0.108	-0.304
1.416	0.000	0.000	0.000

M=0.9 BLOWING REGION AFTER 7 ROWS OF HOLES, X=168 CM AND Z/P=+0.5

RUN 3237607 TF= 20.00 C PR= 760.00 MM-HG DELM= 3.688 CM DELM1= 0.672 CM DELM2= 0.509 CM

DIMENSIONAL PROFILES

Y (CM)	U (M/S)	V (M/S)	W (M/S)	R (M/S)	UP2 (M2/S2)	VP2 (M2/S2)	WP2 (M2/S2)	Q2 (M2/S2)	UV (M2/S2)	UW (M2/S2)	VW (M2/S2)
0.419	12.27	1.40	0.26	12.36	1.137	1.442	1.491	4.070	-0.300	-0.065	0.028
0.575	12.71	1.69	0.57	12.83	0.540	1.181	1.634	3.355	-0.307	-0.075	0.084
1.000	12.39	2.26	1.03	12.64	0.632	1.349	1.996	3.977	-0.246	-0.179	0.449
1.250	12.52	1.96	0.45	12.68	0.772	1.568	1.778	4.118	-0.463	-0.207	0.410
1.500	13.49	1.64	0.20	13.59	0.793	1.485	1.402	3.680	-0.374	0.047	0.114
1.750	13.95	1.42	0.84	14.05	0.519	1.089	1.129	2.738	0.070	0.026	0.254
2.300	14.06	0.93	0.57	14.10	0.557	0.685	0.521	1.764	-0.260	-0.045	0.113
2.500	14.56	0.80	0.55	14.59	0.632	0.610	0.431	1.673	-0.278	-0.013	0.059
3.100	15.88	0.63	0.72	15.91	0.498	0.352	0.263	1.114	-0.170	0.042	0.052
3.500	16.48	0.60	0.88	16.52	0.201	0.173	0.132	0.507	-0.066	0.033	0.031
4.000	16.78	0.63	1.05	16.82	0.040	0.050	0.037	0.127	-0.010	0.009	0.011
5.000	16.82	0.66	1.12	16.87	0.008	0.007	0.005	0.021	0.000	0.002	0.001
6.100	16.82	0.66	1.14	16.88	0.006	0.004	0.002	0.013	0.001	0.001	0.001

NON-DIMENSIONAL PROFILES

Y/DELM	U/RF	V/RF	W/RF	GAMA	BETA	UP/RF	VP/RF	WP/RF	Q/RF	UV/RF2	UW/RF2	VW/RF2
0.114	0.727	0.083	0.015	6.5	1.2	0.063	0.071	0.072	0.120	-0.11D-02	-0.23D-03	0.98D-04
0.156	0.753	0.100	0.034	7.6	2.6	0.044	0.064	0.076	0.109	-0.11D-02	-0.26D-03	0.29D-03
0.271	0.734	0.134	0.061	10.3	4.8	0.047	0.069	0.084	0.118	-0.86D-03	-0.63D-03	0.16D-02
0.339	0.742	0.116	0.027	8.9	2.1	0.052	0.074	0.079	0.120	-0.16D-02	-0.73D-03	0.14D-02
0.407	0.799	0.097	0.012	6.9	0.8	0.053	0.072	0.070	0.114	-0.13D-02	0.16D-03	0.40D-03
0.474	0.826	0.084	0.050	5.8	3.4	0.043	0.062	0.063	0.098	0.25D-03	0.91D-04	0.89D-03
0.624	0.833	0.055	0.034	3.8	2.3	0.044	0.049	0.043	0.079	-0.91D-03	-0.16D-03	0.40D-03
0.678	0.863	0.047	0.033	3.1	2.2	0.047	0.046	0.039	0.077	-0.98D-03	-0.46D-04	0.21D-03
0.840	0.941	0.037	0.043	2.3	2.6	0.042	0.035	0.030	0.063	-0.60D-03	0.15D-03	0.18D-03
0.949	0.976	0.036	0.052	2.1	3.1	0.027	0.025	0.022	0.042	-0.23D-03	0.12D-03	0.11D-03
1.084	0.994	0.037	0.062	2.2	3.6	0.012	0.013	0.011	0.021	-0.35D-04	0.32D-04	0.39D-04
1.356	0.996	0.039	0.066	2.2	3.8	0.005	0.005	0.004	0.009	0.00D 00	0.70D-05	0.35D-05
1.654	0.996	0.039	0.068	2.2	3.9	0.005	0.004	0.003	0.007	0.35D-05	0.35D-05	0.35D-05

Y/DELM	L/DELM	UV/Q2	UV/(UP*VP)
0.114	0.048	-0.074	-0.234
0.156	0.098	-0.092	-0.384
0.271	0.146	-0.062	-0.266
0.339	0.071	-0.112	-0.421
0.407	0.049	-0.102	-0.345
0.474	0.108	0.026	0.093
0.624	0.085	-0.147	-0.421
0.678	0.054	-0.166	-0.448
0.840	0.061	-0.153	-0.406
0.949	0.064	-0.130	-0.354
1.084	0.100	-0.079	-0.224
1.356	0.000	0.000	0.000
1.654	******	0.077	0.204

M=0.9 BLOWING REGION AFTER 7 ROWS OF HOLES, X=168 CM AND Z/P= 0.0

RUN 3237605 TF= 20.00 C PR= 760.00 MM-HG DELM= 3.943 CM DELM1= 0.722 CM DELM2= 0.513 CM

DIMENSIONAL PROFILES

Y (CM)	U (M/S)	V (M/S)	W (M/S)	R (M/S)	UP2 (M2/S2)	VP2 (M2/S2)	WP2 (M2/S2)	Q2 (M2/S2)	UV (M2/S2)	UW (M2/S2)	VW (M2/S2)
0.419	9.35	2.93	-1.04	9.86	1.837	4.244	8.079	14.161	-1.309	0.000	0.765
0.575	12.30	3.01	-4.50	13.44	2.285	4.954	4.841	12.080	-1.644	1.420	-1.442
1.000	14.24	3.04	2.49	14.77	0.759	2.062	4.420	7.242	0.046	-0.279	2.019
1.250	13.56	2.27	0.98	13.78	0.465	0.849	1.466	2.780	-0.166	-0.081	0.445
1.500	13.67	2.02	0.83	13.84	0.387	0.723	0.918	2.029	-0.105	-0.024	0.197
1.750	13.78	1.80	0.66	13.91	0.399	0.777	0.810	1.986	-0.160	-0.080	0.230
2.300	14.62	1.35	0.69	14.70	0.344	0.584	0.498	1.426	-0.112	-0.008	0.084
2.500	14.77	1.23	0.77	14.84	0.325	0.498	0.416	1.240	-0.106	-0.021	0.092
3.100	15.58	0.98	0.81	15.63	0.471	0.413	0.280	1.164	-0.206	-0.002	0.050
3.500	16.32	0.87	0.93	16.37	0.343	0.301	0.184	0.828	-0.148	0.028	0.039
4.000	16.86	0.80	1.10	16.92	0.105	0.129	0.067	0.302	-0.049	0.021	0.015
5.000	16.97	0.75	1.18	17.03	0.011	0.012	0.006	0.030	-0.001	0.003	0.002
6.100	16.95	0.72	1.21	17.05	0.005	0.005	0.004	0.014	0.001	0.000	0.001

NON-DIMENSIONAL PROFILES

Y/DELM	U/RF	V/RF	W/RF	GAMA	BETA	UP/RF	VP/RF	WP/RF	Q/RF	UV/RF2	UW/RF2	VW/RF2
0.106	0.548	0.172	-0.061	17.4	-6.3	0.079	0.121	0.167	0.221	-0.45D-02	0.00D 00	0.26D-02
0.146	0.721	0.177	-0.26?	13.8	-20.1	0.089	0.131	0.129	0.204	-0.57D-02	0.49D-02	-0.50D-02
0.254	0.835	0.178	0.146	12.1	9.9	0.051	0.084	0.123	0.158	0.16D-03	-0.96D-03	0.69D-02
0.317	0.795	0.133	0.057	9.5	4.1	0.040	0.054	0.071	0.098	-0.57D-03	-0.28D-03	0.15D-02
0.380	0.802	0.118	0.049	8.4	3.5	0.036	0.050	0.056	0.084	-0.36D-03	-0.83D-04	0.68D-03
0.444	0.808	0.106	0.039	7.4	2.7	0.037	0.052	0.053	0.083	-0.55D-03	-0.28D-03	0.79D-03
0.583	0.857	0.079	0.040	5.3	2.7	0.034	0.045	0.041	0.070	-0.39D-03	-0.28D-04	0.29D-03
0.634	0.866	0.072	0.045	4.8	3.0	0.033	0.041	0.038	0.065	-0.36D-03	-0.72D-04	0.32D-03
0.786	0.914	0.057	0.048	3.6	3.0	0.040	0.038	0.031	0.063	-0.71D-03	-0.69D-05	0.17D-03
0.888	0.957	0.051	0.055	3.1	3.3	0.034	0.032	0.025	0.053	-0.51D-03	0.96D-04	0.13D-03
1.014	0.989	0.047	0.065	2.7	3.7	0.019	0.021	0.015	0.032	-0.17D-03	0.72D-04	0.52D-04
1.268	0.995	0.044	0.069	2.5	4.0	0.006	0.006	0.005	0.010	-0.34D-05	0.10D-04	0.69D-05
1.547	0.996	0.042	0.071	2.4	4.1	0.004	0.004	0.004	0.007	0.34D-05	0.00D 00	0.34D-05

Y/DELM	L/DELM	UV/Q2	UV/(UP*VP)
0.106	0.014	-0.092	-0.469
0.146	0.021	-0.136	-0.489
0.254	0.024	0.006	0.037
0.317	0.076	-0.060	-0.264
0.380	0.109	-0.052	-0.199
0.444	0.126	-0.081	-0.287
0.583	0.078	-0.079	-0.250
0.634	0.109	-0.085	-0.263
0.786	0.063	-0.177	-0.467
0.888	0.060	-0.179	-0.461
1.014	0.092	-0.162	-0.421
1.268	0.105	-0.033	-0.087
1.547	******	0.071	0.200

M=0.9 BLOWING REGION AFTER 7 ROWS OF HOLES, X=168 CM AND Z/P=-0.5

RUN 3237606 TF= 20.00 C PR= 760.00 MM-HG DELM= 3.366 CM DELM1= 0.547 CM DELM2= 0.428 CM

DIMENSIONAL PROFILES

Y (CM)	U (M/S)	V (M/S)	W (M/S)	R (M/S)	UP2 (M2/S2)	VP2 (M2/S2)	WP2 (M2/S2)	Q2 (M2/S2)	UV (M2/S2)	UW (M2/S2)	VW (M2/S2)
0.419	12.89	1.49	0.26	12.98	0.698	1.695	1.799	4.193	-0.438	-0.086	0.103
0.575	13.38	1.87	0.58	13.52	0.661	1.450	1.975	4.086	-0.384	-0.108	0.183
1.000	13.33	2.81	1.24	13.67	0.768	1.554	2.649	4.971	-0.311	-0.316	0.518
1.250	13.19	2.56	1.03	13.47	0.851	1.840	2.441	5.132	-0.474	-0.348	0.718
1.500	13.92	2.07	0.45	14.08	1.023	1.924	1.959	4.906	-0.577	-0.124	0.367
1.750	14.63	1.76	0.98	14.77	0.783	1.647	1.778	4.208	-0.024	-0.018	0.330
2.300	14.42	1.09	0.71	14.48	0.638	0.834	0.717	2.189	-0.282	-0.071	0.247
2.500	14.90	0.94	0.63	14.94	0.704	0.678	0.484	1.866	-0.306	-0.017	0.098
3.100	16.30	0.72	0.83	16.34	0.401	0.330	0.225	0.956	-0.147	0.049	0.050
3.500	16.75	0.67	0.98	16.80	0.105	0.121	0.086	0.312	-0.038	0.022	0.023
4.000	16.88	0.69	1.07	16.93	0.020	0.028	0.019	0.067	-0.002	0.005	0.005
5.000	16.84	0.68	1.18	16.90	0.007	0.005	0.005	0.018	0.001	0.001	0.001
6.100	16.81	0.70	1.20	16.87	0.005	0.003	0.003	0.012	0.001	0.001	0.001

NON-DIMENSIONAL PROFILES

Y/DELM	U/RF	V/RF	W/RF	GAMA	BETA	UP/RF	VP/RF	WP/RF	Q/RF	UV/RF2	UW/RF2	VW/RF2
0.124	0.764	0.088	0.015	6.6	1.2	0.050	0.077	0.080	0.121	-0.15D-02	-0.30D-03	0.36D-03
0.171	0.793	0.111	0.034	8.0	2.5	0.048	0.071	0.083	0.120	-0.13D-02	-0.38D-03	0.64D-03
0.297	0.790	0.167	0.074	11.9	5.3	0.052	0.074	0.096	0.132	-0.11D-02	-0.11D-02	0.18D-02
0.371	0.782	0.152	0.061	11.0	4.5	0.055	0.080	0.093	0.134	-0.17D-02	-0.12D-02	0.25D-02
0.446	0.825	0.123	0.027	8.5	1.9	0.060	0.082	0.083	0.131	-0.20D-02	-0.44D-03	0.13D-02
0.520	0.867	0.104	0.058	6.9	3.8	0.052	0.076	0.079	0.122	-0.84D-04	-0.63D-04	0.12D-02
0.683	0.855	0.065	0.042	4.3	2.8	0.047	0.054	0.050	0.088	-0.99D-03	-0.25D-03	0.87D-03
0.743	0.883	0.056	0.037	3.6	2.4	0.050	0.049	0.041	0.081	-0.11D-02	-0.60D-04	0.34D-03
0.921	0.966	0.043	0.049	2.5	2.9	0.038	0.034	0.028	0.058	-0.52D-03	0.17D-03	0.18D-03
1.040	0.993	0.040	0.058	2.3	3.3	0.019	0.021	0.017	0.033	-0.13D-03	0.77D-04	0.81D-04
1.189	1.001	0.041	0.063	2.3	3.6	0.008	0.010	0.008	0.015	-0.70D-05	0.18D-04	0.18D-04
1.486	0.998	0.040	0.070	2.3	4.0	0.005	0.004	0.004	0.008	0.35D-05	0.35D-05	0.35D-05
1.812	0.996	0.041	0.071	2.4	4.1	0.004	0.003	0.003	0.006	0.35D-05	0.35D-05	0.35D-05

Y/DELM	L/DELM	UV/Q2	UV/(UP*VP)
0.124	0.059	-0.104	-0.403
0.171	0.087	-0.094	-0.392
0.297	0.134	-0.063	-0.285
0.371	0.170	-0.092	-0.379
0.446	0.063	-0.118	-0.411
0.520	0.035	-0.006	-0.021
0.683	0.139	-0.129	-0.387
0.743	0.060	-0.164	-0.443
0.921	0.067	-0.154	-0.404
1.040	0.091	-0.122	-0.337
1.189	0.337	-0.030	-0.085
1.486	0.159	0.056	0.169
1.812	******	0.083	0.258

M=0.9 START OF RECOVERY AFTER 11 ROWS OF HOLES, X=188 CM AND Z/P=+0.5

RUN 3177605 TF= 20.50 C PR= 760.50 MM-HG DELM= 4.457 CM DELM1= 0.660 CM DELM2= 0.535 CM

DIMENSIONAL PROFILES

Y (CM)	U (M/S)	V (M/S)	W (M/S)	R (M/S)	UP2 (M2/S2)	VP2 (M2/S2)	WP2 (M2/S2)	Q2 (M2/S2)	UV (M2/S2)	UW (M2/S2)	VW (M2/S2)
0.419	13.39	0.80	-0.18	13.42	0.607	1.277	1.466	3.350	-0.272	0.171	-0.092
0.575	13.71	1.25	0.11	13.76	0.568	1.213	1.870	3.651	-0.211	0.099	-0.090
1.000	13.09	1.94	0.25	13.24	0.689	1.771	2.070	4.530	-0.219	0.018	0.093
1.250	13.12	1.62	-0.27	13.22	0.776	1.806	1.746	4.329	-0.449	0.018	0.092
1.500	14.01	1.45	-0.37	14.09	0.734	1.488	1.674	3.897	-0.270	0.196	-0.122
1.750	14.23	1.33	0.35	14.30	0.539	1.057	1.220	2.816	0.181	0.034	0.144
2.300	13.63	0.81	0.01	13.65	0.285	0.619	0.458	1.363	-0.070	-0.019	0.038
2.500	13.77	0.67	-0.04	13.79	0.305	0.591	0.416	1.312	-0.094	-0.024	0.003
3.100	14.42	0.46	-0.03	14.43	0.508	0.521	0.390	1.419	-0.201	-0.037	0.008
3.500	15.12	0.37	-0.02	15.12	0.573	0.432	0.335	1.340	-0.219	0.004	0.003
4.000	15.91	0.31	0.08	15.92	0.339	0.258	0.200	0.797	-0.121	0.030	0.013
5.000	16.54	0.32	0.32	16.54	0.020	0.028	0.017	0.066	-0.003	0.003	0.002
6.100	16.52	0.32	0.36	16.53	0.008	0.007	0.004	0.019	0.001	0.001	0.000

NON-DIMENSIONAL PROFILES

Y/DELM	U/RF	V/RF	W/RF	GAMA	BETA	UP/RF	VP/RF	WP/RF	Q/RF	UV/RF2	UW/RF2	VW/RF2
0.094	0.810	0.048	-0.011	3.4	-0.8	0.047	0.068	0.073	0.111	-0.10D-02	0.63D-03	-0.34D-03
0.129	0.829	0.076	0.007	5.2	0.5	0.046	0.067	0.083	0.116	-0.77D-03	0.36D-03	-0.33D-03
0.224	0.792	0.117	0.015	8.4	1.1	0.050	0.081	0.087	0.129	-0.80D-03	0.66D-04	0.34D-03
0.280	0.794	0.098	-0.016	7.0	-1.2	0.053	0.081	0.080	0.126	-0.16D-02	0.66D-04	0.34D-03
0.337	0.848	0.088	-0.022	5.9	-1.5	0.052	0.074	0.078	0.119	-0.99D-03	0.72D-03	-0.45D-03
0.393	0.861	0.080	0.021	5.3	1.4	0.044	0.062	0.067	0.102	0.66D-03	0.12D-03	0.53D-03
0.516	0.825	0.049	0.001	3.4	0.0	0.032	0.048	0.041	0.071	-0.26D-03	-0.70D-04	0.14D-03
0.561	0.833	0.041	-0.002	2.8	-0.2	0.033	0.047	0.039	0.069	-0.34D-03	-0.88D-04	0.11D-04
0.696	0.872	0.028	-0.002	1.8	-0.1	0.043	0.044	0.038	0.072	-0.74D-03	-0.14D-03	0.29D-04
0.785	0.915	0.022	-0.001	1.4	-0.1	0.046	0.040	0.035	0.070	-0.80D-03	0.15D-04	0.11D-04
0.898	0.962	0.019	0.005	1.1	0.3	0.035	0.031	0.027	0.054	-0.44D-03	0.11D-03	0.48D-04
1.122	1.001	0.019	0.019	1.1	1.1	0.009	0.010	0.008	0.016	-0.11D-04	0.11D-04	0.73D-05
1.369	0.999	0.019	0.022	1.1	1.2	0.005	0.005	0.004	0.008	0.37D-05	0.37D-05	0.00D 00

Y/DELM	L/DELM	UV/Q2	UV/(UP*VP)
0.094	0.051	-0.081	-0.309
0.129	0.138	-0.058	-0.254
0.224	0.072	-0.048	-0.198
0.280	0.064	-0.104	-0.379
0.337	0.042	-0.069	-0.258
0.393	0.219	0.064	0.240
0.516	1.500	-0.051	-0.167
0.561	0.074	-0.072	-0.221
0.696	0.067	-0.142	-0.391
0.785	0.058	-0.163	-0.440
0.898	0.062	-0.152	-0.409
1.122	0.068	-0.045	-0.127
1.369	******	0.053	0.134

M=0.9 START OF RECOVERY AFTER 11 ROWS OF HOLES, X=188 CM AND Z/P=+0.3

RUN 3177604 TF= 20.50 C PR= 760.50 MM-HG DELM= 4.506 CM DELM1= 0.507 CM DELM2= 0.430 CM

DIMENSIONAL PROFILES

Y (CM)	U (M/S)	V (M/S)	W (M/S)	R (M/S)	UP2 (M2/S2)	VP2 (M2/S2)	WP2 (M2/S2)	Q2 (M2/S2)	UV (M2/S2)	UW (M2/S2)	VW (M2/S2)
0.419	14.19	-0.21	-0.01	14.19	0.161	0.242	0.249	0.652	-0.001	-0.003	-0.020
0.575	14.19	-0.42	0.05	14.20	0.189	0.293	0.230	0.712	-0.005	-0.013	-0.012
1.000	14.05	-0.73	0.16	14.07	0.263	0.522	0.335	1.120	-0.032	-0.034	0.054
1.250	14.02	-0.68	0.23	14.04	0.309	0.583	0.417	1.309	-0.039	-0.049	0.102
1.500	14.02	-0.52	0.25	14.03	0.344	0.620	0.495	1.460	-0.067	-0.071	0.151
1.750	14.07	-0.35	0.22	14.08	0.379	0.625	0.534	1.538	-0.099	-0.083	0.178
2.300	14.34	-0.09	0.11	14.34	0.413	0.553	0.522	1.488	-0.142	-0.065	0.152
2.500	14.49	-0.01	0.08	14.49	0.421	0.525	0.500	1.446	-0.150	-0.046	0.133
3.100	15.04	0.11	0.03	15.04	0.424	0.414	0.403	1.241	-0.153	0.001	0.081
3.500	15.46	0.15	0.01	15.46	0.366	0.326	0.321	1.013	-0.121	0.038	0.051
4.000	15.92	0.20	0.06	15.92	0.232	0.198	0.198	0.628	-0.067	0.048	0.021
5.000	16.40	0.32	0.28	16.41	0.022	0.030	0.024	0.077	-0.004	0.007	-0.002
6.100	16.40	0.32	0.28	16.41	0.009	0.006	0.003	0.018	0.001	0.001	0.001

NON-DIMENSIONAL PROFILES

Y/DELM	U/RF	V/RF	W/RF	GAMA	BETA	UP/RF	VP/RF	WP/RF	Q/RF	UV/RF2	UW/RF2	VW/RF2
0.093	0.865	-0.013	-0.001	-0.8	-0.0	0.024	0.030	0.030	0.049	-0.37D-05	-0.11D-04	-0.74D-04
0.128	0.865	-0.026	0.003	-1.7	0.2	0.026	0.033	0.029	0.051	-0.19D-04	-0.48D-04	-0.45D-04
0.222	0.856	-0.044	0.010	-3.0	0.7	0.031	0.044	0.035	0.064	-0.12D-03	-0.13D-03	0.20D-03
0.277	0.854	-0.041	0.014	-2.8	0.9	0.034	0.047	0.039	0.070	-0.14D-03	-0.18D-03	0.38D-03
0.333	0.854	-0.032	0.015	-2.1	1.0	0.036	0.048	0.043	0.074	-0.25D-03	-0.26D-03	0.56D-03
0.388	0.857	-0.021	0.013	-1.4	0.9	0.038	0.048	0.045	0.076	-0.37D-03	-0.31D-03	0.66D-03
0.510	0.874	-0.005	0.007	-0.4	0.4	0.039	0.045	0.044	0.074	-0.53D-03	-0.24D-03	0.56D-03
0.555	0.883	-0.001	0.005	-0.0	0.3	0.040	0.044	0.043	0.073	-0.56D-03	-0.17D-03	0.49D-03
0.688	0.917	0.007	0.002	0.4	0.1	0.040	0.039	0.039	0.068	-0.57D-03	0.37D-05	0.30D-03
0.777	0.942	0.009	0.001	0.6	0.0	0.037	0.035	0.035	0.061	-0.45D-03	0.14D-03	0.19D-03
0.888	0.970	0.012	0.004	0.7	0.2	0.029	0.027	0.027	0.048	-0.25D-03	0.18D-03	0.78D-04
1.110	0.999	0.020	0.017	1.1	1.0	0.009	0.011	0.009	0.017	-0.15D-04	0.26D-04	-0.74D-05
1.354	0.999	0.020	0.017	1.1	1.0	0.006	0.005	0.003	0.008	0.37D-05	0.37D-05	0.37D-05

Y/DELM	L/DELM	UV/Q2	UV/(UP*VP)
0.093	0.028	-0.002	-0.005
0.128	0.061	-0.007	-0.021
0.222	0.219	-0.029	-0.086
0.277	0.745	-0.030	-0.092
0.333	0.551	-0.046	-0.145
0.388	0.241	-0.064	-0.203
0.510	0.124	-0.095	-0.297
0.555	0.108	-0.104	-0.319
0.688	0.087	-0.123	-0.365
0.777	0.079	-0.119	-0.350
0.888	0.075	-0.107	-0.313
1.110	0.064	-0.052	-0.156
1.354	******	0.056	0.136

M=0.9 START OF RECOVERY AFTER 11 ROWS OF HOLES, X=188 CM AND Z/P= 0.0

RUN 3177601 TF= 20.50 C PR= 760.50 MM-HG DELM= 4.806 CM DELM1= 0.737 CM DELM2= 0.558 CM

DIMENSIONAL PROFILES

Y (CM)	U (M/S)	V (M/S)	W (M/S)	R (M/S)	UP2 (M2/S2)	VP2 (M2/S2)	WP2 (M2/S2)	Q2 (M2/S2)	UV (M2/S2)	UW (M2/S2)	VW (M2/S2)
0.419	10.18	2.12	-1.30	10.48	2.094	6.311	7.321	15.727	-1.635	0.256	0.617
0.575	13.61	2.20	-5.22	14.74	2.361	5.065	5.412	12.838	-1.574	2.057	-2.160
1.000	14.65	2.66	1.66	14.98	0.756	2.100	3.419	6.275	0.309	-0.149	1.568
1.250	13.87	1.74	0.10	13.98	0.450	0.857	1.159	2.467	-0.142	0.089	0.119
1.500	13.93	1.51	-0.05	14.01	0.383	0.847	0.818	2.048	-0.069	0.058	0.007
1.750	13.88	1.25	-0.23	13.94	0.374	0.869	0.746	1.989	-0.099	0.017	0.055
2.300	14.15	0.80	-0.23	14.18	0.355	0.652	0.585	1.593	0.007	-0.035	0.020
2.500	14.14	0.69	-0.23	14.16	0.370	0.557	0.515	1.442	-0.039	-0.066	0.042
3.100	14.63	0.51	-0.23	14.64	0.433	0.441	0.380	1.255	-0.158	-0.066	-0.037
3.500	15.10	0.42	-0.16	15.11	0.451	0.402	0.320	1.174	-0.173	-0.046	-0.022
4.000	15.78	0.33	-0.10	15.79	0.430	0.327	0.227	0.985	-0.169	-0.003	-0.004
5.000	16.75	0.23	0.16	16.75	0.046	0.072	0.033	0.151	-0.020	0.009	0.002
6.100	16.77	0.22	0.19	16.77	0.007	0.008	0.004	0.020	0.001	0.001	0.001

NON-DIMENSIONAL PROFILES

Y/DELM	U/RF	V/RF	W/RF	GAMA	BETA	UP/RF	VP/RF	WP/RF	Q/RF	UV/RF2	UW/RF2	VW/RF2
0.087	0.607	0.126	-0.078	11.8	-7.3	0.086	0.150	0.161	0.236	-0.58D-02	0.91D-03	0.22D-02
0.120	0.812	0.131	-0.311	9.2	-21.0	0.092	0.134	0.139	0.214	-0.56D-02	0.73D-02	-0.77D-02
0.208	0.874	0.159	0.099	10.3	6.5	0.052	0.086	0.110	0.149	0.11D-02	-0.53D-03	0.56D-02
0.260	0.827	0.104	0.006	7.2	0.4	0.040	0.055	0.064	0.094	-0.50D-03	0.32D-03	0.42D-03
0.312	0.831	0.090	-0.003	6.2	-0.2	0.037	0.055	0.054	0.085	-0.25D-03	0.21D-03	0.25D-04
0.364	0.828	0.075	-0.014	5.1	-0.9	0.036	0.056	0.052	0.084	-0.35D-03	0.60D-04	0.20D-03
0.479	0.844	0.048	-0.014	3.2	-0.9	0.036	0.048	0.046	0.075	0.25D-04	-0.12D-03	0.71D-04
0.520	0.843	0.041	-0.014	2.8	-0.9	0.036	0.045	0.043	0.072	-0.14D-03	-0.23D-03	0.15D-03
0.645	0.872	0.030	-0.014	2.0	-0.9	0.039	0.040	0.037	0.067	-0.56D-03	-0.23D-03	-0.13D-03
0.728	0.900	0.025	-0.010	1.6	-0.6	0.040	0.038	0.034	0.065	-0.62D-03	-0.16D-03	-0.78D-04
0.832	0.941	0.020	-0.006	1.2	-0.4	0.039	0.034	0.028	0.059	-0.60D-03	-0.11D-04	-0.14D-04
1.040	0.999	0.014	0.010	0.8	0.5	0.013	0.016	0.011	0.023	-0.71D-04	0.32D-04	0.71D-05
1.269	1.000	0.013	0.011	0.8	0.6	0.005	0.005	0.004	0.008	0.36D-05	0.36D-05	0.36D-05

Y/DELM	L/DELM	UV/Q2	UV/(UP*VP)
0.087	0.011	-0.104	-0.450
0.120	0.016	-0.123	-0.455
0.208	0.028	0.049	0.245
0.260	0.063	-0.058	-0.229
0.312	0.159	-0.034	-0.121
0.364	0.898	-0.050	-0.174
0.479	0.119	0.004	0.015
0.520	0.516	-0.027	-0.086
0.645	0.072	-0.126	-0.362
0.728	0.068	-0.147	-0.406
0.832	0.064	-0.172	-0.451
1.040	0.062	-0.132	-0.348
1.269	******	0.050	0.134

M=0.9 START OF RECOVERY AFTER 11 ROWS OF HOLES, X=188 CM AND Z/P=-0.3

RUN 3177602 TF= 20.50 C PR= 760.50 MM-HG DELM= 4.061 CM DELM1= 0.441 CM DELM2= 0.378 CM

DIMENSIONAL PROFILES

Y (CM)	U (M/S)	V (M/S)	W (M/S)	R (M/S)	UP2 (M2/S2)	VP2 (M2/S2)	WP2 (M2/S2)	Q2 (M2/S2)	UV (M2/S2)	UW (M2/S2)	VW (M2/S2)
0.419	14.61	-0.58	0.45	14.63	0.165	0.246	0.270	0.681	0.011	-0.003	0.010
0.575	14.66	-0.80	0.52	14.69	0.180	0.289	0.244	0.713	0.017	-0.017	0.016
1.000	14.58	-1.16	0.44	14.63	0.245	0.497	0.361	1.104	0.015	-0.021	0.038
1.250	14.55	-1.16	0.33	14.60	0.284	0.582	0.439	1.306	0.004	-0.005	0.041
1.500	14.53	-1.04	0.16	14.56	0.317	0.634	0.509	1.460	-0.019	0.033	0.024
1.750	14.51	-0.87	-0.02	14.54	0.356	0.650	0.547	1.554	-0.054	0.079	0.007
2.300	14.61	-0.46	-0.33	14.62	0.416	0.637	0.515	1.569	-0.142	0.121	-0.039
2.500	14.72	-0.36	-0.37	14.73	0.439	0.615	0.477	1.531	-0.167	0.120	-0.040
3.100	15.32	-0.14	-0.40	15.32	0.510	0.474	0.411	1.395	-0.181	0.116	-0.018
3.500	15.84	-0.01	-0.30	15.85	0.406	0.333	0.324	1.063	-0.128	0.095	-0.004
4.000	16.35	0.11	-0.12	16.35	0.183	0.176	0.165	0.525	-0.058	0.046	0.001
5.000	16.58	0.20	0.08	16.58	0.017	0.022	0.012	0.052	-0.002	0.002	0.002
6.100	16.56	0.23	0.16	16.57	0.009	0.006	0.003	0.018	0.001	0.001	0.001

NON-DIMENSIONAL PROFILES

Y/DELM	U/RF	V/RF	W/RF	GAMA	BETA	UP/RF	VP/RF	WP/RF	Q/RF	UV/RF2	UW/RF2	VW/RF2
0.103	0.882	-0.035	0.027	-2.3	1.8	0.025	0.030	0.031	0.050	0.40D-04	-0.11D-04	0.36D-04
0.142	0.885	-0.048	0.031	-3.1	2.0	0.026	0.032	0.030	0.051	0.62D-04	-0.62D-04	0.58D-04
0.246	0.880	-0.070	0.027	-4.5	1.7	0.030	0.043	0.036	0.063	0.55D-04	-0.76D-04	0.14D-03
0.308	0.878	-0.070	0.020	-4.6	1.3	0.032	0.046	0.040	0.069	0.15D-04	-0.18D-04	0.15D-03
0.369	0.877	-0.063	0.010	-4.1	0.6	0.034	0.048	0.043	0.073	-0.69D-04	0.12D-03	0.87D-04
0.431	0.876	-0.053	-0.001	-3.4	-0.1	0.036	0.049	0.045	0.075	-0.20D-03	0.29D-03	0.25D-04
0.566	0.882	-0.028	-0.020	-1.8	-1.3	0.039	0.048	0.043	0.076	-0.52D-03	0.44D-03	-0.14D-03
0.616	0.888	-0.022	-0.022	-1.4	-1.4	0.040	0.047	0.042	0.075	-0.61D-03	0.44D-03	-0.15D-03
0.763	0.925	-0.008	-0.024	-0.5	-1.5	0.043	0.042	0.039	0.071	-0.66D-03	0.42D-03	-0.66D-04
0.862	0.956	-0.001	-0.018	-0.0	-1.1	0.038	0.035	0.034	0.062	-0.47D-03	0.35D-03	-0.15D-04
0.985	0.987	0.007	-0.007	0.4	-0.4	0.026	0.025	0.025	0.044	-0.21D-03	0.17D-03	0.36D-05
1.231	1.001	0.012	0.005	0.7	0.3	0.008	0.009	0.007	0.014	-0.73D-05	0.73D-05	0.73D-05
1.502	0.999	0.014	0.010	0.8	0.6	0.006	0.005	0.003	0.008	0.36D-05	0.36D-05	0.36D-05

Y/DELM	L/DELM	UV/Q2	UV/(UP*VP)
0.103	2.027	0.016	0.055
0.142	0.708	0.024	0.075
0.246	0.220	0.014	0.043
0.308	0.123	0.003	0.010
0.369	0.377	-0.013	-0.042
0.431	17.556	-0.035	-0.112
0.566	0.202	-0.091	-0.276
0.616	0.143	-0.109	-0.321
0.763	0.086	-0.130	-0.368
0.862	0.074	-0.120	-0.348
0.985	0.082	-0.110	-0.323
1.231	0.764	-0.038	-0.103
1.502	******	0.056	0.136

M=0.9 START OF RECOVERY AFTER 11 ROWS OF HOLES, X=188 CM AND Z/P=-0.5

RUN 3177603 TF= 20.50 C PR= 760.50 MM-HG DELM= 4.152 CM DELM1= 0.605 CM DELM2= 0.493 CM

DIMENSIONAL PROFILES

Y (CM)	U (M/S)	V (M/S)	W (M/S)	R (M/S)	UP2 (M2/S2)	VP2 (M2/S2)	WP2 (M2/S2)	Q2 (M2/S2)	UV (M2/S2)	UW (M2/S2)	VW (M2/S2)
0.419	13.38	0.69	-0.29	13.40	0.548	1.258	1.426	3.232	-0.269	0.176	-0.204
0.575	13.67	1.11	-0.01	13.72	0.508	1.167	1.704	3.379	-0.200	0.111	-0.206
1.000	13.15	1.63	0.11	13.25	0.657	1.789	1.775	4.221	-0.279	0.058	0.001
1.250	13.34	1.40	-0.49	13.43	0.827	1.839	1.681	4.348	-0.491	0.077	-0.058
1.500	14.26	1.42	-0.49	14.34	0.710	1.447	1.704	3.861	-0.208	0.173	-0.166
1.750	14.28	1.33	0.20	14.34	0.527	1.046	1.190	2.763	0.214	0.009	0.107
2.300	13.63	0.78	-0.21	13.65	0.296	0.642	0.456	1.394	-0.096	-0.020	0.026
2.500	13.79	0.66	-0.25	13.81	0.322	0.627	0.413	1.362	-0.129	-0.019	-0.004
3.100	14.58	0.38	-0.25	14.59	0.493	0.564	0.368	1.425	-0.216	-0.025	0.001
3.500	15.30	0.27	-0.26	15.30	0.541	0.474	0.306	1.321	-0.235	0.011	-0.002
4.000	16.07	0.18	-0.15	16.07	0.265	0.262	0.163	0.690	-0.113	0.035	0.004
5.000	16.43	0.16	0.07	16.43	0.016	0.020	0.013	0.050	0.000	0.002	-0.001
6.100	16.39	0.16	0.15	16.39	0.007	0.005	0.003	0.016	0.001	0.001	0.001

NON-DIMENSIONAL PROFILES

Y/DELM	U/RF	V/RF	W/RF	GAMA	BETA	UP/RF	VP/RF	WP/RF	Q/RF	UV/RF2	UW/RF2	VW/RF2
0.101	0.816	0.042	-0.018	3.0	-1.2	0.045	0.068	0.073	0.110	-0.10D-02	0.66D-03	-0.76D-03
0.138	0.834	0.068	-0.001	4.6	-0.0	0.043	0.066	0.080	0.112	-0.74D-03	0.41D-03	-0.77D-03
0.241	0.802	0.099	0.007	7.1	0.5	0.049	0.082	0.081	0.125	-0.10D-02	0.22D-03	0.37D-05
0.301	0.814	0.085	-0.030	6.0	-2.1	0.055	0.083	0.079	0.127	-0.18D-02	0.29D-03	-0.22D-03
0.361	0.870	0.087	-0.030	5.7	-2.0	0.051	0.073	0.080	0.120	-0.77D-03	0.64D-03	-0.82D-03
0.422	0.871	0.081	0.012	5.3	0.8	0.044	0.062	0.067	0.101	0.80D-03	0.34D-04	0.40D-05
0.554	0.832	0.048	-0.013	3.3	-0.9	0.033	0.049	0.041	0.072	-0.36D-03	-0.74D-04	0.97D-04
0.602	0.841	0.040	-0.015	2.7	-1.0	0.035	0.048	0.039	0.071	-0.48D-03	-0.71D-04	-0.15D-04
0.747	0.890	0.023	-0.015	1.5	-1.0	0.043	0.046	0.037	0.073	-0.80D-03	-0.93D-04	0.37D-05
0.843	0.933	0.016	-0.016	1.0	-1.0	0.045	0.042	0.034	0.070	-0.87D-03	0.41D-04	-0.74D-05
0.963	0.980	0.011	-0.009	0.6	-0.5	0.031	0.031	0.025	0.051	-0.42D-03	0.13D-03	0.15D-04
1.204	1.002	0.010	0.004	0.6	0.2	0.008	0.009	0.007	0.014	0.00D 00	0.74D-05	-0.37D-05
1.469	1.000	0.010	0.009	0.6	0.5	0.005	0.004	0.003	0.008	0.37D-05	0.37D-05	0.37D-05

Y/DELM	L/DELM	UV/Q2	UV/(UP*VP)
0.101	0.060	-0.083	-0.324
0.138	0.163	-0.059	-0.260
0.241	0.145	-0.066	-0.257
0.301	0.059	-0.113	-0.398
0.361	0.047	-0.054	-0.205
0.422	0.099	0.077	0.288
0.554	0.877	-0.069	-0.220
0.602	0.080	-0.095	-0.287
0.747	0.068	-0.152	-0.410
0.843	0.064	-0.178	-0.464
0.963	0.072	-0.164	-0.429
1.204	0.000	0.000	0.000
1.469	******	0.063	0.169

M=0.9 RECOVERY REGION, 27 DIAM DOWNSTREAM, X=214 CM AND Z/P=+0.5

RUN 3237601 TF= 20.00 C PR= 760.00 MM-HG DELM= 4.986 CM DELM1= 0.748 CM DELM2= 0.583 CM

DIMENSIONAL PROFILES

Y (CM)	U (M/S)	V (M/S)	W (M/S)	R (M/S)	UP2 (M2/S2)	VP2 (M2/S2)	WP2 (M2/S2)	Q2 (M2/S2)	UV (M2/S2)	UW (M2/S2)	VW (M2/S2)
0.419	11.68	0.83	0.18	11.71	0.736	1.058	0.854	2.649	-0.243	0.082	0.114
0.575	12.26	0.85	0.35	12.29	0.662	0.835	0.791	2.289	-0.199	0.105	0.107
1.000	13.35	1.08	0.66	13.41	0.387	0.414	0.598	1.399	-0.098	0.056	0.087
1.250	13.68	1.11	0.74	13.75	0.277	0.326	0.461	1.064	-0.074	0.019	0.079
1.500	13.92	1.09	0.76	13.98	0.217	0.291	0.364	0.872	-0.056	0.002	0.066
1.750	14.08	1.05	0.76	14.14	0.189	0.277	0.309	0.775	-0.047	-0.012	0.061
2.300	14.38	0.97	0.76	14.43	0.200	0.266	0.285	0.751	-0.050	-0.029	0.050
2.500	14.50	0.94	0.76	14.55	0.224	0.267	0.296	0.787	-0.061	-0.032	0.047
3.100	14.95	0.93	0.78	15.00	0.341	0.279	0.348	0.968	-0.106	-0.029	0.040
3.500	15.34	0.92	0.82	15.39	0.392	0.284	0.357	1.033	-0.124	-0.016	0.043
4.000	15.89	0.94	0.89	15.94	0.384	0.251	0.314	0.950	-0.120	0.004	0.047
5.000	16.70	1.00	1.12	16.77	0.134	0.094	0.103	0.331	-0.032	0.020	0.021
6.100	16.86	1.03	1.27	16.94	0.015	0.016	0.013	0.044	0.000	0.003	0.004

NON-DIMENSIONAL PROFILES

Y/DELM	U/RF	V/RF	W/RF	GAMA	BETA	UP/RF	VP/RF	WP/RF	Q/RF	UV/RF2	UW/RF2	VW/RF2
0.084	0.689	0.049	0.011	4.1	0.9	0.051	0.061	0.055	0.096	-0.85D-03	0.29D-03	0.40D-03
0.115	0.724	0.050	0.021	4.0	1.6	0.048	0.054	0.053	0.089	-0.69D-03	0.37D-03	0.37D-03
0.201	0.788	0.064	0.039	4.6	2.8	0.037	0.038	0.046	0.070	-0.34D-03	0.20D-03	0.30D-03
0.251	0.808	0.066	0.044	4.6	3.1	0.031	0.034	0.040	0.061	-0.26D-03	0.66D-04	0.28D-03
0.301	0.822	0.064	0.045	4.5	3.1	0.027	0.032	0.036	0.055	-0.20D-03	0.70D-05	0.24D-03
0.351	0.831	0.062	0.045	4.3	3.1	0.026	0.031	0.033	0.052	-0.16D-03	-0.42D-04	0.21D-03
0.461	0.849	0.057	0.045	3.9	3.0	0.026	0.030	0.032	0.051	-0.17D-03	-0.10D-03	0.17D-03
0.501	0.856	0.055	0.045	3.7	3.0	0.028	0.031	0.032	0.052	-0.21D-03	-0.11D-03	0.16D-03
0.622	0.883	0.055	0.046	3.6	3.0	0.034	0.031	0.035	0.058	-0.37D-03	-0.10D-03	0.14D-03
0.702	0.906	0.054	0.048	3.4	3.1	0.037	0.031	0.035	0.060	-0.43D-03	-0.56D-04	0.15D-03
0.802	0.938	0.055	0.053	3.4	3.2	0.037	0.030	0.033	0.058	-0.42D-03	0.14D-04	0.16D-03
1.003	0.986	0.059	0.066	3.4	3.8	0.022	0.018	0.019	0.034	-0.11D-03	0.70D-04	0.73D-04
1.223	0.995	0.061	0.075	3.5	4.3	0.007	0.007	0.007	0.012	0.00D 00	0.10D-04	0.14D-04

Y/DELM	L/DELM	UV/Q2	UV/(UP*VP)
0.084	0.029	-0.092	-0.275
0.115	0.028	-0.087	-0.268
0.201	0.034	-0.070	-0.245
0.251	0.048	-0.070	-0.246
0.301	0.063	-0.064	-0.223
0.351	0.075	-0.061	-0.205
0.461	0.080	-0.067	-0.217
0.501	0.079	-0.078	-0.249
0.622	0.074	-0.110	-0.344
0.702	0.067	-0.120	-0.372
0.802	0.065	-0.126	-0.387
1.003	0.077	-0.097	-0.285
1.223	0.000	0.000	0.000

M=0.9 RECOVERY REGION, 67 DIAM DOWNSTREAM, X=256 CM AND Z/P=+0.5

RUN 3237604 TF= 20.00 C PR= 760.00 MM-HG DELM= 5.685 CM DELM1= 0.818 CM DELM2= 0.627 CM

DIMENSIONAL PROFILES

Y (CM)	U (M/S)	V (M/S)	W (M/S)	R (M/S)	UP2 (M2/S2)	VP2 (M2/S2)	WP2 (M2/S2)	Q2 (M2/S2)	UV (M2/S2)	UW (M2/S2)	VW (M2/S2)
0.419	11.18	0.28	0.33	11.19	0.985	0.990	0.736	2.711	-0.281	0.167	0.156
0.500	11.44	0.25	0.37	11.45	0.942	0.919	0.703	2.564	-0.270	0.161	0.148
0.625	11.94	0.27	0.47	11.95	0.883	0.766	0.650	2.300	-0.248	0.159	0.133
0.750	12.35	0.29	0.54	12.36	0.787	0.662	0.603	2.052	-0.232	0.131	0.119
1.000	12.97	0.32	0.63	12.99	0.612	0.489	0.505	1.607	-0.174	0.085	0.107
1.250	13.51	0.33	0.70	13.53	0.471	0.367	0.400	1.239	-0.134	0.049	0.082
1.500	13.90	0.32	0.77	13.93	0.361	0.286	0.319	0.967	-0.103	0.024	0.065
1.850	14.33	0.33	0.83	14.36	0.271	0.223	0.251	0.745	-0.083	-0.001	0.047
2.400	14.78	0.31	0.88	14.81	0.238	0.204	0.232	0.675	-0.078	-0.011	0.037
3.000	15.21	0.31	0.91	15.24	0.259	0.223	0.262	0.744	-0.090	-0.004	0.038
3.750	15.75	0.30	0.96	15.78	0.286	0.242	0.288	0.817	-0.105	0.005	0.040
4.500	16.27	0.33	1.05	16.31	0.265	0.217	0.246	0.728	-0.097	0.016	0.039
6.100	17.08	0.38	1.34	17.14	0.034	0.047	0.032	0.114	-0.011	0.004	0.009

NON-DIMENSIONAL PROFILES

Y/DELM	U/RF	V/RF	W/RF	GAMA	BETA	UP/RF	VP/RF	WP/RF	Q/RF	UV/RF2	UW/RF2	VW/RF2
0.074	0.652	0.016	0.019	1.4	1.7	0.058	0.058	0.050	0.096	-0.96D-03	0.57D-03	0.53D-03
0.088	0.667	0.015	0.022	1.3	1.9	0.057	0.056	0.049	0.093	-0.92D-03	0.55D-03	0.50D-03
0.110	0.697	0.016	0.027	1.3	2.3	0.055	0.051	0.047	0.088	-0.84D-03	0.54D-03	0.45D-03
0.132	0.721	0.017	0.032	1.3	2.5	0.052	0.047	0.045	0.084	-0.79D-03	0.45D-03	0.41D-03
0.176	0.757	0.019	0.037	1.4	2.8	0.046	0.041	0.041	0.074	-0.59D-03	0.29D-03	0.36D-03
0.220	0.788	0.019	0.041	1.4	3.0	0.040	0.035	0.037	0.065	-0.46D-03	0.17D-03	0.28D-03
0.264	0.811	0.019	0.045	1.3	3.2	0.035	0.031	0.033	0.057	-0.35D-03	0.82D-04	0.22D-03
0.325	0.836	0.019	0.048	1.3	3.3	0.030	0.028	0.029	0.050	-0.28D-03	-0.34D-05	0.16D-03
0.422	0.862	0.018	0.051	1.2	3.4	0.028	0.026	0.028	0.048	-0.27D-03	-0.37D-04	0.13D-03
0.528	0.887	0.018	0.053	1.2	3.4	0.030	0.028	0.030	0.050	-0.31D-03	-0.14D-04	0.13D-03
0.660	0.919	0.018	0.056	1.1	3.5	0.031	0.029	0.031	0.053	-0.36D-03	0.17D-04	0.14D-03
0.792	0.949	0.019	0.061	1.2	3.7	0.030	0.027	0.029	0.050	-0.33D-03	0.54D-04	0.13D-03
1.073	0.996	0.022	0.078	1.3	4.5	0.011	0.013	0.010	0.020	-0.37D-04	0.14D-04	0.31D-04

Y/DELM	L/DELM	UV/Q2	UV/(UP*VP)
0.074	0.026	-0.104	-0.285
0.088	0.025	-0.105	-0.290
0.110	0.025	-0.108	-0.302
0.132	0.028	-0.113	-0.321
0.176	0.032	-0.108	-0.318
0.220	0.035	-0.108	-0.322
0.264	0.040	-0.107	-0.321
0.325	0.050	-0.111	-0.338
0.422	0.068	-0.116	-0.354
0.528	0.074	-0.121	-0.374
0.660	0.079	-0.129	-0.399
0.792	0.087	-0.133	-0.405
1.073	******	-0.096	-0.275

M=0.9 RECOVERY REGION, 67 DIAM DOWNSTREAM, X=256 CM AND Z/P= 0.0

RUN 3237602 TF= 20.00 C PR= 760.00 MM-HG DELM= 5.585 CM DELM1= 0.814 CM DELM2= 0.622 CM

DIMENSIONAL PROFILES

Y (CM)	U (M/S)	V (M/S)	W (M/S)	R (M/S)	UP2 (M2/S2)	VP2 (M2/S2)	WP2 (M2/S2)	Q2 (M2/S2)	UV (M2/S2)	UW (M2/S2)	VW (M2/S2)
0.419	11.10	0.43	0.29	11.11	0.910	1.001	0.762	2.673	-0.263	0.160	0.162
0.500	11.39	0.41	0.36	11.40	0.890	0.916	0.733	2.539	-0.256	0.154	0.160
0.625	11.84	0.44	0.45	11.86	0.827	0.781	0.688	2.296	-0.226	0.156	0.142
0.750	12.28	0.48	0.53	12.30	0.763	0.646	0.645	2.054	-0.196	0.158	0.125
1.000	12.87	0.55	0.64	12.90	0.595	0.485	0.568	1.648	-0.143	0.122	0.106
1.250	13.35	0.60	0.72	13.38	0.441	0.363	0.472	1.276	-0.097	0.075	0.084
1.500	13.69	0.63	0.76	13.73	0.354	0.292	0.393	1.040	-0.083	0.038	0.074
1.850	14.08	0.65	0.78	14.11	0.273	0.232	0.299	0.804	-0.070	-0.004	0.055
2.400	14.56	0.64	0.80	14.60	0.286	0.232	0.275	0.793	-0.091	-0.029	0.044
3.000	15.05	0.63	0.85	15.08	0.312	0.241	0.288	0.841	-0.108	-0.033	0.037
3.750	15.62	0.62	0.94	15.66	0.317	0.238	0.289	0.844	-0.109	-0.023	0.033
4.500	16.17	0.63	1.06	16.22	0.265	0.197	0.223	0.685	-0.086	-0.008	0.029
6.100	16.90	0.64	1.26	16.96	0.078	0.073	0.058	0.209	-0.023	0.009	0.015

NON-DIMENSIONAL PROFILES

Y/DELM	U/RF	V/RF	W/RF	GAMA	BETA	UP/RF	VP/RF	WP/RF	Q/RF	UV/RF2	UW/RF2	VW/RF2
0.075	0.654	0.025	0.017	2.2	1.5	0.056	0.059	0.051	0.096	-0.91D-03	0.56D-03	0.56D-03
0.090	0.672	0.024	0.021	2.1	1.8	0.056	0.056	0.050	0.094	-0.89D-03	0.54D-03	0.56D-03
0.112	0.698	0.026	0.027	2.1	2.2	0.054	0.052	0.049	0.089	-0.79D-03	0.54D-03	0.49D-03
0.134	0.724	0.028	0.031	2.2	2.5	0.052	0.047	0.047	0.085	-0.68D-03	0.55D-03	0.43D-03
0.179	0.759	0.032	0.038	2.4	2.8	0.045	0.041	0.044	0.076	-0.50D-03	0.42D-03	0.37D-03
0.224	0.787	0.035	0.042	2.6	3.1	0.039	0.036	0.041	0.067	-0.34D-03	0.26D-03	0.29D-03
0.269	0.807	0.037	0.045	2.6	3.2	0.035	0.032	0.037	0.060	-0.29D-03	0.13D-03	0.26D-03
0.331	0.830	0.038	0.046	2.6	3.2	0.031	0.028	0.032	0.053	-0.24D-03	-0.14D-04	0.19D-03
0.430	0.858	0.038	0.047	2.5	3.1	0.032	0.028	0.031	0.053	-0.32D-03	-0.10D-03	0.15D-03
0.537	0.887	0.037	0.050	2.4	3.2	0.033	0.029	0.032	0.054	-0.38D-03	-0.11D-03	0.13D-03
0.671	0.921	0.037	0.055	2.3	3.4	0.033	0.029	0.032	0.054	-0.38D-03	-0.80D-04	0.11D-03
0.806	0.953	0.037	0.063	2.2	3.8	0.030	0.026	0.028	0.049	-0.30D-03	-0.28D-04	0.10D-03
1.092	0.996	0.038	0.074	2.2	4.3	0.016	0.016	0.014	0.027	-0.80D-04	0.31D-04	0.45D-04

Y/DELM	L/DELM	UV/Q2	UV/(UP*VP)
0.075	0.026	-0.098	-0.276
0.090	0.025	-0.101	-0.284
0.112	0.025	-0.098	-0.281
0.134	0.026	-0.095	-0.279
0.179	0.031	-0.087	-0.266
0.224	0.035	-0.076	-0.242
0.269	0.042	-0.080	-0.258
0.331	0.048	-0.087	-0.278
0.430	0.066	-0.115	-0.353
0.537	0.075	-0.128	-0.394
0.671	0.078	-0.129	-0.397
0.806	0.081	-0.126	-0.376
1.092	******	-0.110	-0.305

M=0.9 RECOVERY REGION, 67 DIAM DOWNSTREAM, X=256 CM AND Z/P=-0.5

RUN 3237603 TF= 20.00 C PR= 760.00 MM-HG DELM= 5.543 CM DELM1= 0.761 CM DELM2= 0.591 CM

DIMENSIONAL PROFILES

Y (CM)	U (M/S)	V (M/S)	W (M/S)	R (M/S)	UP2 (M2/S2)	VP2 (M2/S2)	WP2 (M2/S2)	Q2 (M2/S2)	UV (M2/S2)	UW (M2/S2)	VW (M2/S2)
0.419	11.50	0.21	0.32	11.51	1.024	0.972	0.714	2.710	-0.262	0.200	0.165
0.500	11.78	0.18	0.37	11.79	0.995	0.878	0.687	2.560	-0.242	0.209	0.150
0.625	12.27	0.20	0.47	12.29	0.932	0.731	0.633	2.297	-0.229	0.211	0.135
0.750	12.66	0.22	0.54	12.67	0.803	0.615	0.593	2.012	-0.198	0.187	0.124
1.000	13.28	0.26	0.63	13.30	0.623	0.453	0.489	1.566	-0.149	0.137	0.105
1.250	13.75	0.27	0.71	13.77	0.454	0.341	0.389	1.185	-0.109	0.085	0.085
1.500	14.16	0.29	0.78	14.18	0.330	0.270	0.313	0.913	-0.086	0.047	0.070
1.850	14.51	0.30	0.84	14.54	0.245	0.217	0.253	0.715	-0.071	0.017	0.051
2.400	14.92	0.29	0.86	14.95	0.226	0.214	0.243	0.683	-0.075	0.004	0.046
3.000	15.30	0.28	0.88	15.33	0.262	0.237	0.272	0.771	-0.092	0.021	0.047
3.750	15.81	0.29	0.92	15.84	0.291	0.239	0.268	0.798	-0.096	0.037	0.046
4.500	16.36	0.29	0.98	16.39	0.270	0.230	0.247	0.748	-0.094	0.047	0.041
6.100	17.06	0.37	1.26	17.11	0.074	0.064	0.062	0.201	-0.012	0.024	0.007

NON-DIMENSIONAL PROFILES

Y/DELM	U/RF	V/RF	W/RF	GAMA	BETA	UP/RF	VP/RF	WP/RF	Q/RF	UV/RF2	UW/RF2	VW/RF2
0.076	0.672	0.012	0.019	1.0	1.6	0.059	0.058	0.049	0.096	-0.89D-03	0.68D-03	0.56D-03
0.090	0.688	0.011	0.022	0.9	1.8	0.058	0.055	0.048	0.094	-0.83D-03	0.71D-03	0.51D-03
0.113	0.717	0.012	0.027	0.9	2.2	0.056	0.050	0.046	0.089	-0.78D-03	0.72D-03	0.46D-03
0.135	0.740	0.013	0.032	1.0	2.4	0.052	0.046	0.045	0.083	-0.68D-03	0.64D-03	0.42D-03
0.180	0.776	0.015	0.037	1.1	2.7	0.046	0.039	0.041	0.073	-0.51D-03	0.47D-03	0.36D-03
0.226	0.804	0.016	0.041	1.1	3.0	0.039	0.034	0.036	0.064	-0.37D-03	0.29D-03	0.29D-03
0.271	0.828	0.017	0.046	1.2	3.2	0.034	0.030	0.033	0.056	-0.29D-03	0.16D-03	0.24D-03
0.334	0.848	0.018	0.049	1.2	3.3	0.029	0.027	0.029	0.049	-0.24D-03	0.58D-04	0.17D-03
0.433	0.872	0.017	0.050	1.1	3.3	0.028	0.027	0.029	0.048	-0.26D-03	0.14D-04	0.16D-03
0.541	0.894	0.016	0.051	1.0	3.3	0.030	0.028	0.030	0.051	-0.31D-03	0.72D-04	0.16D-03
0.677	0.924	0.017	0.054	1.1	3.3	0.032	0.029	0.030	0.052	-0.33D-03	0.13D-03	0.16D-03
0.812	0.956	0.017	0.057	1.0	3.4	0.030	0.028	0.029	0.051	-0.32D-03	0.16D-03	0.14D-03
1.101	0.997	0.022	0.074	1.2	4.2	0.016	0.015	0.015	0.026	-0.41D-04	0.82D-04	0.24D-04

Y/DELM	L/DELM	UV/Q2	UV/(UP*VP)
0.076	0.025	-0.097	-0.263
0.090	0.025	-0.095	-0.259
0.113	0.025	-0.100	-0.277
0.135	0.027	-0.098	-0.282
0.180	0.032	-0.095	-0.280
0.226	0.035	-0.092	-0.277
0.271	0.040	-0.094	-0.288
0.334	0.055	-0.099	-0.308
0.433	0.076	-0.110	-0.341
0.541	0.086	-0.119	-0.369
0.677	0.076	-0.120	-0.364
0.812	0.085	-0.126	-0.377
1.101	******	-0.060	-0.174

A.2. Spanwise-Averaged Profiles

This section contains the spanwise-averaged profiles of streamwise mean velocity component $(\overline{U})$, turbulent kinetic energy and streamwise turbulent shear stress component $(-\overline{u'v'})$ for blowing ratios $M = 0.4$ and 0.9. There is a pair of pages for each location. On the first page are the run numbers, spanwise positions, and profiles for which the spanwise averages were obtained. The dimensional and non-dimensional spanwise-averaged profiles are given on the second page.

M=0.4 BLOWING REGION AFTER 3 ROWS OF HOLES, X=148 CM

RUN(1): 12157602 RUN(2): 12157601 RUN(3): 12147604 RUN(4): 12157603 RUN(5): 12157604
Z/P(1): 0.5 Z/P(2): 0.3 Z/P(3): 0.0 Z/P(4): -0.3 Z/P(5): -0.5

Y (CM)	U(1) (M/S)	U(2) (M/S)	U(3) (M/S)	U(4) (M/S)	U(5) (M/S)
0.419	8.000	10.960	5.400	10.680	7.960
0.500	8.170	11.140	5.650	10.920	8.160
0.600	8.380	11.540	6.540	11.340	8.450
0.750	8.780	11.990	8.600	11.850	9.010
0.950	9.680	12.570	10.060	12.440	10.120
1.200	11.300	13.200	10.840	13.070	11.900
1.500	13.060	13.960	12.230	13.780	13.610
1.800	14.120	14.660	13.640	14.430	14.600
2.100	14.910	15.280	14.770	15.020	15.280
2.400	15.520	15.830	15.490	15.540	15.840
2.700	16.020	16.230	15.970	15.950	16.250
3.000	16.320	16.430	16.280	16.150	16.460
4.000	16.450	16.470	16.390	16.240	16.510

Y (CM)	UV(1) (M2/S2)	UV(2) (M2/S2)	UV(3) (M2/S2)	UV(4) (M2/S2)	UV(5) (M2/S2)
0.419	-0.354	-0.295	-0.655	-0.335	-0.371
0.500	-0.341	-0.298	-0.772	-0.306	-0.381
0.600	-0.397	-0.306	-0.916	-0.261	-0.477
0.750	-0.589	-0.324	-0.780	-0.248	-0.690
0.950	-0.824	-0.356	-0.258	-0.240	-0.923
1.200	-0.824	-0.332	-0.462	-0.243	-0.818
1.500	-0.458	-0.293	-0.591	-0.245	-0.387
1.800	-0.283	-0.239	-0.474	-0.217	-0.233
2.100	-0.202	-0.179	-0.242	-0.174	-0.163
2.400	-0.130	-0.116	-0.127	-0.118	-0.098
2.700	-0.068	-0.061	-0.055	-0.065	-0.047
3.000	-0.025	-0.021	-0.017	-0.025	-0.015
4.000	0.000	0.000	0.000	0.000	0.000

Y (CM)	Q2(1) (M2/S2)	Q2(2) (M2/S2)	Q2(3) (M2/S2)	Q2(4) (M2/S2)	Q2(5) (M2/S2)
0.419	3.363	2.757	5.295	2.532	3.777
0.500	3.400	2.694	5.667	2.445	3.788
0.600	3.624	2.626	5.825	2.344	4.041
0.750	4.186	2.596	4.804	2.300	4.698
0.950	5.034	2.538	2.223	2.218	5.421
1.200	4.943	2.266	2.813	2.047	4.761
1.500	3.015	1.920	3.383	1.775	2.556
1.800	1.896	1.534	2.806	1.484	1.610
2.100	1.345	1.147	1.668	1.143	1.117
2.400	0.913	0.743	0.961	0.778	0.721
2.700	0.517	0.398	0.512	0.436	0.372
3.000	0.227	0.164	0.210	0.190	0.146
4.000	0.019	0.020	0.019	0.018	0.017

SPANWISE AVERAGED PROFILES M=0.4 BLOWING REGION AFTER 3 ROWS OF HOLES, X=148 CM

AVERAGE UINF = 16.41 M/S

DIMENSIONAL PROFILES

Y(CM)	U(M/S)	UDERV(1/S)	Q2(M2/S2)	UV(M2/S2)
0.419	8.634	0.2800 03	3.316	-0.432
0.500	8.853	0.3980 03	3.399	-0.463
0.600	9.393	0.6150 03	3.429	-0.512
0.750	10.382	0.6030 03	3.352	-0.502
0.950	11.318	0.3810 03	2.735	-0.378
1.200	12.169	0.3450 03	2.758	-0.430
1.500	13.277	0.3580 03	2.454	-0.397
1.800	14.246	0.2940 03	1.948	-0.312
2.100	15.042	0.2030 03	1.324	-0.199
2.400	15.646	0.1740 03	0.833	-0.120
2.700	16.084	0.1130 03	0.452	-0.060
3.000	16.328	0.5570 02	0.189	-0.021
4.000	16.412	0.1000-07	0.019	0.000

DELM= 2.872 CM DELM1= 0.684 CM DELM2= 0.428 CM

NON-DIMENSIONAL PROFILES

Y/DELM	U/UE	Q/UE	UV/UE2	L/DELM	UV/Q2
0.146	0.526	0.111	-0.16D-02	0.082	-0.130
0.174	0.539	0.112	-0.17D-02	0.060	-0.138
0.209	0.572	0.113	-0.19D-02	0.040	-0.149
0.261	0.633	0.112	-0.19D-02	0.041	-0.150
0.331	0.690	0.101	-0.14D-02	0.056	-0.138
0.418	0.741	0.101	-0.16D-02	0.066	-0.156
0.522	0.809	0.095	-0.15D-02	0.061	-0.162
0.627	0.868	0.085	-0.12D-02	0.056	-0.160
0.731	0.917	0.070	-0.74D-03	0.067	-0.150
0.836	0.953	0.056	-0.44D-03	0.069	-0.144
0.940	0.980	0.041	-0.22D-03	0.075	-0.132
1.044	0.995	0.026	-0.76D-04	0.090	-0.109
1.393	1.000	0.008	0.00D 00	0.000	0.000

M=0.4 BLOWING REGION AFTER 7 ROWS OF HOLES, X=168 CM

RUN(1): 12147601 RUN(2): 12137606 RUN(3): 12147602
Z/P(1): 0.5 Z/P(2): 0.0 Z/P(3): -0.5

Y (CM)	U(1) (M/S)	U(2) (M/S)	U(3) (M/S)
0.419	7.820	5.060	7.750
0.575	8.070	5.850	7.980
1.000	8.430	9.120	8.380
1.250	9.230	5.480	9.250
1.500	10.260	9.940	10.330
1.750	11.190	10.630	11.390
2.300	13.190	12.590	13.490
2.500	13.940	13.260	14.180
3.100	15.560	15.100	15.660
3.500	16.210	15.850	16.160
4.000	16.530	16.240	16.370
5.000	16.540	16.240	16.380
6.100	16.510	16.170	16.360

Y (CM)	UV(1) (M2/S2)	UV(2) (M2/S2)	UV(3) (M2/S2)
0.419	-0.400	-0.747	-0.314
0.575	-0.366	-0.881	-0.274
1.000	-0.603	-0.280	-0.555
1.250	-0.722	-0.357	-0.739
1.500	-0.734	-0.473	-0.787
1.750	-0.692	-0.609	-0.716
2.300	-0.619	-0.641	-0.554
2.500	-0.505	-0.570	-0.433
3.100	-0.183	-0.268	-0.131
3.500	-0.063	-0.093	-0.040
4.000	-0.011	-0.011	-0.005
5.000	0.000	0.000	0.000
6.100	0.000	0.000	0.000

Y (CM)	Q2(1) (M2/S2)	Q2(2) (M2/S2)	Q2(3) (M2/S2)
0.419	4.113	5.485	3.626
0.575	4.073	5.886	3.603
1.000	4.802	2.747	4.499
1.250	5.144	3.149	4.993
1.500	4.940	3.587	4.809
1.750	4.472	4.052	4.389
2.300	3.762	3.897	3.349
2.500	3.164	3.470	2.660
3.100	1.316	1.760	0.912
3.500	0.524	0.725	0.345
4.000	0.125	0.145	0.081
5.000	0.021	0.021	0.019
6.100	0.014	0.012	0.012

SPANWISE AVERAGED PROFILES M=0.4 BLOWING REGION AFTER 7 ROWS OF HOLES, X=168 CM

AVERAGE UINF = 16.35 M/S

DIMENSIONAL PROFILES

Y(CM)	U(M/S)	UDERV(1/S)	Q2(M2/S2)	UV(M2/S2)
0.419	6.342	0.331D 03	4.564	-0.565
0.575	6.879	0.405D 03	4.777	-0.619
1.000	8.818	0.334D 03	3.589	-0.420
1.250	9.400	0.238D 03	4.025	-0.531
1.500	10.138	0.319D 03	4.194	-0.607
1.750	10.972	0.351D 03	4.233	-0.653
2.300	12.980	0.399D 03	3.733	-0.616
2.500	13.676	0.337D 03	3.202	-0.523
3.100	15.387	0.220D 03	1.455	-0.216
3.500	16.058	0.117D 03	0.589	-0.074
4.000	16.391	0.302D 02	0.125	-0.010
5.000	16.396	-0.104D 02	0.021	0.000
6.100	16.347	0.100D-07	0.012	0.000

DELM= 3.613 CM DELM1= 1.149 CM DELM2= 0.620 CM

NON-DIMENSIONAL PROFILES

Y/DELM	U/UF	Q/UF	UV/UF2	L/DELM	UV/Q2
0.116	0.388	0.131	-0.21D-02	0.063	-0.124
0.159	0.421	0.134	-0.23D-02	0.054	-0.130
0.277	0.539	0.116	-0.16D-02	0.054	-0.117
0.346	0.575	0.123	-0.20D-02	0.085	-0.132
0.415	0.620	0.125	-0.23D-02	0.068	-0.145
0.484	0.671	0.126	-0.24D-02	0.064	-0.154
0.637	0.794	0.118	-0.23D-02	0.061	-0.165
0.692	0.837	0.109	-0.20D-02	0.059	-0.163
0.858	0.941	0.074	-0.81D-03	0.059	-0.149
0.969	0.982	0.047	-0.28D-03	0.064	-0.125
1.107	1.003	0.022	-0.36D-04	0.090	-0.077
1.384	1.003	0.009	0.00D 00	0.000	0.000
1.688	1.000	0.007	0.00D 00	0.000	0.000

M=0.4 START OF RECOVERY AFTER 11 ROWS OF HOLES, X=188 CM

RUN(1): 12137605 RUN(2): 12137604 RUN(3): 12137603 RUN(4): 12177601 RUN(5): 12177602
Z/P(1): 0.5 Z/P(2): 0.3 Z/P(3): 0.0 Z/P(4): -0.3 Z/P(5): -0.5

Y (CM)	U(1) (M/S)	U(2) (M/S)	U(3) (M/S)	U(4) (M/S)	U(5) (M/S)
0.419	8.590	10.690	6.510	10.400	8.350
0.575	8.550	10.800	8.850	10.590	8.330
1.000	8.970	10.990	9.440	10.800	8.640
1.250	9.760	11.250	9.660	11.030	9.440
1.500	10.480	11.580	10.020	11.340	10.140
1.750	11.000	11.970	10.530	11.710	10.700
2.300	12.300	13.010	11.850	12.750	12.180
2.500	12.810	13.400	12.340	13.130	12.710
3.100	14.330	14.640	13.840	14.320	14.250
3.500	15.210	15.390	14.860	15.070	15.110
4.000	16.040	16.130	15.860	15.800	15.870
5.000	16.560	16.480	16.600	16.300	16.220
6.100	16.490	16.400	16.540	16.260	16.170

Y (CM)	UV(1) (M2/S2)	UV(2) (M2/S2)	UV(3) (M2/S2)	UV(4) (M2/S2)	UV(5) (M2/S2)
0.419	-0.223	-0.138	-0.474	-0.112	-0.307
0.575	-0.238	-0.150	-0.364	-0.097	-0.337
1.000	-0.588	-0.295	-0.303	-0.224	-0.590
1.250	-0.564	-0.383	-0.351	-0.317	-0.545
1.500	-0.444	-0.467	-0.461	-0.389	-0.483
1.750	-0.513	-0.501	-0.531	-0.436	-0.538
2.300	-0.627	-0.516	-0.590	-0.451	-0.659
2.500	-0.624	-0.511	-0.621	-0.439	-0.607
3.100	-0.469	-0.373	-0.577	-0.350	-0.405
3.500	-0.335	-0.264	-0.450	-0.263	-0.267
4.000	-0.143	-0.115	-0.222	-0.130	-0.099
5.000	-0.004	-0.003	-0.005	-0.004	-0.002
6.100	0.000	0.000	0.000	0.000	0.000

Y (CM)	Q2(1) (M2/S2)	Q2(2) (M2/S2)	Q2(3) (M2/S2)	Q2(4) (M2/S2)	Q2(5) (M2/S2)
0.419	3.235	2.212	4.573	2.031	3.191
0.575	3.384	2.387	3.652	2.216	3.407
1.000	4.172	3.013	2.893	2.930	4.180
1.250	3.909	3.300	3.243	3.269	3.925
1.500	3.468	3.520	3.590	3.428	3.577
1.750	3.627	3.620	3.876	3.564	3.762
2.300	3.953	3.541	3.933	3.461	4.081
2.500	3.879	3.382	3.906	3.297	3.814
3.100	2.896	2.541	3.426	2.483	2.659
3.500	2.058	1.770	2.627	1.771	1.735
4.000	0.955	0.789	1.411	0.866	0.719
5.000	0.079	0.083	0.104	0.085	0.064
6.100	0.023	0.021	0.022	0.021	0.021

SPANWISE AVERAGED PROFILES M=0.4 START OF RECOVERY AFTER 11 ROWS OF HOLES, X=188 CM

AVERAGE UINF = 16.37 M/S

DIMENSIONAL PROFILES

Y(CM)	U(M/S)	UDERV(1/S)	Q2(M2/S2)	UV(M2/S2)
0.419	8.908	0.560D 03	2.861	-0.260
0.575	9.726	0.371D 03	2.847	-0.227
1.000	10.076	0.482D 02	3.119	-0.327
1.250	10.402	0.158D 03	3.367	-0.383
1.500	10.797	0.167D 03	3.516	-0.444
1.750	11.244	0.193D 03	3.693	-0.498
2.300	12.429	0.222D 03	3.715	-0.544
2.500	12.868	0.222D 03	3.594	-0.545
3.100	14.223	0.224D 03	2.838	-0.444
3.500	15.078	0.198D 03	2.060	-0.330
4.000	15.906	0.124D 03	1.014	-0.154
5.000	16.432	0.791D 01	0.088	-0.004
6.100	16.372	0.1000-07	0.021	0.000

DELM= 4.284 CM DELM1= 1.091 CM DELM2= 0.709 CM

NON-DIMENSIONAL PROFILES

Y/DELM	U/UF	Q/UF	UV/UF2	L/DELM	UV/Q2
0.098	0.544	0.103	-0.97D-03	0.021	-0.091
0.134	0.594	0.103	-0.85D-03	0.030	-0.080
0.233	0.615	0.108	-0.12D-02	0.277	-0.105
0.292	0.635	0.112	-0.14D-02	0.091	-0.114
0.350	0.660	0.115	-0.17D-02	0.093	-0.126
0.408	0.687	0.117	-0.19D-02	0.085	-0.135
0.537	0.759	0.118	-0.20D-02	0.078	-0.146
0.584	0.786	0.116	-0.20D-02	0.078	-0.152
0.724	0.869	0.103	-0.17D-02	0.070	-0.157
0.817	0.921	0.088	-0.12D-02	0.068	-0.160
0.934	0.972	0.062	-0.58D-03	0.074	-0.152
1.167	1.004	0.018	-0.15D-04	0.184	-0.044
1.424	1.000	0.009	0.00D 00	0.000	0.000

M=0.9 BLOWING REGION AFTER 7 ROWS OF HOLES, X=168 CM

RUN(1): 3237607 RUN(2): 3237605 RUN(3): 3237606
Z/P(1): 0.5 Z/P(2): 0.0 Z/P(3): -0.5

Y (CM)	U(1) (M/S)	U(2) (M/S)	U(3) (M/S)
0.419	12.270	9.350	12.890
0.575	12.710	12.300	13.380
1.000	12.390	14.240	13.330
1.250	12.520	13.560	13.190
1.500	13.490	13.670	13.920
1.750	13.950	13.780	14.630
2.300	14.060	14.620	14.420
2.500	14.560	14.770	14.900
3.100	15.880	15.580	16.300
3.500	16.480	16.320	16.750
4.000	16.780	16.860	16.880
5.000	16.820	16.570	16.840
6.100	16.820	16.990	16.810

Y (CM)	UV(1) (M2/S2)	UV(2) (M2/S2)	UV(3) (M2/S2)
0.419	-0.300	-1.309	-0.438
0.575	-0.307	-1.644	-0.384
1.000	-0.246	0.046	-0.311
1.250	-0.463	-0.166	-0.474
1.500	-0.374	-0.105	-0.577
1.750	0.070	-0.160	-0.024
2.300	-0.260	-0.112	-0.282
2.500	-0.278	-0.106	-0.306
3.100	-0.170	-0.206	-0.147
3.500	-0.066	-0.148	-0.038
4.000	-0.010	-0.049	-0.002
5.000	0.000	-0.001	0.001
6.100	0.001	0.001	0.001

Y (CM)	Q2(1) (M2/S2)	Q2(2) (M2/S2)	Q2(3) (M2/S2)
0.419	4.070	14.161	4.193
0.575	3.355	12.080	4.086
1.000	3.977	7.242	4.971
1.250	4.118	2.780	5.132
1.500	3.680	2.029	4.906
1.750	2.738	1.986	4.208
2.300	1.764	1.426	2.189
2.500	1.673	1.240	1.866
3.100	1.114	1.164	0.956
3.500	0.507	0.828	0.312
4.000	0.127	0.302	0.067
5.000	0.021	0.030	0.018
6.100	0.013	0.014	0.012

SPANWISE AVERAGED PROFILES M=0.9 BLOWING REGION AFTER 7 ROWS OF HOLES, X=168 CM

AVERAGE UINF = 16.87 M/S

DIMENSIONAL PROFILES

Y(CM)	U(M/S)	UDERV(1/S)	Q2(M2/S2)	UV(M2/S2)
0.419	10.844	0.122D 04	8.713	-0.870
0.575	12.624	0.885D 03	8.039	-1.038
1.000	13.565	-0.170D 03	6.021	-0.105
1.250	13.202	0.165D 02	3.627	-0.307
1.500	13.658	0.204D 03	3.097	-0.278
1.750	13.991	0.894D 02	2.706	-0.075
2.300	14.412	0.124D 03	1.682	-0.186
2.500	14.721	0.169D 03	1.489	-0.193
3.100	15.787	0.178D 03	1.102	-0.184
3.500	16.425	0.126D 03	0.629	-0.103
4.000	16.812	0.396D 02	0.206	-0.029
5.000	16.870	-0.646D 01	0.025	-0.000
6.100	16.873	0.100D-07	0.013	0.001

DELM= 3.790 CM DELM1= 0.669 CM DELM2= 0.498 CM

NON-DIMENSIONAL PROFILES

Y/DELM	U/UF	Q/UF	UV/UF2	L/DELM	UV/Q2
0.111	0.643	0.175	-0.31D-02	0.020	-0.100
0.152	0.748	0.168	-0.36D-02	0.030	-0.129
0.264	0.804	0.145	-0.37D-03	0.050	-0.018
0.330	0.782	0.113	-0.11D-02	0.884	-0.085
0.396	0.809	0.104	-0.98D-03	0.068	-0.090
0.462	0.829	0.097	-0.26D-03	0.081	-0.028
0.607	0.854	0.077	-0.65D-03	0.092	-0.111
0.660	0.872	0.072	-0.68D-03	0.069	-0.130
0.818	0.936	0.062	-0.65D-03	0.063	-0.167
0.924	0.973	0.047	-0.36D-03	0.067	-0.164
1.055	0.996	0.027	-0.10D-03	0.113	-0.141
1.319	1.000	0.009	-0.11D-05	0.071	-0.012
1.610	1.000	0.007	0.35D-05	******	0.075

M=0.9 START OF RECOVERY AFTER 11 ROWS OF HOLES, X=188 CM

RUN(1): 3177605 RUN(2): 3177604 RUN(3): 3177601 RUN(4): 3177602 RUN(5): 3177603
Z/P(1): 0.5 Z/P(2): 0.3 Z/P(3): 0.0 Z/P(4): -0.3 Z/P(5): -0.5

Y (CM)	U(1) (M/S)	U(2) (M/S)	U(3) (M/S)	U(4) (M/S)	U(5) (M/S)
0.419	13.390	14.190	10.180	14.610	13.380
0.575	13.710	14.190	13.610	14.660	13.670
1.000	13.090	14.050	14.650	14.580	13.150
1.250	13.120	14.020	13.870	14.550	13.340
1.500	14.010	14.020	13.930	14.530	14.260
1.750	14.230	14.070	13.880	14.510	14.280
2.300	13.630	14.340	14.150	14.610	13.630
2.500	13.770	14.490	14.140	14.720	13.790
3.100	14.420	15.040	14.630	15.320	14.580
3.500	15.120	15.460	15.100	15.840	15.300
4.000	15.910	15.920	15.780	16.350	16.070
5.000	16.540	16.400	16.750	16.580	16.430
6.100	16.520	16.400	16.770	16.560	16.390

Y (CM)	UV(1) (M2/S2)	UV(2) (M2/S2)	UV(3) (M2/S2)	UV(4) (M2/S2)	UV(5) (M2/S2)
0.419	-0.272	-0.001	-1.635	0.011	-0.269
0.575	-0.211	-0.005	-1.574	0.017	-0.200
1.000	-0.219	-0.032	0.309	0.015	-0.279
1.250	-0.449	-0.039	-0.142	0.004	-0.491
1.500	-0.270	-0.067	-0.069	-0.019	-0.208
1.750	0.181	-0.099	-0.099	-0.054	0.214
2.300	-0.070	-0.142	0.007	-0.142	-0.096
2.500	-0.094	-0.150	-0.039	-0.167	-0.129
3.100	-0.201	-0.153	-0.158	-0.181	-0.216
3.500	-0.219	-0.121	-0.173	-0.128	-0.235
4.000	-0.121	-0.067	-0.169	-0.058	-0.113
5.000	-0.003	-0.004	-0.020	-0.002	0.000
6.100	0.001	0.001	0.001	0.001	0.001

Y (CM)	Q2(1) (M2/S2)	Q2(2) (M2/S2)	Q2(3) (M2/S2)	Q2(4) (M2/S2)	Q2(5) (M2/S2)
0.419	3.350	0.652	15.727	0.681	3.232
0.575	3.651	0.712	12.838	0.713	3.379
1.000	4.530	1.120	6.275	1.104	4.221
1.250	4.329	1.309	2.467	1.306	4.348
1.500	3.897	1.460	2.048	1.460	3.861
1.750	2.816	1.538	1.989	1.554	2.763
2.300	1.363	1.488	1.593	1.569	1.394
2.500	1.312	1.446	1.442	1.531	1.362
3.100	1.419	1.241	1.255	1.395	1.425
3.500	1.340	1.013	1.174	1.063	1.321
4.000	0.797	0.628	0.985	0.525	0.690
5.000	0.066	0.077	0.151	0.052	0.050
6.100	0.019	0.018	0.020	0.018	0.016

SPANWISE AVERAGED PROFILES M=0.9 START OF RECOVERY AFTER 11 ROWS OF HOLES, X=188 CM

AVERAGE UINF = 16.53 M/S

DIMENSIONAL PROFILES

Y(CM)	U(M/S)	UDERV(1/S)	Q2(M2/S2)	UV(M2/S2)
0.419	12.862	0.785D 03	4.889	-0.567
0.575	14.012	0.520D 03	4.891	-0.536
1.000	14.192	-0.156D 03	3.291	0.055
1.250	13.947	-0.476D 01	2.140	-0.131
1.500	14.108	0.518D 02	2.037	-0.083
1.750	14.119	-0.605D 01	1.888	-0.039
2.300	14.200	0.345D 02	1.526	-0.085
2.500	14.288	0.581D 02	1.450	-0.112
3.100	14.858	0.121D 03	1.315	-0.171
3.500	15.366	0.149D 03	1.127	-0.157
4.000	15.960	0.101D 03	0.731	-0.106
5.000	16.532	0.210D 02	0.091	-0.008
6.100	16.528	0.1000-07	0.019	0.001

DELM= 4.526 CM DELM1= 0.584 CM DELM2= 0.479 CM

NON-DIMENSIONAL PROFILES

Y/DELM	U/UF	Q/UF	UV/UF2	L/DELM	UV/Q2
0.093	0.778	0.134	-0.21D-02	0.021	-0.116
0.127	0.848	0.134	-0.20D-02	0.031	-0.110
0.221	0.859	0.110	0.20D-03	0.033	0.017
0.276	0.844	0.089	-0.48D-03	1.679	-0.061
0.331	0.854	0.086	-0.30D-03	0.123	-0.041
0.387	0.854	0.083	-0.14D-03	0.725	-0.021
0.508	0.859	0.075	-0.31D-03	0.186	-0.055
0.552	0.864	0.073	-0.41D-03	0.128	-0.078
0.685	0.899	0.069	-0.63D-03	0.076	-0.130
0.773	0.930	0.064	-0.57D-03	0.068	-0.139
0.884	0.966	0.052	-0.39D-03	0.071	-0.144
1.105	1.000	0.018	-0.30D-04	0.096	-0.090
1.348	1.000	0.008	0.37D-05	******	0.054

APPENDIX B

WIRING DIAGRAMS OF THE 3-D TURBULENT FLOW ANALYZER

Nomenclature

V_x, V_y, V_z	Linearizer outputs.
U_x, U_y, U_z	Normalized effective velocities, same as U_{eff_1}, U_{eff_2}, U_{eff_3}.
$D_x, D_y, D_z, E_x, E_y, E_z, F_x, F_y, F_z$	Coefficients in the inverted Jorgensen's matrix M.
X, Y, Z	Normalized velocities in wire coordinates.
$X_u, Y_u, Z_u, X_v, Y_v, Z_v, X_w, Y_w, Z_w$	Coefficients of the coordinate transformation matrix N.
U, V, W	Normalized velocities in laboratory coordinates.

FLOW COMPUTER FRONT PANEL SCHEMATIC DIAGRAM

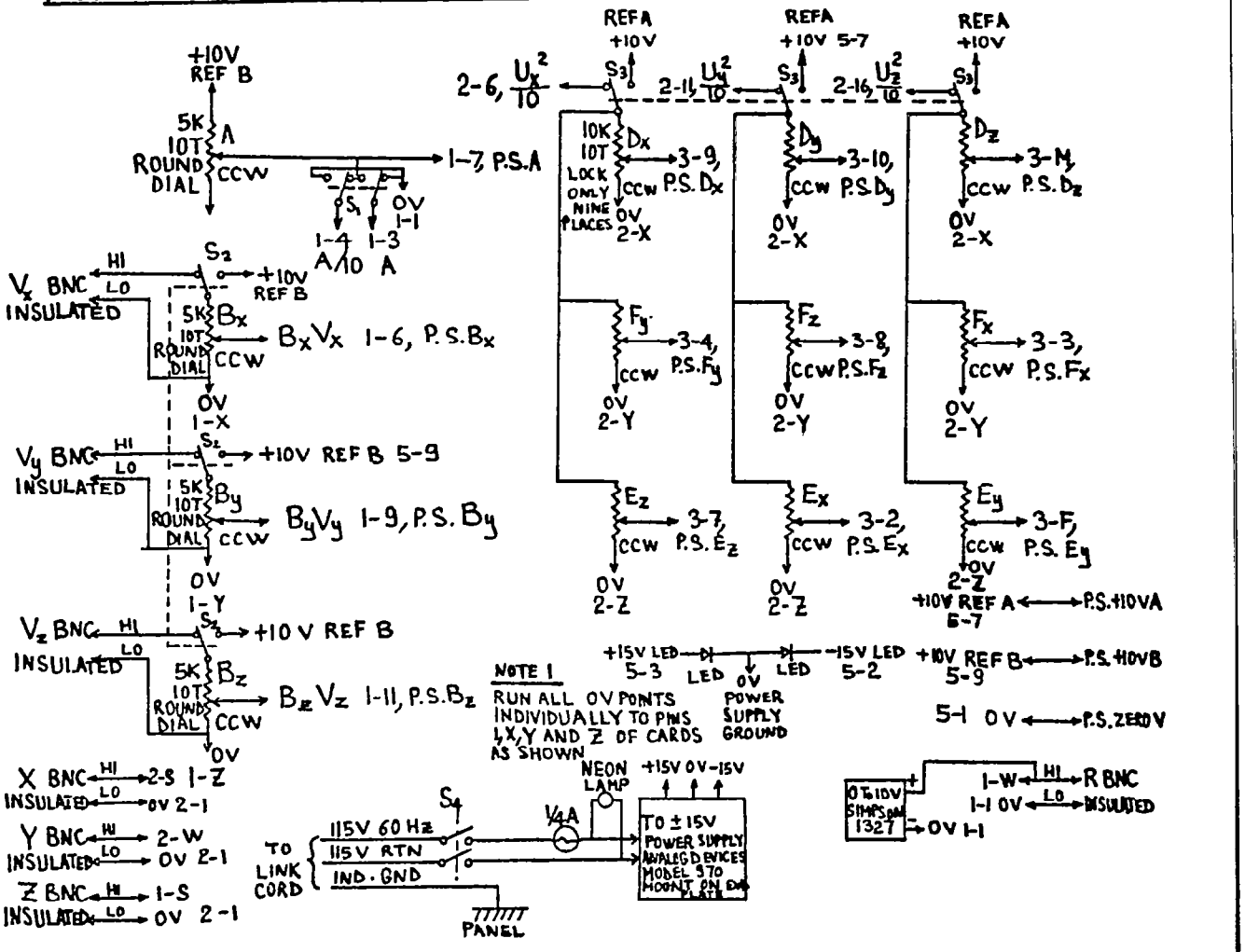

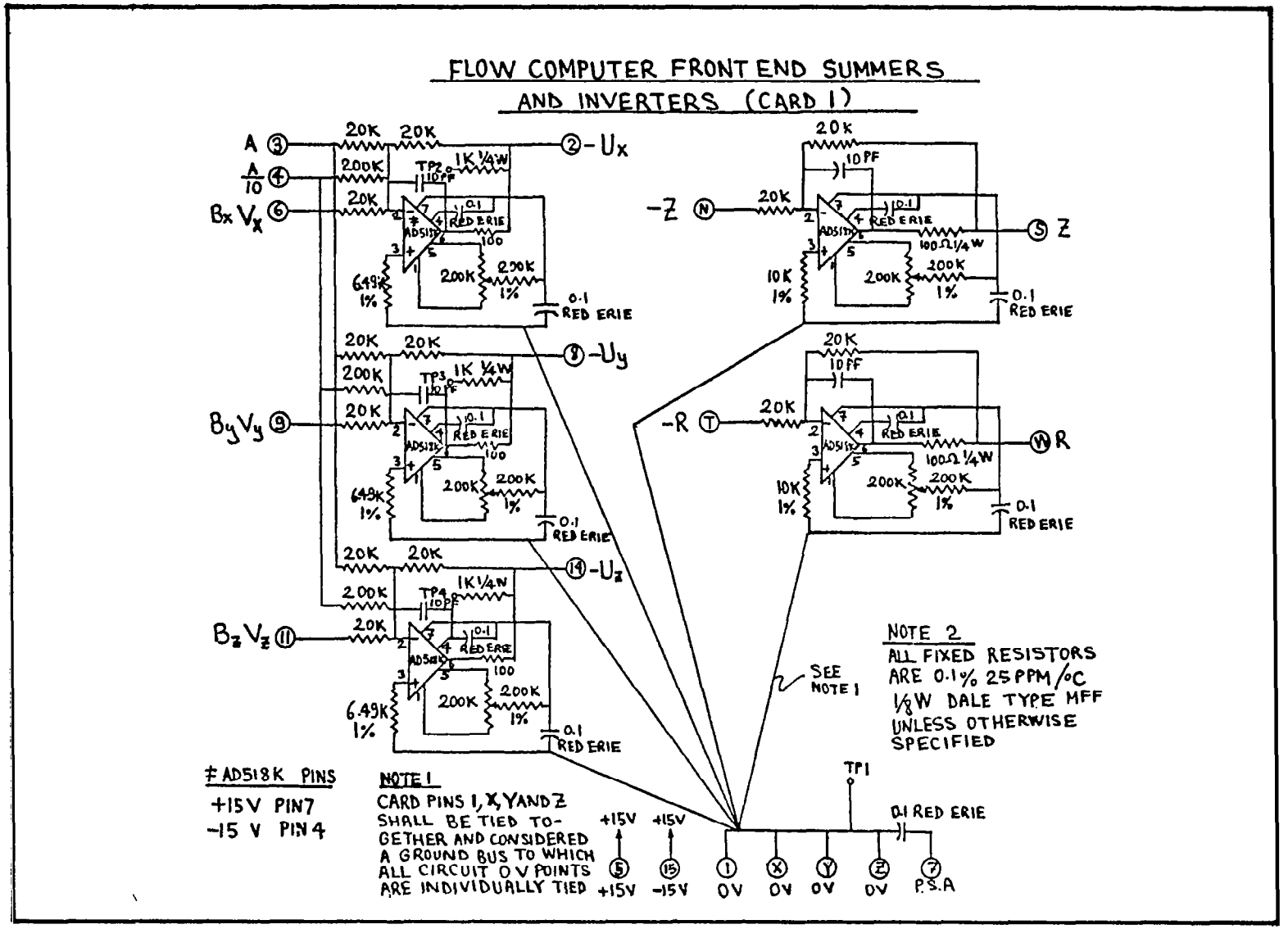
FLOW COMPUTER FRONT END SUMMERS
AND INVERTERS (CARD 1)
A ③
A/10 ④
Bx Vx ⑥
20K
200K
10PF
1K 1/4W
TP2
0.1 RED ERIE
100
649K 1%
200K 1%
-Ux ②
By Vy ⑨
TP3
-Uy ⑧
Bz Vz ⑪
TP4
-Uz ⑭
-Z ⑭
Z ⑤
-R ⑦
R ⑩
10K 1%
100Ω 1/4W
SEE NOTE 1
NOTE 2
ALL FIXED RESISTORS ARE 0.1% 25PPM/°C 1/8W DALE TYPE MFF UNLESS OTHERWISE SPECIFIED
AD518K PINS
+15V PIN 7
-15 V PIN 4
NOTE 1
CARD PINS 1, X, Y AND Z SHALL BE TIED TOGETHER AND CONSIDERED A GROUND BUS TO WHICH ALL CIRCUIT 0 V POINTS ARE INDIVIDUALLY TIED
+15V ⑤
-15V ⑮
0V ①
0V Ⓧ
0V Ⓨ
0V Ⓩ
P.S.A ⑦
TP1
0.1 RED ERIE

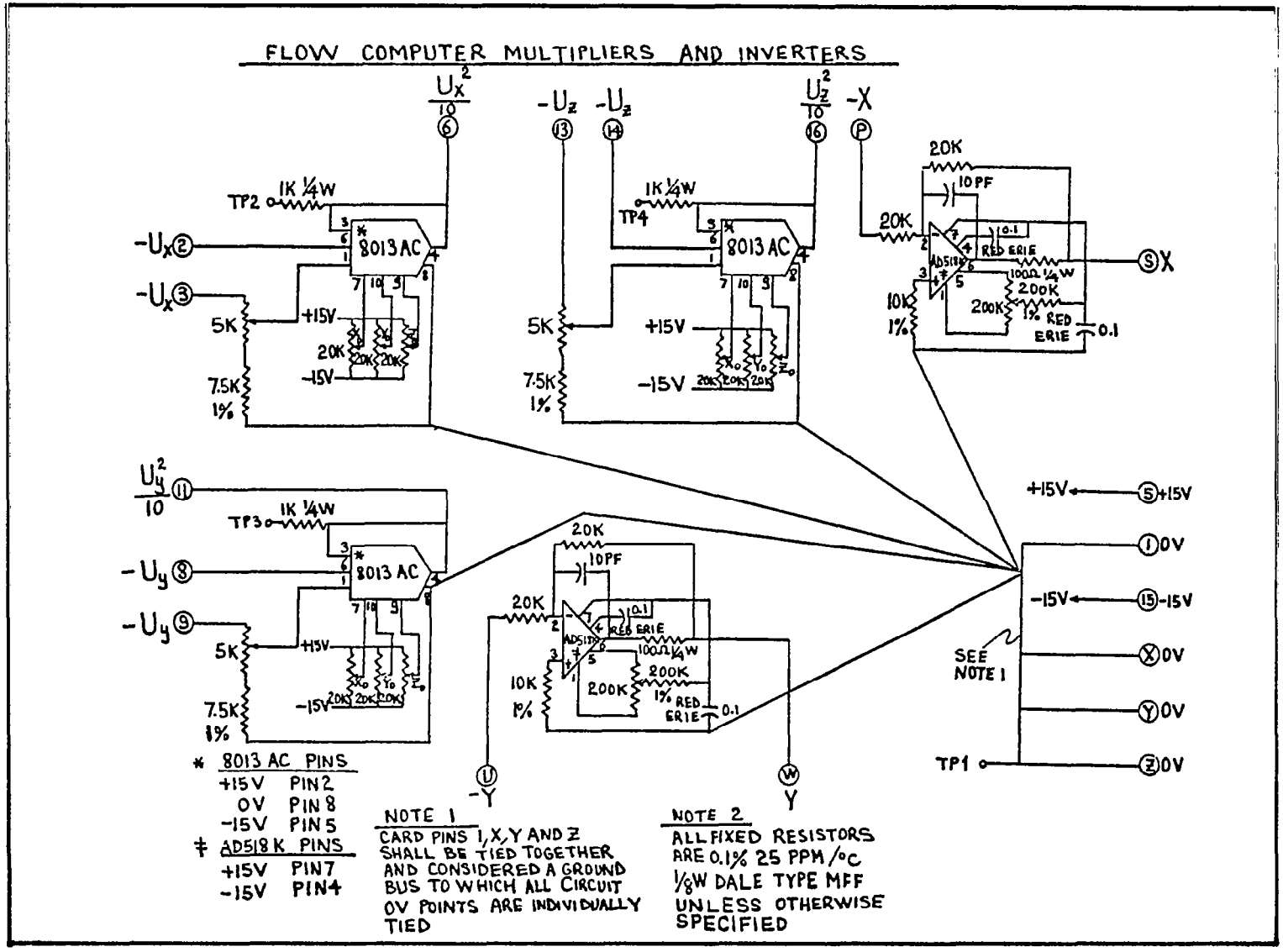
FLOW COMPUTER MULTIPLIERS AND INVERTERS
$\frac{U_x^2}{10}$
$-U_z$
$-U_z$
$\frac{U_z^2}{10}$
$-X$
$\frac{U_y^2}{10}$
1K ¼W
TP2
TP3
TP4
8013 AC
5K
7.5K 1%
+15V
-15V
20K
10PF
10K 1%
200K
100Ω ¼W
1% RED ERIE
0.1
RED ERIE
AD518K
+15V
0V
-15V
SEE NOTE 1
TP1
-Y
Y
* 8013 AC PINS
+15V PIN 2
0V PIN 8
-15V PIN 5
‡ AD518K PINS
+15V PIN 7
-15V PIN 4
NOTE 1
CARD PINS 1, X, Y AND Z SHALL BE TIED TOGETHER AND CONSIDERED A GROUND BUS TO WHICH ALL CIRCUIT 0V POINTS ARE INDIVIDUALLY TIED
NOTE 2
ALL FIXED RESISTORS ARE 0.1% 25 PPM/°C 1/8W DALE TYPE MFF UNLESS OTHERWISE SPECIFIED

FLOW COMPUTER SUMMING AMPLIFIERS (CARD 3)

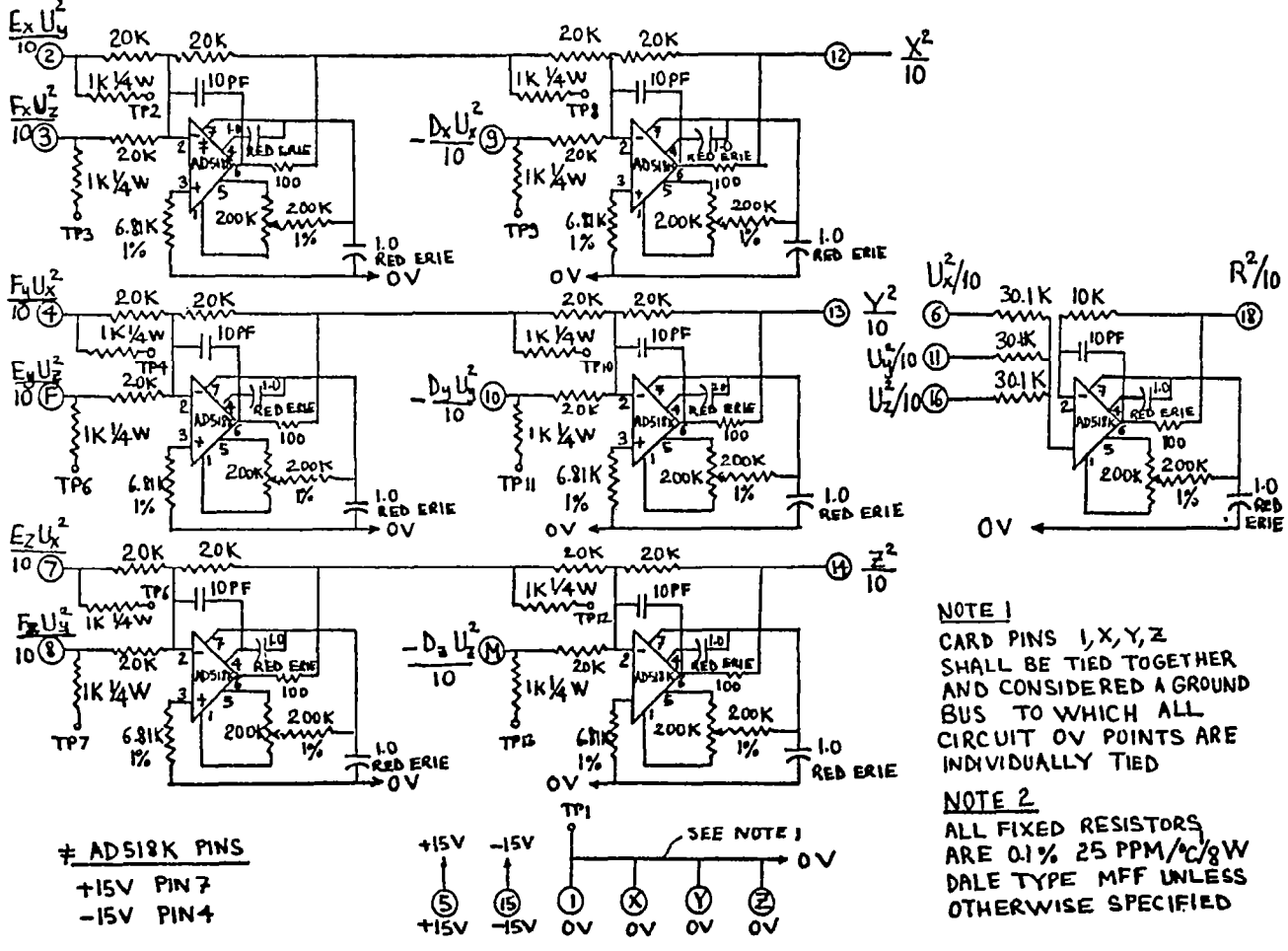

NOTE 1

CARD PINS 1, X, Y, Z SHALL BE TIED TOGETHER AND CONSIDERED A GROUND BUS TO WHICH ALL CIRCUIT 0V POINTS ARE INDIVIDUALLY TIED

NOTE 2

ALL FIXED RESISTORS ARE 0.1% 25 PPM/°C/⅛W DALE TYPE MFF UNLESS OTHERWISE SPECIFIED

FLOW COMPUTER SQUARE ROOTS (CARD 4)

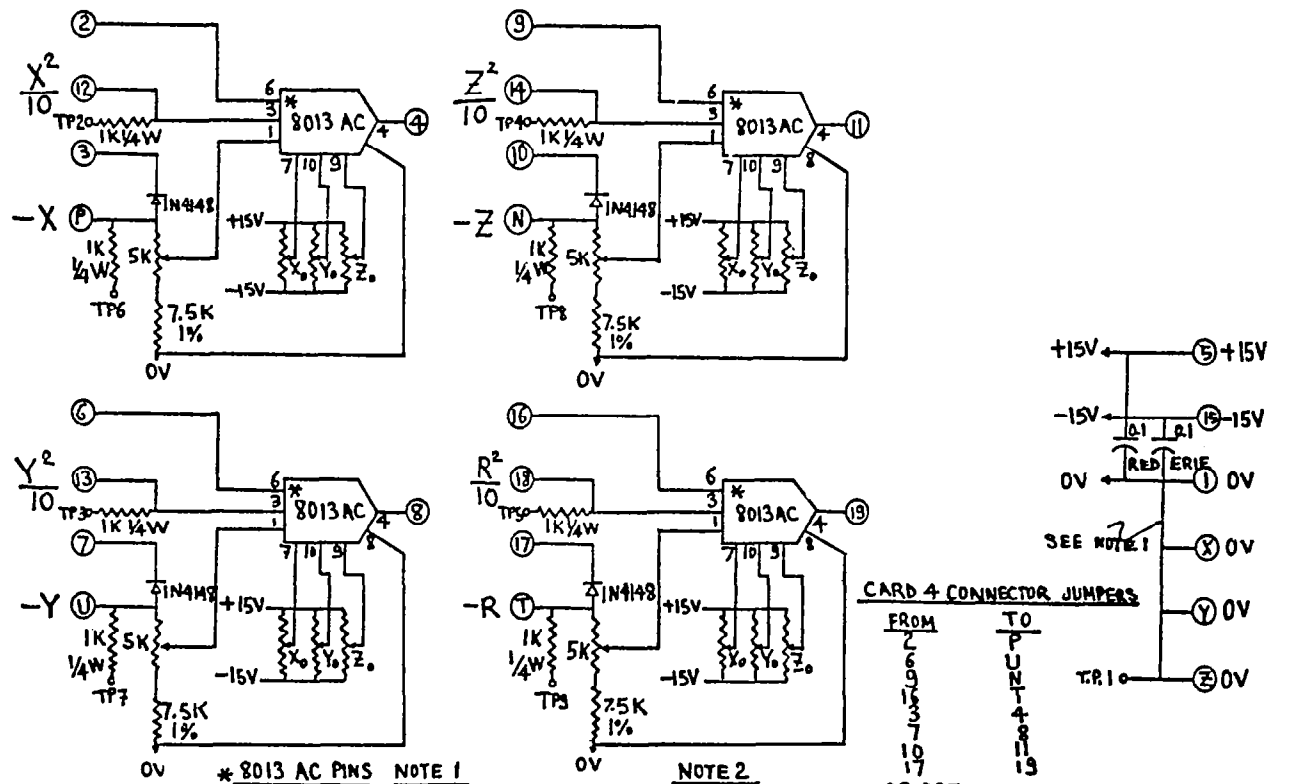

CARD 4 CONNECTOR JUMPERS	
FROM	TO PC BOARD UNIT
2	4
6	8
9	11
13	19
3	
7	
10	
17	

* 8013 AC PINS
+15V PIN 2
0V PIN 8
-15V PIN 5

NOTE 1
CARD PINS 1, X, Y, Z SHALL BE TIED TOGETHER AND CONSIDERED A GROND BUS TO WHICH ALL CIRCUIT 0V POINTS ARE INDIVIDUALLY TIED

NOTE 2
ALL FIXED RESISTORS ARE 0.1% 25 PPM/°C 1/8 W DALE TYPE MFF UNLESS OTHERWISE SPECIFIED

FLOW COMPUTER PRECISION +10V REFERENCE SCHEMATIC DIAGRAM (CARD 5)

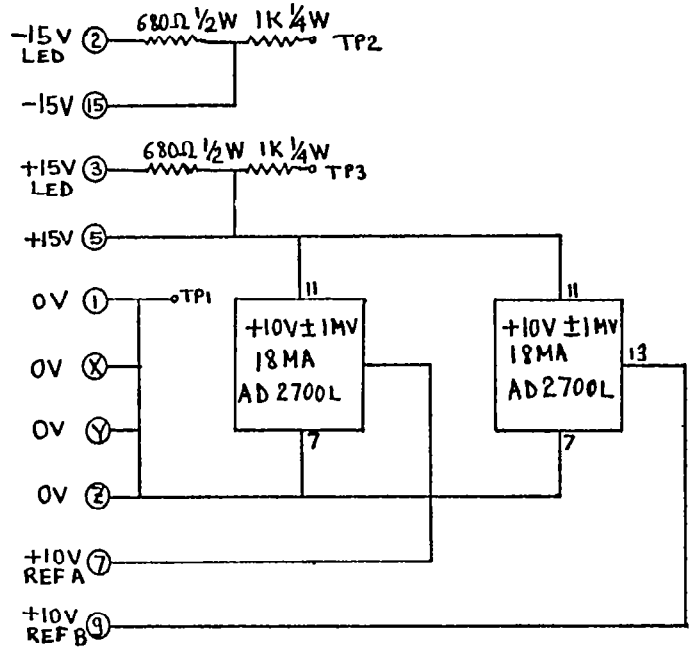

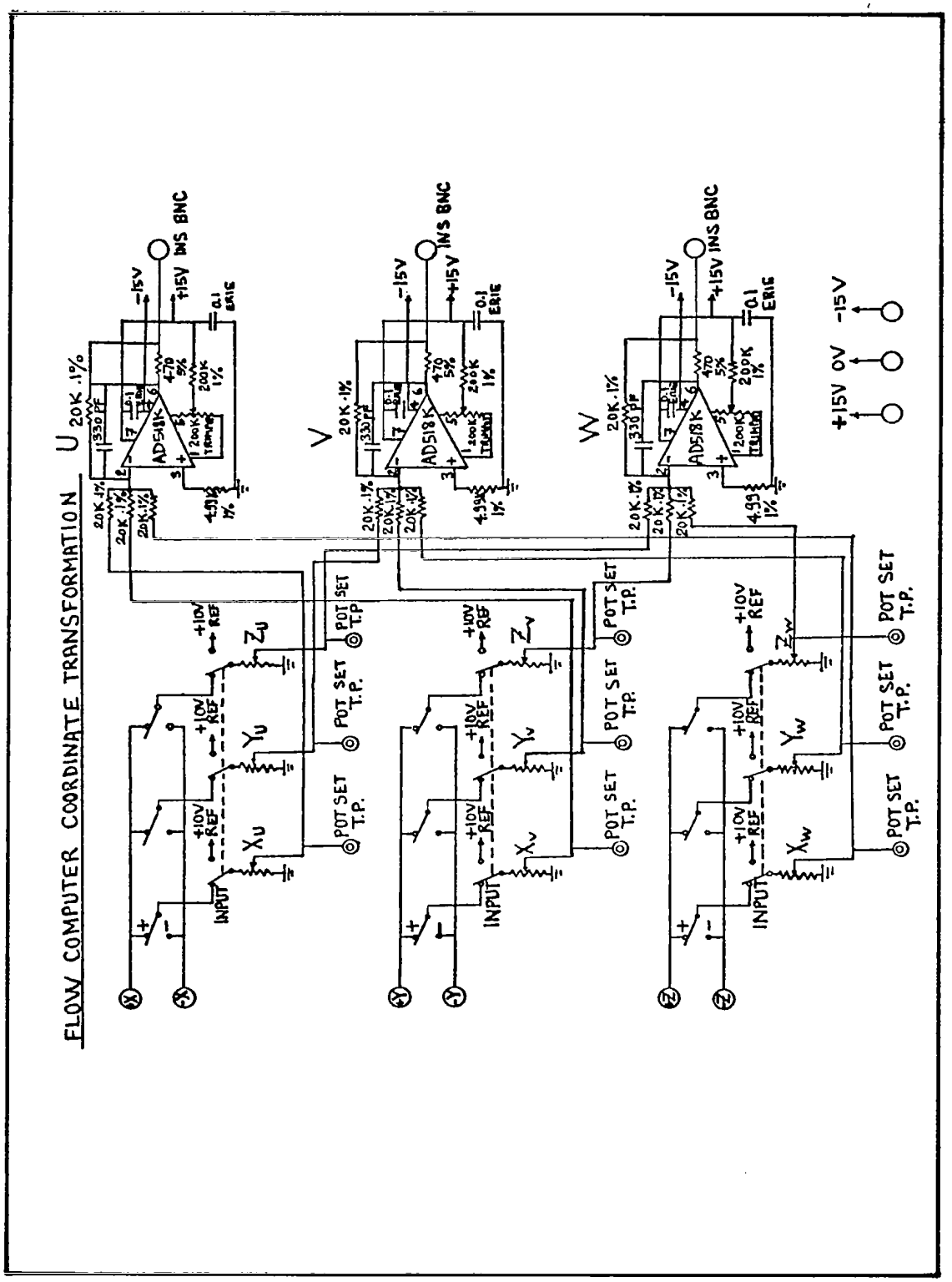
FLOW COMPUTER COORDINATE TRANSFORMATION
U
V
W
20K .1%
330 PF
AD518K
+15V INS BNC
-15V
+15V
0.1 ERIE
470 5%
200K 1%
4.99K 1%
+10V REF
POT SET T.P.
INPUT
+15V 0V -15V

1. Report No.	2. Government Accession No.	3. Recipient's Catalog No.
NASA CR-3104		

4. Title and Subtitle	5. Report Date
FULL-COVERAGE FILM COOLING: 3-DIMENSIONAL MEASUREMENTS OF TURBULENCE STRUCTURE AND PREDICTION OF RECOVERY REGION HYDRODYNAMICS	March 1979
	6. Performing Organization Code
7. Author(s)	8. Performing Organization Report No.
S. Yavuzkurt, R. J. Moffat, and W. M. Kays	HMT-27
	10. Work Unit No.
9. Performing Organization Name and Address	
Stanford University Stanford, California 94305	11. Contract or Grant No. NAS3-14336
	13. Type of Report and Period Covered
12. Sponsoring Agency Name and Address	Contractor Report
National Aeronautics and Space Administration Washington, D.C. 20546	14. Sponsoring Agency Code

15. Supplementary Notes

Final report. Project Manager, Raymond E. Gaugler, Fluid System Components Division, NASA Lewis Research Center, Cleveland, Ohio 44135.

16. Abstract

Hydrodynamic measurements were made with a triaxial hot-wire in the full-coverage region and the recovery region following an array of injection holes inclined downstream, at 30^{o} to the surface. The data were taken under isothermal conditions at ambient temperature and pressure for two blowing ratios: $M = 0.9$ and $M = 0.4$. ($M = \rho_{jet}U_{jet}/\rho_{\infty}U_{\infty}$ where U is the mean velocity and ρ is the density. Subscripts "jet" and "∞" stand for injectant and free stream, respectively.) Profiles of the three main velocity components and the six Reynolds stresses were obtained at several spanwise positions at each of the five locations down the test plate. A one-equation model of turbulence (using turbulent kinetic energy with an algebraic mixing length) was used in a two-dimensional computer program to predict the mean velocity and turbulent kinetic energy profiles in the recovery region. A new real-time hot-wire scheme was developed to make measurements in the three-dimensional turbulent boundary layer over the full-coverage surface.

17. Key Words (Suggested by Author(s))	18. Distribution Statement
Boundary layer; Heat transfer; Film cooling; Computer program; Turbulence; Numerical	Unclassified - unlimited STAR Category 34

19. Security Classif. (of this report)	20. Security Classif. (of this page)	21. No. of Pages	22. Price*
Unclassified	Unclassified	187	A09

* For sale by the National Technical Information Service, Springfield, Virginia 22161

NASA-Langley, 1979